JOURNAL OF TELECOMMUNICATIONS AND INFORMATION TECHNOLOGY

3/2018

(*Contents Continued on Back Cover*)

ISSN 1509-4553 on-line: ISSN 1899-8852

Circulation: 300 copies Sowa – Druk na życzenie, www.sowadruk.pl, tel. 22 431-81-40

Ministry of Science and Higher Education
Republic of Poland

Improvement of language quality; Assigning DOIs; Subscription to the plagiarism detection system – tasks financed under 556/P-DUN/2017 agreement from the budget of the Ministry of Science and Higher Education under the science dissemination fund.

JOURNAL OF TELECOMMUNICATIONS AND INFORMATION TECHNOLOGY

Preface

This issue of the *Journal of Telecommunications and Information Technology* is dominated by a set of papers presenting theoretical studies and computer simulations devoted to optimization of several types of multiuser wireless systems.

This part begins with two papers written by M. Addad and A. Djebbari. The first one, titled *A New Code Family for QS-CDMA Visible Light Communication Systems*, presents new codes for broadband Visible Light Communications (VLC) – a method relying on modulated light emitted by light emitting diodes (LEDs) for short-range data transmission in various environments. Optical Code Division Multiple Access (OCDMA) is a strong candidate for VLC applications. Multiple access interference is the predominant source of bit errors, as it causes transmission errors when system users are transmitting asynchronously. In this case, the so-called Zero Cross-Correlation (ZCC) codes (orthogonal sets of sequences where no overlapping of ones occurs and a zero zone exists) ensure the best system performance, also in the presence of synchronization problems and multipath propagation.

The same authors look, in the second paper titled *Suitable Spreading Sequences for Asynchronous MC-CDMA Systems*, at ways to improve performance of the multi-carrier Code Division Multiple Access (MC-CDMA) technology which combines Orthogonal Frequency Division Multiplexing (OFDM) and Code Division Multiple Access (CDMA), and is frequently used in radio communication systems. However, an MC-CDMA network serving a large number of users suffers from a high Peak-To-Average Power Ratio (PAPR), causing poor utilization of transmitter power. In addition, asynchronous MC-CDMA suffers from the effect of multiple access interference. Both harmful effects shall be reduced for maintaining a low error rate. After computer simulations, it was concluded that Zero Correlation Zone (ZCZ) sequences are the most suitable spreading sequences.

The issue of reducing PAPR and efficiently utilizing transmitter power in OFDM systems is analyzed also by Y. Aimer, B. Seddik Bouazza, S. Bachir, and C. Duvanaud in their paper titled *Interleaving Technique Implementation to Reduce PAPR of OFDM Signal in Presence of Nonlinear Amplification with Memory Effects*. The authors show that it is possible to interleave multicarrier signals to prevent grouping of errors (which cannot be removed by means of forward error correction), to use null subcarriers to transmit side information to the receiver, with the said transmission augmented with a new method for coding interleaver

keys at the transmitter and a robust decoding procedure at the receiver. Simulations of such a WLAN 802.11a system, including a nonlinear power amplifier with memory, indicate a reduction of PAPR by 5.2 dB.

The next paper, titled *Using Least Mean p-Power Algorithm to Correct Channel Distortion in MC-CDMA Systems*, by M. Zidane, S. Safi, M. Sabri, and M. Frikel, is also about MC-CDMA 4G mobile radio systems, but focuses on adaptive downlink equalization to compensate for channel distortion in terms of the bit error rate, investigated analytically using the Least Mean p-Power Algorithm (LMP). The results of numerical simulations, performed for various values of signal-to-noise ratio and the p threshold, show that the presented algorithm is able to simulate the standard BRAN C channel measured with different accuracy levels.

There are many novel technologies that are proposed for inclusion in 5G wireless networks. One of them is the device-to-device (D2D) communications: a direct communication between two or more user devices across a short distance without participation of the base station. D2D can ensure more efficient handling of certain types of mobile data traffic, but produces more interference, as it uses the same frequency band as the underlying cellular network. In their study *Interference Management Using Power Control for Device-to-Device Communication in Future Cellular Networks*, T. A. Nugraha, M. P. Pamungkas, and A. N. N. Chamim investigate the use of adaptive power control to mitigate such interference. Simulations show that the signal to interference plus noise ratio (SINR) can be improved by 0.5–1 dB compared to operation at a fixed power level.

Errors produced by noise and adverse propagation phenomena in wireless and wired communication systems render the use of error correcting codes mandatory in many cases. Their implementations, however, tend to be complex. In their paper titled *Low Density Parity Check Codes Constructed from Hankel Matrices*, M. A. Tehami and A. Djebbari present a new technique for constructing Low Density Parity Check Codes (LDPC) based on the Hankel matrix and circulant permutation matrices. The new codes are exempt of any cycle of length 4 to ensure low-complexity hardware implementations, with a reduced number of logic gates and the use of simple shift registers. Simulations show that the proposed codes perform very well over additive white Gaussian noise channels.

Telephone systems must often work in noisy environments, such as interior of a car, train station or a place where other persons speak at the same time. Several methods of speech enhancement relying on digital signal processing to remove noise and improve intelligibility have been developed. None of them, however, is equally effective in different conditions, especially when the interfering sound is of the non-stationary nature. In the paper titled *Incoherent Discriminative Dictionary Learning for Speech Enhancement*, D. Shaheen, O. Al Dakkak, and M. Wainakh have proposed and tested a new Incoherent Discriminative Dictionary Learning (IDDL) algorithm to model both speech and noise, where the cost function accounts for both "source confusion" and "source distortion" errors, with a regularization term that penalizes the coherence between speech and noise sub-dictionaries. At the enhancement stage, sparse coding is used on the learnt dictionary to estimate both clean speech and noise spectrum. Finally, the Wiener filter is used to refine the clean speech estimate. Experiments on the Noizeus dataset, demonstrated that the proposed algorithm outperforms other dictionary learning speech enhancement algorithms: K-SVD, GDL and FDDL, using two objective measures: frequency-weighted segmental SNR and Perceptual Evaluation of Speech Quality (PESQ) in the presence of structured non-stationary noise, but not white noise.

The next two papers are devoted to cognitive radio, a promising technology capable of adaptive and more efficient use of the scarce spectrum available currently, by additional or "secondary" users, when the primary (licensed) users do not transmit. However, this requires new methods of spectrum allocation and reception of signals in adverse conditions to be applied.

In the paper titled *Interference Aware Routing Game for Cognitive Radio Ad-hoc Networks* by S. Amiri-Doomari, G. Mirjalily and J. Abouei, an interference-aware routing game is proposed that connects flow initiators to the destinations. A network formation game among secondary users is formulated in which each secondary user aims to maximize its utility, and to reduce the aggregate interference on the primary users and the end-to-end delay. In order to reduce end-to-end delay and the accumulated interference, the new algorithm selects upstream neighbors, looking from the point of view of the sender. It avoids congested network

zones and forms at least one path from the flow initiator to the destination. To model interference between secondary users, a signal-to-interference-plus noise (SINR) model is employed. Numerical simulations show that the proposed algorithm works better than Interference Aware Routing (IAR) in cognitive radio mesh networks, with fewer hops between the initiator and the destination required.

Optimization of receiver designs for cognitive networks is the subject of the paper titled *Theoretical Investigation of Different Diversity Combining Techniques in Cognitive Radio* by R. Agarwal, N. Srivastava and H. Katiyar. The authors compare the performance of energy detectors in cognitive radio using different diversity combining techniques. While the Maximal Ratio Combining (MRC) receiver works best, it is complex and expensive, so less complex combining techniques are preferred, such as switched diversity. Two such schemes were analyzed: Switch Examine Combining (SEC) and Switch Examine Combining with post examining selection (SECp). General formulas for the probability of detection using MRC, SEC and SECp diversity combining techniques over the Rayleigh fading channel were derived for various numbers of branches, and a trade-off between detection performance and receiver complexity was observed.

In their article titled *Swarm Intelligence-based Partitioned Recovery in Wireless Sensor Networks*, G. Kumar and V. Ranga look at the ways to improve reliability and resilience of heterogeneous wireless sensor networks, because battery-powered sensor nodes operate in a hostile, noisy environment and fail frequently (usually due to a discharged battery) or lose connections to other nodes. A network partition recovery solution called Grey Wolf was presented, which is an optimizer algorithm for repairing segmented heterogeneous wireless sensor networks. This solution provides strong bi-connectivity in the damaged area, but also distributes traffic load among the multiple deployed nodes to enhance the repaired network's lifetime. Computer simulations show that the Grey Wolf algorithm offers considerable performance advantages over other approaches.

Concluding this issue of JTIT is the paper titled *Non-crossing Rectilinear Shortest Minimum Bend Paths in the Presence of Rectilinear Obstacles* by Shylashree Nagaraja, in which a new algorithm to determine the shortest, non-crossing, rectilinear paths in a two-dimensional grid graph is presented. The shortest paths are determined which do not cross each other and bypass all obstacles. This is useful in the design of integrated circuits and printed circuit boards, in the routing of traffic in wireless sensor networks, etc. When more than one equal length non-crossing path is present between the source and the destination, the proposed algorithm selects the path which has the least number of corners (bends) along the path. In this method, the grid points are the vertices of the graph and the lines joining the grid points are the edges of the graph. The obstacles are represented by their boundary grid points. Once the graph is ready, an adjacency matrix is generated and the Floyd-Warshall all-pairs shortest path algorithm is used iteratively to identify the shortest, non-crossing paths. To get the minimum number of bends in a path, the author made a modification of the Floyd-Warshall algorithm, which is a novel element.

Krzysztof Borzycki
Guest Editor

https://doi.org/10.26636/jtit.2018.preface3

Paper

A New Code Family for QS-CDMA Visible Light Communication Systems

Mouad Addad and Ali Djebbari

Faculty of Electrical Engineering, Djillali Liabes University of Sidi Bel Abbes, Sidi Bel Abbès, Algeria

https://doi.org/10.26636/jtit.2018.124318

Abstract—Visible light communication (VLC) is a promising technology for wireless communication networks. Optical code division multiple access (OCDMA) is a strong candidate for VLC-based applications. The predominant source of bit error in OCDMA is the multiple access interference (MAI). To eliminate MAI in synchronous OCDMA, zero cross correlation (ZCC) codes have been proposed. However, synchronization problems and multipath propagation introduce relative non-zero time delays. Therefore, the zero correlation zone (ZCZ) concept was introduced. In this paper, we propose a new method for generating ZCC codes. The proposed construction can accommodate any number of users with flexible Hamming weight. The numerical results obtained show that the proposed codes significantly reduce MAI, compared to ZCC, as well as ZCZ codes.

Keywords—CDMA, visible light communication, zero correlation zone, zero cross correlation.

1. Introduction

Wireless access technologies have been continuously evolving in response to the rapid increase in the use of mobile devices [1]. The scarcity of radio frequency spectrum is a limiting factor in meeting this demand [2]. In applications where high bandwidth is required, visible light communication (VLC) is a promising technology, complementary to radio frequency systems. A key advantage of VLC is its potential to simultaneously provide energy sufficient lighting and high-speed communication using light emitting diodes (LEDs) [1]–[5]. VLC is being adopted in, to name a few, vehicle-to-vehicle communication [3], indoor positioning [4], and underwater communications [5].

A crucial aspect of a VLC system is the multiple access technique. The optical medium is suited for spread spectrum multiple access (SSMA) communications due to its large bandwidth. Code division multiple access (CDMA) is one class of SSMA, in which many users access a common channel simultaneously through the use of encoding. In an optical CDMA system (OCDMA), the received signal is the superposition of light waves from the individual users.

The performance of OCDMA systems depends on the code set employed. The design of proper codes for OCDMA must take into consideration many criteria, such as: large set size, equal Hamming weight, minimum length, and most importantly low cross correlation properties. Zero cross correlation (ZCC) codes were proposed to eliminate the MAI effect in synchronous OCDMA systems [6], [7]. However, synchronization problems and multipath propagation introduce a relative non-zero time delay. Therefore, zero correlation zone (ZCZ) codes were introduced for the optical quasi-synchronous (QS) CDMA [8].

The remaining content of the paper is organized as follows. New family of ZCC codes is introduced in Section 2. In Section 3, the system model for optical QS-CDMA is given. Performance of the system using various optical codes is evaluated in Section 4. We give our concluding remarks in Section 5.

2. Preliminaries

ZCC code is an orthogonal set of sequences where no overlapping of ones occurs. The code parameters must be flexible, so that it can suit any application: number of users can take any integer and is independent of the code Hamming weight (number of ones in any single code). Let $\mathbf{S}$ be a set with M codes each with length N where $\mathbf{S} = \{\mathbf{s}^1, \ldots, \mathbf{s}^i, \ldots, \mathbf{s}^M\}$, and $\mathbf{s}^i = \{s_1^i, \ldots, s_l^i, \ldots, s_N^i\}$:

$$\mathbf{S} = \begin{bmatrix} \mathbf{s}^1 \\ \vdots \\ \mathbf{s}^i \\ \vdots \\ \mathbf{s}^M \end{bmatrix} = \begin{bmatrix} s_1^1 & \ldots & s_l^1 & \ldots & s_N^1 \\ \vdots & \ddots & \vdots & \ddots & \vdots \\ s_1^i & \ldots & s_l^i & \ldots & s_N^i \\ \vdots & \ddots & \vdots & \ddots & \vdots \\ s_1^M & \ldots & s_l^M & \ldots & s_N^M \end{bmatrix} \tag{1}$$

and $s_l^i \in \{0,1\}$.

The periodic cross-correlation function (CCF) is defined as follows:

$$R_{\mathbf{s}^i,\mathbf{s}^j}(\tau) = \sum_{l=1}^{N} s_l^i s_{(l+\tau) \bmod N}^j, \tag{2}$$

when $i = j$ the CCF becomes the auto-correlation function (ACF).

The code set $\mathbf{S}$ is called optical ZCZ set if the correlation functions satisfy [6], [7]:

$$R_{\mathbf{s}^i,\mathbf{s}^j}(\tau) = \begin{cases} w & i = j,\ \tau = 0 \\ 0 & i \neq j,\ \tau = 0 \end{cases}, \tag{3}$$

where w represents the code's Hamming weight. The code length for ZCC codes is $N = Mw$.
A code set $\mathbf{S}$ is called ZCZ if the correlation functions satisfy [8]:

$$R_{\mathbf{s}^i,\mathbf{s}^j}(\tau) = \begin{cases} w & i = j,\ \tau = 0 \\ 0 & i \neq j,\ \tau = 0 \\ 0 & 0 < |\tau| \leq Z \end{cases}, \tag{4}$$

where Z is the zero-zone length. The code length for ZCZ codes is $N = Mw(Z+1)$.

2.1. New ZCC Code Family

In this section, a simple and flexible construction method of ZCC codes is presented. The number of codes as well as the code Hamming weight can be easily adjusted. The construction procedure is as follows. For $w = 2$, a starter ZCC code is obtained as:

$$\mathbf{ZCC}_{w=2}^{M=2} = \begin{bmatrix} 1 & 1 & 0 & 0 \\ 0 & 0 & 1 & 1 \end{bmatrix}. \tag{5}$$

To increase the number of codes to $M+1$, a mapping technique is used as:

$$\mathbf{ZCC}_{w}^{M+1} = \begin{bmatrix} \mathbf{A} & \mathbf{B} \\ \mathbf{C} & \mathbf{D} \end{bmatrix}, \tag{6}$$

where $\mathbf{A}$ is the original ZCC set of $[M,N]$, $\mathbf{B}$ consists of $[M,w]$ zeros, $\mathbf{C}$ consists of $[1,N]$ zeros, and $\mathbf{D}$ of a $[1,w]$ ones. Example: by using the mapping technique (6) on ZCC given by (5), we obtain:

$$\mathbf{ZCC}_{w=2}^{M=3} = \begin{bmatrix} 1 & 1 & 0 & 0 & 0 & 0 \\ 0 & 0 & 1 & 1 & 0 & 0 \\ 0 & 0 & 0 & 0 & 1 & 1 \end{bmatrix}. \tag{7}$$

The ZCC code length is $N = wM$.

3. System Model

The optical QS-CDMA for VLC system is designed in [8] to support M active users, each containing an information source and a destination. Each user employs a white LED for signal transmission and a photodiode for signal reception. The optical source is assumed to be ideally flat over a bandwidth $\left[v_0 - \frac{\Delta_v}{2} \quad v_0 + \frac{\Delta_v}{2}\right]$ where v_0 denotes the optical central frequency and Δ_v the bandwidth. Users are considered to have an equal transmitted and received power. The LED broadband spectrum is divided into N wavelengths, where each user is assigned a set of wavelengths. Each bit "1" of the user's assigned code picks a wavelength. When the information is carried on the intensity of light, the signals that modulate the LEDs must be real and non-negative. Therefore, unipolar codes made up of "1" and "0" are used.
The main sources of LED-based OCDMA degradation are phase-induced intensity noise (PIIN), shot noise, and thermal noise. PIIN generated at the photodiode output can be suppressed using ZCC and ZCZ codes [6]–[8]. Therefore, only the shot noise and thermal noise are present in the photodiode current. The current variance at the receiver can be expressed as [6], [8]:

$$\mathrm{Var}(i) = 2eIB + \frac{4k_{\mathrm{B}}T_nB}{R_L}, \tag{8}$$

where e is the electron charge, I is the average photocurrent, B is the receiver electrical bandwidth, k_{B} is the Boltzmann's constant, T_n the receiver noise temperature, and R_L is the receiver load resistor. The average photo current is given as [8]:

$$I = \frac{RP_{sr}}{N}\left(wd_j + \sum_{i=1,i\neq j}^{M} d_i \sum_{l=1}^{N} s_{l-\tau_i}^i s_l^j\right), \tag{9}$$

where P_{sr} is the received power, d_j is the desired user's transmitted data bit, d_i is the interferer's transmitted bit, and R is the responsivity of the photodiode given as [8]:

$$R = \frac{\eta e}{hv_0}, \tag{10}$$

where η is the photo detector's quantum efficiency and h is Planck's constant.
When ZCC and ZCZ codes are used, the desired user's current for a time delay $\tau_i = 0$ is:

$$I_d = \frac{RP_{sr}wd_j}{N}. \tag{11}$$

For quasi-synchronous transmission $(\tau_i \neq 0)$ and worst case scenario $(d_i = d_j = 1)$, the averaged average current $\bar{I}$ is given as [8]:

$$\bar{I} = \frac{RP_{sr}}{N}\left(w + \frac{1}{Z}\sum_{\tau_i=1}^{Z}\sum_{i=1,i\neq j}^{M}\sum_{l=1}^{N} s_{l-\tau_i}^i s_l^j\right). \tag{12}$$

The average signal to noise ratio (SNR) for optical QS-CDMA system is [8]:

$$SNR = \frac{I_d^2}{\mathrm{Var}(i)} = \frac{\left(\frac{RP_{sr}w}{N}\right)^2}{\frac{2eBRP_{sr}}{N}\left(w + \frac{MAI(\tau_i)}{Z}\right) + \frac{4k_{\mathrm{B}}T_nB}{R_L}}, \tag{13}$$

where Z is the maximum time delay between all users and $MAI(\tau_i)$ is the multiple access interference (MAI) defined as:

$$MAI(\tau_i) = \sum_{\tau_i=1}^{Z}\sum_{i=1,i\neq j}^{M}\sum_{l=1}^{N} s_{l-\tau_i}^i s_l^j. \tag{14}$$

4. Performance Analysis

The MAI is a significant cause of bit decision errors for an optical QS-CDMA system. The correlation properties of codes are crucial to the system's capacity to eliminate MAI and provide reliable communication. In this section, we first investigate MAI reduction of the proposed ZCC

codes based on time delay, code length, and the number of codes. Next, ZCC codes are compared to ZCZ codes.
In order to evaluate the impact of correlation properties on the code's performance, we compare the proposed ZCC family to two ZCC codes proposed in [6], [7]. The same number of codes $M = 10$, code length $N = 80$, and Hamming weight $w = 8$ were used. From Fig. 1, it is clear that when the time delay between active users increases, MAI also increases in the system. This is because a longer time delay results in higher cumulative correlation function values. With their good correlation properties, the ZCC codes proposed provide lower MAI.

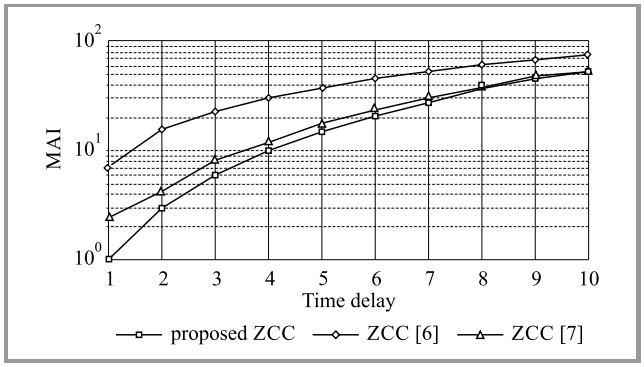

Fig. 1. MAI vs. time delay.

The impact of code length on MAI is analyzed and plotted in Fig. 2. ZCC codes with $M = 10$ active users having maximum time delay of $Z = 5$ were evaluated. The MAI level increases with code length N. Since M is fixed, longer codes can be obtained by increasing the Hamming weight w. This results in more ones "1" in the code and, consequently, higher correlation values. Note that the proposed ZCC codes not only have the lowest MAI level but also remain constant for code length N higher than 50.

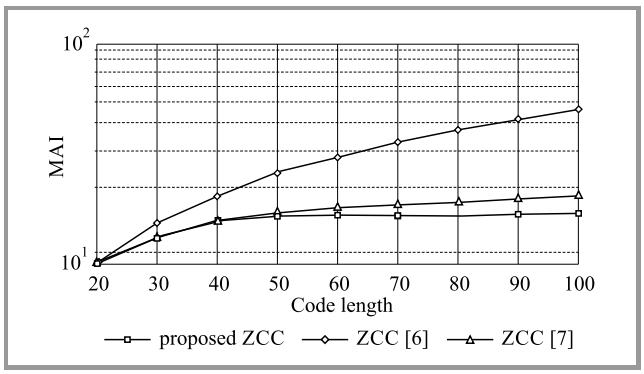

Fig. 2. MAI vs. code length.

Next, the interferer effect on MAI is analyzed. Figure 3 shows MAI values versus the number of active users M. ZCC codes with Hamming weight $w = 8$, code length $N = 10$, and time delay $Z = 3$ were evaluated. One can see that admitting more users to the system results in a high level of MAI. Note that the proposed ZCC codes still maintain the lowest values of MAI.

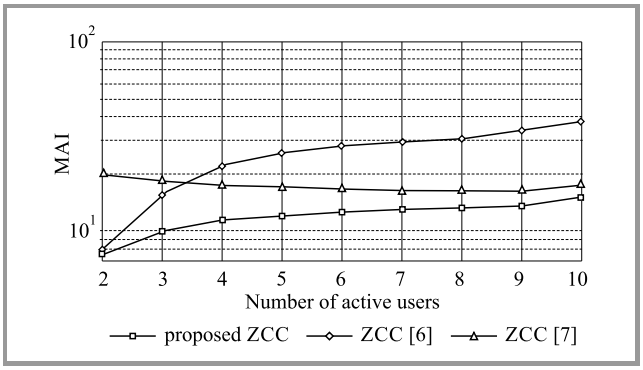

Fig. 3. MAI vs. number of active users.

4.1. Comparison between ZCC and ZCZ Codes

Due to their zero-correlation property, ZCZ codes have been extensively studied for radio frequency systems (more details can be found in [9], [10]). In [8], the authors introduced optical ZCZ codes to eliminate MAI in an optical QS-CDMA VLC system. Optical ZCZ codes can eliminate interference $MAI(\tau_i) = 0$ for $\tau_i \leq Z$. The SNR for ZCZ codes is:

$$SNR = \frac{\left(\frac{RP_{sr}w}{N}\right)^2}{\frac{2eBRP_{sr}w}{N} + \frac{4k_B T_n B}{R_L}}. \tag{15}$$

Since MAI cannot be used to compare ZCC and ZCZ codes performance, BER will be used instead. BER can be computed as follows [8]:

$$BER = 0.5 \cdot \mathrm{erfc}\sqrt{\frac{SNR}{8}}. \tag{16}$$

Table 1
System parameters

Symbol	Quantity	Value
v_0	Blue light center frequency	480 nm
Δ_v	Modulation bandwidth	650 MHz
η	Photo detector quantum efficiency	0.6
T_n	Receiver noise temperature	300 K
R_L	Receiver load resistor	1030 Ω
B	Receiver electrical bandwidth	311 MHz
e	Electron charge	$1.602189 \cdot 10^{-19}$ C
k_B	Boltzmann's constant	$1.3806505 \cdot 10^{-23}$ $\frac{\mathrm{J}}{\mathrm{K}}$
h	Planck's constant	$6.626196 \cdot 10^{-34}$ J · s

The parameters used in the computation of analytical results are listed in Table 1 [8].

Figure 4 shows BER performance with respect to the received power P_{sr}. ZCC and ZCZ codes with $M = 4$ active users and a different time delay were evaluated. The Ham-

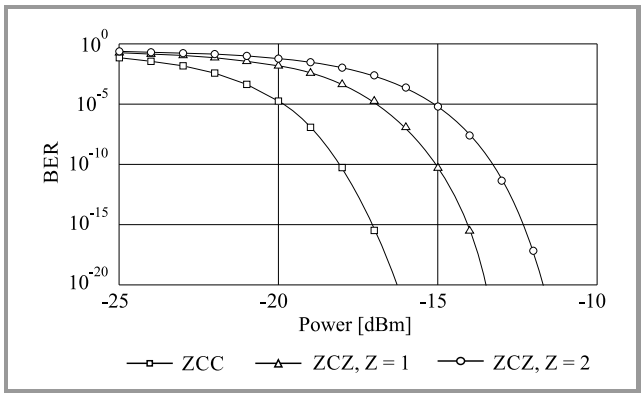

Fig. 4. BER comparison between ZCC and ZCZ codes.

ming weight is $w = 3$. We can readily see that ZCC codes outperform ZCZ codes by a large extent. Although ZCZ codes eliminate MAI, their code length is proportional to the zero zone Z. A large time delay requires long ZCZ codes which results in poor BER performance.

5. Conclusion

In this paper, we evaluate the performance of an optical QS-CDMA VLC system. MAI caused by the quasi-synchronous transmission was investigated with respect to ZCC correlation properties, code length, and number of codes in the set. New ZCC codes with a flexible construction and good correlation properties were presented in this paper. It was shown that the proposed ZCC codes have the best performance according to the criteria previously mentioned. It was also shown that ZCZ could eliminate MAI, but their length is not practical and results in poor BER performance. Therefore, we conclude that the new ZCC codes provide robust communication in a QS-CDMA VLC system.

References

[1] K. Werfli *et al.*, "Experimental demonstration of high-speed 4×4 imaging multi-CAP MIMO visible light communications", *J. of Lightwave Technol.*, vol. 36, no. 10, pp. 1944–1951, 2018 (doi: 10.1109/JLT.2018.2796503).

[2] A. K. Gupta and A. Chockalingam, "Performance of MIMO modulation schemes with imaging receivers in visible light communication", *J. of Lightwave Technol.*, vol. 36, no. 10, pp. 1912–1927, 2018 (doi: 10.1109/JLT.2018.2795698).

[3] V. T. B. Tram and M. Yoo, "Vehicle-to-vehicle distance estimation using a low-resolution camera based on visible light communications", *IEEE Access*, vol. 6, pp. 4521–4527, 2018 (doi: 10.1109/ACCESS.2018.2793306).

[4] A. Naz, H. M. Asif, T. Umer, and B. S. Kim, "PDOA based indoor positioning using visible light communication", in *IEEE Access*, vol. 6, pp. 7557–7564, 2018 (doi: 10.1109/ACCESS.2018.2796623).

[5] F. Miramirkhani and M. Uysal, "Visible light communication channel modeling for underwater environments with blocking and shadowing", *IEEE Access*, vol. 6, pp. 1082–1090, 2018 (doi: 10.1109/ACCESS.2017.2777883).

[6] T. H. Abd, S. A. Aljunid, H. A. Fadhil, R. A. Ahmed, and N. Saad, "Developpment of a new code family based on SAC-OCDMA system with large cardinality for OCDMA network", *Optic. Fiber Technol.*, vol. 17, no. 4, pp. 273–280, 2011 (doi: 10.1016/j.yofte.2011.04.002).

[7] A. Garadi A. and A. Djebbari, "New technique for construction of a zero cross correlation code", *Optik*, vol. 123, no. 15, pp. 1382–1384, 2012 (doi: 10.1016/j.ijleo.2011.08.017).

[8] L. Feng, J. Wang, R. Q. Qingyang, and L. Liu, "New design of optical zero correlation zone codes in quasi-synchronous VLC CDMA systems", *EURASIP J. on Wireless Communic. and Network.*, vol. 2015, no. 1, pp. 1–7, 2015 (doi: 10.1186/s13638-015-0360-z).

[9] M. Addad and A. Djebbari, "A ternary zero correlation zone sequence sets construction procedure", *Turkish J. of Electr. Engin. and Comp. Sciences*, vol. 25, no. 3, pp. 2455–2463, 2017 (doi: 10.3906/elk-1603-115).

[10] M. Addad and A. Djebbari, "Suitable Sequences for Asynchronous MC-CDMA Systems", *J. of Telecommun. and Inform. Technol.*, no. 3, pp. 9–13, 2018 (doi: 10.26636/jtit.2018.118217).

Mouad Addad received his M.Sc. degree in Telecommunications in 2013 from the University of Djillali Liabes In Sidi Bel Abbes, Algeria. He is currently pursuing his Ph.D. degree at the same university. His main research interests include sequences design for communication applications, signal processing, and wireless communication systems over multipath and fading channel.
E-mail: ad-mouad@hotmail.fr
Faculty of Electrical Engineering
Djillali Liabes University of Sidi Bel Abbes
Sidi Bel Abbès, Algeria

Ali Djebbari received his B.Sc. degree in 1988, from the University of Sciences and Technology of Oran (USTO, Algeria), M.Sc. degree in 1991, from the University of Sidi Bel Abbes, and the Ph.D. degree in 1997, from USTO. He works at the Department of Telecommunications at the University of Sidi Bel Abbes and does his research at the Telecommunications and Digital Signal Processing Laboratory. His research interests include signal processing for telecommunications, communication over multipath and fading channels, wireless networks, channel coding and optical communication networks.
E-mail: adjebari2002@yahoo.fr
Faculty of Electrical Engineering
Djillali Liabes University of Sidi Bel Abbes
Sidi Bel Abbès, Algeria

Paper

Suitable Spreading Sequences for Asynchronous MC-CDMA Systems

Mouad Addad and Ali Djebbari

Faculty of Electrical Engineering, Djillali Liabes University of Sidi Bel Abbes, Sidi Bel Abbès, Algeria

https://doi.org/10.26636/jtit.2018.118217

Abstract—In order to meet the demand of high data rate transmission with good quality maintained, the multi-carrier code division multiple access (MC-CDMA) technology is considered for the next generation wireless communication systems. However, their high crest factor (CF) is one of the major drawbacks of multi-carrier transmission systems. Thus, CF reduction is one of the most important research areas in MC-CDMA systems. In addition, asynchronous MC-CDMA suffers from the effect of multiple access interference (MAI), caused by all users active in the system. Degradation of the system's bit error rate (BER) caused by MAI must be taken into consideration as well. The aim of this paper is to provide a comparative study on the enhancement of performance of an MC-CDMA system. The spreading sequences used in CDMA play an important role in CF and interference reduction. Hence, spreading sequences should be selected to simultaneously ensure low CF and low BER values. Therefore, the effect that correlation properties of sequences exert on CF values is investigated in this study. Furthermore, a numerical BER evaluation, as a function of the signal-to-noise ratio (SNR) and the number of users, is provided. The results obtained indicate that a trade-off between the two criteria is necessary to ensure good performance. It was concluded that zero correlation zone (ZCZ) sequences are the most suitable spreading sequences as far as the satisfaction of the above criteria is concerned.

Keywords—BER, crest factor, multiple access interference, MC-CDMA, peak-to-average power ratio, zero-correlation zone.

1. Introduction

Multi-carrier (MC) is the predominant transmission technique in today's communication systems. In particular, the multi-carrier code division multiple access (MC-CDMA) transmission scheme combines orthogonal frequency division multiplexing (OFDM) and code division multiple access (CDMA). The main advantages of the combined system are: variable data rate, high spectral efficiency and robustness against frequency selective fading [1]–[7]. However, one major drawback of this technology is the large peak-to-average power ratio (PAPR). High PAPR reduces power efficiency and causes implementation-related issues [3]. Therefore, achieving very low PAPR values is of major importance. The unique structure of CDMA can be utilized by considering the signal design aspect. PAPR can be minimized through finding a suitable family of sequences [3], [4]. MC-CDMA encounters another problem, i.e. the multiple access interference (MAI). This type of interference occurs when system users are transmitting asynchronously, i.e. there is a timing misalignment among users, such as the uplink channel of cellular mobile systems. To mitigate MAI, several techniques were proposed recently [1], [5], [6]. However, these techniques only add to the complexity of MC-CDMA systems. In contrast, MAI interference could be eliminated through the design of a set of sequences with impulsive auto-correlation function (ACF) and zero cross-correlation functions (CCF) [6], [8]. Unfortunately, such ideal sequences are impossible to construct [8]. Instead, various sequences could be used: Walsh-Hadamard (WH), orthogonal Gold, orthogonal Golay complementary (OGC), and zero-correlation zone (ZCZ). Each sequence set has specific ACF and CCF properties. ZCZ sequences have been proposed and studied in [9]–[13].

The objective of this paper is to investigate the performance of ZCZ sequences based on two criteria: PAPR and bit error rate (BER) in an MC-CDMA system. In this study, we consider two MAI effects, i.e. inter-symbol interference (ISI) and inter-channel interference (ICI). Furthermore, we evaluate the performance of ZCZ sequences against conventional sequences. The sequence set with both a low crest factor and low BER performance is defined as optimal.

The remaining content of the paper is organized as follows. In Section 2 we give preliminaries to correlation functions, sequences generation, and the concept of an MC-CDMA system. In Section 3, the performance of ZCZ sequences in terms of both PAPR and BER is evaluated. Finally, concluding remarks on the optimal sequences are given in Section 4.

2. Preliminaries

First, the correction function are defined. A sequence of length N is denoted by $\mathbf{a}_N = [a_0, a_1, \ldots, a_n, \ldots, a_{N-1}]$. A set of M sequences $\{\mathbf{a}^1, \mathbf{a}^2, \ldots, \mathbf{a}^M\}$ is denoted by $\{\mathbf{a}^m\}_{m=1}^{M}$. The discrete periodic $R_{\mathbf{a}^x\mathbf{a}^y}(\tau)$ and aperiodic $\theta_{\mathbf{a}^x\mathbf{a}^y}(\tau)$ cross-correlation functions of a pair of sequences $\mathbf{a}^x$ and $\mathbf{a}^y$ are defined as [14]:

$$R_{\mathbf{a}^x\mathbf{a}^y}(\tau) = \sum_{n=0}^{N-1} a_n^x \left[a^y_{(n+\tau) \bmod N}\right]^*, \tag{1}$$

$$\theta_{\mathbf{a}^x\mathbf{a}^y}(\tau) = \sum_{n=0}^{N-1-\tau} a_n^x \left[a^y_{n+\tau}\right]^*, \tag{2}$$

where τ is the sequence shift variable and $[a_n]^*$ denotes the complex conjugate of sequence element a_n. The notation $(.) \bmod N$ denotes a modulo N operation. When $x = y$, CCF becomes ACF and will be denoted simply by $R_{\mathbf{a}^x}(\tau)$ and $\theta_{\mathbf{a}^x}(\tau)$.

Next, the ZCZ sequences are defined using binary construction methods. A set of binary sequences $\{\mathbf{a}^m\}_{m=1}^{M}$ that satisfy the following conditions is a ZCZ sequence set denoted by $ZCZ(N,M,Z_0)$, where Z_0 is the zeros zone length [8].

$$R_{\mathbf{a}^x,\mathbf{a}^y}(\tau) = \begin{cases} N & \tau = 0,\ x = y \\ 0 & \tau = 0,\ x \neq y \\ 0 & 0 < |\tau| \leq Z_0 \end{cases}, \tag{3}$$

where $\tau = 0$ means that CCF is computed at the in-phase. Among the flexible construction methods considered in this study are those proposed in [11]–[13].

WH sequence set is obtained directly from the Hadamard matrix. Any pair of sequences verifies the following property [15]:

$$R_{\mathbf{a}^x\mathbf{a}^y}(\tau) = \begin{cases} N & \tau = 0\ x = y \\ 0 & \tau = 0,\ x \neq y \end{cases}, \tag{4}$$

The orthogonal Gold sequences are generated from their corresponding Gold sequences [14] by appending $+1$ at the subset end [16].

OGC can be generated using the following recursive method [15]:

$$\mathbf{a}_{2N} = \begin{bmatrix} \mathbf{a}_N & \overline{\mathbf{a}}_N \\ \mathbf{a}_N & -\overline{\mathbf{a}}_N \end{bmatrix}, \tag{5}$$

where $\mathbf{a}_N$ is a square matrix of order N with complementary rows. Two binary sequences $(\mathbf{a}^x,\mathbf{a}^y)$ of length N are complementary if the sum of their aperiodic ACFs satisfies [14]:

$$\theta_{\mathbf{a}^x}(\tau) + \theta_{\mathbf{a}^y}(\tau) = \begin{cases} 2N & \tau = 0 \\ 0 & \tau \neq 0 \end{cases}. \tag{6}$$

The $\overline{\mathbf{a}}_N$ means that the right half columns of $\mathbf{a}_N$ are reversed.

In the MC-CDMA scheme of K users, the same information symbol $b_k(m)$ is spread over N carriers, each multiplied by a different element of the spreading sequence $\mathbf{c}_k = \{c_{k,n}\}_{n=1}^{N}$ assigned to user k. After spreading, the user bit is modulated onto successive subcarriers such that one information symbol is spread over several subcarriers. Binary phase-shift keying (BPSK) modulation is used. The MC-CDMA transmitter for user k is shown in Fig. 1.

The transmitted signal for user k is [16], [17]:

$$s_k(t) = \sqrt{\frac{2P}{N}} \sum_{m=-\infty}^{\infty} b_k(m) u_{T_b}(t - mT_b) \sum_{n=1}^{N} c_{k,n} \mathrm{e}^{\mathrm{j}(w_n t + \theta_k)}, \tag{7}$$

where P is the power of data bits, $u_{T_b}(t)$ is the rectangular pulse defined in $[0,T_b]$ with T_b denoting the bit duration, $w_n = \frac{2\pi n}{T_b}$ is the n-th subcarrier angular frequency, and the random phase θ_k is uniformly distributed over $[0,2\pi]$. The

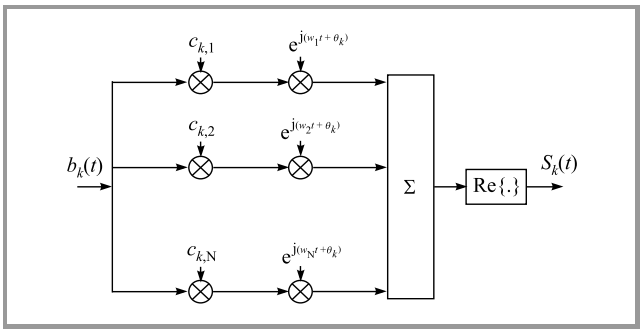

Fig. 1. MC-CDMA Transmitter for the k-th user.

neighboring subcarriers are orthogonal and separated by $\Delta w = \frac{2\pi}{T_b}$.

An asynchronous MC-CDMA system in the additive white Gaussian noise (AWGN) channel is considered. We restrict our analysis to line of sight conditions where the multipath replicas have insignificant power compared to the line of sight signal [18]. The received signal can be written as [16], [17]:

$$r(t) = \sqrt{\frac{2P}{N}} \sum_{k=1}^{K} \sum_{m=-\infty}^{\infty} b_k(m) u_{T_b}(t - mT_b - \tau_k) \times \sum_{n=1}^{N} c_{k,n} \mathrm{e}^{\mathrm{j}(w_n t + \varphi_{k,n})} + n(t), \tag{8}$$

where τ_k is the random time delay of user k uniformly distributed over bit duration $[0,T_b]$, $\varphi_{k,n} = \theta_k - w_n \tau_k$, and $n(t)$ is is a zero-mean bandpass white noise with equivalent low pass signal that has a power spectral density N_0. The MC-CDMA receiver for the i-th user is shown in Fig. 2.

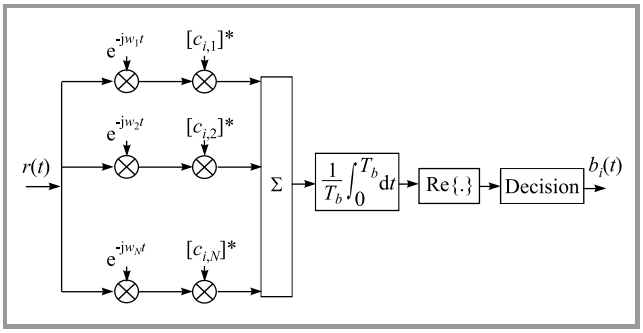

Fig. 2. MC-CDMA receiver for the i-th user.

We consider a coherent correlation receiver synchronized to the desired user i ($\tau_i = 0$). Time delays are quantized to integer multiple of the code element (chip) duration $T_c = \frac{T_b}{N}$. The decision variable of the 0th data bit of user i is given by [16]–[17]:

$$Z_{i,0} = \mathrm{Re}\left\{ \frac{1}{T_b} \int_0^{T_b} \sum_{n'=1}^{N} r(t) [c_{i,n'}]^* \mathrm{e}^{-\mathrm{j}w_{n'}t} \mathrm{d}t \right\} = D_i + n_i + MAI_i, \tag{9}$$

where D_i, n_i, MAI_i are the desired signal, the AWGN, and the multiple access interference terms, respectively. With-

out any loss of generality, we divide both sides of Eq. (9) by $\sqrt{\frac{2P}{N}}$.

The desired symbol $b_{i,0}$ is influenced by the corresponding $b_{k,0}$ and previous symbols $b_{k,-1}$ of each interferer k, thus the interference between users at the access point or multiple access interference MAI_i term is given by [17]:

$$MAI_i = \mathrm{Re}\left\{ \frac{1}{T_b} \sum_{n'=1}^{N} [c_{i,n'}]^* \sum_{\substack{k=1 \\ k\neq i}}^{K} \sum_{n=1}^{N} c_{k,n} \left[b_{k,-1} \times \int_0^{\tau_k} \mathrm{e}^{\mathrm{j}([w_n - w_{n'}]t + \varphi_{k,n})} \mathrm{d}t + b_{k,0} \int_{\tau_k}^{T_b} \mathrm{e}^{\mathrm{j}([w_n - w_{n'}]t + \varphi_{k,n})} \mathrm{d}t \right] \right\}. \quad (10)$$

Or, in a compact form:

$$MAI_i = \sum_{\substack{k=1 \\ k\neq i}}^{K} MAI_{i,k} = \sum_{\substack{k=1 \\ k\neq i}}^{K} ISI_{i,k} + ICI_{i,k}. \quad (11)$$

We can distinguish two cases: $n = n'$ and $n \neq n'$. In the first case, interference from the same subcarriers of user k is called inter-symbol interference (ISI). If $n \neq n'$, interference from other subcarriers of user k is called inter-channel interference (ICI).

$$ISI_{i,k} = \mathrm{Re}\left\{ \frac{1}{T_b} \sum_{n=1}^{N} [c_{i,n}]^* c_{k,n} \left[b_{k,-1}\tau_k + b_{k,0}(T_b - \tau_k) \right] \mathrm{e}^{\mathrm{j}\varphi_{k,n}} \right\}, \quad (12)$$

$$ICI_{i,k} = \mathrm{Re}\left\{ \frac{2}{T_b} \sum_{n'=1}^{N} \sum_{\substack{n=1 \\ n\neq n'}}^{N} [c_{i,n'}]^* c_{k,n} \frac{b_{k,-1} - b_{k,0}}{w_n - w_{n'}} \times \left[e^{\mathrm{j}\left(\frac{[w_n - w_{n'}]\tau_k}{2} + \varphi_{k,n}\right)} \sin \frac{[w_n - w_{n'}]\tau_k}{2} \right] \right\}. \quad (13)$$

It is worth noting that for a synchronous transmission ($\tau_k = 0, \forall k$), ICI does not exist and the ISI reduces to:

$$ISI_{i,k} = \mathrm{Re}\left\{ b_{k,0} \mathrm{e}^{\mathrm{j}\theta_k} \sum_{n=1}^{N} [c_{i,n}]^* c_{k,n} \right\}. \quad (14)$$

Thus, we can conclude that the offset (time delays) between users generates ICI and degrades BER performance, as shown in [17]. In a synchronous case, ISI can be eliminated using a set of orthogonal sequences.

Since we considered an AWGN channel, the decision variable can be regarded as a Gaussian random variable [17]. The BER of user i, conditioned on $\{\tau_k\}, \{\theta_k\}, \{b_{k,-1}\}$, and $\{b_{k,0}\}$, is [17]:

$$P_{e,i/\tau_k,\theta_k,b_{k,-1},b_{k,0}(k\neq i)} = \frac{1}{2}\mathrm{erfc}\left[\sqrt{\frac{E_b}{N_0}} \left(1 + \frac{MAI_i}{N} \right) \right], \quad (15)$$

where $\frac{E_b}{N_0}$ is defined as SNR. To obtain the unconditional BER for user i, we average $P_{e,i/\tau_k,\theta_k,b_{k,-1},b_{k,0}(k\neq i)}$ over all variables via Monte Carlo integration. A more appropriate performance measure is the averaged BER over all users [17]:

$$P_e = \frac{1}{K} \sum_{i=1}^{K} P_{e,i}. \quad (16)$$

Note that the results obtained for an asynchronous transmission using the Gaussian model do agree with system simulations for a relatively large number of users [19].

Another important criterion for the selection of spreading sequences for MC-CDMA is PAPR. The PAPR parameter of a signal is defined as the ratio of peak to average signal power. In this study, we consider crest factor (CF) as a measure of signal envelope compactness, its relation to PAPR is [16]:

$$CF = \sqrt{PAPR}. \quad (17)$$

The CF of an MC-CDMA signal must satisfy the following inequality [16]:

$$\mathrm{CF} \leq \frac{\max|S(f)|}{\sqrt{\frac{E}{2}}}, \quad (18)$$

where $S(f)$ is the Fourier transform of the spreading sequences and E is the energy of the same sequence. The Fourier transform of the spreading sequence can be calculated by applying the well-known auto-correlation theorem, given by [16]:

$$|S(f)|^2 = \sum_{\tau=-(N-1)}^{N-1} \theta_{\mathbf{a}^x}(\tau) \mathrm{e}^{-\mathrm{j}2\pi\tau f}. \quad (19)$$

3. Numerical Analysis

In this section, the conventional sequences in CDMA systems and ZCZ sequences are analyzed in terms of CF and BER. First, we evaluate the CF values of various sequences and then simulate their performance in an asynchronous MC-CDMA environment.

3.1. CF Analysis

The evaluation procedure of CF values is performed as follows. First, sequence sets each of lengths $N = 8$, 16, 32, 64, and 128, were generated. Second, the CF is computed for each sequence in the set and all values are averaged. Figure 3 illustrates CF performance of various sequences. Note that as the sequence's length increases, CF increases as well, except for OGC for $N \geq 32$ and ZCZ in [12] for $N \geq 64$ where it remains constant. In addition to their low CF levels, OGC and ZCZ in [12] also have a steady CF, which constitutes a major advantage in MC-CDMA systems. Note also that only OGC and ZCZ sequences remain under CF value of 3 for all lengths. The second-best sequences are those in [11] and the well known orthogonal Gold. The CF level for these codes is relatively low and slowly increases with the increase of sequence's length N. WH sequences have, by far, the highest values of CF.

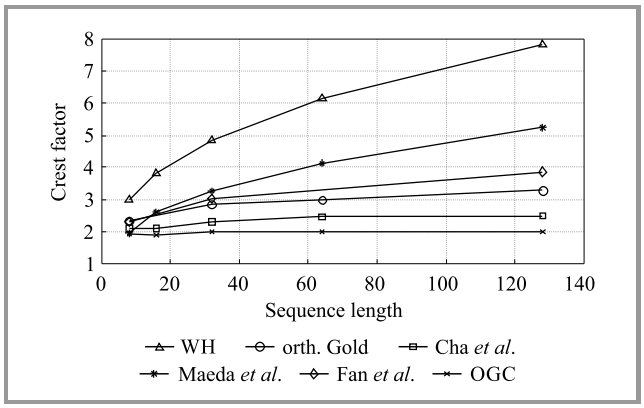

Fig. 3. Average CF of sequences for various lengths.

3.2. BER Analysis

This section focuses on interference related issues in asynchronous MC CDMA systems. The performance of an MC-CDMA system using various spreading codes in the presence of MAI in an AWGN channel is simulated using Matlab. We have considered an asynchronous MC-CDMA system, where a number of mobile users transmit their signal to a common receiver such as the uplink cellular system. First, the effect of the sequence length on BER performance of 4 users was analyzed and plotted in Fig. 4. For simulation, orthogonal Gold sequences were used with lengths 7, 31, and 63. As it can be seen in Fig. 4, the BER performance improves with the increase of the sequence length. To obtain a BER of 10^{-4}, MC-CDMA using sequences of length $N = 63$ requires 2 dB less SNR than sequence of length $N = 31$.

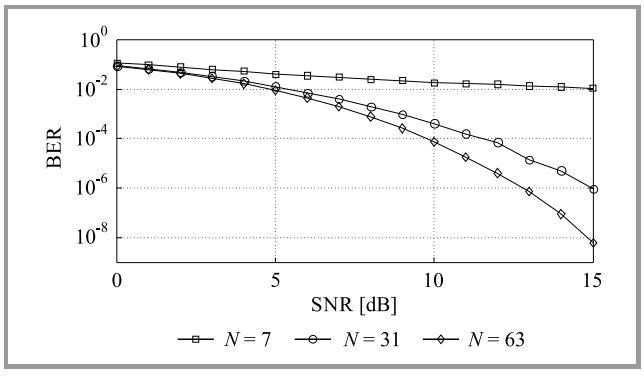

Fig. 4. BER versus SNR at different lengths of orthogonal Gold spreading sequence.

The effect of the number of active users on BER performance is analyzed next. Figure 5 shows BER performance of MC-CDMA versus the number of users at different values of SNR $= 5, 10$, and 15. For simulation, orthogonal Gold sequences were used ($N = 31$). As anticipated, a high number of active users causes degradation in BER performance. This is because admitting more users to the system results in higher level of interference (MAI).

We conclude this section with a comparative study of various spreading sequences. In this simulation, the number

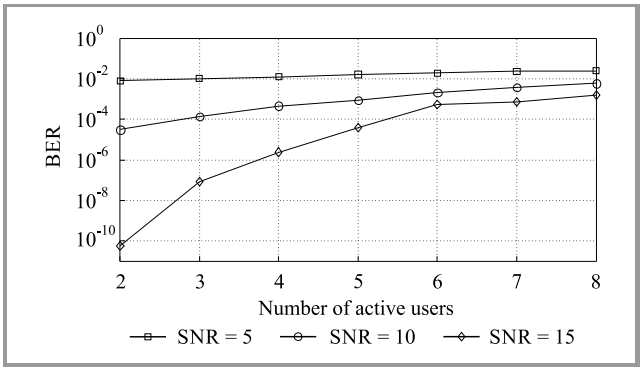

Fig. 5. BER versus number of active users for orthogonal Gold sequence at different SNR values.

of users is $K = 8$, the sequence length is $N = 32$ for WH, ZCZ and OGC sequences and $N = 31$ for orthogonal Gold sequences, and the bit rate is taken as 100 Mbps. For SNR ≥ 20 dB, BER remains constant and is equal to $5 \cdot 10^{-3}$ for WH and OGC sequences, $2 \cdot 10^{-3}$ for ZCZ sequences and $7.5 \cdot 10^{-4}$ for orthogonal Gold sequences. From the results obtained, it is observable that Gold outperforms WH and OGC sequences by a factor of 6.6 and ZCZ by a factor of 2.6.

3.3. Discussion

According to the BER criterion, the best results are obtained when orthogonal Gold sequences are used for

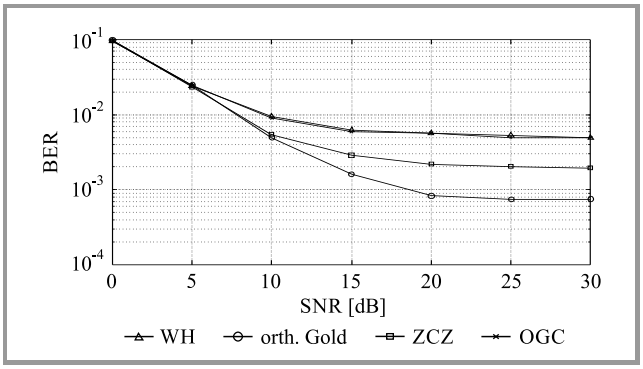

Fig. 6. BER versus SNR curves of various spreading sequences.

spreading (Fig. 6). In addition, BER performance of the system also improves with the increase of the spreading sequence length (Fig. 4). However, MC-CDMA systems using orthogonal Gold sequences suffer from considerably

Table 1
System parameters

Sequences	CF	BER
ZCZ	Low	Low
WH	Highest	Highest
Orthogonal Gold	High	Lowest
OGC	Lowest	High

high values of CF, which leads to signal distortion (Fig. 3). Moreover, increasing the sequence length would lead to even higher values of CF in the case of orthogonal Gold sequences (Fig. 3). Thus, a trade-off must be established between low BER and low CF. From the simulation results, it can be observed that ZCZ sequences have both low BER and low CF (see Table 1). Therefore, we conclude that ZCZ sequences are the suitable candidate for asynchronous MC-CDMA systems.

4. Conclusion

This work was carried out to enhance the performance of an MC-CDMA system through the proper choice of the spreading sequences. The performance of CDMA-based wireless systems is mainly governed by the characteristics of the spreading sequences i.e. their length and correlation properties. In this paper, CF performance of ZCZ, WH, orthogonal Gold, and OGC sequences was analyzed and compared. In addition, BER performance of an asynchronous MC-CDMA system in the AWGN channel was evaluated as well. With the use of an efficient spreading sequence, the system enjoys low CF and BER levels. Based on the results obtained for different sequences, it is observed that BER performance of the system degrades with an increase of the number of users and improves with an increase the spreading sequence length. The system with ZCZ sequences shows good performance in terms of both CF and BER. We conclude that ZCZ sequences have the best trade-off possible and therefore are the suitable candidate for asynchronous MC-CDMA systems.

References

[1] K. S. Vishvaksenan and P. T. Vasanth Raj, "Coded downlink multiuser MC-CDMA system using transmitter pre-processing: Performance results", *IEEE Access*, vol. 4, pp. 4534–4542 (doi: 10.1109/ACCESS.2016.2596774).

[2] J. O. M. Amok and N. M. Saad, "Error rate performance analysis of multiantenna MC DS-CDMA system over μ–μ frequency selective fading channels with arbitrary parameters", *Int. J. of Electron. Commun.*, vol. 70, no. 5, pp. 517–529, 2015 (doi: 10.1016/j.aeue.2015.11.007).

[3] W.-J. Huang, W.-W. Hu, C.-P. Li, and J.-C. Chen, "Novel metric-based PAPR reduction schemes for MC-CDMA systems", *IEEE Transact. on Vehic. Technol.*, vol. 64, no. 9, pp. 3982-3989, 2015 (doi: 10.1109/TVT.2014.2361353).

[4] H.-H. Chang, S.-C. Lin, and C.-D. Lee, "A CDMA scheme based on perfect Gaussian integer sequences", *Int. J. of Electron. Commun.*, vol. 75, pp. 70-81, 2017 (doi: 10.1016/j.aeue.2017.03.008).

[5] R. AliHemmati, P. Azmi, and F. Marvasti, "Joint multi-user interference and clipping noise cancellation in uplink MC-CDMA system", *Int. J. of Electron. Commun.*, vol. 64, no. 5, pp. 425–432, 2010 (doi: 10.1016/j.aeue.2009.02.006).

[6] D. Judson and A. Albert, "Performance of multicarrier complementary-coded CDMA under frequency-selective Nakagami-*m* fading channels", *EURASIP J. of Wireless Commun. and Network.*, vol. 67, pp. 1–9, 2016 (doi: 10.1186/s13638-016-0563-y).

[7] A. B. Djebbar, A. Djebbari, M. Bouziani, and J. M. Rouvaen, "Derivation of new expressions of bit error rate for MC-CDMA system in Nakagami fading channel", *Int. J, of Electron. Commun.*, vol. 57, no. 6, pp. 395–402, 2003 (doi: 10.1078/1434-8411-54100191).

[8] P. Fan, "Spreading sequence design and theoretical limits for quasi-synchronous CDMA", *EURASIP J. of Wireless Commun. and Network.*, vol. 2004, no. 1, pp. 19–31, 2014 (doi: 10.1155/S1687147204405015).

[9] M. Addad and A. Djebbari, "A ternary zero correlation zone sequence sets construction procedure", *Turkish J. of Electr. Engin. Comp. Sciences*, vol. 25, no. 3, 2016 (doi: 10.3906/elk-1603-115).

[10] Z. Zhang, L. Ge, F. Zeng, and G. Xuan, "Zero correlation zone sequence set with inter-group orthogonal and inter-subgroup complementary properties", *Adv. in Math. of Commun.*, vol. 9, no. 1, pp. 9–21, 2015 (doi: 10.3934/amc.2015.9.9).

[11] P. Fan, N. Suehiro, N. Kuroyanagi, and X. Deng, "Class of binary sequences with zero correlation zone", *Electron. Let.*, vol. 35, no. 10, pp. 777–779, 1999 (doi: 10.1049/el:19990567).

[12] J. Cha, S. Kameda, M. Yokoyama, H. Nakase, K. Masu, and K. Tsubouchi, "New binary sequences with zero-correlation duration for approximately synchronised CDMA", *Electron. Let.*, vol. 36, no. 11, pp. 991–993, 2000 (doi: 10.1049/el:20000703).

[13] T. Maeda, S. Kanemoto, and T. Hayashi, "A novel class of binary zero-correlation zone sequence set", in *Proc. 2010 IEEE Region 10 Conf. TENCON 2010*, Fukuoka, Japan, 2010, pp. 708–711 (doi: 10.1109/TENCON.2010.5686619).

[14] P. Fan and M. Darnell, *Sequence Design for Communications Applications*, 1st ed. Baldock, UK: Research Studies Press, Electronic & Electrical Engineering Research Studies. Communications Systems, Techniques, and Applications Series, 1, 1996 (ISBN: 978-0863802010).

[15] H. Ochiai and H. Imai, "OFDM CDMA with peak power reduction based on the spreading sequences", in *Proc. 1998 IEEE int. Conf on Commun. (ICC'98)*, Atlanta, GA, USA, 1998, pp. 1299–1303 (doi: 10.1109/ICC.1998.683035).

[16] B. M. Povovic, "Spreading sequences for multicarrier CDMA systems", *IEEE Transact. on Commun.*, vol. 47, no. 6, pp. 918–926, 1999 (doi: 10.1109/26.771348).

[17] Q. Shi and M. Latva-aho, "Spreading sequences for asynchronous MC-CDMA revisited: Accurate bit error rate analysis", *IEEE Transact. on Commun.*, vol. 51, no. 1, pp. 8-11, 2003 (doi: 10.1109/TCOMM.2002.807631).

[18] D. Boudreau *et al.*, "Wide-band CDMA for the UMTS/IMT-2000 satellite component", *IEEE Transact. on Vehic. Technol.*, vol. 51, no. 2, pp. 306–331, 2002 (doi: 10.1109/25.994808).

[19] Q. Shi and M. Latva-aho, "Performance analysis of MC-CDMA in Rayleigh fading channels with correlated envelopes and phases", *IEE Proc. – Commun.*, vol. 150, no. 3, pp. 214–220 (doi: 10.1049/ip-com:20030177).

Mouad Addad, **Ali Djebbari** – for biographies, see this issue, p. 8.

Paper

Interleaving Technique Implementation to Reduce PAPR of OFDM Signal in Presence of Nonlinear Amplification with Memory Effects

Younes Aimer[1,2], Boubakar Seddik Bouazza[1], Smail Bachir[2], and Claude Duvanaud[2]

[1] *Laboratory Technology of Communication, Faculty of Technology, University of Saida, Saida, Algeria*
[2] *XLIM Laboratory UMR-CNRS 7252, Institute of Technology of Angoulême, University of Poitiers, Angoulême, France*

https://doi.org/10.26636/jtit.2018.123517

Abstract—In OFDM systems, peak-to-average power ratio (PAPR) reduction of the signal is one of the main challenges that need to be overcome in order to use the transmitter in an efficient manner. As one of attractive techniques, interleaving can be used in PAPR reduction for multicarrier signals without spectrum distortion. In this paper, the authors propose to extend the possibilities of interleaving to improve PAPR reduction, to use a new coding of interleaver keys at the transmitter and a robust decoding procedure at the receiver. In order not to degrade the data rate, the use of null subcarriers to transmit side information to the receiver is proposed and evaluated.

Simulation results in the context of the WLAN 802.11a standard in the presence of a nonlinear power amplifier model with memory, show a reduction of PAPR of approximately 5.2 dB, and an improvement of bit error rate and error vector magnitude of about 2 decades and 4% respectively, while respecting the spectral mask specification.

Keywords—downward compatibility, interleaving technique, interleaver key, OFDM systems, PAPR reduction.

1. Introduction

The next generations of wireless communication systems have to satisfy the customers' requirements in terms of quality and quantity of information. Because of its high spectral efficiency, robustness against interferences and frequency selective fading [1], as well as low complexity and implementation flexibility, Orthogonal Frequency Division Multiplexing (OFDM) has become the most common technique. For these reasons, OFDM is widely adopted as a physical layer (PHY) technology in recent wireless communication standards, such as Digital Audio/Video Broadcasting (DAB/DVB), Wireless Local Area Networks (WLAN), Wireless Metropolitan/Personal Area Networks (WMAN/WPAN), and WiMAX. OFDM is also included in the fifth generation (5G) cellular networks to support a high data transmission rate and to meet the required level of quality of service (QoS).

However, the major drawback of this technique is its high envelope fluctuation of the transmitted signal defined by the PAPR value [2]. Such a signal with high instantaneous values is degraded by the nonlinear characteristics of radio-frequency (RF) circuits, mainly the RF power amplifier (PA) [3]. To limit degradation, a back-off of the level is used, leading to the use of the PA with low power efficiency. Such a solution is costly, because it sacrifices the transmitter performance.

The objective of PAPR reduction methods is to limit these fluctuations to operate near the PA saturation region (high efficiency area), while maintaining the original data-rate and respecting such communication criteria as BER, EVM, downward compatibility[1] and spectrum occupancy specifications.

PAPR reduction in OFDM systems has been a subject of intense research, based on which various techniques have been proposed in the literature. Among them, we can mention methods like clipping, clipping and filtering [4]– [6], active constellation extension (ACE) [7], [8], tone reservation (TR) [6], [9], [10], selected mapping (SLM) [11], [12], switching [13], coding methods [14] and partial transmit sequence (PTS) [8], [15], [16].

The authors in [17] proposed a PAPR reduction technique based on frequency interleaving of mapped symbols and the selection of the one that presents the lowest PAPR. However, the problem of the side information (SI) transmission is not addressed and only the principle of PAPR reduction is presented. In [18], a proposal to send SI on the chosen interleaver via pilots is made. This has the advantage of not affecting the data rate, but it influences the equalization and channel estimation at the receiver.

In this paper, we propose to use interleaving for PAPR reduction in WLAN 802.11a (Fig. 1) and to use null subcarriers (NS) available in the Wi-Fi-OFDM standard to transmit interleaver key-codes. The newly proposed technique

[1]Downward compatibility: additional signal processing at the transmitter do not need change at the receiver.

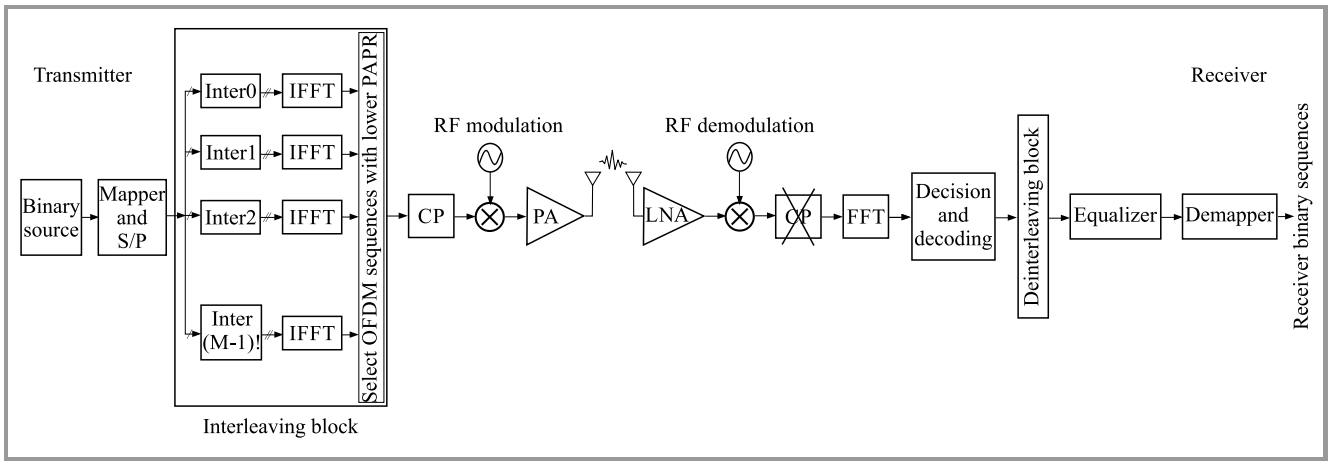

Fig. 1. Digital communication system with PAPR reduction based on frequency interleaving method.

provides a realistic solution by taking into account nonlinearity of RF-PA, without the need to transmit SI and respecting downward compatibility. The main idea is to test several interleaving possibilities, select the most efficient one and transmit its key-code on the minimum number of NS. A critical point of the proposed method is to ensure a correct transmission of the key-code despite degradation introduced by the transmission channel To ensure the quality level required, we propose a proper decoding process.

The proposed interleaving method is evaluated for WLAN 802.11a, in the presence of a PA model estimated from the measurements of a commercial PA, class AB with memory. Also, the key-code decoding process is evaluated and presents a low complexity and a high probability of error immunization against the AWGN channel. An effective scheme is proposed here, which constructs a favorable OFDM transmit signal with reduced PAPR.

Notation: Throughout this paper, small letters for vectors and matrices in the time-domain and capital letters for vectors and matrices in the frequency-domain are used.

2. OFDM System

2.1. Problem Position

In discrete time, the transmitted OFDM signals x_n are obtained by taking Inverse Fast Fourier Transform (IFFT):

$$x_n = \frac{1}{\sqrt{N}} \sum_{k=0}^{N-1} X_k \, \mathrm{e}^{\frac{\mathrm{j}2\pi nk}{N}}, \quad 0 \le n \le N-1, \tag{1}$$

where X_k, $k = 0,1,\ldots,N-1$ are input mapped symbols, usually modulated by a Quadrature Amplitude Modulation (QAM), and k is the discrete-time index.

It is known that OFDM modulation is a particular case of multi-carrier transmission, where a single data stream is transmitted over a number of lower rate orthogonal subcarriers with the advantage of its high spectral distribution and efficiency, high data rate, robustness to multi-path channel and easier implementation. However, as shown in Eq. (1), the resulting signal is the superposition of N independent narrow-band channels that can generate constructive and/or destructive sums, and consequently, high envelope fluctuations. These high instantaneous peaks limit the nonlinear RF-PA to operate at a lower average power efficiency, known as linear region, leading to a degradation of the transmitter efficiency. Improvement of power efficiency requires a reduction in fluctuations to maintain a higher average power without signal degradation. PAPR value quantifies this problem and defines the ratio between the maximum instantaneous power and average power for each OFDM symbol:

$$\begin{aligned} PAPR_{\mathrm{dB}} &= 10 \cdot \log \frac{P_{peak}}{P_{average}} \\ P_{peak} &= 10 \cdot \log \frac{\max\limits_{0 \le n \le N-1} |x_n|^2}{\mathbb{E}|x_n|^2} \end{aligned}, \tag{2}$$

where P_{peak} represents the peak output power, $P_{average}$ means the average output power, $\mathbb{E}[\cdot]$ denotes the expected value operation and x the vector of OFDM samples in time-domain such as $\mathbf{x} = [x_0, x_1, \ldots, x_{(N-1)}]^T$.

The complementary cumulative distribution function (CCDF) of PAPR is one of the most frequently used performance evaluation method for PAPR reduction techniques. It denotes the probability that PAPR of a data block exceeds a given threshold and is expressed as:

$$CCDF = \mathbb{P}[PAPR > PAPR_0], \tag{3}$$

where $\mathbb{P}[\cdot]$ is the probability function.

3. Interleaving Method

Interleaving is among the most commonly used techniques in digital communication systems, for its important benefits related to preventing the grouping of errors. Because coding is not capable of correcting a burst of errors, interleaving is used and consists in transforming these bursts

into isolated errors, which makes their correction easier. The principle of interleaving is based on a simple breakdown of mapped symbols into more code words, before their transmission over the ODFM modulator. Thus, we define the number of code words M (also called the depth of the interleaver) and the number of symbols per code word, called the word-length, and the denoted K. Figure 2 shows an example of an interleaver with $N = 16$ subcarriers per OFDM symbol, $M = 4$ code words and $K = 4$ word-length. The mapped symbols are spread in a series over a matrix of 4×4 and sent-out in parallel, i.e. column-by-column, to the OFDM modulator. Note that we choose $N = 16$ subcarriers to facilitate comprehension of the interleaving method.

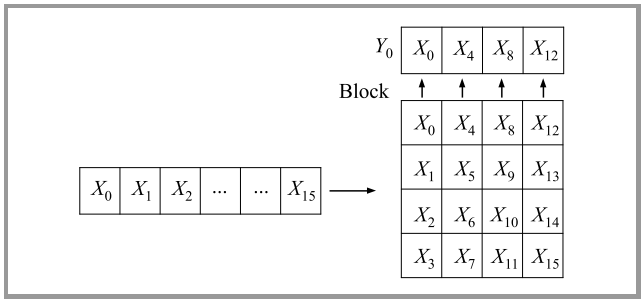

Fig. 2. Illustration of interleaving ($N = 16$, $M = K = 4$).

Let us define the vector of modulated symbols such as:

$$\mathbf{X}^{1\times N} = [X_0\, X_1\, \cdots\, X_{N-1}]\,. \tag{4}$$

To split this vector into M code words, denoted as Y_f, we use the modulus function. If we denote the remainder after division of the code word position f by M as s_f, the code word Y_f contains a group of mapped symbols which have the same remainder. We can describe the mathematical expression of the f-th codeword as follows:

$$\mathbf{Y}_f^{K\times 1} = \left[X_{M\cdot 0+s_f}\; X_{M\cdot 1+s_f}\; \cdots\; X_{M\cdot(K-1)+s_f}\right]^T. \tag{5}$$

At the receiver, there is no additional complexity to the system and only the inverse process is performed with the deinterleaver.

3.1. Interleaving for PAPR Reduction

The design of the interleaving method presented above is one of these proposed in the literature as a solution for reducing the risk of deformations of successive symbols in the same code word. In practice, only one kind of interleaving is performed as a function of the channel characteristics and the used coding. For PAPR reduction, the idea is to apply several kinds of interleaving at the transmitter. After IFFT operation, the smallest PAPR among them is chosen to be transmitted (Fig. 1). The major advantage of this technique is it its low complexity compared to the block coding techniques [14] or the PTS method [15], [16]. However, its major drawback is the need for the transmission of information about the used interleaver to carry out its decoding at the receiver, which degrades the data rate. Also, to insure the best reduction of the PAPR, a large number of interleaving possibilities is used, which increases the key length of each interleaver and degrades the data rate. In this work, we propose to deal with reducing PAPR using all possibilities of interleaving without the loss of in data rate, by:

- coding inter-key[2] in within a minimum of length,
- transmitting used the inter-key via a minimum number of null subcarriers,
- and decoding the received inter-key with the use of a robust process.

3.2. Interleaving Method Used

In communication systems, adding redundancy in source coding and forward error correction (FEC) provides correlated data which influence the PAPR value. In [17], it is shown that the sequence of highly correlated binary data in multicarrier systems has a large PAPR. Thus, it is important to break down long correlation patterns to reduce high values of the complex envelope. In the proposed scheme (Fig. 3), we proposed to generate all $M!$ possibilities (where

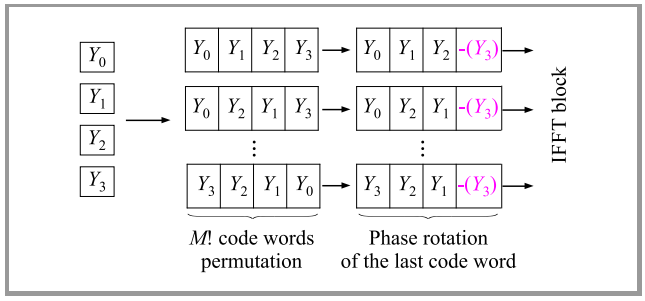

Fig. 3. Example of interleaving possibilities with $M = 4$ code words.

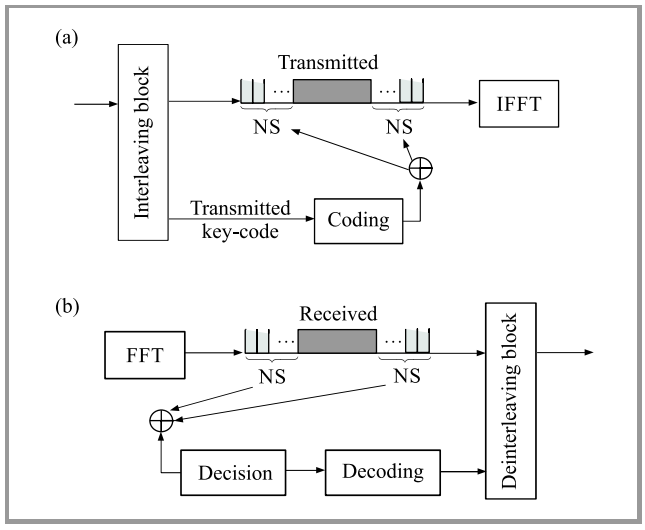

Fig. 4. Key-code on NS at the: (a) transmitter (b) receiver.

[2]inter-key: the code of the interleaver.

M is the number of code words) by permuting blocks in the new OFDM symbol and finally, reverse the last block. IFFT operation generates the time-domain signals and the sequence presenting the smallest PAPR is selected.
Each possibility of interleaving has its inter-key and the one chosen is transmitted to the receiver via null subcarriers (Fig. 4a). Here, the rank of the interleaver is coded in binary and mapped using quadrature amplitude modulation (QAM), by choosing the high-energy symbols of the constellation used.
Table 1 shows inter-keys in binary words of 6 bits and their equivalent in mapped symbols, where ± 1 and $\pm$j indicate their position within the chosen 4-QAM constellation.

Table 1
Interleaver keys

Interleaver	Binary code	4-QAM code
0	[0 0,0 0,0 0]	$[-1-1\text{j}, -1-1\text{j}, -1-1\text{j}]$
1	[0 0,0 0,0 1]	$[-1-1\text{j}, -1-1\text{j}, -1+1\text{j}]$
⋮	⋮	⋮
23	[0 1,0 1,1 1]	$[-1+1\text{j}, -1+1\text{j}, 1+1\text{j}]$

3.3. Inter-key Transmission via NS and Decoding Process

In communication standards, one OFDM symbol is used to transmit data, pilots and also some reserved subcarriers which are set to zero (called null subcarriers). For example, in a Wi-Fi system, the OFDM symbol is presented in Fig. 5. Here, we propose to use these subcarriers in the interleaving method, where the inter-key of the optimal interleaver is transmitted with some of them. As a reminder, null subcarriers are used to prevent adjacent channel interference (ACI). In [19], [20] and [21] it has been shown for DVB-T, WiMAX and WLAN standards, respectively, that it results in a slight broadening of the spectrum but remains inside the spectrum mask.

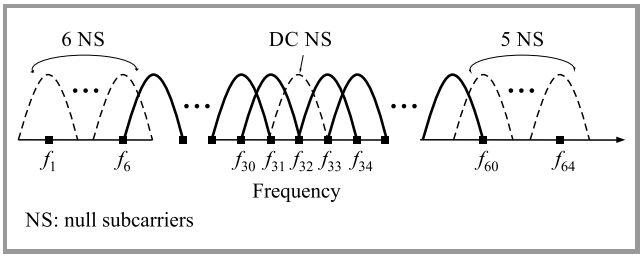

Fig. 5. OFDM symbol in WLAN 802.11a standard.

3.4. Inter-key Decoding Process

Unfortunately and as for data subcarriers, PA nonlinearities and channel noise may affect the inter-key subcarriers transmitted, which will adversely affect the decoding process at the receiver.
To reduce the risk of error, we define a decoding process based on the comparison of the received inter-key with all possibilities using the XOR gate on each QAM position. The one that renders the maximum number of zeros is selected (Fig. 4b). The proposed decoding process is invoked for each OFDM symbol with the following operations:
Variables:

$\mathbf{CK}_r^{M\times 1}$: received code-key,

$\mathbf{CK}^{M\times K}$: matrix of all code-keys used at the transmitter,

$\mathbf{CK}_c^{M\times 1}$: the correct code-key,

$\mathbf{R}^{M\times K}$: resulting XOR operation matrix.

Step 1: extract $\text{CK}_r^{M\times 1}$ from the received null-subcarriers and convert QAM symbols to binary.

Step 2: in k-th iteration, compare $\mathbf{CK}_r^{M\times 1}$ to each code-key row of matrix $\mathbf{CK}$ according to $\mathbf{R}[:,k] = \text{CK}_r \oplus \mathbf{CK}[:,k]$, where $\mathbf{R}[:,k]$ denotes the k-th row of matrix $\mathbf{R}^{M\times K}$ and operation $\oplus$ is the binary XOR gate.

Step 3: Repeat step 2 for the chosen number M of interleavers or stop when $\mathbf{R}[:,k]$ is a vector of zeros.

Step 4: $\mathbf{CK}_c$ corresponds to the line providing a maximum number of zeros.

Step 5: Select $\mathbf{CK}_c$ and deinterleave.

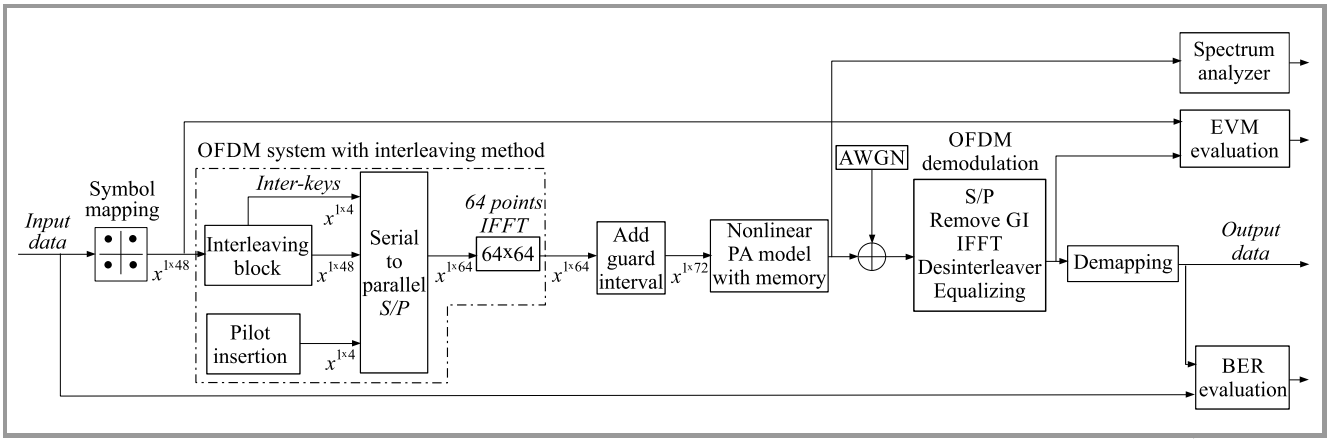

Fig. 6. Simulation block of Wi-Fi standard with interleaving method.

4. Simulation Results

The proposed method is evaluated using the Matlab Mathworks platform for the WLAN 802.11a standard presented in Fig. 6. It adopts OFDM technique for its uplink (UP) and downlink (DL), with a frequency band of 5 GHz, and support data rate up to 54 Mbps for an area coverage between user and transmitter of up to several meters.

Table 2
Simulation parameters

Parameter	Value
No. of sub-carriers	64 (48 data, 4 pilots and 12 NS)
Frequency band	5 GHz
Bandwidth	20 MHz
Modulation	16-QAM
No. of binary data	4608000 bits
No. of OFDM blocks	2000
Performance metrics	CCDF, BER, spectrum
Num. of interleavers:	
Case 1	$4! = 24$ possibilities coded on 3 NS
Case 2	$5! = 120$ possibilities coded on 4 NS

According to the parameters presented in Table 2, three contexts are studied:

- signals properties as a function of the number of interleaving possibilities,
- communication criteria (BER, EVM) using Gaussian channels,
- and frequency response in the presence of a nonlinear RF PA model.

Figure 7 presents a variation of the PAPR value as a function of the number of OFDM symbols for several interleaving possibilities (24 and 120 possibilities of interleaving). We can see that, increasing number of possibilities offers better performance in terms of PAPR reduction.

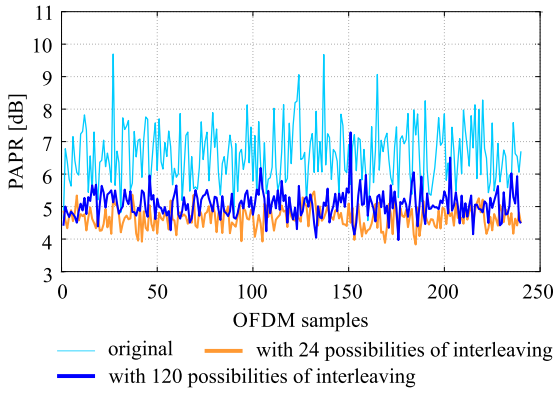

Fig. 7. PAPR in time-domain with and without interleaving. (For color pictures visit www.nit.eu/publications/journal-jtit)

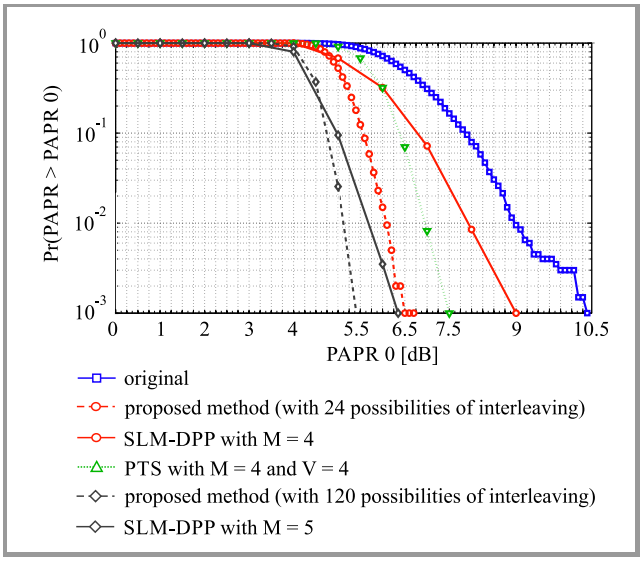

Fig. 8. Comparison of CCDF curves.

Figure 8 shows a comparison (in terms of CCDF) of the proposed method with the PTS method presented in [16] and the SLM-DPP method given in [17]. The results obtained confirm those shown in Fig. 7, i.e., PAPR can be further reduced when we increase the number of interleaving possibilities.

For the probability of 10^{-3}, it illustrates also a decrease in PAPR of up to 3.75 dB and 5.2 dB for 24 and 120 interleaving possibilities respectively, in comparison with the SLMDPP (for 4 and 5 blocks) and PTS method (for 4 blocks and 4 phases), which shows a reduction of 1.5 dB (SLMDPP for 4 blocks), 4 dB (SLM-DPP for 5 blocks) and 3 dB, respectively.

4.1. Nonlinear PA Model with Memory Effects

To validate the solution, we perform several simulations in the presence of a nonlinear RF PA model.

Table 3
Model parameters

	Values
$b_{0,1}$	$-3,1+\mathrm{j}2.93$
$b_{1,1}$	$-2,86\cdot10^{-1}+\mathrm{j}2.19\cdot10^{-1}$
$b_{0,3}$	$5.15\cdot10^{-2}-\mathrm{j}4.2\cdot10^{-2}$
$b_{1,3}$	$7.58\cdot10^{-3}-\mathrm{j}4.34\cdot10^{-3}$
$b_{0,5}$	$-3.49\cdot10^{-4}+\mathrm{j}2.75\cdot10^{-4}$
$b_{1,5}$	$-4.93\cdot10^{-5}+\mathrm{j}1.37\cdot10^{-5}$

We consider a model with memory of a commercial class AB power amplifier (SZP-2026Z from RF Micro Devices)

designed for WLAN 802.11 equipment, where its input to output relationship, in baseband format, is expressed as [21]:

$$y(t) = \sum_{i=0}^{m} \sum_{p=0}^{P} b_{i,2p+1} \cdot |u(t-i)|^{2p} \cdot u(t-i), \quad (6)$$

where P is the nonlinearity order and m the memory depth. For $P = 2$ and $m = 1$, parameters $b_{i,2p+1}$ are estimated using a multicarrier signal with a bandwidth of 20 MHz. Table 3 summarizes the model parameters.

In Fig. 9 we have plotted the AM/AM static characteristic presented by the output signal power depending on the input signal power, which describes the SZP-2026Z power amplifier. The 1 dB compression point corresponding to IBO= 0 dB, is achieved for input power equal to 20 dBm.

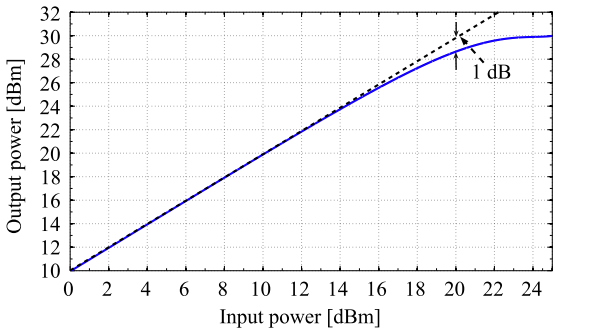

Fig. 9. AM/AM static characteristics of the SZP-2026Z amplifier.

To see the effect of the power amplifier used on the Wi-Fi-OFDM signal with application of the reduction method, we have plotted the AM/AM dynamic characteristic with and without the interleaving method (Fig. 10).

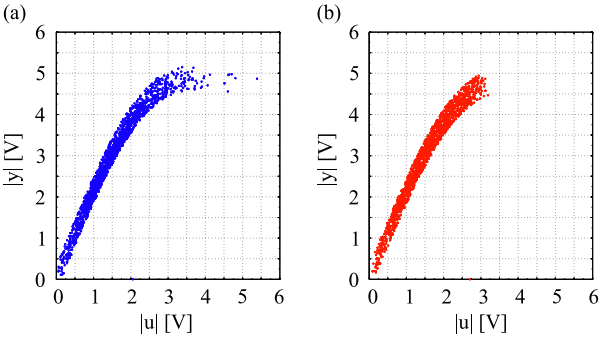

Fig. 10. AM/AM dynamic characteristics without (a) and with (b) interleaving method.

After comparison of the two figures, we note that the application of the interleaving method reduces the signal dynamic and then the nonlinear distortion generated by the amplifier.

To evaluate the proposed system we estimate its sensibility to channel noise in the presence of a power amplifier.

Figure 11 presents EVM of the received signal versus SNR for IBO= −2 dB, with and without interleaving (for 24 and 120 possibilities of interleaving) for a Gaussian channel and in the presence of a nonlinear power amplifier.

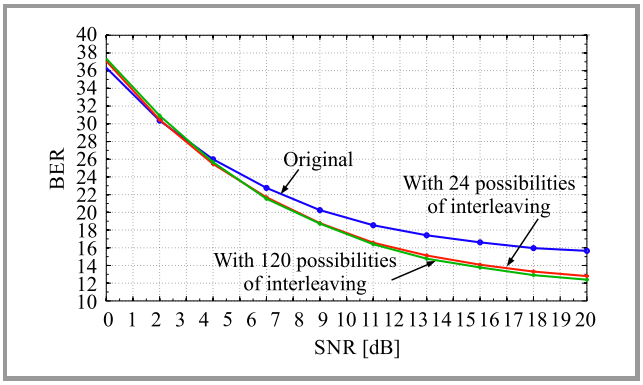

Fig. 11. EVM versus SNR for Gaussian channels (IBO= −2 dB).

From these results, one can observe that for a low SNR value (SNR< 6 dB), the curves with and without the interleaving method behave almost in the same manner. At this SNR level, the noise power to be added is important. Consequently, the impact of channel noise is preponderant compared to the nonlinearity of the amplifier, and that prevents improvement in EVM.

On the other hand, at higher SNR values (SNR> 12 dB), the impact of noise is negligible compared to the nonlinearity of the amplifier. In this case the interleaving method allows a good improvement in the EVM result.

In the same context, Fig. 12 presents BER results versus SNR for an IBO= −2 dB, where we can observe that the use of the proposed method offers an improvement in BER, with high SNR values (SNR> 12 dB).

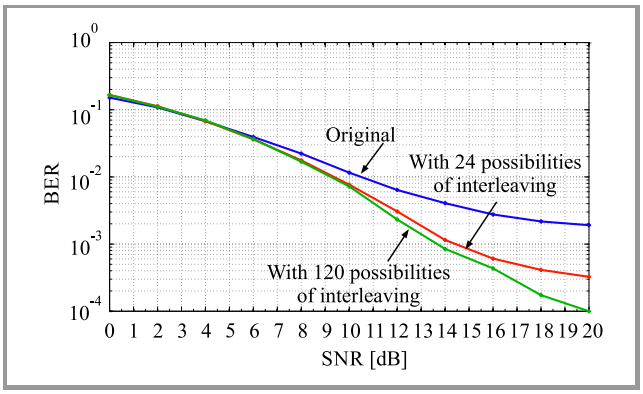

Fig. 12. BER versus SNR for Gaussian channels (IBO= −2 dB).

Figures 13 and 14 present the comparison of EVM and BER curves versus IBO, for SNR= 16 dB. These results confirm the suitability of the interleaving method proposed, as it allows for an improvement in EVM of about 2.5% and 3%, and in BER with a factor of one decade, one decade and a half for 24 and 120 possibilities of interleaving, respectively.

Based on the above and with the same transmission quality (identical EVM or identical BER), the interleaving method makes it possible to obtain a gain of 2 dB in IBO. In other words, by applying the interleaving method, the am-

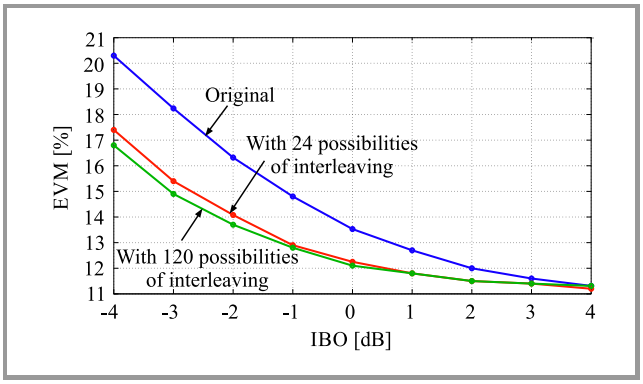

Fig. 13. EVM curves vs. IBO (SNR= 16 dB).

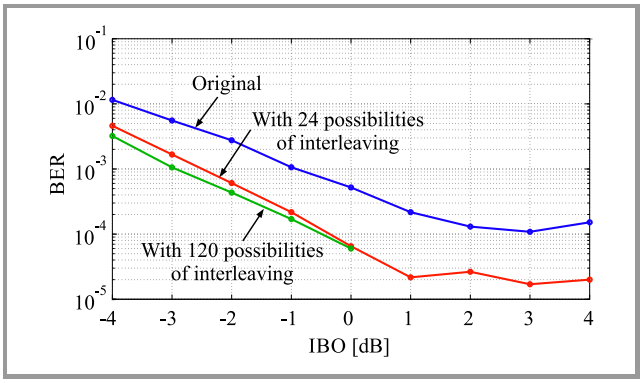

Fig. 14. BER curves vs. IBO (SNR= 16 dB).

plifier can be used with an increase of 2 dB of the input power level, and with a higher power efficiency compared to the scenario without the method being applied, for the same QoS.

Figure 15 shows a constellation, with (see Fig. 15a) and without the interleaving method (see Fig. 15b) at the amplifier output for an IBO equal to -2 dB. Application of the interleaving method makes it possible to reduce the dispersion on the constellation points.

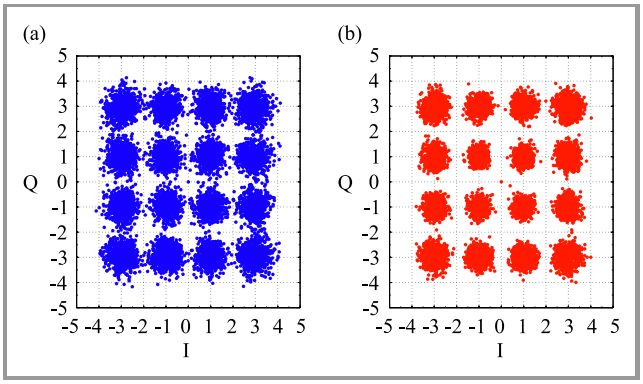

Fig. 15. Constellation at the amplifier output without (a), and with (b) the application of the interleaving method (IBO= -2 dB).

In Fig. 16 the impact of NS is shown for Wi-Fi-OFDM signal at an IBO= -2 dB, before and after application of the interleaving method (for 24 and 120 possibilities of interleaving).

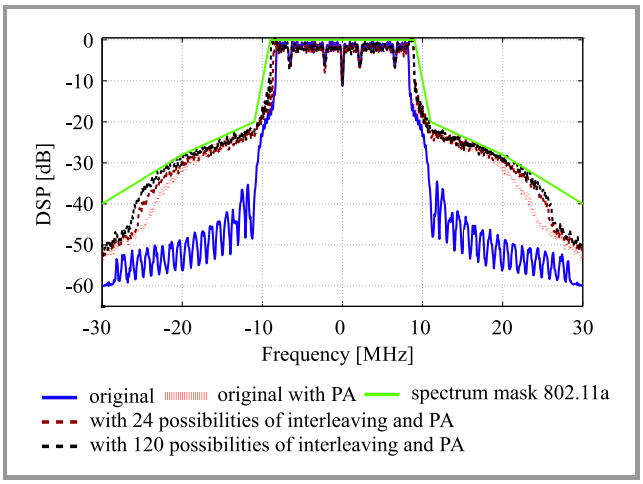

Fig. 16. Impact of nonlinear PA model with memory on frequency responses with and without interleaving (IB= -2 dB).

As expected, the use of null subcarriers affects the spectrum with a larger bandwidth and spurious component in the adjacent bands due to nonlinear effects. However, they will remain still under the mask specification of the standard used.

ACPR values are calculated after the amplifier for different IBO levels, with the lower and upper bandwidth of 25 MHz for each, with and without the interleaving method. The results are shown in Table 4. In terms of ACPR, they are very close, both without and with the interleaving method for 24 and 120 possibilities.

5. Conclusions

In this paper, an original implementation of the interleaving method is proposed for PAPR reduction and is evaluated in terms of its robustness, against a nonlinear PA and noisy channel. The principle is based on the selection of the interleaving possibility with the lowest PAPR. The main objective of the method is to avoid optimization processes, such as those applied in TR [21].

In practice, we proposed a coding process where the selected interleaver is coded with an inter-key. In order not to degrade the data rate, the interleaver is transmitted to the receiver via a minimum number of null subcarriers. Such a technique ensures downward compatibility and offers a PAPR improvement of about 5.2 dB over the original signal.

In order to find the correct interleaver at the receiver, despite the transmission errors, a practical decoding process has been presented. A nonlinear power amplifier with memory was inserted to evaluate the proposed method in terms of QoS and energy efficiency. From these results, we observed an improvement in EVM of about 3% and an improvement in BER by a factor of more than one decade.

So, for a given quality in terms of EVM or BER, the interleaving method enables to use the power amplifier at a higher IBO (-2 dB) rate, leading to greater power efficiency values.

Table 4
ACPR Results

	Adjacent Channel Power Ratio [dB]					
	Original		With 24 possibility		With 120 possibility	
	Lower	Upper	Lower	Upper	Lower	Upper
IBO= −4 dB	−22.13	−22.00	−21.83	−21.74	−21.78	−21.75
IBO= −2 dB	−25.09	−24.94	−24.88	−24.77	−24.26	−24.20
IBO= 0 dB	−28.39	−28.21	−28.12	−28.00	−27.25	−27.10
IBO= 2 dB	−31.53	−31.32	−31.03	−30.92	−30.00	−30.00
IBO= 4 dB	−34.04	−33.88	−33.22	−33.12	−32.00	−31.90

The power amplifier output spectrum demonstrates the possibilities offered in terms of performance improvement, while observing WLAN 802.11a specifications. The use of null subcarriers for transmitting SI is therefore not an obstacle to the generalization of the interleaving method and its application to next generation of wireless communication systems.

6. Acknowledgments

Research reported in this publication is supported by PHC-Tassili project of the Hubert Curien Partnership.

References

[1] M.-O. Pun, M. Morelli, and C.-C. J. Kuo, *Multi-carrier Techniques for Broadband Wireless Communications: A Signal Processing Perspective*, Communication and Signal Processing (Book 3). London: Imperial College Press, 2007 (ISBN: 978-1860949463).

[2] R. Prasad, *OFDM for Wireless Communications Systems*. Norwood, MA: Artech House, 2004 (ISBN: 978-1580537964).

[3] T. Jiang and Y. Wu, "An Overview: Peak-to-Average Power Ratio Reduction Techniques for OFDM Signals", *IEEE Transact. on Broadcast.*, vol. 54, no. 2, pp. 257–268, 2008 (doi: 10.1109/TBC.2008.915770).

[4] D. Guel and J. Palicot, "Clipping Formulated As an Adding Signal Technique for OFDM Peak Power Reduction", in *Proc. VTC Spring 2009 – IEEE 69th Vehicul. Technol. Conf.*, Barcelona, Catalonia, Spain, 2009, pp. 1–5 (doi: 10.1109/VETECS.2009.5073442).

[5] R. Saroj, "A Cooperative Additional Hybrid and Clipping technique for PAPR reduction in OFDM System", in *Proc. 2016 Fifth Int. Conf. on Eco-friendly Comput. and Commun. Sys. (ICECCS)*, Bhopal, Madhya Pradesh, India, 2016, pp. 53–57 (doi: 10.1109/Eco-friendly.2016.7893241).

[6] M. J. Azizipour and K. Mohamed-pour, "Clipping noise estimation in uniform tone reservation scenario using OMP algorithm", in *Proc. 2016 8th Int. Symp. on Telecommun. (IST)*, Teheran, IRI, 2016, pp. 500–505 (doi: 10.1109/ISTEL.2016.7881871).

[7] Z. Zheng and G. Li, "An Efficient FPGA Design and Performance Testing of the ACE Algorithm for PAPR Reduction in DVB-T2 Systems", *IEEE Transact. on Broadcast.*, vol. 63, no. 1, pp. 134–143, 2017 (doi: 10.1109/TBC.2016.2593401).

[8] R. Saroj, "Performance evaluation of hybrid ACE-PTS PAPR reduction techniques", in *Proc. 2016 11th Int. Conf. on Computer Engineer. Sys. (ICCES)*, Cairo, Egypt, 2016, pp. 407–413 (doi: 10.1109/ICCES.2016.7822039).

[9] J. Tellado-Mourelo, "Peak to Average Power Ratio Reduction for Multicarrier Modulation", *PhD thesis, Stanford University*, 1999.

[10] H. Sohtsinda, S. Bachir, C. Perrine, and C. Duvanaud, "An evaluation of hybrid tone reservation method for PAPR reduction using power amplifier with memory effects", *IEEE Int. Conf. on Electron., Circuits and Sys. (ICECS)*, Monte Carlo, 2016, pp. 676–679 (doi: 10.1109/ICECS.2016.7841292).

[11] R. W. Bauml, R. G. H. Fischer, and J. B. Huber, "Reducing the peak-to-average power ratio of multicarrier modulation by selected mapping", *Electron. Let.*, vol. 32, no. 22, pp. 2056–2057, 1996 (doi: 10.1049/el:19961384).

[12] J. Ji, G. Ren, and H. Zhang, "A Semi-Blind SLM Scheme for PAPR Reduction in OFDM Systems With Low-Complexity Transceiver", *IEEE Transact. on Vehicul. Technol.*, vol. 64, no. 6, pp. 2698–2703, 2015 (doi: 10.1109/TVT.2014.2345262).

[13] M. S. Hossain and T. Shimamura, "Low-complexity null subcarrier-assisted OFDM PAPR reduction with improved BER", *IEEE Commun. Let.*, vol. 20, no. 11, pp. 2249–2252, 2016 (doi: 10.1109/LCOMM.2016.2598801).

[14] A. E. Jones, T. A. Wilkinson, and S. K. Barton, "Block coding scheme for reduction of peak to mean envelope power ratio of multicarrier transmission schemes", *Electron. Let.*, vol. 30, no. 25, pp. 2098–2099, 1994, (doi: 10.1049/el:19941423).

[15] S. H. Muller and J. B. Huber, "OFDM with reduced peak-to-average power ratio by optimum combination of partial transmit sequences", *Electron. Let.*, vol. 33, no. 5, pp. 368–369, 1997 (doi: 10.1049/el:19970266).

[16] A. Hanprasitkum, A. Numsomran, P. Boonsrimuang, and P. Boonsrimuang, "Improved PTS method with new weighting factor technique for FBMC-OQAM systems", in *Proc. 19th Int. Conf. on Adv. Communic. Technol. (ICACT)*, Bongpyeong, South Korea, 2017, pp. 143–147 (doi: 10.23919/ICACT.2017.7890073).

[17] J. H. Wen, G. R. Lee, C. C. Kung, and C. Y. Yang, "Coding schemes applied to peak-to-average power ratio (PAPR) reduction in OFDM systems", in *Proc. 2008 Int. Wirel. Communic. and Mob. Comput. Conf.*, Crete Island, Greece, 2008, pp. 807–812 (doi: 10.1109/IWCMC.2008.139).

[18] H.-G. Ryu, S.-K. Kim, and S.-B. Ryu, "Interleaving method without side information for the PAPR reduction of OFDM system", in *Proc. Int. Symp. on Communic. and Inform. Technol.*, Sydney, NSW, Australia, 2007, pp. 72–76 (doi: 10.1109/ISCIT.2007.4391987).

[19] I. M. Mahafeno, Y. Louet, and J.-F. Helard, "Peak-to-average power ratio reduction using second order cone programming based tone reservation for terrestrial digital video broadcasting systems', *IET Communic.*, vol. 3, no. 7, pp. 1250–1261, 2009 (doi: 10.1049/iet-com.2008.0372).

[20] S. Hu, G. Wu, Q. Wen, Y. Xiao, and S. Li, "Nonlinearity reduction by tone reservation with null subcarriers for WiMAX system", *Wireless Person. Communic.*, vol. 54, no. 2, pp. 289–305, 2010 (doi: 10.1007/s11277-009-9726-z).

[21] B. Koussa, S. Bachir, C. Perrine, C. Duvanaud, and R. Vauzelle, "A comparison of several gradient based optimization algorithms for PAPR reduction in OFDM systems", in *Proc. 2nd International Conference on Communications, Computing and Control Applications CCCA'12*, Marseilles, France, 2012, pp. 1–6 (doi: 10.1109/CCCA.2012.6417865).

Younes Aimer received his B.Sc. and M.Sc. in Electronics and Telecommunications from the University of Saida, Algeria in 2011 and 2013, respectively. Since 2014 he has been a Ph.D. student in Signal Processing and Telecommunications at the Laboratory of Technologies and Communications, University of Saida, Algeria, and since 2016 at the XLIM laboratory, Department of Smart Networks, University of Poitiers, France in co-tutelle (in: electronics, microelectronics, nanoelectronics and microwaves). His current research interests are in digital communications, wireless and mobile communications and signal processing.

E-mail: aimer.younes@univ-saida.dz
Laboratory Technology of Communication
Faculty of Technology
University of Saida
BP 138 En-Nasr
20000 Saida, Algeria.

E-mail: younes.aimer@univ-poitiers.fr
XLIM Laboratory UMR-CNRS 7252
Institute of Technology of Angoulême
University of Poitiers
4 avenue de Varsovie
16021 Angoulême cedex, France

Boubakar Seddik Bouazza received his B.Sc., M.Sc. and Ph.D. degrees, all in electrical engineering, from University of Sidi Bel Abbes, Algeria, in 1996, 1999 and 2006, respectively. In 1999 he joined the University of Saida (Algeria) as an assistant professor and he is a lecturer at the Electronics Department since 2006. Since 2012, he is a director of the communications technology laboratory. He held visiting positions at École Nationale Supérieure de Télécommunications de Bretagne (ENST), Brest, France, as a Ph.D student. His current research interests are in digital communications, wireless and mobile communications, channel coding, turbo codes and bandwidth-efficient coded modulation schemes.

E-mail: boubakar.bouazza@univ-saida.dz
Laboratory Technology of Communication
Faculty of Technology
University of Saida
BP 138 En-Nasr
20000 Saida, Algeria

Smail Bachir received both B.Sc. and M.Sc. in Signal Theory from Polytechnic School of Algeria in 1997. He joined the scientific department of Leroy Somer Society and the University of Poitiers in France where he received his Ph.D. degree in Automatic and Electrical Engineering in 2002. He is presently an Associate Professor at the University of Poitiers and a researcher at XLIM laboratory with the Department of Smart Networks and Systems. His research interests include signal processing, parameter identification, electronic devices and wireless circuits.

E-mail: smail.bachir@univ-poitiers.fr
XLIM Laboratory UMR-CNRS 7252
Institute of Technology of Angoulême
University of Poitiers
4 avenue de Varsovie
16021 Angoulême cedex, France

Claude Duvanaud received his Ph.D. in Electronics and Communication Engineering from the University of Limoges, France, in 1993 and the a habilitation degree (Diriger des Recherches) from the University of Poitiers in 2003. He currently is an Associate Professor at the University Institute of Technology, Angoulême, University of Poitiers, France. His research interests include modeling, simulation and design of nonlinear power amplifiers and communication systems.

E-mail: claude.duvanaud@univ-poitiers.fr
XLIM Laboratory UMR-CNRS 7252
Institute of Technology of Angoulême
University of Poitiers
4 avenue de Varsovie
16021 Angoulême cedex, France

Paper

Using Least Mean *p*-Power Algorithm to Correct Channel Distortion in MC-CDMA Systems

Mohammed Zidane[1], Said Safi[2], Mohamed Sabri[1], and Miloud Frikel[3]

[1]*Department of Physics, Faculty of Sciences and Techniques, Sultan Moulay Slimane University, Morocco*
[2]*Department of Mathematics and Informatics, Polydisciplinary Faculty, Sultan Moulay Slimane University, Morocco*
[3]*GREYC Lab UMR 6072 CNRS, ENSICAEN, Caen, France*

https://doi.org/10.26636/jtit.2018.114717

Abstract—This work focuses on adaptive Broadband Radio Access Network (BRAN) channel identification and on downlink Multi-Carrier Code Division Multiple Access (MC-CDMA) equalization. We use the normalized BRAN C channel model for 4G mobile communications, distinguishing between indoor and outdoor scenarios. On the one hand, BRAN C channel parameters are identified using the Least Mean *p*-Power (LMP) algorithm. On the other, we consider these coefficients in the context of adaptive equalization. We provide an overview and a mathematic formulation of MC-CDMA systems. According to these fundamental concepts, the equalizer technique is investigated analytically to compensate for channel distortion in terms of the bit error rate (BER). The numerical simulation results, for various signal-to-noise ratios and different *p* threshold, show that the presented algorithm is able to simulate the BRAN C channel measured with different accuracy levels. Furthermore, as far as the adaptive equalization problem is concerned, the results obtained using the zero-forcing equalizer demonstrate that the algorithm is adequate for some particular cases of threshold *p*.

Keywords—adaptive equalization, adaptive identification, BER, BRAN C, LMP, MC-CDMA system, ZF.

1. Introduction

The need to develop more efficient wireless communication systems, offering higher data rates, is prevalent today. Different channel accessing techniques exist, such as frequency division multiple access (FDMA), time division multiple access (TDMA), code division multiple access (CDMA) or orthogonal frequency division multiple access (OFDMA). The mix of CDMA and OFDMA offers us a multi carrier-code division multiple access (MC-CDMA) technique which is a good candidate to meet the requirements stated. In the case of very high-speed wireless access of 100 Mbps to 1 Gbps, the channel is severely frequency-selective due to the presence of many interfering paths with different time delays, as well as due to equipment imperfection and presence of noise.

To remedy the perturbation introduced by the transmission channel, it is necessary to identify the distortion and to implement an equalization device. However, the calculation of equalizer coefficients requires knowledge of the parameters of the transmission channel's impulse response parameters, i.e. identification.

There are different identification techniques that can be implemented. In this work we use the LMP algorithm [1]–[3] for radio channel identification. Recently, adaptive algorithms are receiving increasing attention, and are widely studied in various works [1]–[7]. There are several applications, such as interference cancelation, spectral subtraction, wireless localization, adaptive beamforming, and channel equalization [2], in which these can be used. In this paper we address the application of the LMP algorithm in identification of the BRAN C channel and in downlink MC-CDMA equalization. However, LMP is a stochastic gradient-based adaptive filtering algorithm, which uses the p-power of error as the adaptation cost, and it is robust to outliers when $p < 2$ [1], [3]. Here, we address the application of the presented algorithm in the context of adaptive equalization of MC-CDMA systems. However, MC-CDMA offers a high bit rate and high capacity transmission, and is one of the most promising techniques for future mobile communications. Indeed, MC-CDMA is actually a fusion of CDMA and OFDM techniques. MC-CDMA is an effective scheme that reduces such problems as spectral limitation and distortions due to multipath channels.

The principle of MC-CDMA systems is that the multicarrier transmission combines with frequency domain spreading, and the original data stream from a user is spread with this user's specific code, in this case the Walsh-Hadamard code, in the frequency domain but not in the time domain. Each symbol is transmitted simultaneously in a number of subcarriers. However, in digital communication, synchronization between the transmitter and the receiver is considered to constitute a major problem. Synchronization errors cause the loss of orthogonality between subcarriers and considerably degrade performance, especially when a large number of subcarriers exists, provoked by wireless environments. There are many different propagation paths caused by obstacles in the channels, such as buildings, mountains and walls between the transmitter and

receiver [8]–[9]. To compensate for the degradation of the transmitter signal, it is necessary to identify the origin of the distortion and to apply the equalization technique. In this paper, we use the zero forcing (ZF) equalizer after channel identification, to correct channel distortion. However, we have considered a practical frequency selective fading channel, such as BRAN C [10]–[11] normalized for MC-CDMA systems, exited by non-Gaussian sequences, for different SNR and fixed data inputs. The performance of the presented algorithm and equalizer is demonstrated in terms of effectiveness of BRAN C channel identification on the one hand, and BER degradation of downlink MC-CDMA equalization on the other.

The remainder of the paper is organized as follows. The problem is formulated in Section 2. The MC-CDMA system and the equalizer used are described in Section 3. In Section 4, an overview of the LMP algorithm is presented. Numerical simulation results and analyses are considered in Section 5. Finally, the study is concluded in Section 6.

2. Problem Formulation

The BRAN adaptive channel identification problem, as illustrated in Fig. 1, is considered with a discrete time model. One common application of such a solution is linked with the use of adaptive filters to identify an unknown system, such as the impulse response of an unknown communications channel.

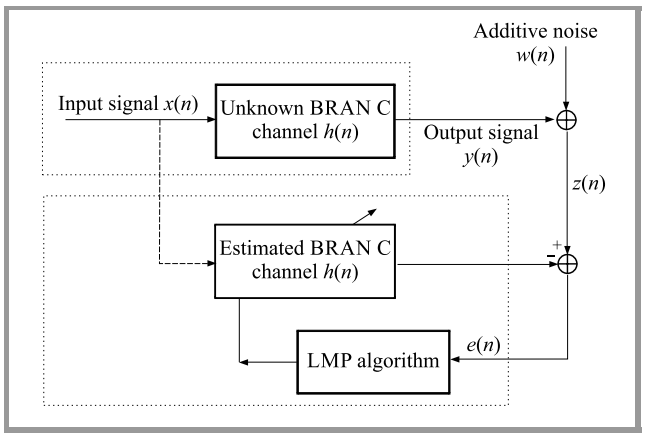

Fig. 1. Adaptive system identification configuration.

Typically, a digital communication channel can be modeled as a finite impulse response filter with an additive noise source. Specifically, the received signal at sample n is:

$$z(n) = \sum_{i=0}^{L-1} h(i)x(n-i) + w(n) \ , \tag{1}$$

where:

$$h = \left[h_0, h_1, \ldots, h_{L-1}\right]$$

and

$$x(n) = \left[x(n), x(n-1), \ldots, x(n-L+1)\right]$$

denotes channel coefficient, with L size, and input signal vector $x(n)$, respectively. $w(n)$ is additive Gaussian noise. The impulse response of the system model is chosen to minimize the mean square error.

For this system we assume that:

- the input sequence $x(n)$ is independent and identically distributed (i.i.d.) zero mean and non-Gaussian,
- the measurement noise sequence $w(n)$ is as assumed zero mean, i.i.d., Gaussian and independent of $x(n)$ with an unknown variance,
- the adaptive filter has the same number of taps as the unknown system represented by $h(n)$.

The problem statement is to identify the parameters of the system $h(n)_{(n=1,\ldots,L)}$ using the LMP algorithm, for various SNR levels and different thresholds p, in order to exploit these coefficients in an adaptive equalization problem. The purpose is to compensate the fading channel, in MC-CDMA systems, in terms of the BER.

3. MC-CDMA System Description

3.1. MC-CDMA Systems

The MC-CDMA signal originates from the concatenation of direct sequence spectrum spreading and multi-carrier modulation operations. However, as it is the case with the OFDM signal, the MC-CDMA signal can be generated by an inverse fast Fourier transform (IFFT) performed on the spreading code chips. Thus, the choice of spreading codes is fundamental. The complex symbol a_i of each user i is, firstly, multiplied by each chip $c_{i,k}$ of the Walsh-Hadamard spreading code, and then applied to the modulator of the multicarriers. Each subcarrier transmits an element of information multiplied by a code chip of that subcarrier (an overview of MC-CDMA systems can be found in [6], [12]–[14]).

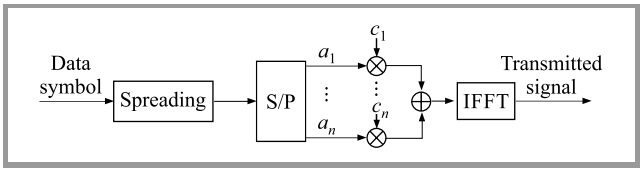

Fig. 2. Transmitter of downlink MC-CDMA systems.

Figure 2 shows the MC-CDMA modulator in a scenario where the spreading code has a length L_c equal to the number of subcarriers N_p, based on the hypothesis of L_c being equal to N_p, and the expression of the signal transmitted at the output of the modulator is given by:

$$x = \frac{1}{\sqrt{N_p}} Ca \ , \tag{2}$$

where matrix C represents the spreading codes:

$$\begin{aligned} \mathrm{C} &= \left[c_0, c_1, \ldots, c_{N_u-1}\right] \\ &= \begin{bmatrix} c_{0,0} & \cdots & c_{N_u-1,0} \\ c_{0,1} & \cdots & c_{N_u-1,1} \\ \cdot & \cdot & \cdot \\ \cdot & \cdot & \cdot \\ \cdot & \cdot & \cdot \\ c_{0,L_c-1} & \cdots & c_{N_u-1,L_c-1} \end{bmatrix}, \end{aligned} \tag{3}$$

where $c_i = [c_{i,0}, c_{i,1}, \ldots, c_{i,L_c-1}]^T$.

When N_u users are active, the multi-user downlink MC-CDMA signal received at the input of the receiver, denoted by $r(t)$, is:

$$r(t) = \frac{1}{\sqrt{N_p}} \sum_{p=0}^{P-1} \sum_{k=0}^{N_p-1} \sum_{i=0}^{N_u-1} \times \Re\{\beta_p e^{j\theta_p} a_i c_{i,k} e^{2j\pi(f_0+k/T_c)(t-\tau_p)}\} + n(t)\,. \tag{4}$$

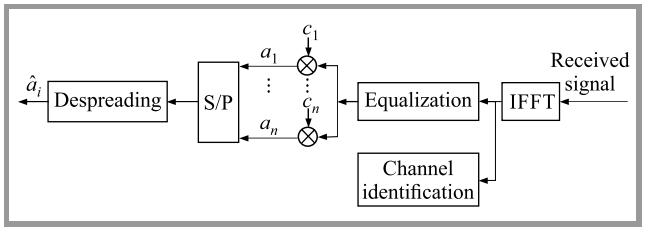

Fig. 3. Receiver of downlink MC-CDMA systems.

In Fig. 3 we represent the receiver for downlink MC-CDMA systems. After equalization, the expression of the signal s_k is given in a vector form, by the following expression:

$$s = \mathrm{G}r = \mathrm{GHC}a + \mathrm{G}n\,, \tag{5}$$

where $\mathrm{H} = \mathrm{diag}[h_0, \ldots, h_{N_p-1}]$ represents the complex channel frequency response.

The matrix $\mathrm{G} = \mathrm{diag}\left[g_0, \ldots, g_{N_p-1}\right]$ represents the diagonal matrix composed of the equalization of coefficients g_k equalization, or, in a scalar form, by:

$$s_k = g_k h_k \left(\sum_{i=0}^{N_u-1} c_{i,k} a_i \right) + g_k n_k\,. \tag{6}$$

After despreading and threshold detection, the data symbol of the user detected corresponds to the sign of the scalar produced between the vector of the received equalized signals, s, and the user-specific spreading code i, c_i^T, that is:

$$\widehat{a_i} = < c_i^T, s > = \sum_{k=0}^{N_p-1} c_{i,k} s_k\,. \tag{7}$$

Using Eqs. (6) and (7), the general expression of the symbol detected for i user is given by the following equation:

$$\begin{aligned} \widehat{a_i} &= \sum_{q=0}^{N_u-1} \sum_{k=0}^{N_p-1} c_{i,k}(g_k h_k c_{q,k} a_q + g_k n_k) \\ &= \underbrace{\sum_{k=0}^{N_p-1} c_{i,k}^2 g_k h_k a_i}_{U \quad (i=q)} + \underbrace{\sum_{q=0}^{N_u-1} \sum_{k=0}^{N_p-1} c_{i,k} c_{q,k} g_k h_k a_q}_{M \quad (i\neq q)} \\ &\quad + \underbrace{\sum_{k=0}^{N_p-1} c_{i,k} g_k n_k}_{N}\,, \end{aligned} \tag{8}$$

where the terms U, M and N of Eq. (8) are, respectively, the signal of the considered user, signals of other users (multiple access interferences) and the noise pondered by the equalization coefficient and by spreading the code of the chip.

If we suppose that the spreading codes are orthogonal, i.e.:

$$c_i^T c_q = \sum_{k=0}^{N_p-1} c_{i,k} c_{q,k} = 0\,, \quad \forall\ i \neq q\,, \tag{9}$$

Equation (8) will become:

$$\widehat{a_i} = \underbrace{\sum_{k=0}^{N_p-1} c_{i,k}^2 g_k h_k a_i}_{U} + \underbrace{\sum_{k=0}^{N_p-1} c_{i,k} g_k n_k}_{N}\,. \tag{10}$$

The probability of binary error is written as [15]:

$$\begin{aligned} P_e &= P_r\left\{X < 0 | \Re(a) = +\sqrt{E_a}\right\} \\ &= \frac{1}{2}\mathrm{erfc}\left(\frac{E\{X\}}{\sqrt{2\mathrm{var}\{X\}}}\right)\,, \end{aligned} \tag{11}$$

with X being the decision variable equal to $\Re(\widehat{a})$ for a given value of a.

The mean $E(X)$ of the decision variable, conditional upon h_k is written as:

$$\begin{aligned} E\{X\} &= \Re\left\{\sum_{k=0}^{L_c-1} c_{i,k}^2 g_k h_k\right\}\sqrt{E_a} \\ &= \sqrt{E_a}\frac{1}{L_c}\sum_{k=0}^{L_c-1} \Re\{g_k h_k\} \underset{L_c\to\infty}{\longrightarrow} 0\,, \end{aligned} \tag{12}$$

and the variance of the decision variable is:

$$\begin{aligned} \mathrm{Var}\{X\} &= E\left[\left(\sum_{k=0}^{L_c-1} c_{i,k}\Re\{g_k n_k\}\right)^2\right] \\ &= \frac{1}{L_c}\sum_{k=0}^{L_c-1} |g_k|^2 \frac{E\{n_k^2\}}{2}\,. \end{aligned} \tag{13}$$

The power P_U of the information bearing component U is:

$$P_U = E[UU^*] = \frac{\sum_{k=0}^{L_c-1} |g_k h_k|^2}{L_c^2}\sigma_a^2 \ . \tag{14}$$

The power P_N of the signal's noise component is:

$$P_N = E[NN^*] = \frac{1}{L_c}\sum_{k=0}^{L_c-1} |g_k|^2 \sigma_{n_k}^2 \ . \tag{15}$$

The SNR of the MC-CDMA signal after despreading as a function of the length of the spreading codes L_c is:

$$\frac{P_U}{P_N} = \frac{\sum_{k=0}^{L_c-1} |g_k h_k|^2 \sigma_a^2}{L_c \sum_{k=0}^{L_c-1} |g_k|^2 \sigma_{n_k}^2} \ . \tag{16}$$

3.2. Equalization of MC-CDMA Systems using ZF

The goal of ZF is to minimize the peak distortion of the equalized channel, i.e. the inverse of the channel is applied to the received signal the restored signal is defined as:

$$g_k = \frac{1}{h_k} \ . \tag{17}$$

The estimated received symbol, $\widehat{a_i}$ of symbol a_i of the user i is:

$$\widehat{a_i} = \sum_{k=0}^{N_p-1} c_{i,k}^2 a_i + \sum_{k=0}^{N_p-1} c_{i,k}\frac{1}{h_k} n_k \ . \tag{18}$$

The goal of equalization is to extract a_i. After equalization and despreading, SNR of the MC-CDMA signal obtained in Eq. (16) reduces to:

$$\frac{P_U}{P_N} = \frac{\sigma_a^2}{\sum_{k=0}^{L_c-1} \frac{1}{|h_k|^2}\sigma_{n_k}^2} \ . \tag{19}$$

Determination of the subcarrier weighing coefficients is to be performed adaptively, using the LMP algorithm and will be described in Section 4.

4. Adaptive Identification using LMP Algorithm

LMP [1], [3] is one of the most popular adaptive filtering algorithms. With a proper p value, the LMP can outperform the traditional least mean square (LMS) ($p = 2$).
The cost function of the LMP algorithm is [1]:

$$L_{LMP} = |e(n)|^p = |z(n) - h^T(n)x(n)|^p \ , \tag{20}$$

where p is a positive constant value. Furthermore, we can keep the filter stable under impulsive noise conditions when $1 < p < 2$. Gradient descent methods can be used to estimate the filter weights, and an iteration equation can be derived as:

$$\begin{aligned} h(n+1) &= h(n) - \eta \frac{\partial J_{LMP}(n)}{\partial h(n)} \\ &= h(n) - \eta\left[-p|e(n)|^{p-1}\text{sign}(e(n))x(n)\right] \\ &= h(n) + \eta p|e(n)|^{p-1}\text{sign}(e(n))x(n), \end{aligned} \tag{21}$$

where $\mu = p\eta$ is the step size, and

$$\text{sign}(x) = \begin{cases} 1 & \text{if} \quad x > 0 \\ 0 & \text{if} \quad x = 0 \\ -1 & \text{if} \quad x < 0 \end{cases} \ . \tag{22}$$

5. Simulation Results

Performance is evaluated using the normalized mean square error (NMSE):

$$NMSE = \sum_{i=1}^{L}\left[\frac{h(i) - \widehat{h}(i)}{h(i)}\right]^2 \ , \tag{23}$$

where $\widehat{h}(i)$ and $h(i)$, $i = 1, \ldots, L$, are the estimated and real parameters, respectively, in each run.
Table 1 shows a summary of the real model of the BRAN C channel identified using the LMP algorithm presented. The length of this channel is $L = 18$.

Table 1
Delay and magnitudes of 18 targets of BRAN C channel

Delay τ_i [ns]	Mag. A_i [dB]	Delay τ_i [ns]	Mag. A_i [dB]
0	–3.3	230	–3.0
10	–3.6	280	–4.4
20	–3.9	330	–5.9
30	–4.2	400	–5.3
50	0.0	490	–7.9
80	–0.9	600	–9.4
110	–1.7	730	–13.2
140	–2.6	880	–16.3
180	–1.5	1050	–21.2

5.1. Adaptive Identification of BRAN C Channel

Here, an adaptive algorithm, such as LMP is introduced for system identification, It adjusts its coefficients to minimize the mean square error between its output and the output of an unknown system. The goal is to adapt the coefficients of the filter to match, as closely as possible, the response of an unknown BRAN C channel.
Figures 4, 5 and 6 represent the estimations of the BRAN C parameters using LMP, where SNR = 0, 4 and 8 dB, respectively, the data length of non-Gaussian signal input is

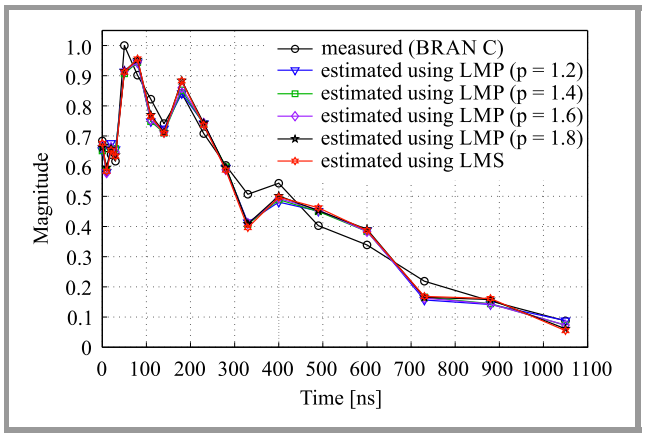

Fig. 4. BRAN C channel identification performance versus parameter threshold p, for SNR = 0 dB.

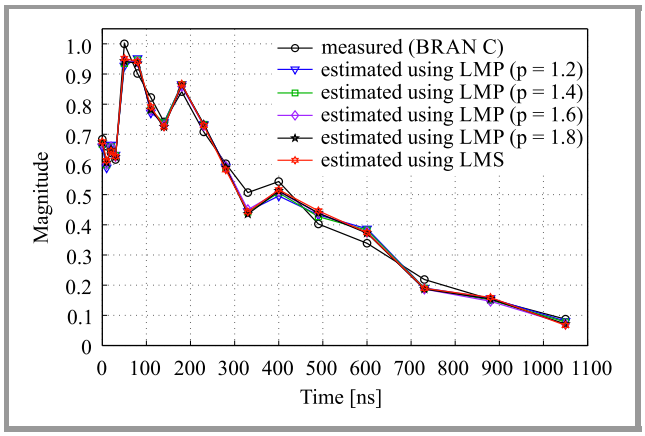

Fig. 5. BRAN C channel identification performance versus parameter threshold p, for SNR = 4 dB.

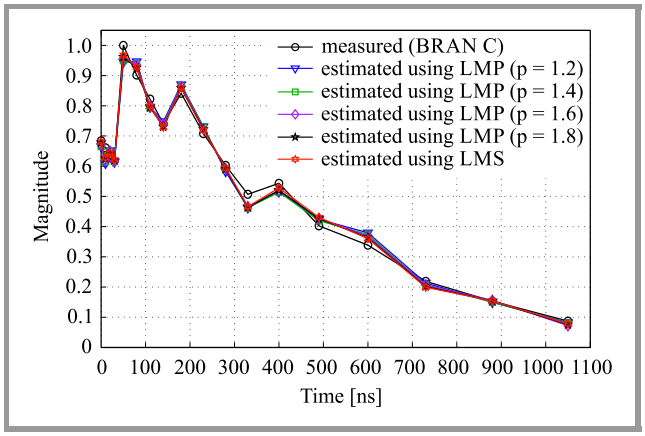

Fig. 6. BRAN C channel identification performance versus parameter threshold p, for SNR = 8 dB.

N = 2048, and for 100 Monte Carlo runs, in order to study the effect of the noise power on the estimated parameters. The parameter, in numerical simulations, is set as $\mu = 0.01$ and various thresholds p are applied.

In a very noisy environment (SNR = 0 dB), Gaussian noise influenced the estimated parameters of the BRAN C channel model (Fig. 4). We would also like to point out a difference between the estimated and true BRAN C parameters, which do not follow the real model in this SNR scenario. Simulation results (Figs. 5 and 6) confirm better accuracy levels, especially when SNR $>$ 4 dB. However, the estimated models, using the standard LMP algorithm, follow the real model of the BRAN C channel and a minor difference is observed. For example, if SNR = 8 dB, we have a perfect agreement between the estimated and measured channel, using all algorithms considered.

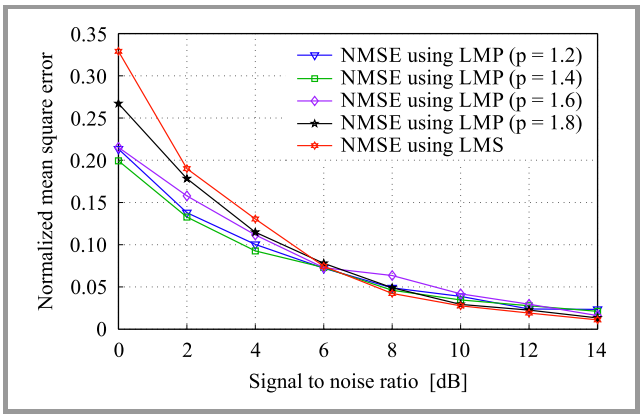

Fig. 7. NMSE values as a function of SNR using the LMP algorithms.

Figure 7 shows the performance of NMSE versus threshold p values for different SNRs. This figure gives us a good idea about the precision of these algorithms in terms of NMSE defined in the Eq. (23). Indeed, in the interval of 0–6 dB, we can note that the standard LMP is more efficient than the traditional LMS ($p = 2$), for all threshold p values, with LMP presenting a higher advantage ($p = 1.4$) than other options within the interval in question. In addition,

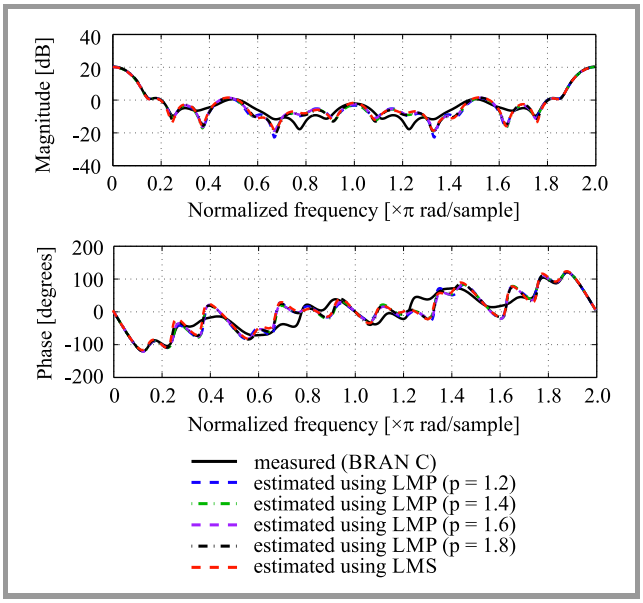

Fig. 8. Estimated magnitude and phase of the BRAN C channel when SNR = 0 dB and N = 2048.

for SNR higher than 6 dB, we observe that the traditional LMS becomes more effective compared to the LMP algorithm. In conclusion, LMP ($p = 1.4$) is very adequate in a noisy environment 0 dB $\leq$ SNR $\leq$ 6 dB. If SNR $>$ 6 dB, we have a minor difference between NMSE obtained using LMP ($p = 1.4$) and that obtained using LMS.

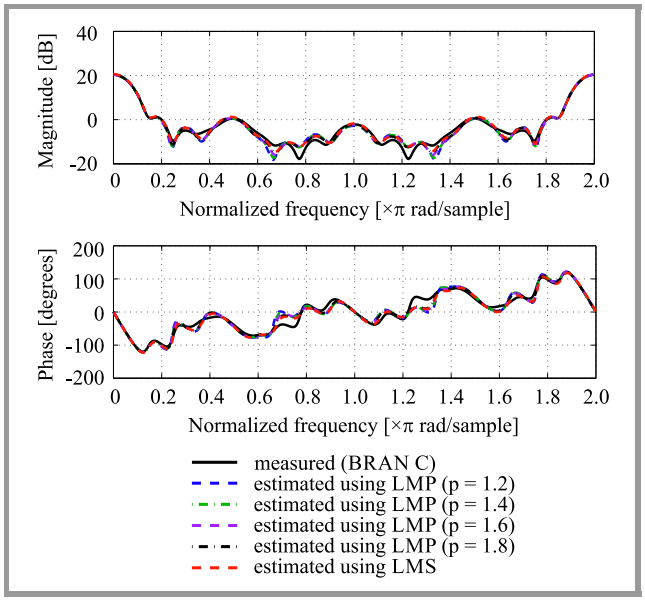

Fig. 9. Estimated magnitude and phase of the BRAN C channel when SNR = 8 dB and N = 2048.

In order to test accuracy in the frequency domain, we represent – in Figs. 8 and 9 – the estimation magnitude and the phase of the impulse response of BRAN C radio channel, for SNR = 0 dB and SNR = 8 dB, respectively, for various thresholds p. From these figures we can conclude that:

- for a high noise environment (SNR = 0 dB), the estimated magnitude and phase follow the real model of BRAN C channel, with a certain difference,
- for SNR $\geq$ 8 dB, the estimated magnitude and phase converge with the real model, with the highest accuracy value.

5.2. Adaptive Equalization of MC-CDMA Systems

As far as the problem of adaptive equalization is concerned, we use the ZF equalizer technique after channel identification to correct channel distortion. The performance is evaluated in terms of BER.

In Fig. 10 we represent the BER estimation of the BRAN C radio channel using the ZF equalizer in MC-CDMA systems, for different SNRs and various thresholds p of the LMP algorithm.

BER simulation for various SNRs differing from 0 to 14 dB, demonstrates that the BER estimated using LMP ($p = 1.4$) and LMS algorithms is more precise and offers better results than in the case of the LMP algorithm. However, if SNR $\geq$ 14 dB and LMP ($p = 1.4$) and LMS algorithms are used, we obtain a 1 bit error if 10^4 bits are

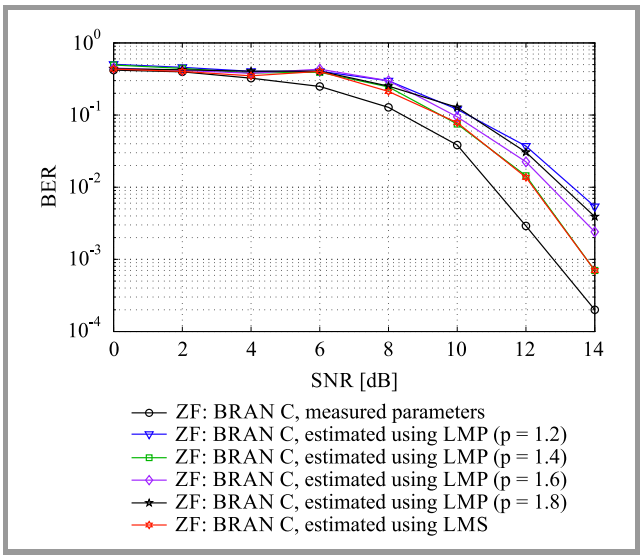

Fig. 10. BER of the estimated and measured BRAN C channel, for different SNR and various thresholds p.

received. In the other case ($p = 1.2$, 1.6 and 1.8), we obtain a 1 bit error if 10^3 bits are received, which is an advantage over LMP ($p = 1.6$).

6. Conclusion

In this paper, the BRAN channel identification problem and downlink MC-CDMA equalization have been investigated. We have presented an overview of the LMP algorithm. To illustrate identification performance, we applied this algorithm to the BRAN C channel model for various thresholds p and different SNRs. According to the results of numerical simulations, it has been demonstrated that LMP ($p = 1.4$) is preferred in a very noise environment (0 dB $\leq$ SNR $\leq$ 6 dB), and is more efficient than traditional LMS ($p = 2$) for all thresholds p. Furthermore, where SNR $>$ 6 dB, the LMS algorithm becomes more efficient than LMP with a minor difference, principally in the case of $p = 1.4$. These interesting, identification-related results encouraged us to exploit the estimated BRAN C channel coefficients in the context of adaptive equalization for MC-CDMA systems. Indeed, we have used the ZF equalizer to reduce BER. The results obtained here prove that BER rates estimated using LMP ($p = 1.4$) and LMS algorithms are similar and more precise than other cases involving the use of the LMP algorithm, and, thus, the objective assumed has been reached.

References

[1] W. Ma, B. Chen, H. Qu, and J. Zhao, "Sparse least mean p-power algorithms for channel estimation in the presence of impulsive noise", *Signal, Image and Video Process.*, vol. 10, no. 3, pp. 503–510, 2016 (doi: 10.1007/s11760-015-0757-5).

[2] G. Gui, W. Peng, and F. Adachi, "Adaptive system identification using robust LMS/F algorithm", *Int. J. of Commun. Syst.*, vol. 27, no. 11, pp. 2956–2963, 2014 (doi: 10.1002/dac.2517).

[3] S. C. Pei and C. C. Tseng, "Least mean p-power error criterion for adaptive FIR filter", *IEEE J. on Selec. Areas in Commun.*, vol. 12, no. 9, pp. 1540–1547, 1994 (doi: 10.1109/49.339922).

[4] W. Ma, H. Qu, J. Zhao, B. Chen, and G. Gui, "Sparsity aware normalized least mean p-power algorithms with correntropy induced metric penalty", in *IEEE Int. Conf. on Digit. Signal Proces. DSP 2015*, Singapore, Singapore, 2015, pp. 638–642 (doi: 10.1109/ICDSP.2015.7251952).

[5] M. L. Aliyu, M. A. Alkassim, and M. S. Salman, "A p-norm variable step-size LMS algorithm for sparse system identification", *Signal, Image and Video Process.*, vol. 9, no. 7, pp. 1559–1565, 2015 (doi: 10.1007/s11760-013-0610-7).

[6] M. Zidane, S. Safi, M. Sabri, A. Boumezzough, and M. Frikel, "Adaptive algorithms versus higher order cumulants for identification and equalization of MC-CDMA", *J. of Telecommun. and Inform. Technol.*, no. 3, pp. 53–62, 2014.

[7] N. Ishibushi, Y. Kajikawa, and S. Miyoshi, "Statistical-mechanical analysis of LMS algorithm for time-varying unknown system", *J. of the Phys. Society of Japan*, vol. 86, no. 2, ID: 024803, 2017 (doi: 10.7566/JPSJ.86.024803).

[8] N. Yee, J.-P. M. G. Linnartz, and G. Fettweis, "Multi-Carrier-CDMA in indoor wireless networks", in *Proc. Int. Symp. on Pers., Indoor, and Mob. Radio Commun. PIMRC 1993*, Yokohama, Japan, 1993, pp. 109–113.

[9] M. Frikel, B. Targui, M. M'Saad, and F. Hamon, "Adaptive equalization using controlled equal gain combining for uplink/downlink MC-CDMA systems, *Int. J. of Signal Process.*, vol. 4, no. 3, pp. 230–237, 2008.

[10] "Broadband Radio Access Networks (BRAN); High Performance Radio Logical Area Network (HIPERLAN) Type 2; Requirements and architectures for wireless broadband access", ETSI, Jan. 1999.

[11] "Broadband Radio Access Networks (BRAN); HIPERLAN Type 2; Physical Layer", ETSI, Dec. 2001.

[12] M. Zidane, S. Safi, and M. Sabri, "Compensation of fading channels using partial combining equalizer in MC–CDMA Systems", *J. of Telecommun. and Inform. Technol.*, no. 1, pp. 5–11, 2017.

[13] M. Zidane, S. Safi, M. Sabri, and A. Boumezzough, "Identification and equalization using higher order cumulants in MC-CDMA systems", in *Proc. 5th Worksh. on Codes, Cryptography and Commun. Syst. WCCCS 2014*, El Jadida, Morocco, 2014, pp. 81–85 (doi: 10.1109/WCCCS.2014.7107925).

[14] M. Zidane, S. Safi, M. Sabri, A. Boumezzough, and M. Frikel, "Broadband radio access network channel identification and downlink MC-CDMA equalization", *Int. J. of Energy, Inform. and Commun.*, vol. 5, no. 2, pp. 13-34, 2014 (doi: 10.14257/ijeic.2014.5.2.02).

[15] J. Y. Baudais, "Étude des modulations à porteuses multiples et à spectre étalé: analyse et optimisation", Doctoral dissertation, INSA de Rennes, France, 2001 (in French).

Mohammed Zidane received his M.Sc. degree in Electronic Engineering from the Faculty of Science and Techniques Sultan Moulay Slimane University, Beni Mellal, Morocco, his M.Sc. degree in Optoelectronics and Laser Instrumentation from the Faculty of Science and Techniques Hassan First University, Settat, Morocco, and his Ph.D. in Signal Processing and Telecommunications from Sultan Moulay Slimane University, Beni Mellal, Morocco. His research interests include digital communications and signal processing, linear and non-linear broadband radio access network (BRAN) channels identification, higher order statistics, blind identification and equalization in MC-CDMA systems – the subjects on which he has published 9 journal and 4 conference papers.
E-mail: zidane.ilco@gmail.com
Department of Physics
Faculty of Sciences and Techniques
Sultan Moulay Slimane University
PO box 523, Beni Mellal, Morocco

Said Safi received his B.Sc. degree in Physics (option Electronics) from Cadi Ayyad University, Marrakech, Morocco in 1995, M.Sc. and Doctorate degrees from Chouaib Doukkali University and Cadi Ayyad Univerrsity, in 1997 and 2002, respectively. He was a Professor of Information Theory and Telecommunication Systems at the National School for Applied Sciences, Tangier, Morocco, from 2003 to 2005. Since 2006, he has been a Professor of Applied Mathematics and Programming at the Faculty of Science and Technics, Beni Mellal, Morocco. In 2008 he received his Ph.D. degree in Telecommunication and Informatics from the Cadi Ayyad University. His general interests span the areas of communications and signal processing, estimation, time-series analysis and system identification – subjects on which he has published 14 journal and more than 60 conference papers. His current research topics focus on transmitter and receiver diversity techniques for single- and multi-user fading communication channels, and wide-band wireless communication systems.
E-mail: safi.said@gmail.com
Department of Mathematics and Informatics
Sultan Moulay Slimane University
PO box 592, Sultan Beni Mellal, Morocco

Mohamed Sabri received his Ph.D. degree in Signal Processing and Telecommunications, from Rennes I University, France. His current research interests include evolution of communication networks, human face detection and recognition. He is currently working as a Professor at the Department of Physics, Faculty of Sciences and Techniques, University of Sultan Moulay Slimane, Beni Mellal, Morocco.
E-mail: sipt03@yahoo.fr
Department of Physics
Faculty of Sciences and Techniques
Sultan Moulay Slimane University
PO box 523, Beni Mellal, Morocco

Miloud Frikel received his Ph.D. degree from the center of mathematics and scientific computation CNRS URA 2053, France, in array processing. Currently, he is with the GREYC laboratory and the ENSICAEN, as Assistant Professor. Between 1998 and 2003 he was with the Signal Processing Lab, Institute for Systems and Robotics, Institute Superior Tecnico, Lisbon, as a researcher in the field of wireless location and statistical array processing. Later he worked as a research engineer for a software company in Munich, Germany, and was an employee of the Institute for Circuit and Signal Processing of the Technical University of Munich, Germany. Mr. Frikel's research interests span several areas, including statistical signal and array processing, cellular geolocation (wireless location), space-time coding, direction finding and source localization, blind channel identification for wireless communication systems, and MC-CDMA systems.

E-mail: mfrikel@greyc.ensicaen.fr
GREYC UMR 6072 CNRS
ENSICAEN
6, B. Maréchal Juin
14050 Caen, France

Paper

Interference Management using Power Control for Device-to-Device Communication in Future Cellular Network

Toha Ardi Nugraha, Muhammad Putra Pamungkas, and Anna Nur Nazilah Chamim

Department of Electrical Engineering, Universitas Muhammadiyah Yogyakarta, Yogyakarta, Indonesia

https://doi.org/10.26636/jtit.2018.125418

Abstract—There are many scenarios that have been proposed for fifth generation (5G) networks. Some of them, if implemented, will bring fundamental changes at the architectural and node level. One example of such proposed technologies is device-to-device (D2D) communications which will change the nature of conventional cellular network design. D2D permits direct communication between two or more user devices without intervention of the base station (i.e. eNB). D2D can ensure network performance improvement over the traditional cellular network, because it can offload the mobile data traffic from the other devices. However, applying D2D features in a cellular network will bring about more complex interference problems, since D2D communication uses the same band as its underlying cellular communication network. The aim of this research is to investigate interference-related problems caused by D2D communications, affecting the underlying cellular networks, during downlink and uplink transmissions. The paper examines the use of power control methods to mitigate interference. A comparison is offered between fixed power level (FC) with or without power control, and adaptive power controls using two methods (AC1 and AC2), on a base station or on each of the D2D devices, based on the measured signal to interference plus noise ratio (SINR). The simulation results show that both power control methods contribute to improvement of network performance. AC1 and AC2 can improve SINR by about 1 dB and 0.5 dB compared to FC in a downlink transmission, and by 0.5 dB in an uplink transmission.

Keywords—cellular network, device-to-device communication, interference management, power control.

1. Introduction

There are many concepts, design criteria and scenarios that have been proposed for fifth generation (5G) cellular networks. Some of them, if implemented, will bring about fundamental changes at the architectural and node level. One example of such proposed technologies is device-to-device (D2D) communications [1]. D2D is a new feature for future cellular systems. In conventional cellular networks, each device or user equipment (UE) communicates directly with the base station (BS) via downlink (DL) and uplink (UL) paths [2]. The infrastructure of cellular networks will be changed in the new system. D2D permits direct communication between two user devices, without using the BS. D2D can improve performance of a traditional cellular network, due to D2D offloading the mobile data traffic from other devices.

Some researches has already been performed to investigate D2D communication in a cellular network [3]. Since no D2D standard has been proposed for 5G systems yet, the D2D model remains widely open [4]. However, D2D communications may results in cellular networks suffering from interference-related problems, as D2D communication shares the same frequency band as its underlying cellular network. Therefore, interference management aiming to reduce the adverse effects is crucial.

Many studies have been performed to investigate D2D's underlying cellular networks, and to assess various aspects related to coverage [5], [6]. One of the solutions adopted to manage interference-related problems is to separate the frequency allocation for D2D communications and macro cell communications, as presented in [7], [8]. However, limitation of the frequency spectrum is a common and serious problem, because of numerous devices staying on within a macro cell cellular network [9]. One of the solutions is to use a different frequency for each device, but this scheme is less effective, because in areas in which D2D communication is not used frequently, frequency domain allocated to D2D communications will be wasted.

In order to solve the frequency spectrum allocation problems, paper [10] proposes a shared/dedicated resource allocation method for D2D communications using underlying cellular networks. Therefore, some researchers have made proposed other solutions to manage the interference-related problems occurring within the same frequency spectrum for D2D communication, by implementing power control methods, e.g. [11]. This paper proposes a random network model for a D2D underlying cellular system using stochastic geometry, as well as developed centralized and distributed power control algorithms, but this method turned out to be very complex. Paper [12] investigated joint resource allocation and power control for D2D communications and the

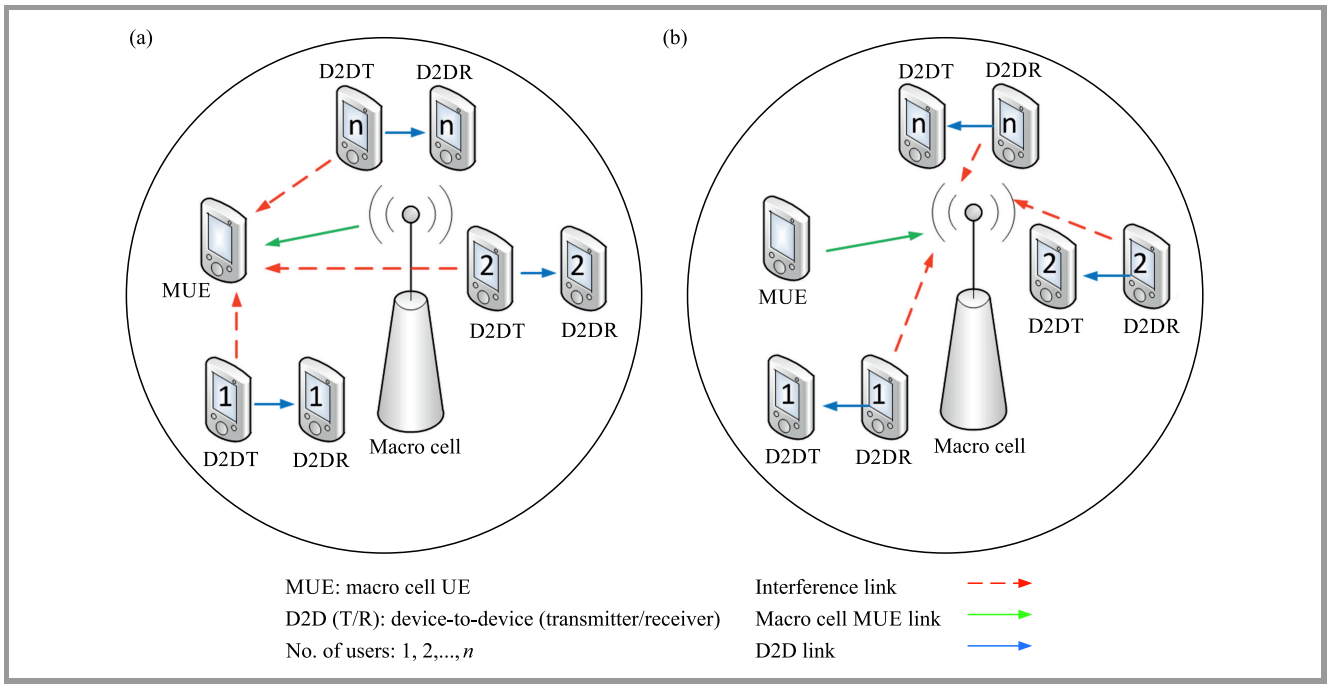

Fig. 1. Downlink and uplink transmissions of cellular network with D2D deployed in the single macro cell scenario: (a) first analyzed scenario, (b) second case.

underlying cellular networks, and the result focused on optimizing energy efficiency (EE) of D2D communications. The other method implemented the adaptive power control method [13]. In that paper, the simulation focused solely on DL transmissions. Another paper [14] also investigated D2D communication within an underlying cellular system, but only focused on UL transmissions.

The objective of this research is to manage interference-related problems in D2D communications and underlying cellular networks, affecting both types of transmissions, i.e. DL and UL. This research proposes the use of power control methods to mitigate interference in both directions. The methods compare two schemes, i.e. fixed power level (FC) and adaptive power controls (AC1 and AC2). The methods are implemented on BS or on D2D UE, based on the signal to interference plus noise ratio (SINR) measured in each device.

The rest of the paper is organized as follows. Section 2 describes the system models. Section 3 verifies the model proposed by using simulation results. Finally, Section 4 summarizes the conclusions and described further work required.

2. System Model

This research simulates a single macro cell in a cellular networks system, implementing some user devices to establish D2D communication. The simulations investigate the implementation of power control methods in both types of transmission, i.e. downlink and uplink transmissions used within D2D communication's underlying macro cell coverage. The simulation assumes also that D2D communications uses the same frequency spectrum as is used in the macro cell. Therefore, interference between each devices and the base station should be the main problem encountered.

In the first scenario, the simulation investigates the problem of interference caused DL signal sent from D2D UE (D2DT) to the macro cell's receiver MUE. A number of D2D communications will interfere with the MUE that is being served by the macro cell. The SINR distribution of MUE will be analyzed. This first scenario is shown in Fig. 1a. The second scenario analyzes the impact of interference on the receiver of the macro cell, caused by uplink interference of the devices, as presented in Fig. 1b.

For the first scenario, let P_{T_M} be the transmit power of the macro cell. Then, $P^{DL}_{R\_MUE}$ is the power received at the receiver side (at the MUE that desires to receive the of the signal) can be formulated as [13]:

$$P^{DL}_{R\_MUE} = P_{T\_M}.G_{T\_M}\,, \tag{1}$$

where P_{T_M} is the transmit power of the macro cell and G_{T_M} is the channel gain from the macro cell to MUE. For simulating G_{T_M}, the Eq. (1) can be used as:

$$G_{T\_M} = PL_M.h_M\,, \tag{2}$$

where PL_M is the propagation loss between the macro cell and MUE, and h_M is the channel's small scale fading factor from the macro cell to MUE. However, this research does not take into account the effect of small scale fading. Therefore, it characterizes only the propagation loss caused by the distance between the transmitter and the receiver.

In this system, $P_{T\_M}.G_{T\_M}$ means the received signal power at the distance d. Since this paper does not consider the ef-

fect of small scale fading, G_{T_M} could be denoted as a propagation model. This paper adopts the propagation model formulated in [9] and [15].
This formula describes the path-loss link between pieces of user equipment, which calculates the propagation loss from D2D UE/D2DT of D2DR and MUE to the macro cell or vice versa:

$$PL_M[\text{dB}] = 128.1 + 37.6 \log d[\text{km}], \quad (3)$$

and this equation reflects D2D links and calculates the link propagation level between the transmitter of D2D UE (D2DT) and the receiver of D2D UE (D2DR):

$$Pl_{D2D}[\text{dB}] = 148 + 40 \log d\,[\text{km}], \quad (4)$$

where Pl_{D2D} is the propagation loss from UE (D2D equipment or MUE) to the macro cell or vice versa), Pl_{D2D} is propagation loss from D2D communication pairs between D2DT and D2DR, and d is the distance between the transmitter and the receiver in km.
In a DL transmission, the signal quality of MUE is measured by SINR:

$$SINR^{DL}_{MUE_1,M} = \frac{P^{DL}_{R\_MUE}}{rd(k)P_{D2DT_k,MUE_1}.G_{D2DT_k,MUE_1} + N}, \quad (5)$$

where $SINR_{MUE_1}$ is the SINR values on MUE with the signal received from the macro cell. $P^{DL}_{R\_MUE}$ is the received power at MUE for the desired signal from the macro cell. $rd(k)$ is the equality indicator used for downlink resources, 0 and 1 are for the different and same resource used, respectively [13]. G_{D2DT_k,MUE_1} is the channel gain between D2DT that interferes and MUE, and N is the power of system noise.
$P^{DL}_{R\_MUE}$ can be calculated using Eq. (1) and the interference from $D2DR_K$ that uses the same frequency resource as the cellular networks can be formulated using Eq. (1), by replacing eNB indices with those for the transmitter, and the MUE1 indices remain the same as those of the receiver serving as the terminal under observation. As mentioned earlier, this paper does not consider the small scale fading factor and the same assumption applies to the link between D2DT and MUE.
In UL, SINR measured on eNB can be calculated as:

$$SINR^{UL}_{eNB_1,M} = \frac{P^{UL}_{R\_eNB}}{rd(k)P_{D2DR_k,MUE_1}.G_{D2DR_k,MUE_1} + N}, \quad (6)$$

where $SINR_{MUB_1}$ is the SINR values on eNB receiver with the signal received from the MUE transmitter. $P^{UL}_{R\_MUE}$ is the received power at eNB. G_{D2DR_k,MUE_1} is the channel gain between D2D and N is the power of system noise.

2.1. Power Control

The power control method is implemented on both sides: D2D and the cellular network. This paper considers interference-related problems affecting cellular communication first. In the case of D2D communication, all equations presented in the following descriptions apply, with the indices replaced accordingly.
In order to reduce interference, the transmit power of the desired transmitter, i.e. eNB in this case, may be adjusted. The transmit power of the eNB macro cell, P_{T_M} is established in the numerator of Eq. (5). The transmit power of the desired transmitter, at the frame transmission time, $P_{T\_M}(t_i)$ will be adjusted at the next time of frame transmission, producing a new transmit power value $P_{T\_M}(t_{i+1})$.
This paper uses γ as a parameter of the TX power control method change occurring at the next frame transmission and based on the estimated value of current time of $SINR(SINR_{est}(t_i)).SINR_{est}(t_i)$ will be compared with the predetermined $SINR_{tar}$ value. Based on this argument, this paper introduces a k parameter, to indicate whether the value of γ will increase the transmit power or decrease the transmit power or whether the same transmit power will be kept for the next time of frame transmission. The general expression of $P_{T\_M}(t_{i+1})$ can be written as:

$$P_{T\_M}(t_{i+1}) = P_{T\_M}(t_i) + k.\gamma. \quad (7)$$

The value of k will be determined according to the SINR(t_i). In this case, there are three likely conditions of SINR$_{est}$(t$_i$) [13]:

- first, if $SINR_{est}$ is smaller than $SINR_{tar}$, then k will be a positive value,
- second, if $SINR_{est}$ is same as $SINR_{tar}$, then k will be equal to 0,
- third, if $SINR_{est}$ is greater than $SINR_{tar}$, then k will be a negative value.

The exact values of k and γ depend on the power control method that is going to be applied. This paper uses two power control methods: AC1 and AC2. The manner in which the values of k and γ impact the two power control methods is explained later on in this section.
And then, another scenario has to be met by the power control method. The value of $P_{T\_M}(t_{i+1})$ in Eq. (7) must not exceed the value of maximum and must not be lower the minimum transmit power of eNB, i.e. $P_{\max}$ and $P_{\min}$, respectively. Then, the final value of $P_{T\_M}(t_{i+1})$ at the next frame transmission using the output of the power control method will be determined based on the expression below. To avoid the confusion, $P_{T\_M}(t_{i+1})$ that is formulated in Eq. (7) is re-denoted as $P_{T\_M}(t_{i+1})$:

$$P_{T\_M}(t_{i+1}) = \begin{cases} \min\left\{P^*_{T\_M}(t_{i+1}), P_{\max}\right\} & \text{if } SINR_{est}(t_i) < SINR_{tar} \\ P^*_{T\_M}(t_{i+1}) & \text{if } SINR_{est}(t_i) = SINR_{tar} \\ \max\left\{P^*_{T\_M}(t_{i+1}), P_{\min}\right\} & \text{if } SINR_{est}(t_i) > SINR_{tar} \end{cases}. \quad (8)$$

Equation (8) will guarantee that the power output of the power control methods will be within the permitted transmit power limits of UE (MUE and D2DT) and eNB.

2.2. AC1 Power Control

The AC1 power scheme procedure is simple and can be implemented easily in practice. As in [13], the paper has applied this power control method to a two-tier heterogeneous (femto-cell and macro cell) network. AC1 uses a fixed value for multiplication of k and γ. The value of γ is set to be a constant and is a simulation parameter. The value of k, in turn, depend on the values of $SINR_{est}(t_i)$, as explained earlier, and can be expressed as:

$$k = \begin{cases} +2 & \text{if } SINR_{est}(t_i) < SINR_{tar} \\ 0 & \text{if } SINR_{est}(t_i) = SINR_{tar} \\ -2 & \text{if } SINR_{est}(t_i) > SINR_{tar} \end{cases}. \quad (9)$$

2.3. AC2 Power Control

This research uses the different values of multiplication between k and γ in order to increase or decrease the transmit power in the AC2 power control method:

$$k = \begin{cases} +3 & \text{if } SINR_{est}(t_i) < SINR_{tar} \\ 0 & \text{if } SINR_{est}(t_i) = SINR_{tar} \\ -3 & \text{if } SINR_{est}(t_i) > SINR_{tar} \end{cases}, \quad (10)$$

The different values of k when $SINR_{est}(t_i) < SINR_{tar}$ and $SINR_{est}(t_i) > SINR_{tar}$ are intended to affect the controlled transmit power when it is increased or decreased.
The γ is based on the average received interference power at the observed terminal (D2D UE). Calculation of the average interference power is based on the moving average method, as illustrated in Fig. 1a-b. The shift register is used to store the interference power detected at the observed terminal (MUE or eNB). Then, the average value of interference power is:

$$\bar{I} = \frac{1}{n}\sum_{i=1}^{n} I_i . \quad (11)$$

Then, γ is calculated:

$$\gamma = |P_{TM}(t_i) - \bar{I}| . \quad (12)$$

SINR values at the MUE for DL and eNB for UL transmission are analyzed through simulation.

3. Simulation Results

This paper presents some simulations investigating interference management by considering D2D communication in an underlying cellular network BS. A single macro cell is considered with the position of eNB base station at the center of the macro cell network, as discussed earlier. This simulation is set up to randomize the location of D2D devices 10 times in each simulation, throughout the macro cell network's coverage.
Table 1 shows the values of simulation parameters. The maximum and minimum transmit power of eNB and D2D equipment are set to 46 dBm and 26 dBm, respectively. The macro cell radius of eNB is set up to 900 m, which is typical of a cellular network in an urban area. In a cell edge situation, UL transmit power will be a big problem if each device uses the same frequency band, since devices that are far away from its pair will maximize the power level to maintain the communication link.

Table 1
Simulation parameters

Parameter	Value
Number of macro cell networks	1
Macro cell network radius	1000 m
Radius DUE (D2DT to D2DR)	100 m
Macro cell TX power (maximum)	46 dBm
UE TX power (maximum)	26 dBm
Frequency carrier	1800 MHz
Antenna pattern	Omni-directional
Channel bandwidth	10 MHz
Number of transmitters	1
Number of receivers	1
White noise spectral density	–174 dBm/Hz
Radius MUE to macro cell	0 s.d. 600 m
Radius D2DT to macro cell	600 s.d. 900 m

This simulation divides the coverage of the macro cell into two areas, cell center (0–600 m) and cell edge (600–900 m). The distance is measured from the base station eNB. For evaluating interference in DL and UL transmissions in this paper, both MUE and D2D devices pairs are randomly deployed at the edge of the cell (600–900 m). The system bandwidth is set to 10 MHz and the system noise is set to –174 dBm/Hz. The value of γ for AC1 is set to be 2 dB, and the SINR target is set to 0 dB, which corresponds to a SINR value typical for data traffic. Note that these experiments used software simulation and were repeated for 10 times. The average simulation results are shown in the graph.

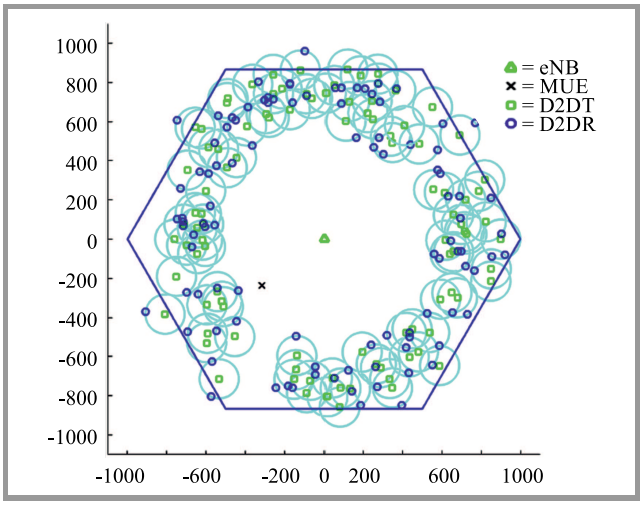

Fig. 2. Simulations of a single cellular network (eNB) with D2D deployment.

The first scenario investigates the power control scheme to manage SINR in a DL transmission. In this case, eNB in the center of a macro cell sends the signal to the MUE device, while D2D equipment (as D2DT) also transmits the signal to another piece of D2D equipment (D2DR). So, the transmission signal from D2DT will interfere with MUE. This scenario uses QoS parameters, such as level of SINR in the receiver part, measured on MUE devices in DL [16].

The second scenario involved an UL transmission, where MUE transmitted an UL signal to eNB, while D2DR equipment also transmitted a signal to D2DT equipment. So, the D2DR transmission signal interfered with the MUE signal uplink to eNB. This scheme utilized the same QoS parameters as used on the base station eNB in the first scheme.

Figure 2 shows the simulation scenario using a cellular network system with an eNB as a macro cell, MUE equipment and the number of D2D pairs increased to 100 devices. In a DL transmission, as shown in Fig. 3, the increased number of pieces of D2D equipment could decrease the SYSTEM's performance. With UE only, SINR values achieved approximately 30 dB for every power transmit method, without AC1 or AC2. If the number of D2D pairs was increased to 50, SINR dropped to about 25.5 dB, 25 dB, and 24 for AC1, AC2, and without power control (PC) or fixed power level (FC), respectively.

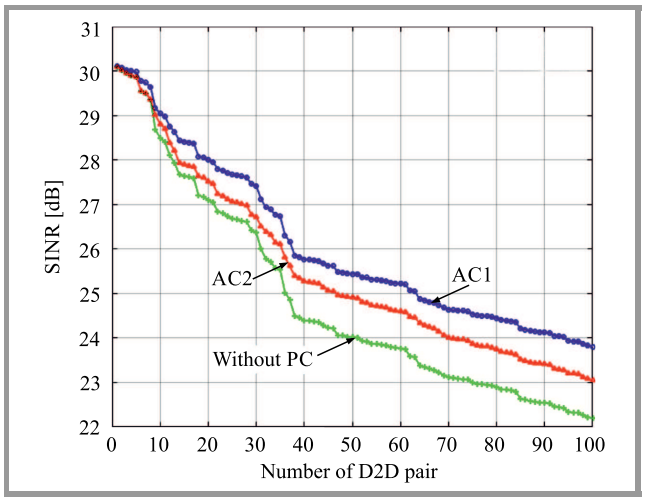

Fig. 3. SINR downlink values measured in a MUE as the number of increased D2D pairs, under a single cell scenario of a macro cell network without power control and with adaptive power control.

Figure 4 shows the result of UL transmission simulation. In this result, the increased number of pieces of D2D equipment also could decrease the system's performance. It can be noticed in Fig. 4 that when there is no interference at MUE, SINR achieves up to 18 dB for systems without PC, with AC1 and AC2 methods, respectively. When the number of D2D pairs equals 50 devices, SINR drops to about 2 dB and less than 0 when 100 D2D pairs are used without PC. With AC1 and AC2 implemented, SINR

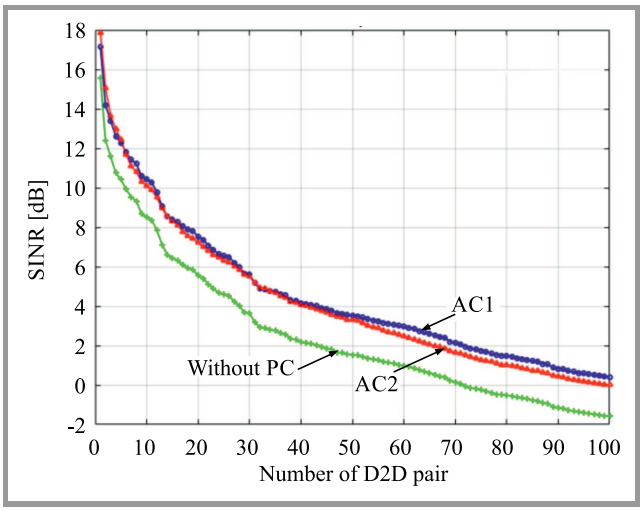

Fig. 4. SINR uplink values measured in eNB as the number of increased D2D pairs under a single cell scenario of a macro cell network with MUE, without power control and with AC1 and AC2 adaptive power control.

dropped to about 3.5 dB for both schemes and remained at above 0 when D2D communication setup involved 100 pairs within a macro cell network.

Based on those simulations, it can be noticed that AC1 and AC2 methods are capable of managing SINR performance, as shown in Figs. 3–4. These power control methods could work because the transmitter of each device adjusts the transmit power according to the estimated SINR and interference values. In summary, based on the result shown in Fig. 4, these power control methods can only manage up to 100 D2D pairs to ensure SINR level of up to 0 dB.

4. Conclusion

This paper investigates different power control methods used to mitigate interference between two or more user devices, with the number of D2D pairs equaling up to 100. The decision whether to increase or decrease the power level on BS or on the transmitter of the D2D pair is based on the estimated current SINR. The power control methods may be divided based on two aspects. The first of them is based on the fixed power level or uses no power control to manage the power level of the transmitter. The second uses adaptive power controls with two schemes (AC1 and AC2). Based on the measured SINR, the simulation results show that both power control methods contribute to managing SINR and network performance. AC1 and AC2 can improve SINR by up to 1 dB in each method compared to FC in both DL and UL transmissions.

Acknowledgements

The authors would like to thank Universitas Muhammadiyah Yogyakarta for supporting this research and Mr. Slamet Riyadi for his suggestions about this paper.

References

[1] A. Gupta and R. K. Jha, "A survey of 5G network: Architecture and emerging technologies", *IEEE Access*, vol. 3, pp. 1206–1232, 2015 (doi: 10.1109/ACCESS.2015.2461602).

[2] R.-G. Cheng, N.-S. Chen, Y.-F. Chou, and Z. Becvar, "Offloading multiple mobile data contents through opportunistic device-to-device communications", *Wirel. Personal Commun.*, vol. 84, no. 3, pp. 1963–1979, 2015 (doi: 10.1007/s11277-015-2492-1).

[3] P. Mach, Z. Becvar, and T. Vanek, "In-band device-to-device communication in ofdma cellular networks: A survey and challenges", *IEEE Commun. Surveys & Tutor.*, vol. 17, no. 4, pp. 1885–1922, 2015 (doi: 10.1109/COMST.2015.2447036).

[4] M. N. Tehrani, M. Uysal, and H. Yanikomeroglu, "Device-to-device communication in 5G cellular networks: Challenges, solutions, and future directions", *IEEE Commun. Mag.*, vol. 52, no. 5, pp. 86–92, 2014 (doi: 10.1109/MCOM.2014.6815897).

[5] A. Asadi, Q. Wang, and V. Mancuso, "A survey on device-to-device communication in cellular networks", *IEEE Commun. Surveys & Tutor.*, vol. 16, no. 4, pp. 1801–1819, 2014 (doi: 10.1109/COMST.2014.2319555).

[6] L. Wei, R. Hu, Y. Qian, and G. Wu, "Enable device-to-device communications underlaying cellular networks: Challenges and research aspects", *IEEE Commun. Mag.*, vol. 52, no. 6, pp. 90–96, 2014 (doi: 10.1109/MCOM.2014.6829950).

[7] S. T. Shah, S. F. Hasan, B.-C. Seet, P. H. J. Chong, and M. Y. Chung, "Device-to-device communications: A contemporary survey", *Wirel. Personal Commun.*, vol. 98, no. 1, pp. 1247–1284, 2018 (doi: 10.1007/s11277-017-4918-4).

[8] R. Yin, C. Zhong, G. Yu, Z. Zhang, K. K. Wong, and X. Chen, "Joint spectrum and power allocation for D2D communications underlaying cellular networks", *IEEE Trans. on Vehicular Technol.*, vol. 65, no. 4, pp. 2182–2195, 2016 (doi: 10.1109/TVT.2015.2424395).

[9] S. Y. Shin and T. A. Nugraha, "Cooperative water filling (CoopWF) algorithm for small cell networks", in *Proc. Int. Conf. on ICT Convergence ICTC 2013*, Jeju, South Korea, 2013, pp. 959–961 (doi: 10.1109/ICTC.2013.6675527).

[10] P. Mach and Z. Becvar, "Combined shared/dedicated resource allocation for device-to-device communication", *arXiv preprint arXiv:1711.01866*, 2017.

[11] N. Lee, X. Lin, J. G. Andrews, and R. W. Heath, "Power control for D2D underlaid cellular networks: Modeling, algorithms, and analysis", *IEEE J. on Selec. Areas in Commun.*, vol. 33, no. 1, pp. 1–13, 2015 (doi: 10.1109/JSAC.2014.2369612).

[12] Y. Jiang, Q. Liu, F. Zheng, X. Gao, and X. You, "Energy-efficient joint resource allocation and power control for D2D communications", *IEEE Trans. on Vehicular Technol.*, vol. 65, no. 8, pp. 6119–6127, 2016 (doi: 10.1109/TVT.2015.2472995).

[13] M. Susanto, H. Fitriawan, A. Abadik, and Herlinawati, "On the reduction of interference effect using power control for device-to-device communication underlying cellular communication network", in *Proc. Int. Conf. on Elec. Engin. and Comp. Sci. ICECOS 2017*, Palembang, Indonesia, 2017, pp. 28–32 (doi: 10.1109/ICECOS.2017.8167149).

[14] A. Ramezani-Kebrya, M. Dong, B. Liang, G. Boudreau, and S. H. Seyedmehdi, "Joint power optimization for device-to-device communication in cellular networks with interference control", *IEEE Trans. on Wirel. Commun.*, vol. 16, no. 8, pp. 5131–5146, 2017 (doi: 10.1109/TWC.2017.2706259).

[15] S. K. Pal, T. A. Nugraha, S. Shams, and A. Rahman, "Resource allocation strategy using optimal power control for mitigating two-tier interference in heterogeneous networks", in *Proc. Wirel. Commun. and Networking Conf. Worksh. WCNCW 2014*, Istanbul, Turkey, 2014, pp. 104–109 (doi: 10.1109/WCNCW.2014.69348769).

[16] V. Tikhvinskiy, G. Bochechka, and A. Gryazev, "QoS requirements as factor of trust to 5G network", *J. of Telecommun. and Inform. Technol.*, no. 1, pp. 3–8, 2016.

Toha Ardi Nugraha received his B.Sc. degree in Telecommunication Engineering from Telkom University, Indonesia, in 2011 and M.Sc. degree in IT Convergence Engineering from Kumoh National Institute of Technology, South Korea, in 2014. He joined the Department of Electrical Engineering, Universitas Muhammadiyah Yogyakarta, Indonesia, as a lecturer in 2016. He has worked at the R&D Center PT Telkom Indonesia in 2009–2012 as a research assistant. His current research interests include wireless and mobile networks, D2D, Li-Fi, and IoT.
E-mail: toha@ft.umy.ac.id
Universitas Muhammadiyah Yogyakarta
Jl. Brawijaya, Bantul
Yogyakarta 55183, Indonesia

Muhammad Putra Pamungkas received his B.Sc. degree in Electrical Engineering from Universitas Muhamadiyah Yogyakarta, Indonesia, in 2017. He is currently pursuing M.Sc. degree at the Department of Electrical Engineering, Institut Teknologi Bandung, Indonesia, with a focus on telecommunications. His research interests include computer networking, mobile communications, wireless networks and D2D communications.
E-mail: putrapamungkas.15031995@gmail.com
Universitas Muhammadiyah Yogyakarta
Jl. Brawijaya, Bantul
Yogyakarta 55183, Indonesia

Anna Nur Nazilah Chamim received her B.Sc. degree in Electrical Engineering from Universitas Muhammadiyah Yogyakarta, Indonesia in 2001, and M.Sc. degree from the Department of Electrical Engineering, Universitas Gadjah Mada, Indonesia in 2014. Since 2009 she has worked as a Head of Department of Telecommunication Engineering Politeknik PPKP Yogyakarta. She also worked as a lecturer at the Department of Electrical Eng., Universitas Muhammadiyah Yogyakarta. Her research interests include telecommunications, digital signal and image processing.
E-mail: anna_nnc@umy.ac.id
Universitas Muhammadiyah Yogyakarta
Jl. Brawijaya, Bantul
Yogyakarta 55183, Indonesia

Paper

Low Density Parity Check Codes Constructed from Hankel Matrices

Mohammed Amine Tehami and Ali Djebbari

Faculty of Electrical Engineering, Djillali Liabes University of Sidi Bel Abbes, Sidi Bel Abbès, Algeria

https://doi.org/10.26636/jtit.2018.121717

Abstract—In this paper, a new technique for constructing low density parity check codes based on the Hankel matrix and circulant permutation matrices is proposed. The new codes are exempt of any cycle of length 4. To ensure that parity check bits can be recursively calculated with linear computational complexity, a dual-diagonal structure is applied to the parity check matrices of those codes. The proposed codes provide a very low encoding complexity and reduce the stored memory of the matrix H in which this matrix can be easily implemented comparing to others codes used in channel coding. The new LDPC codes are compared, by simulation, with uncoded bi-phase shift keying (BPSK). The result shows that the proposed codes perform very well over additive white Gaussian noise (AWGN) channels.

Keywords—dual diagonal matrix, error correcting codes, girth, Hankel matrix, low density parity check codes.

1. Introduction

The field of error correcting codes was developed by introducing them into iterative decoding [1]. Nowadays, low density parity check (LDPC) codes are considered to the best solution, thanks to their considerable importance in error correcting performance and possibility to be represented by a specific parity check binary matrix $M \times N$ [2], [3]. The Tanner graph is a bipartite graph with two sets, i.e. the columns and the rows are depicted as follows: columns represent variable nodes, and rows represent check nodes. The edge is a connection between these two sets [4]. A cycle in the Tanner graph is defined as the path which starts and ends at the same node. If a cycle of this graph is considered, the minimum length of such a cycle is called girth [4]. LDPC codes are classified into two classes: regular, if the number of 1s in each row and column is constant, and irregular, if it varies [5], [6].

In this context, we present a special class of LDPC codes which benefit from low-complexity of decoding implementations due to the absence of cycle of length 4. Such a proposed construction has the following advantages:

- the proposed method guarantees that the constructing matrix avoids any cycles of length 4, which is essential for decoding simplicity,
- this method uses the permutation matrix, which makes the implementation easier, i.e. reduces the number of logical gates required and uses simple shift registers,
- a dual diagonal structure is applied to the parity check matrix of those codes, which ensures that parity check bits can be recursively implemented with linear computational complexity [7], [8].

The remainder of this paper is organized as follows. In Section 2, a description of the Hankel matrix and several conditions required to avoid a girth of length 4 is given. Section 3 presents the encoding concept and shows the advantages of the proposed construction of LDPC codes. Section 4 discusses the simulation results and, finally, Section 5 is devoted to conclusions.

2. Proposed Construction of Matrix

Girth is one of the most important keys that affect the performance of LDPC codes [1], [9]. Recent research indicates that small cycles affect the decoding complexity of these codes. Therefore, research on the construction of LDPC codes with a comparatively large girth, e.g. greater than 4, is still valuable for practical applications [6].

Let $\mathbf{H}$ be the parity check matrix $M \times N$ size, where M is the number of rows and N is the number of columns. It can be represented in the following form:

$$\mathbf{H} = [\mathbf{H}_1 \, \mathbf{H}_2] \, . \tag{1}$$

$\mathbf{H}_2$ is a dual diagonal matrix of size $M \times M$, which ensures that parity check bits can be recursively calculated with linear computational complexity [7], [8]. The proposed matrix $\mathbf{H}_1$ is of the square type, with $M \times M$ size and can be constructed as follows.

First, we use the Hankel matrix [10] where its elements (indexes) are:

$$a_{i,j} = i + j - 1 \, , \tag{2}$$

where i, j are the numbers of rows and columns respectively.

The structure of the Hankel matrix of size $m \times m$ [2] is:

$$\mathbf{H}_a = \begin{bmatrix} 1 & 2 & \dots & m \\ 2 & 3 & \dots & m+1 \\ \vdots & \vdots & \ddots & \vdots \\ m & m+1 & \dots & 2m-1 \end{bmatrix} , \tag{3}$$

with $M = m \times (m-1)$ and m restricted to an even number, greater than 2.
Next, by applying the process of symmetry in relation to an ascending diagonal m of matrix $\mathbf{H}_a$ a new $\mathbf{H}_b$ matrix is obtained:

$$\mathbf{H}_b = \begin{bmatrix} 1 & 2 & \dots & m \\ 2 & 3 & \dots & m-1 \\ \vdots & \vdots & \ddots & \vdots \\ m & m-1 & \dots & 1 \end{bmatrix}. \quad (4)$$

We also construct matrix $\mathbf{H}_b$ having the elements of $a_{i,j}, 1 \leq i \leq m$ and $1 \leq j \leq m$, and defined by:

$$a_{i,j} = \begin{cases} a_{i,j} \text{ of } \mathbf{H}_a & \text{if } i+j \leq m+1 \\ a_{(m+1)-i,(m+1)-j} & \text{otherwise} \end{cases}. \quad (5)$$

An example is given to clarify the analysis, with $m = 4$, $\mathbf{H}_b$ is:

$$\mathbf{H}_b = \begin{bmatrix} 1 & 2 & 3 & 4 \\ 2 & 3 & 4 & 3 \\ 3 & 4 & 3 & 2 \\ 4 & 3 & 2 & 1 \end{bmatrix}.$$

Each index of matrix $\mathbf{H}_b$ is assigned by sub-permutation matrices of size $(m-1) \times (m-1)$, and all indexes with a value equal to m are replaced by a zero matrix of size $(m-1) \times (m-1)$.
For $m = 4$, the sub-permutation matrices are given as follows. The sub-matrix of index '1' is an identity matrix.

$$\text{'1'} = \begin{bmatrix} 1 & 0 & 0 \\ 0 & 1 & 0 \\ 0 & 0 & 1 \end{bmatrix}$$

The sub-matrix of index '2' is a sub-identity matrix permuted once to the right.

$$\text{'2'} = \begin{bmatrix} 0 & 1 & 0 \\ 0 & 0 & 1 \\ 1 & 0 & 0 \end{bmatrix}$$

The sub-matrix of index '3' is a sub-identity matrix permuted twice to the right.

$$\text{'3'} = \begin{bmatrix} 0 & 0 & 1 \\ 1 & 0 & 0 \\ 0 & 1 & 0 \end{bmatrix}$$

The sub-matrix of index '4' is a zero matrix.

$$\text{'4'} = \begin{bmatrix} 0 & 0 & 0 \\ 0 & 0 & 0 \\ 0 & 0 & 0 \end{bmatrix}$$

To avoid repeating the sub-matrices in matrix $\mathbf{H}_b$, a choice of their size was performed.

A new matrix noted $\mathbf{H}_c$ is obtained as:

$$\mathbf{H}_c = \begin{bmatrix} 1 & 0 & 0 & 0 & 1 & 0 & 0 & 0 & 1 & 0 & 0 & 0 \\ 0 & 1 & 0 & 0 & 0 & 1 & 1 & 0 & 0 & 0 & 0 & 0 \\ 0 & 0 & 1 & 1 & 0 & 0 & 0 & 1 & 0 & 0 & 0 & 0 \\ 0 & 1 & 0 & 0 & 0 & 1 & 0 & 0 & 0 & 0 & 0 & 1 \\ 0 & 0 & 1 & 1 & 0 & 0 & 0 & 0 & 0 & 1 & 0 & 0 \\ 1 & 0 & 0 & 0 & 1 & 0 & 0 & 0 & 0 & 0 & 1 & 0 \\ 0 & 0 & 1 & 0 & 0 & 0 & 0 & 0 & 1 & 0 & 1 & 0 \\ 1 & 0 & 0 & 0 & 0 & 0 & 1 & 0 & 0 & 0 & 0 & 1 \\ 0 & 1 & 0 & 0 & 0 & 0 & 0 & 1 & 0 & 1 & 0 & 0 \\ 0 & 0 & 0 & 0 & 0 & 1 & 0 & 1 & 0 & 1 & 0 & 0 \\ 0 & 0 & 0 & 1 & 0 & 0 & 0 & 0 & 1 & 0 & 1 & 0 \\ 0 & 0 & 0 & 0 & 1 & 0 & 1 & 0 & 0 & 0 & 0 & 1 \end{bmatrix}$$

Many cycles of length 4 are included in $\mathbf{H}_c$ as depicted in the Tanner graph and shown in Fig. 1: Now, we can easily

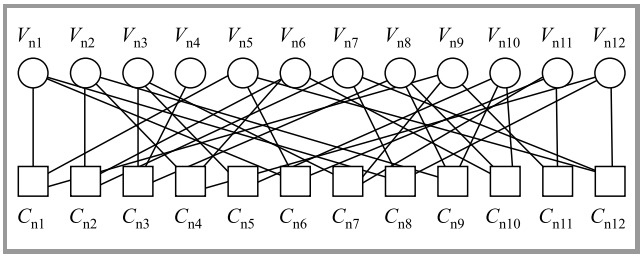

Fig. 1. The Tanner graph of $\mathbf{H}_c(12,3,3)$.

construct matrix $\mathbf{H}_1$ from $\mathbf{H}_c$ by applying the principle of activation on matrix $\mathbf{H}_b$ and using only two indexes (x and y) of matrix $\mathbf{H}_c$.
The sum of these two indexes is equal to the index which is situated on the ascending diagonal m, by applying:

$$x + y = m, \quad (6)$$

with x, y and m being the indexes of permutation matrices. For example, when $m = 4$, there are two combinations. This means that we can activate the indexes ($x = 1$ with $y = 3$), which helps obtain matrix $\mathbf{H}_1$.

$$\mathbf{H}_1 = \begin{bmatrix} 1 & 0 & 0 & 0 & 0 & 0 & 0 & 0 & 1 & 0 & 0 & 0 \\ 0 & 1 & 0 & 0 & 0 & 0 & 1 & 0 & 0 & 0 & 0 & 0 \\ 0 & 0 & 1 & 0 & 0 & 0 & 0 & 1 & 0 & 0 & 0 & 0 \\ 0 & 0 & 0 & 0 & 0 & 1 & 0 & 0 & 0 & 0 & 0 & 1 \\ 0 & 0 & 0 & 1 & 0 & 0 & 0 & 0 & 0 & 1 & 0 & 0 \\ 0 & 0 & 0 & 0 & 1 & 0 & 0 & 0 & 0 & 0 & 1 & 0 \\ 0 & 0 & 1 & 0 & 0 & 0 & 0 & 0 & 1 & 0 & 0 & 0 \\ 1 & 0 & 0 & 0 & 0 & 0 & 1 & 0 & 0 & 0 & 0 & 0 \\ 0 & 1 & 0 & 0 & 0 & 0 & 0 & 1 & 0 & 0 & 0 & 0 \\ 0 & 0 & 0 & 0 & 0 & 1 & 0 & 0 & 0 & 1 & 0 & 0 \\ 0 & 0 & 0 & 1 & 0 & 0 & 0 & 0 & 0 & 0 & 1 & 0 \\ 0 & 0 & 0 & 0 & 1 & 0 & 0 & 0 & 0 & 0 & 0 & 1 \end{bmatrix}$$

Hence, the matrix $\mathbf{H}$ can be represented as:

$$\mathbf{H} = \left[\begin{array}{cccccccccccccccccccccc}
1 & 0 & 0 & 0 & 0 & 0 & 0 & 0 & 1 & 0 & 0 & 0 & 1 & 0 & 0 & 0 & 0 & 0 & 0 & 0 & 0 & 0 & 0 & 0 \\
0 & 1 & 0 & 0 & 0 & 0 & 1 & 0 & 0 & 0 & 0 & 0 & 1 & 1 & 0 & 0 & 0 & 0 & 0 & 0 & 0 & 0 & 0 & 0 \\
0 & 0 & 1 & 0 & 0 & 0 & 0 & 1 & 0 & 0 & 0 & 0 & 0 & 1 & 1 & 0 & 0 & 0 & 0 & 0 & 0 & 0 & 0 & 0 \\
0 & 0 & 0 & 0 & 0 & 1 & 0 & 0 & 0 & 0 & 0 & 1 & 0 & 0 & 1 & 1 & 0 & 0 & 0 & 0 & 0 & 0 & 0 & 0 \\
0 & 0 & 0 & 1 & 0 & 0 & 0 & 0 & 0 & 1 & 0 & 0 & 0 & 0 & 0 & 1 & 1 & 0 & 0 & 0 & 0 & 0 & 0 & 0 \\
0 & 0 & 0 & 0 & 1 & 0 & 0 & 0 & 0 & 0 & 1 & 0 & 0 & 0 & 0 & 0 & 1 & 1 & 0 & 0 & 0 & 0 & 0 & 0 \\
0 & 0 & 1 & 0 & 0 & 0 & 0 & 0 & 1 & 0 & 0 & 0 & 0 & 0 & 0 & 0 & 0 & 1 & 1 & 0 & 0 & 0 & 0 & 0 \\
1 & 0 & 0 & 0 & 0 & 0 & 1 & 0 & 0 & 0 & 0 & 0 & 0 & 0 & 0 & 0 & 0 & 0 & 1 & 1 & 0 & 0 & 0 & 0 \\
0 & 1 & 0 & 0 & 0 & 0 & 0 & 1 & 0 & 0 & 0 & 0 & 0 & 0 & 0 & 0 & 0 & 0 & 0 & 1 & 1 & 0 & 0 & 0 \\
0 & 0 & 0 & 0 & 0 & 1 & 0 & 0 & 0 & 1 & 0 & 0 & 0 & 0 & 0 & 0 & 0 & 0 & 0 & 0 & 1 & 1 & 0 & 0 \\
0 & 0 & 0 & 1 & 0 & 0 & 0 & 0 & 0 & 0 & 1 & 0 & 0 & 0 & 0 & 0 & 0 & 0 & 0 & 0 & 0 & 1 & 1 & 0 \\
0 & 0 & 0 & 0 & 1 & 0 & 0 & 0 & 0 & 0 & 0 & 1 & 0 & 0 & 0 & 0 & 0 & 0 & 0 & 0 & 0 & 0 & 1 & 1
\end{array}\right]$$

3. Encoding Concept

Gallager has shown that codes of column-weight-two have a minimum distance increasing logarithmically with code length, compared to a linear increase when the column weight is at least three [1]. Despite the low increase in minimum distance, these codes have shown good potential in some applications, such as partial response channels [11], [12] and also require less computation due to column weight.

Although LDPC code performance is high, the hardware implementation still remains a challenge due to the large size and complex random (unstructured) row-column connections [13]. This complexity has been reduced by using structured codes [13]. However, the girth (smallest cycle) has been reduced by using a constraint over row-column connections [14]. It has been shown that if the girth increases, the decoding performance is higher [15], [16].

LDPC codes are linear codes. Thus, they can be expressed as the null space of a parity check matrix $\mathbf{H}$ [2]. Considered c as a codeword written as $c = [d\ p]$, where d and p are the data and parity bits respectively. The parity relationship can be written as [17]:

$$\mathbf{H}c^T = 0^T\,. \tag{7}$$

In the proposed method, $\mathbf{H}$ is decomposed into $\mathbf{H} = [\mathbf{H}_1\ \mathbf{H}_2]$, such that:

$$[\mathbf{H}_1\ \mathbf{H}_2][d\ p]^T = 0^T\,, \tag{8}$$

$$\mathbf{H}_1 d^T = \mathbf{H}_2 p^T\,, \tag{9}$$

$$p^T = (\mathbf{H}_2^{-1}\mathbf{H}_1)d^T\,, \tag{10}$$

where $\mathbf{H}_2$ is the dual diagonal matrix and $\mathbf{H}_1$ is built deterministically, as seen above.

Based on the structure of $\mathbf{H}_2$ and Eq. (8), the parity check bits $p = \{p_i\}$ can be easily computed from a given data $d = \{d_i\}$ and matrix $\mathbf{H}_1$ as in [18]:

$$p_1 = \sum_j h1_j d_j\,, \tag{11}$$

$$p_i = p_{i-1} + \sum_j h_{ij}^1 d_j \bmod 2\,, \tag{12}$$

where h_{ij}^1 are the elements of $\mathbf{H}_1$.

In [18], a comparative study with an LDPC code defined from a randomly generated parity check matrix [6] has shown that if $\mathbf{H}$ is brought into $[\mathbf{H}_2, \mathbf{H}_1]$, and $\mathbf{H}_2$ has a dual diagonal structure, several advantages are obtained:

- there is no need of Gaussian elimination for the encoding process,
- $\mathbf{H}_2$ is always non-singular i.e. $\mathbf{H}_2$ is always invertible,
- if $\mathbf{H}_1$ is sparse, it requires very little memory to store $\mathbf{H}$ in the encoder.

Besides the advantages cited above, there are two other advantages offered by the proposed construction:

- $\mathbf{H}_1$ is effectively sparse, comprising largely 0s $\left(\frac{M-w}{M}\right)$ and has a low density of 1s $\left(\frac{w}{M}\right)$ where w is the weight (number of ones in each column or row) of $\mathbf{H}_1$, which ensures a very low encoding complexity [19];
- The particularity structure of the obtained matrix $\mathbf{H}_1$ (can be built from identity sub-matrix only, with some permutations) considerably reduces memory usage.

4. Simulation Results

Monte Carlo simulations were used to estimate the bit error rate (BER) of an LDPC code. Iterative belief propagation and additive white Gaussian Noise (AWGN) were applied as the decoding algorithm and channel, respectively. For simulation purposes, we used the rate $R = \frac{1}{2}$ and block length $N = 4324$. This simulation is running for at least 1000 code words and the maximum iteration is 80.

The performance of uncoded BPSK is presented with the aim of comparing it with coded BPSK, using the new LDPC code and other LDPC codes. The signal to noise ratios (SNR) for the coded BPSK and the uncoded BPSK are defined, as in [20], with the first one being:

$$SNR_1 = 10\log\frac{E_b}{2\sigma^2 R} \tag{13}$$

and the other one defined as:

$$SNR_2 = 10\log\frac{E_b}{2\sigma^2}. \tag{14}$$

Figure 2 represents BER performance of the proposed LDPC codes and of uncoded BPSK with $N = 4324$, $j = 2$ (j represents the weight of columns) and $R = \frac{1}{2}$.

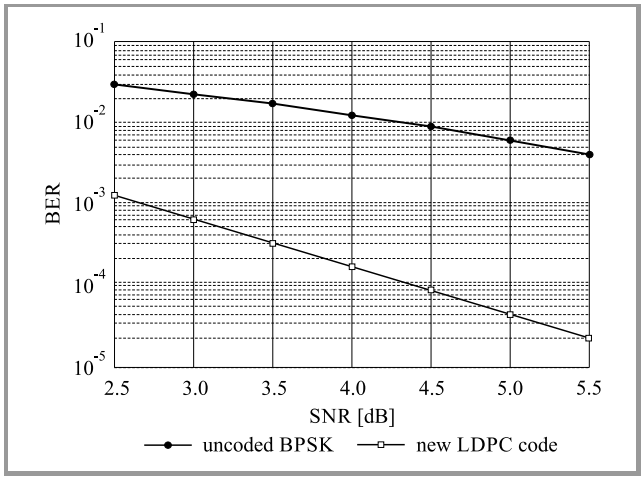

Fig. 2. BER of the proposed LDPC codes and uncoded BPSK with $N = 4324$, $j = 2$ and $R = \frac{1}{2}$.

From Fig. 2, we can observe that the new LDPC code offers better performances compared to the uncoded BPSK transmission. At BER= 10^{-3}, the obtained gain is about 1.9 dB.

Table 1 shows the comparison of BER performance of the proposed LDPC codes, with $N = 4324$, $j = 2$ with three others codes: Random codes, GB-(Geometry Based) LDPC and TS-(Turbo-Structured) LDPC codes [20].

Table 1
BER performance of the proposed LDPC codes with Random codes, GB-LDPC codes and TS-LDPC codes.

BER	Proposed LDPC codes	Random codes [20]	GB-LDPC codes [20]	TS-LDPC codes [20]
	E_b/N_0			
10^{-3}	2.5	3	3	3
10^{-4}	4	4	4	3.8

From Table 1, it can be observed that the proposed codes exhibit a performance gain of about 0.5 dB compared to Random, GB-LDPC and TS-LDPC codes at BER of 10^{-3}. At BER of 10^{-4}, the proposed LDPC codes provide the same performance when compared to the unstructured Random codes, GB-LDPC codes and offer a loss in gain of about 0.2 dB when compared to the TS-LDPC codes. From this, we can say that the proposed LDPC codes can reach the error floor region, for long length. The results demonstrate that the proposed LDPC codes, having a uniform structure and low complexity when it comes to hardware implementation (reduced logic gates and the use of simple shift registers), offer an error rate performance that is slightly better than that of more complex unstructured LDPC codes.

5. Conclusion

In this paper, we have presented a method of constructing a parity check matrix of an LDPC code. The main advantage of such a method is its ability to demonstrate how to avoid girth of length 4 by using the Hankel matrix. Also, a dual diagonal structure is applied to parity check matrices, which ensures that parity check bits can be recursively calculated with linear computational complexity

References

[1] R. G. Gallager, "Low-density parity-check codes", *IRE Transact. Inform. Theory*, vol. 8, no. 1, pp. 21–28, 1962 (doi: 10.1109/TIT.1962.1057683).

[2] W. Sulek, "Seed Graph Expansion for Construction of Structured LDPC Codes", in *Proc. 6th Int. Sym. on Wireless Commun. Sys. ISWCS*, Siena, Italy, 2009, pp. 216–220 (doi: 10.1109/ISWCS.2009.5285248).

[3] D. Xia, H. He, Y. Xu, and Y. Cai, "A novel construction scheme with linear encoding complexity for LDPC codes", in *Proc. 4th Int. Conf. on Wireless Commun. Network. and Mob. Comput.*, Dalian, Liaoning, China, 2008, pp. 1–4 (doi: 10.1109/WiCom.2008.358).

[4] R. Tanner, "A recursive approach to low complexity codes", *IEEE Transact. Inform. Theory*, vol. 27, no. 5, pp. 533–547, 1981 (doi: 10.1109/TIT.1981.1056404).

[5] Y. Abid, O. Sidek, M. F. M. Salleh, and F. Ghani, "A new quasi-cyclic low density parity check codes", in *Proc. 2009 IEEE Sym. on Indust. Electron. & Applic.*, Kuala Lumpur, Malaysia, 2009, pp. 239–242 (doi: 10.1109/ISIEA.2009.5356472).

[6] D. J. C. MacKay, "Good codes based on very sparse matrices", *IEEE Transact. Inform. Theory*, vol. 45, no. 2, pp. 399–431, 1999 (doi: 10.1109/18.748992).

[7] Q. Guo-lei and Z. Dong, "Design of structured LDPC codes with quasi-cyclic and rotation architecture", in *Proc. 2010 3rd Int. Conf. on Adv. Comput. Theory and Engineer. ICACTE*, Chengdu, Sichuan, China, 2010, pp. 655–657 (doi: 10.1109/ICACTE.2010.5578934).

[8] M. Yang, W. E. Ryan, and Y. Li, "Design of efficiently encodable moderate length high-rate irregular LDPC codes", *IEEE Trans. Commun.*, vol. 52, no. 4, pp. 564–571, 2004 (doi: 10.1109/TCOMM.2004.826367).

[9] K. Liu, Z. Fei, J. Kuang, and X. Li. "A novel algorithm for removing cycles in quasi-cyclic LDPC codes", in *Proc. 2009 IEEE 20th Int. Sym. on Person. Indoor and Mob. Radio Commun.*, Tokyo, Japan, 2009, pp. 1054–1058 (doi: 10.1109/PIMRC.2009.5450003).

[10] A. Ahmed and Y. F. Hu, "3M Relationship Pattern for Detection and Estimation of Unknown Frequencies for Unknown Number of Sinusoids Based on Eigenspace Analysis of Hankel Matrix", in *IET 2nd Intel. Sig. Process. Conf. 2013 ISP 2013*, London, UK, 2013, pp. 1–6 (doi: 10.1049/cp.2013.2058).

[11] H. Song, J. Liu, and B. V. K. V. Kumar, "Low complexity LDPC codes for partial response channels", in *Proc. IEEE Global Telecommun. Conf. GLOBECOM'02*, Taipei, Taiwan, 2002, vol. 2, pp. 1294–1299 (doi: 10.1109/GLOCOM.2002.1188406).

[12] H. Song, J. Liu, and B. V. K. V. Kumar, "Large girth cycle codes for partial response channels", *IEEE Transact. on Magnet.*, vol. 40, no. 4, part 2, pp. 3084–3086, 2004 (doi: 10.1109/TMAG.2004.829197).

[13] G. Malema and M. Liebelt, "Quasi-cyclic LDPC codes of column-weight two using a search algorithm", *EURASIP J. Adv. Sig. Process.*, vol. 2007, no. 4, pp. 1–8, 2007 (doi: 10.1155/2007/45768).

[14] M. P. C. Fossorier, "Quasi-cyclic low-density parity-check codes from circulant permutation matrices", *IEEE Transact. Inform. Theory*, vol. 50, no. 8, pp. 1788–1793, 2004 (doi: 10.1109/TIT.2004.831841).

[15] M. E. O'Sulivan, "Algebraic construction of sparse matrices with large girth", *IEEE Transact. Inform. Theory*, vol. 52, no. 2, pp. 718–727, 2006 (doi: 10.1109/TIT.2005.862120).

[16] Y. Mao and A. H. Banihasherni, "A heuristic search for good low-density parity-check codes at short block lengths", *in Proc. IEEE Int. Conf. on Commun. ICC'01*, Helsinki, Finland, vol. 1, 2001, pp. 41–44 (doi: 10.1109/ICC.2001.936269).

[17] T. J. Richardson and R. L. Urbanke, "Efficient encoding of low-density-parity-check codes", *IEEE Transact. Inform. Theory*, vol. 47, no. 2, pp. 638–656, 2001 (doi: 10.1109/18.910579).

[18] L. Ping, W. K. Leung, and N. Phamdo, 'Low density parity check codes with semi-random parity check matrix", *Electron. Let.*, vol. 35, no. 1, pp. 38–39, 1999 (doi: 10.1049/el:19990065).

[19] Z. Hao and Z. Tong, "Block-LDPC: a partial LDPC coding system design approach", *IEEE Transact. Circuits Sys. I*, vol. 52, no. 4, pp. 766–775, 2005 (doi: 10.1109/TCSI.2005.844113).

[20] J. M. F. Moura, J. Lu, and H. Zhang, "Structured low-density-parity-check codes", *IEEE Sig. Process. Mag.*, vol. 21, no. 1, pp. 42–55, 2004 (doi: 10.1109/MSP.2004.1267048).

Mohammed Amine Tehami received his B.Sc. and M.Sc. from the Department of Electronics, University of Djilali Liabes, Sidi Bel Abbès, (Algeria) in 2009 and 2011, respectively. He worked as a Research Scientist specializing in LDPC code construction at (LTTNS) Telecommunication and Digital Signal Processing Laboratory, Sidi Bel Abbès. He is interested in channel coding, as well as construction and analysis of LDPC codes.
E-mail: Chahoub_88@yahoo.com
Faculty of Electrical Engineering
Djillali Liabes University of Sidi Bel Abbes
Sidi Bel Abbès, Algeria

Ali Djebbari – for biography, see this issue, p. 8.

Paper

Incoherent Discriminative Dictionary Learning for Speech Enhancement

Dima Shaheen, Oumayma Al Dakkak, and Mohiedin Wainakh

Telecommunications Department, Higher Institute for Applied Science and Technology HIAST, Damascus, Syria

https://doi.org/10.26636/jtit.2018.121317

Abstract—Speech enhancement is one of the many challenging tasks in signal processing, especially in the case of non-stationary speech-like noise. In this paper a new incoherent discriminative dictionary learning algorithm is proposed to model both speech and noise, where the cost function accounts for both "source confusion" and "source distortion" errors, with a regularization term that penalizes the coherence between speech and noise sub-dictionaries. At the enhancement stage, we use sparse coding on the learnt dictionary to find an estimate for both clean speech and noise amplitude spectrum. In the final phase, the Wiener filter is used to refine the clean speech estimate. Experiments on the Noizeus dataset, using two objective speech enhancement measures: frequency-weighted segmental SNR and Perceptual Evaluation of Speech Quality (PESQ) demonstrate that the proposed algorithm outperforms other speech enhancement methods tested.

Keywords—ADMM, l1 minimization algorithms, sparse coding, speech enhancement, supervised dictionary learning.

1. Introduction

Digital speech is a communication tool that is most frequently used by humans, especially with the proliferation of Voice over the Internet (VoIP) telephony software. Speech can be corrupted by various factors: noise (additive, multiplicative), reverberation (convolutive noise), and interfering speech. Speech enhancement aims to boost its quality. This enhancement involves two quality factors: "speech pleasantness", which refers to how comfortable it is for humans to listen to the speech signal over a prolonged period of time, and "speech intelligibility", which refers to how understandable the speech is (word error rate). Noise is the most common factor that causes speech degradation. Speech de-noising algorithms constitute a major part of the enhancement methods that aim to extract a clean speech signal from a noisy mix. It is a challenging task, as it is hard to remove noise efficiently without distorting the clean signal.

The problem we are tackling in this paper is single channel speech de-noising that deals with non-stationary noise. Mathematically, this problem aims to reconstruct the clean speech signal $s(n)$, based on the received signal $y(n)$ which is an additive mixture of the two unknown signals: the clean speech and a non-stationary noise signal $i(n)$:

$$y(n) = s(n) + i(n)\,. \tag{1}$$

The significance of this problem is based on the fact that communication takes place, nowadays, in noisy environments, such as at airports, in the street or inside a car. The noise in these environments is non-stationary, which means that its statistic values are changing over time. It is crucial to provide the user with a good quality speech, so they can understand others and listen to them comfortably, using communication tools, in these hostile environments. In fact, there are many applications that use speech de-noising algorithms in these adverse environments, such as mobile communications, VoIP, hearing aids and speech recognition software.

Traditional speech enhancement methods, like spectral subtraction (SS) [1], [2], Wiener filtering [3], statistical model-based methods [4] and subspace methods Singular Spectrum Analysis (SSA) [5], [6] perform well in the case of white noise, but have limited performance in the case of non-stationary speech-like noise. SS is based on estimating the noise power spectrum and subtracting it from the noisy power spectrum. The main issue with SS is the generation of isolated peaks in the estimated clean speech spectrum, which is referred to as musical noise. Statistical model-based methods assume that speech and noise obey some probability distribution and propose a least square estimator to estimate the signal. In both cases it is hard to find a good estimate for the noise power spectrum in the case of non-stationary noise. All these methods are unsupervised, which means that they do not use any prior information about the noise and speech. Recently, new supervised methods incorporating prior information to build a model for both speech and noise signals using training samples, have been proposed. These methods achieve better results than non-supervised methods.

Codebook-based approaches [7], [8], Hidden Markov Model (HMM) based approaches [9]–[11], supervised non-negative matrix factorization (NMF) [12]–[14] and sparsity-based method [15]–[19] are examples of supervised speech enhancement approaches. Srinivasan *et al.* [8] used vector quantization to learn codebooks for both speech and noise

LPC features. At the enhancement stage, the closest pair in terms of minimum Itakaru-Saito distance between the noisy power spectrum and linear combination of the speech and noise pair is picked and used as estimators. Mohammadabad *et al*. [14] proposed Bayesian NMF for speech enhancement, where the training data is decomposed into two matrices: bases matrix and activation matrix, while at the enhancement stage the noisy mixture is projected on the concatenation of the two matrices.

Motivated by the great success of the sparsity based signal model achieved in many signal processing tasks, and notably image de-noising [20], Sigg [15] proposed using the approximate K-Singular Value Decomposition (K-SVD) [21], [22] dictionary learning to model the amplitude spectrum of clean speech and noise separately, and then concatenating both dictionaries in one to perform speech enhancement.

Zhao *et al*. [16] proposed using the same K-SVD with a non-negative constraint at the sparse coding stage to learn a dictionary that models the Power Spectral Density (PSD) of clean speech, and used the Least Angle Regression LARS algorithm [34] to find the sparse code of the noisy speech on the learned dictionary. Then, the clean speech PSD estimate is found based on multiplication of the sparse code with the dictionary. Luo *et al*. [17] proposed a complementary joint sparse representation, where two mixture dictionaries to model "mixture and speech" and "mixture and noise" are added to the Generative Dictionary Learning (GDL) problem formulation, and sparse codes of clean speech are forced to represent the noisy mixture on the mixture and clean speech sub-dictionary, while the sparse codes for the noise are forced to represent the noisy mixture on the mixture and noise sub-dictionary. Though this joint sparse representation alleviates, to some extent, the problem of source confusion, it is characterized by high complexity due to the need of learning four sub-dictionaries instead of two.

In the previous studies, "signal approximation" only is considered in the cost function when learning the representative dictionaries, while *source confusion* and *incoherence* between speech and noisy sub-dictionaries are not taken into account in the dictionary learning process. Source confusion means that part of the noise that is coherent with clean speech will have sparse representation over the clean speech dictionary (noise confusion), and part of the clean speech will have sparse representation over the noise dictionary (speech confusion), and thus, residual noise corresponding to noise confusion might still exist in the estimated clean speech at the enhancement stage, which will also suffer from extra distortion from the original clean speech due to the fact that part of it will be omitted as it will be considered as noise. Incoherence refers to the maximum correlation between any two columns of speech and noise dictionaries. As shown in [15], incoherence is directly related to the degree of sparsity (number of non-zero elements) needed for the speech and noise signals to achieve exact recovery by their sparse projection on their corresponding sub-dictionaries. High coherence means a low sparsity degree, which cannot be verified in practice, and thus we are interested in low coherence dictionary.

In this paper, we propose a new Incoherent Discriminative Dictionary Learning (IDDL) algorithm to model both speech and noise jointly. We impose a coherence penalty on the speech and noise sub-dictionaries in the cost function, which also incorporates: a penalty for "speech confusion" when learning the noise sub-dictionary, and a penalty for "noise confusion" when learning the clean speech sub- dictionary. We use the Alternating Direction Method of Multipliers (ADMM) [35] to solve the two sub-dictionaries' learning optimization problems.

The paper is organized as follows. In Section 2 a review of the main problems is provided: dictionary learning algorithms and speech enhancement using sparse coding. In Section 3, the proposed IDDL algorithm is described, along with the overall proposed speech enhancement system. In Section 4, the conducted experiments and their results are presented. Section 5 summarizes and concludes the paper.

2. Problem Review

$\mathbf{Y} \in \mathbb{R}^{N\times n}$ is the matrix whose columns are the n training samples $\mathbf{y}_i \in \mathbb{R}^N$ (N is the dimension of the input signals. In the context of speech enhancement, the input signals $\mathbf{y}_i$ are the amplitude spectrum of every speech frame i, and thus, N is the number of FFT coefficients[1]), $\mathbf{D} \in \mathbb{R}^{N\times K}$ is the dictionary matrix whose columns are K prototype signals that can represent signals of interests *sparsely* (i.e. using a linear combination of a low number of these prototype signals denoted by $\mathbf{d}_i$), $\mathbf{X} \in \mathbb{R}^{k\times n}$ is the matrix whose columns $x_i \in \mathbb{R}^K$ are the sparse codes of $\mathbf{y}_i$. In our setting, $\mathbf{Y}$ contains the extracted features (amplitude of FFT coefficients) of the training audio frames (either clean speech or noise), composed of $\mathbf{Y}_s \in \mathbb{R}^{N\times n_s}$ speech training samples (n_s is the number of clean speech training frames), and $\mathbf{Y}_n \in \mathbb{R}^{N\times n_n}$ the noise training samples (n_n is the number of noise training frames). $\mathbf{X}_s \in \mathbb{R}^{K\times n_s}$ is the sparse codes of $\mathbf{Y}_s$, and $\mathbf{X}_n \in \mathbb{R}^{K\times n_n}$ the sparse codes of $\mathbf{Y}_n$. $\mathbf{D}$ is the concatenation of $\mathbf{D}_s \in \mathbb{R}^{N\times L}$ and $\mathbf{D}_n \in \mathbb{R}^{N\times L}$ the dictionary matrices for representation of the clean speech signal and the noise signal, respectively. They have the same number of columns denoted by L. Clearly in this case $= 2L$, and the total number of training samples $n = n_s + n_n$. $\mathbf{X}_s^s$ are the sparse coefficients of $\mathbf{X}_s$ on $\mathbf{D}_s$, $\mathbf{X}_s^n$ are the sparse coefficients of $\mathbf{X}_s$ on $\mathbf{D}_n$.$\mathbf{X}_n^n$ are the sparse coefficients of $\mathbf{X}_n$ on $\mathbf{D}_n$, and $\mathbf{X}_n^s$ are the sparse coefficients of $\mathbf{X}_n$ on $\mathbf{D}_s$.

2.1. Dictionary Learning

Sparsity-based signal model approximates a signal by a linear combination of a few basic signals out of a larger collection of signals that form what is called the dictionary. In

[1] In fact we take only half of the number of FFT coefficients because of symmetry, so $N = \frac{NFFT}{2} + 1$.

a classic dictionary learning problem, we seek a matrix $\mathbf{D}$ whose columns are the basic signals that can represent, as close as possible, the training signals $\mathbf{y}_i$ *sparsely*:

$$\min_{\mathbf{D},\mathbf{X}} \sum_{i=1}^{n} \left\|\mathbf{y}_i - \mathbf{D}\mathbf{x}_i\right\|_2^2 \quad \text{s.t.} \quad \forall i, \left\|\mathbf{x}_i\right\|_0 \leq k \ , \tag{2}$$

where k is the maximum number of non-zero elements in $\mathbf{x}_i$, $\|\mathbf{x}_i\|_0$ is ℓ_0 a pseudo norm which represents the number of non-zeros in $\mathbf{x}_i$. $\mathbf{X}$ is the matrix composed of all the sparse codes $\mathbf{x}_i$.

This optimization problem is non-convex when both $\mathbf{D}$ and $\mathbf{X}$ are unknown, however it becomes convex if one of $\mathbf{D}$ or $\mathbf{X}$ is fixed – that is why it is generally solved iteratively by fixing the dictionary $\mathbf{D}$ and updating sparse codes $\mathbf{X}$, and then fixing $\mathbf{X}$ and updating $\mathbf{D}$.

In fact, dictionary learning is a generalization of the k-means clustering algorithm [21], the only difference is that in k-means, each training signal is forced to use only one "atom" from the dictionary (the closest cluster center), as its representative, while in dictionary learning each signal is allowed to use multiple dictionary atoms, provided that it can be approximated by a linear combination of these atoms, and that this linear combination uses as few the dictionary atoms as possible.

In k-means, we iterate between finding the representative of each training signal (the cluster center which is equivalent to the dictionary atom that minimizes the suitable metric distance), and updating the cluster centers. However, dictionary learning is solved by iterating between two stages [21]. First, the dictionary is fixed and the sparse code $\mathbf{x}_i$ for each training signal is calculated using any sparse coding solver. Then, the sparse code is fixed and the dictionary atoms are updated to minimize the cost function.

The method used to update the dictionary atoms is the key difference between individual dictionary learning algorithms. Some dictionary learning methods update, in each iteration, the whole set of atoms. This is the case in one of the early and simple dictionary learning solutions – Method of Optimal Direction (MOD) [23], which updates the whole dictionary using the closed form of the Mean Squared Error (MSE) estimator:

$$\mathbf{D} = \mathbf{Y}\mathbf{X}^T(\mathbf{X}\mathbf{X}^T)^{-1} \ . \tag{3}$$

Other dictionary learning algorithms update the dictionary atoms successively, one by one, as is the case in the very famous and successful dictionary learning algorithm known as K-Singular Value Decomposition (K-SVD) [21]. At the sparse coding stage, K-SVD uses greedy Orthogonal Matching Pursuit (OMP) [32], [33] to find the sparse code for each training sample. At the dictionary update stage, in turn, for each dictionary atom $\mathbf{d}_k$, K-SVD selects only those training samples that use this atom, which will be denoted as $\mathbf{x}^k$, and splits the representation error E into two components: the sparse representation on $\mathbf{d}_k$, and the residual error $\mathbf{E}_k$ that accounts for the sparse presentation error using all the dictionary atoms other than $\mathbf{d}_k$:

$$\begin{aligned}\mathbf{E} &= \left\|\mathbf{Y} - \mathbf{D}\mathbf{X}\right\|_F^2 = \left\|\mathbf{Y} - \sum_{i=1}^{K} \mathbf{d}_i \mathbf{x}_T^i\right\|_F^2 \\ &= \left\|\left(\mathbf{Y} - \sum_{\substack{i\neq k \\ i=1}} \mathbf{d}_i \mathbf{x}_T^i\right) - \mathbf{d}_k \mathbf{x}_T^k\right\|_F^2 = \left\|\mathbf{E}_k - \mathbf{d}_k \mathbf{x}_T^k\right\|_F^2 \ , \end{aligned} \tag{4}$$

where $\mathbf{x}_T^i$ represents the sparse coefficients corresponding to the atom $\mathbf{d}_i$, which is the i-th row of the matrix $\mathbf{X}$. As the rows $\mathbf{x}_T^k$ are all zeros except for the indexes of the test examples in $\mathbf{Y}$ that use atoms $\mathbf{d}_k$ $\mathbf{d}_k\mathbf{x}_T^k$ does not affect the whole $\mathbf{E}_k$, but only the *restricted* $\mathbf{E}_k^R$ which is composed of the columns of $\mathbf{E}_k$ that correspond to the examples that use $\mathbf{d}_k$.

To update $\mathbf{d}_k$ and $\mathbf{x}_T^k$ in a way that minimizes the restricted error $\mathbf{E}_k^R$ (which is the only part of the total error representation $\mathbf{E}$ that is affected by atom $\mathbf{d}_k$), K-SVD evaluates the Singular Value Decomposition (SVD) for $\mathbf{E}_k^R = \mathbf{U}\mathbf{\Delta}\mathbf{V}^T$ (where $\mathbf{U}$ and $\mathbf{V}$ are orthonormal matrices, and Δ is a diagonal matrix with non-negative elements on the diagonal known as *eigen* values), and updates $\mathbf{d}_k$ with the first column of $\mathbf{U}$, simultaneously updating the corresponding sparse coefficients $\mathbf{x}_T^k$ as the first column of $\mathbf{V}$ multiplied by $\mathbf{\Delta}(1,1)$ [21].

The cost function in Eq. (4) measures the representation power of dictionary $\mathbf{D}$ only. In the case of a classification task, discriminative power of the sparse code $\mathbf{x}$ should be considered. This leads to a new trend in dictionary learning algorithms called "discriminative" or "supervised" dictionary learning in which the cost function reflects both the representation and classification error. Suo [24] has proposed the most general formulation of the discriminative dictionary learning problem, given below:

$$\min_{\mathbf{D},\mathbf{X}} \sum_{i=1}^{n} \left(\left\|\mathbf{y}_i - \mathbf{D}\mathbf{x}_i\right\|_2^2 + \lambda_1 \left\|\mathbf{x}_i\right\|_1\right) + \lambda_2 f_{\mathbf{x}}(\mathbf{X}) + \lambda_3 f_{\mathbf{D}}(\mathbf{D}) \ , \tag{5}$$

where $f_{\mathbf{X}}(\mathbf{X})$ is a function that measures the discriminative power of the sparse codes $\mathbf{X}$, and $f_{\mathbf{D}}(\mathbf{D})$ is a function that measures the discrimination power of the atoms of $\mathbf{D}$.

Discriminative dictionary learning algorithms fall into one of three categories, depending on the values of λ_2, λ_3. In the first category ($\lambda_3 = 0$), a dictionary shared by all classes is learned, while forcing the sparse codes to be discriminative. For example, Mairal *et al*. [25] proposed to add a logistic loss function to the sparse code, as a discriminative measure. Zhang *et al*. proposed Discriminative K-SVD (D-KSVD) [26] that adds a linear regression term to learn a linear classifier on the sparse coefficients to the objective function in the dictionary learning problem formulation (6), while in the case of label consistent-KSVD (LC-KSVD) [27], a label consistency term is added that measures how consistent the sparse codes are with the class labels.

In the second category ($\lambda_2 = 0$), only the discriminative power of the dictionary atoms is considered. For example,

Ramirez *et al*. [28] proposed learning class-specific sub-dictionaries for each class with a structural incoherence penalty term to make the sub-dictionaries as independent as possible.

A hybrid discriminative dictionary learning forms the third category, where both the dictionary atoms and the sparse codes are forced to be discriminative ($\lambda_2 \neq 0,\ \lambda_3 \neq 0$). It is the case in the COPAR dictionary learning algorithm [29] and Fisher discriminative dictionary learning (FDDL) [30].

FDDL uses label information both in the dictionary update and sparse coding stage. In FDDL, the sparse codes of the training samples are forced to have low within-class scatter, but large between-class scatter. Also, each class-specific sub-dictionary is forced to have good reconstruction capability for the training samples from that class, but poor reconstruction capability for other classes. Therefore, both the representation residual and the representation coefficients of the query sample are discriminative. Thus, the dictionary learning optimization problem is formulated, in FDDL, as follows:

$$\min_{\mathbf{D},\mathbf{X}} \mathrm{r}(\mathbf{Y},\mathbf{D},\mathbf{X}) + \lambda_1 \left\|\mathbf{X}\right\|_1 + \lambda_2 f_{\mathbf{X}}(\mathbf{X}) \quad \text{s.t.} \quad \left\|\mathbf{d}_i\right\|_2 = 1, \quad \forall i \in \{1 \ldots L\} \ , \tag{6}$$

where $\mathrm{r}(\mathbf{Y},\mathbf{D},\mathbf{X})$ is a cost function that measures the discriminative power of dictionary $\mathbf{D}$, $\|\mathbf{X}\|_1$ is the sparsity inducing term, and $f_{\mathbf{X}}(\mathbf{X})$ is the cost function that measures the discriminative power of the sparse codes $\mathbf{X}$.

The cost function that imposes discrimination of atoms of dictionary $\mathbf{D}$ is defined as:

$$\mathrm{r}(\mathbf{Y}_i,\mathbf{D},\mathbf{X}_i) = \left\|\mathbf{Y}_i - \mathbf{D}\mathbf{X}_i\right\|_F + \left\|\mathbf{Y}_i - \mathbf{D}_i\mathbf{X}_i^i\right\|_F + \sum_{\substack{j=1 \\ j\neq i}}^{C} \left\|\mathbf{D}_j\mathbf{X}_i^j\right\|_F^2 , \tag{7}$$

where $\|\mathbf{A}\|_F = \sqrt{\sum_i \sum_j a_{ij}^2}$ is the Frobenius norm, C is the number of classes, $\mathbf{Y}_i$ is the matrix composed of a training sample of class i, $\mathbf{X}_i$ is their corresponding sparse codes over the total dictionary $\mathbf{D}$. $\mathbf{D}_j$ is the sub-dictionary representing the samples of class j. The first term in "r" represents the total representation error of samples $\mathbf{Y}_i$ (of class i) over the total dictionary $\mathbf{D}$, and the second term represents the representation error of $\mathbf{Y}_i$ over the i-class specific sub-dictionary $\mathbf{D}_i$, while the third term represents the contribution of sub-dictionaries other than $\mathbf{D}_i$ in the sparse representation of samples $\mathbf{Y}_i$, which should be small, as those samples belong to a different class, and it accounts for the confusion error in the case of source separation.

Function $f_{\mathbf{X}}(\mathbf{X})$ is a cost function that imposes discrimination on the sparse codes $\mathbf{X}$ according to the Fisher discrimination criterion, which means that the sparse codes $\mathbf{X}$ should have minimum within-class scatter denoted by $S_W(\mathbf{X})$, and maximum between-class scatter denoted by $S_B(\mathbf{X})$. A regularization term that shrinks $\|\mathbf{X}\|_F^2$ is added to make $f_{\mathbf{X}}(\mathbf{X})$ more smooth and convex [30]:

$$f_{\mathbf{X}}(\mathbf{X}) = \mathrm{tr}\big(S_W(\mathbf{X})\big) - \mathrm{tr}\big(S_B(\mathbf{X})\big) + \eta \left\|\mathbf{X}\right\|_F^2 , \tag{8}$$

where:

$$S_W(\mathbf{X}) = \sum_{i=1}^{C} \sum_{x_k \in \mathbf{X}_i} (\boldsymbol{x}_k - \boldsymbol{m}_i)(\boldsymbol{x}_k - \boldsymbol{m}_i)^T \ , \tag{9}$$

$$S_B(\mathbf{X}) = \sum_{i=1}^{C} n_i (\boldsymbol{m}_i - \boldsymbol{m})(\boldsymbol{m}_i - \boldsymbol{m})^T \ . \tag{10}$$

In the above equations, $\boldsymbol{m}_i$ is the mean of sparse codes $\mathbf{X}_i$, $\boldsymbol{m}$ is the mean of all sparse vectors $\mathbf{X}$, n_i is the number of samples that belong to class i, η is a regularization parameter that controls the energy of the samples, tr is the matrix trace operator.

2.2. Speech Enhancement using Sparse Coding

Sigg [15] proposed a supervised speech enhancement method based on learning two dictionaries, one for clean speech and the other for noise, according to the following formulations:

$$\min_{\mathbf{D}_s,\mathbf{X}_s} \left\|\mathbf{Y}_s - \mathbf{D}_s\mathbf{X}_s\right\|_F^2 \ , \quad \|\mathbf{X}_s\|_0 \leq k_s \ , \tag{11}$$

$$\min_{\mathbf{D}_n,\mathbf{X}_n} \left\|\mathbf{Y}_n - \mathbf{D}_n\mathbf{X}_n\right\|_F^2 \ , \quad \|\mathbf{X}_n\|_0 \leq k_n \, . \tag{12}$$

Sigg proposed GDL to solve each of the previous problems. GDL is, in fact, a variation of the approximate K-SVD [22], the only difference is at the sparse coding stage. Sigg proposed least angle regression with coherence criterion (LARC) [15] for sparse coding, instead of the greedy orthogonal matching pursuit (OMP) [33]. LARC is a variation of LARS [34], where the coherence between the residual error and the dictionary is used as the stopping criterion instead of the l_2 norm of the residual error. It has been found that LARC has several advantages over OMP. First, LARC is insensitive to changes in signal energy, as the stopping criterion is related to residual coherence and not to the amplitude of the error. Second, as LARC uses the l_1 norm, which not only penalizes the num-

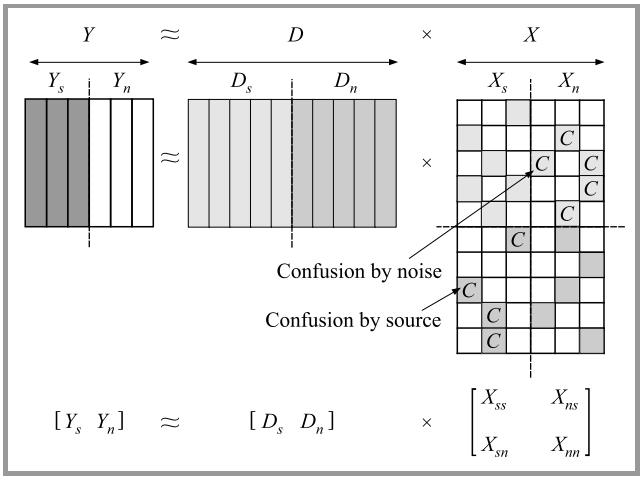

Fig. 1. Columns of $\mathbf{X}$ are the sparse codes of $\mathbf{Y}$ on dictionary $\mathbf{D}$. The sparse coefficient where there is C, means coefficients which cause confusion.

ber of non-zero coefficients (as in the case of l_0 pseudo norm that OMP uses) but also penalizes their magnitudes. This increases the temporal smoothness of the enhanced speech [15].

There are two problems with GDL. First, the two sub-dictionaries $\mathbf{D}_s$ and $\mathbf{D}_n$ are learnt independently – see Eqs. (11) and (12), and thus the source confusion error is not considered. Figure 1 illustrates speech and noise confusion. The second problem is the coherence between $\mathbf{D}_s$ and $\mathbf{D}_n$ that is also not considered in the learning process. These problems will be addressed in our DL algorithm proposed below.

3. IDDL Algorithm

The proposed dictionary learning algorithm defines a new cost function that penalizes coherence between the speech and the noise sub-dictionaries $\|\mathbf{D}_s^T\mathbf{D}_n\|_F^2$, source confusion $\|\mathbf{D}_n\mathbf{X}_s^n\|_F^2$ and noise confusion $\|\mathbf{D}_s\mathbf{X}_n^s\|_F^2$. The proposed algorithm iterates between three steps, after initializing the dictionary, sparse coding using LARC is performed – Eq. (13), then both $\mathbf{X}$ and the noise sub-dictionary $\mathbf{D}_n$ are fixed, while the speech sub-dictionary $\mathbf{D}_s$ is updated using Eq. (14), and in the third step both $\mathbf{X}$ and speech sub-dictionary $\mathbf{D}_s$ are fixed, while the noise sub-dictionary $\mathbf{D}_n$ is updated using Eq. (15).

1. Update $\mathbf{X}$ ($\mathbf{D}-[\mathbf{D}_s,\mathbf{D}_n]$ fixed):

$$\mathbf{X}=\min_{\mathbf{X}}\left\|\mathbf{Y}-\mathbf{D}\mathbf{X}\right\|_F^2+\lambda_l\left\|\mathbf{X}\right\|_1 \tag{13}$$

2. Update $\mathbf{D}_s$ ($\mathbf{X},\mathbf{D}_n$ fixed):

$$\mathbf{D}_s=\min_{\mathbf{D}_s}\left\|\mathbf{Y}_s-\mathbf{D}_s\mathbf{X}_s^s\right\|_F^2+\lambda_{nc}\left\|\mathbf{D}_sX_n^s\right\|_F^2+\lambda_c\left\|D_n^TD_s\right\|_F^2 \tag{14}$$

3. Update $\mathbf{D}_n$ ($\mathbf{X},\mathbf{D}_s$ fixed):

$$\mathbf{D}_n=\min_{\mathbf{D}_n}\left\|\mathbf{Y}_n-\mathbf{D}_n\mathbf{X}_n^n\right\|_F^2+\lambda_{sc}\left\|\mathbf{D}_nX_s^n\right\|_F^2+\lambda_c\left\|\mathbf{D}_s^T\mathbf{D}_n\right\|_F^2 \tag{15}$$

The λ_{nc}, λ_{sc}, $\lambda_c\geq 0$ are regularization parameters to control the importance of noise confusion, speech confusion, and sub-dictionary coherences, respectively.

We propose to use the alternating direction method of multipliers (ADMM) [35] to solve Eqs. (14) and (15). First, we introduce an auxiliary variable $\mathbf{Z}$ with an equality constrained $\mathbf{Z}=\mathbf{D}_s$:

$$\mathbf{D}_s=\arg\min_{\mathbf{D}_s,\mathbf{Z}}+\left\|\mathbf{Y}_s-\mathbf{D}_s\mathbf{X}_s^s\right\|_F^2+\lambda_{nc}\left\|\mathbf{D}_s\mathbf{X}_n^s\right\|_F^2+\lambda_c\left\|\mathbf{D}_n^T\mathbf{Z}\right\|_F^2,\quad \mathbf{Z}=\mathbf{D}_s\,. \tag{16}$$

We can see that Eq. (16), which is exactly equivalent to Eq. (14), is in the form that the ADMM algorithm solves. Next, we introduce the dual Lagrangian variable $\mathbf{U}$, and a scaling parameter p, to formulate the augmented Lagrangian, which is a function of the three variables, denoted as follows:

$$\mathcal{L}_\rho(\mathbf{D}_s,\mathbf{Z},\mathbf{U})=\left\|\mathbf{Y}_s-\mathbf{D}_s\mathbf{X}_s^s\right\|_F^2+\lambda_{nc}\left\|\mathbf{D}_s\mathbf{X}_n^s\right\|_F^2+\lambda_c\left\|\mathbf{D}_n^T\mathbf{Z}\right\|_F^2+\mathbf{U}(\mathbf{D}_s-\mathbf{Z})+\frac{\rho}{2}\left\|\mathbf{D}_s-\mathbf{Z}+\mathbf{U}\right\|_F^2\,. \tag{17}$$

According to ADMM, problem given by Eq. (16) can be solved by alternatingly updating, one at a time, each variable in Eq. (17), to minimize the augmented Lagrangian, while fixing the others. With an initial $\mathbf{Z}^0=\mathbf{U}^0=\mathbf{D}_s^0$ (the upper-script denotes the iteration time index), we alternatively solve the following problems until convergence is achieved:

$$\mathbf{D}_s^{t+1}=\min_{\mathbf{D}_s}\left\|\mathbf{Y}_s-\mathbf{D}_s\mathbf{X}_s^s\right\|_F^2+\lambda_{nc}\left\|\mathbf{D}_s\mathbf{X}_n^s\right\|_F^2+\lambda_c\left\|\mathbf{D}_n^T\mathbf{Z}^t\right\|_F^2+\mathbf{U}^t\left(\mathbf{D}_s-\mathbf{Z}^t\right)+\frac{\rho}{2}\left\|\mathbf{D}_s-\mathbf{Z}^t+\mathbf{U}^t\right\|_F^2\,, \tag{18}$$

$$\mathbf{Z}^{t+1}=\left(2\lambda_c\mathbf{D}_n\mathbf{D}_n^T+\rho\mathbf{I}\right)^{-1}\left(\mathbf{D}_s^{t+1}+\mathbf{U}^T\right)\,, \tag{19}$$

$$\mathbf{U}^{t+1}=\mathbf{U}^T+\rho\left(\mathbf{D}_s^{t+1}-\mathbf{Z}^{t+1}\right)\,. \tag{20}$$

After some matrix manipulation, we can easily see that Eq. (19) is equivalent to the following problem:

$$\mathbf{D}_s^{t+1}=\min_{\mathbf{D}_s}\mathrm{tr}\left(\mathbf{D}_s^T\mathbf{D}_s\mathbf{A}\right)-2\mathrm{tr}\left(\mathbf{D}_s^T\mathbf{B}\right)\,, \tag{21}$$

where

$$\mathbf{A}=\mathbf{Y}_s.\left(\mathbf{X}_s^s\right)^T+\frac{\rho}{2}\left(\mathbf{Z}^t-\mathbf{U}^t\right)\,,$$

$$\mathbf{B}=\mathbf{X}_s^s\left(\mathbf{X}_s^s\right)^T+\lambda_{nc}\mathbf{X}_n^s\left(\mathbf{X}_n^s\right)^T+\frac{\rho}{2}\mathbf{I}\,.$$

We can solve Eq. (21) using the same dictionary update algorithm as proposed by Mairal *et al.* [37] in online dictionary learning (ODL). This dictionary update algorithm is based on block-coordinate descent with warm start, which enjoys being parameter-free [37]. The same procedure procedure applies to the problem of learning the noise sub-dictionary $\mathbf{D}_n$ (Eq. (15)). Algorithm 1 describes the IDDL algorithm, while Algorithm 2 describes how sub-dictionary is updated using ADMM.

Algorithm 1: IDDL

Input: $\mathbf{Y}_s\in\mathbb{R}^{N\times n_s}$; $\mathbf{Y}_n\in\mathbb{R}^{N\times n_n}$; L; max_iter1; μ; λ_{nc}; λ_{sc}; λ_c
Output: $\mathbf{D}\in\mathbb{R}^{N\times 2L}$

Initialize $\mathbf{D}_s^0$, $\mathbf{D}_n^0$
$\mathbf{D}=[\mathbf{D}_s^0,\ \mathbf{D}_n^0]$
$\mathbf{Y}=[\mathbf{Y}_s,\ \mathbf{Y}_n]$
For $t=1$ to max_iter1 **do**
    $\mathbf{X}=\mathrm{LARC}(\mathbf{D},\mathbf{Y},\mu)$
    Update $\mathbf{D}_s$ using Algorithm 2, $i=1,\ j=2,\ \lambda=\lambda_{nc}$
    Update $\mathbf{D}_n$ using Algorithm 2, $i=2,\ j=1,\ \lambda=\lambda_{sc}$
    $\mathbf{D}=[\mathbf{D}_s,\mathbf{D}_n]$
End for

Algorithm 2: Sub-dictionary update

Input: $\mathbf{Y}_s; \mathbf{Y}_n; \mathbf{X}_s; \mathbf{X}_n; L; \mathbf{D} \in \mathbb{R}^{N\times 2L}; i; max\_iter2; \lambda; \lambda_c; \rho$
Output: $\mathbf{D}_i \in \mathbb{R}^{N\times L}$

$\mathbf{D}_i^0 = \mathbf{D}(:,(i-1).L+1:i.L)$
$\mathbf{D}_j = \mathbf{D}(:,(j-1).L+1:j.L)$
initial $\mathbf{Z}^0 = \mathbf{U}^0 = \mathbf{D}_i^0$
$\mathbf{X}_i^i = \mathbf{X}_i\big((i-1).L+1:i.L,:\big)$
$\mathbf{X}_j^i = \mathbf{X}_j\big((i-1).L+1:i.L,:\big)$
For $t = 1$ to max_iter 2 **do**
  Update $\mathbf{D}_i^t$ using Algorithm 2 in [37], where:
    $\mathbf{A} = \mathbf{Y}_i.(\mathbf{X}_i^i)^T + \frac{\rho}{2}(\mathbf{Z}^t - \mathbf{U}^t)$,
    $\mathbf{B} = \mathbf{Y}_i.(\mathbf{X}_i^i)^T + \lambda\mathbf{X}_j^i(\mathbf{X}_j^i)^T + \frac{\rho}{2}\mathbf{I}$
  $\mathbf{Z}^{t+1} = (2\lambda_c\mathbf{D}_j\mathbf{D}_j^T + \rho\mathbf{I})^{-1}(\mathbf{D}_i^{t+1} + \mathbf{U}^t)$
  $\mathbf{U}^{t+1} = \mathbf{U}^t + \rho(D_i^{t+1} - \mathbf{Z}^{t+1})$
End for

It should be noted that IDDL differs from FDDL in four aspects. First, we do not impose discrimination on the sparse codes $\mathbf{X}$ (i.e. $\lambda_2 = 0$). Second, the confusion error terms are weighted with regularization parameters. Third, a coherence penalty term is added to the DL formulation, and last, LARC is used at the sparse coding stage, instead of the fast iterative shrinkage and thresholding algorithm (FISTA) [36].

3.1. Speech Enhancement System based on DL

The overall speech enhancement system is depicted in Fig. 2. The system consists of two stages: training and enhancement. During the training phase, we learn the IDDL dictionary that models the amplitude spectrum of the training speech and noise samples. The amplitude of the short time Fourier coefficients (STFT) for the overlapping time frames of the clean speech and noise training signals is calculated after applying the Hamming window. The amplitude spectrum coefficients for all training frames are concatenated as columns to form $\mathbf{Y}_s$ and $\mathbf{Y}_n$, and fed to the IDDL algorithm that learns the clean speech sub-dictionary $\mathbf{D}_s$, and the noise sub-dictionary $\mathbf{D}_n$. These two sub-dictionaries are concatenated together to form the overall dictionary, that contains $2L$ columns.

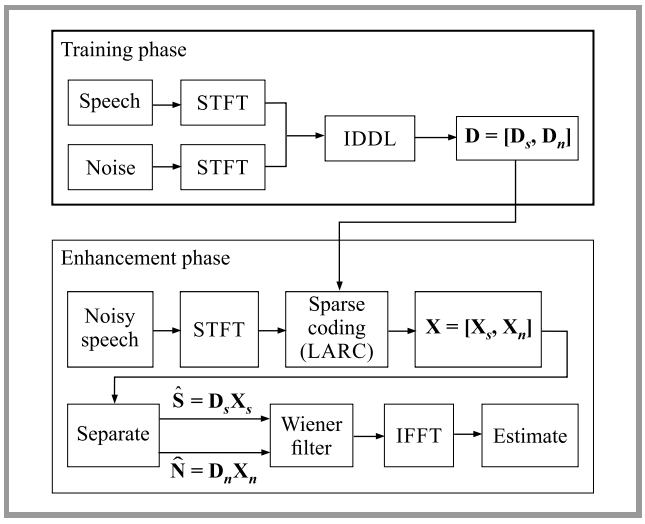

Fig. 2. The overall speech enhancement system.

At the enhancement phase, using LARC and the dictionary $\mathbf{D}$, the sparse codes $\mathbf{X}$ for the amplitude spectrum coefficients of the overlapping frames of the noisy signal are calculated. The sparse code vectors $\mathbf{X}$ contain $2L$ coefficients. The first L ones $\mathbf{X}_s$ that correspond to sub-dictionary $\mathbf{D}_s$ are separated from the last L ones $\mathbf{X}_n$ that correspond to sub-dictionary $\mathbf{D}_n$. By multiplying $\mathbf{X}_s$ and $\mathbf{D}_s$, as well as $\mathbf{X}_n$ and $\mathbf{D}_n$ we get an initial estimation for the amplitude spectrum of the clean speech and noise signals, respectively. These initial estimations are fed to the Wiener filter to find the final clean speech amplitude spectrum estimation. Finally, we apply the inverse Fourier transform to the estimated amplitude spectrum combined with the noisy phase spectrum to get the estimated clean speech.

4. Experiments

4.1. Noizeus Dataset

Noizeus [38] is a noise database that contains 30 IEEE sentences produced by three male and three female speakers, with 5 different sentences per speaker. The sentences are corrupted by eight different real-world noises at different SNRs: (0, 5, 10, 15) dB. The noise was taken from the Aurora database and includes suburban train noise, babble, car, exhibition hall, restaurant, street, airport and train station noise [38]. All speech and noise signals are sampled at 8 kHz.

As the database contains a small number of speakers, and to assure speaker independent cases, which means that the speakers in the training set are different from the speakers in the test set[2], we have divided the dataset into two sets: a training set that contains three speakers and another testing set that contains the remaining three speakers. We have created 12 training/test sets through permutations[3] of three speakers out of 6, and averaged the results. Table 1 shows the list of speakers and their characteristics [40], while Table 2 shows the speakers in the 12 different training/test sets we have created for experiments.

All training sets contain male and female speakers, except for the training set number 11, which is all female speakers (speakers 3, 4, and 6) while the corresponding test set is all male (speakers 1, 2, and 5), and the training set number 12 which is all male, while the corresponding test set is all female. The first 5 training set contain 2 male speakers and

[2] A speaker-independent scenario enables the proposed system to use any available clean speech samples as the training set, not necessarily pertaining to the speaker whose speech we wish to enhance, contrary to the speaker-dependent scenario.

[3] Permutation of 3 speakers out of 6 gives 20 sets. For our experiments we took only 10 sets that contain both male and female speakers, to calculate the average PESQ and fwSegSNR. We conducted the experiment using set number 11 (see Table 2) that contains a female speaker only, and set number 12 that contains a male speaker only, to see if the gender of the speakers in the training set has any impact on the performance achieved. The average does not include results for test groups 11 and 12.

Table 1
Noizeus speaker's characteristics

Speaker	Gender	Pitch frequency F0 [Hz]	Age	State raised	Sentences
1	M	135	21	Texas	sp1–sp5
2	M	134	20	California	sp6–sp10
3	F	225	19	North Carolina and Texas	sp11–sp15
4	F	245	22	Texas	sp16–sp20
5	M	144	20	Texas and Kentucky	sp21–sp25
6	F	225	22	Texas	sp26–sp30

Table 2
Description of different training and test sets

Train/test set	Speakers in the training set	Speakers in the test set
1	[1, 2, 3]	[4, 5, 6]
2	[1, 2, 4]	[3, 5, 6]
3	[1, 2, 6]	[3, 4, 5]
4	[2, 3, 5]	[1, 4, 6]
5	[2, 4, 5]	[1, 3, 6]
6	[1, 3, 4]	[2, 5, 6]
7	[2, 3, 4]	[1, 5, 6]
8	[3, 4, 5]	[1, 4, 5]
9	[3, 4, 6]	[1, 2, 6]
10	[4, 5, 6]	[1, 2, 3]
11	[3, 4, 6]	[1, 2, 5]
12	[1, 2, 5]	[3, 4, 6]

1 female, while the other 5 training sets contain 2 female speakers and 1 male.

For every training set, we collect 15 sentences (15 clean recordings and 15 noisy recordings of a specific type of noise) uttered by the 3 chosen speakers. To have the noise training samples (that belong to the specific type, e.g. a car), we subtract the clean speech recordings from the noisy recordings within the training dataset, and thus we get 15 recordings per noise[4]. Every recording (clean speech and noise) is divided into overlapping frames that are 128 ms long, with a ratio of 75% (overlapping length of 96 ms). After applying the hamming window to these clean speech and noise frames, we calculate the FFT coefficients of these overlapped windows, and stack them together as columnar vectors to form the training matrices $\mathbf{Y}_s$ (the amplitude of the FFT coefficients of the clean speech frames) and $\mathbf{Y}_n$ (the amplitude of the FFT coefficients of the clean speech frames). The same procedure is applied to noisy signals at the enhancement stage.

[4] In the general case, noise samples can be obtained either through a voice activity detector (VAD) from non-speech segments, or from an offline noise database like Noisex-92 [43].

4.2. Performance Metrics

There are two types of measures to assess the performance of speech enhancement algorithms: subjective measures and objective measures. Subjective measures are scores reported by human listeners participating in a subjective listening test. The mean opinion score (MOS) [40] is a result, on the scale from 1 to 5, that a human listener decides to use to express their satisfaction with the quality of speech they are listening to. Due to the high logistic costs needed to perform subjective listening tests, objective measures were sought.

Frequency weighted segmental SNR (fwSegSNR) is the estimated mean frequency domain SNR over all time frames, with a perceptually motivated frequency band weighting. fwSegSNR may be calculated according as follows:

$$\text{fwSegSNR} = \frac{10}{Nw}\sum_{n=1}^{N}\sum_{b=1}^{B} w_b \log \frac{|S(b,n)|^2}{(|S(b,n)| - |\hat{S}(b,n|)^2}\,, \tag{22}$$

where $S(b,n)$ are the complex FFT coefficients of the clean speech, n is the frame index, b is the frequency component index, N is the total number of frames in the speech signal, B is the total number of frequency components, w_b is the corresponding frequency weighting, w is the sum of all the frequency weights, and $\hat{S}(b,n)$ are the estimated complex spectrum coefficients of the enhanced speech.

PESQ [39] is an international measure that simulates MOS, and is widely used to assess the quality of speech conveyed through a telephone network. Its derivation may be found in [39]. It has been shown that PESQ has the highest correlation coefficient ($\rho = 0.89$) with the overall speech quality [41], and correlates well with subjective speech *intelligibility* [42], while fwSegSNR has the second highest correlation coefficients with the overall speech quality ($\rho = 0.85$) [41], and correlates well with subjective speech *quality* [42]. That is why we have used these two measures to assess performance of the proposed algorithm. It should be emphasized that speech quality does not correlate with speech intelligibility, as it is the case of synthesized speech, which generally has low quality, though it could be highly intelligible. We have used the implementation provided by [40] for both fwSegSNR and PESQ.

4.3. The Results

To assess the performance of the proposed IDDL algorithm, we compared its performance in terms of fwSegSNR and PESQ against three other different DL algorithms: K-SVD, GDL, and FDDL. We have used the same speech enhancement system as depicted in Fig. 2, but with the different DL algorithms mentioned.

Different frame lengths were investigated starting with 256 up to 1024 samples (from 32 to 128 ms) with the overlapping rate of 50–75%. We have found that longer frames always render better results. This increases the dimensions of the feature space and, thus, results in a lower coherence between the clean speech and noise sub-dictionaries, which

means a lower source confusion error. Longer enhancement time is a disadvantage of using the longer frame length, as increasing the dimensions of the signal feature space N will increase the time needed for sparse coding.

The number of DFT coefficients varied as well. In one scenario we chose the number of DFT coefficients as the same number of samples in the frame, while for short frame lengths we tried zero padding and used 1024 DFT coefficients, but it was not useful. This is because it does not really increase the dimension of the feature space, as the information content is the same.

The regularization parameters λ_{nc}, λ_{sc}, λ_c are set through a validation test. We found that the optimal experimental values in our setting are: $\lambda_{nc} = 1$, $\lambda_{sc} = 1$, $\lambda_c = 0.0001$.

For LARC, the stopping residual coherence thresholds is set at $\mu = 0.15$ in IDDL and GDL at the training stage, while it's set at $\mu = 0.1$ for sparse coding at the enhancement stage, as described in [15]. We have verified experimentally that those values of μ are optimal for the performance of the proposed system, for all noise types except for the case of white noise and car noise. We have found that using a lower value of $\mu = 0.05$ for sparse coding renders better performance for all dictionaries studied, in the case of car noise and white noise. This is due to the fact that both types of noise experience lower confusion levels (non-speech-like noise) with clean speech signal than other types of speech-like noise, and using a lower value of μ (which means a lower approximation error) will not cause the confusion error to increase. This hints that we can use a dynamic value for μ based on the initial value of the speech confusion error.

For FDDL, we have used the efficient implementation provided by [31] and denoted by E-FDDL. There are two parameters to tune E-FDDL: FISTA l_1 regularization parameter which is set to $\lambda_1 = 0.05$, and Fisher discrimination regularization parameter $\lambda_2 = 0.01$, Eq. (6).

The number of maximum iterations for KSVD is set to 15, for E-FDDL it is set to 7, and for GDL it is set to 20.

The number of maximum iterations (max_iter1 in Algorithm 1) for IDDL is set to 7. In fact we have tested different values in the range of $\{3 \ldots 25\}$ for this parameter. We noticed that increasing the number of maximum iterations over 7 minimizes all sub-costs: source distortion, noise distortion, source confusion, noise confusion and sub-dictionaries coherence even further (see Figs. 6–10), but the resulting dictionary does not perform better on the testing set. This is due to the fact that the model (the dictionary) becomes over-fitted to the training set and does not generalize well.

For initializing IDDL ($\mathbf{D}_s^0, \mathbf{D}_n^0$), we have investigated two scenarios: either to build two initial dictionaries composed of random samples from the training set, or to initialize IDDL with two prebuilt K-SVD dictionaries, one for clean speech and one for noise. We have noticed that IDDL with a random initial dictionary has no performance gain over the other studied DL methods, while IDDL with initial prebuilt K-SVD dictionaries achieves superior performance.

Table 3
The proposed speech enhancement system's general parameter setting

Parameter	Variable and value
Window length	$Tw = 128$ ms
Window shift	$Tsh = 32$ ms
Number of FFT coefficients	$NFFT = 1024$
Signal dimension	$N = \frac{NFFT}{2} + 1 = 513$
Number of atom in the sub-dictionary	$L = 300$
The stopping residual coherence thresholds of LARC (the sparse coding block in the enhancement stage)	$\mu = 0.14$

Table 4
The parameters setting of the 4 used dictionary learning algorithms used in the training stage

Dictionary	Parameter	Variable name
IDDL	The stopping residual coherence thresholds of LARC (sparse coding stage): lines 3, 4 in Algorithm 1	$\mu = 0.15$
	Distortion error penalty	$\lambda_{nc} = 1$, $\lambda_{sc} = 1$
	Coherence penalty	$\lambda_c = 0.0001$
	max_iter1	$q_1 = 7$
	max_iter2	$q_2 = 5$
FDDL	FISTA $l1$ regularization	$\lambda_1 = 0.05$
	Fisher discrimination regularization parameter	$\lambda_2 = 0.01$
	Maximum iterations	$q = 7$
K-SVD	Sparsity degree (for OMP stage)	$k = 30$
	Maximum iterations	$q = 15$
GDL	The stopping residual coherence thresholds of LARC (sparse coding solver)	$\mu = 0.15$
	Maximum iterations	$q = 20$

The results shown in Tables 4 and 5 are for the case $L = 300$ (which means that the dimensions of the total dictionary are $513^7 \times 600$), with a pre-built K-SVD dictionary for initialization.

Experiments were conducted using Matlab 2015Ra on a laptop with 3.16 GHz Intel Core i5 processor and 4 GB RAM.

Table 3 summarizes the general parameters settings of the speech enhancement system, while Table 4 summarizes all dictionary learning parameters, for the 4 dictionary learning algorithms used to get the results reported in Tables 4 and 5.

Table 5 shows the frequency weighted segmental SNR (in dB) for the different dictionary learning algorithms using the parameter settings listed above in Tables 3 and 4. To

Table 5
Frequency weighted segmental SNR (in dB), speaker independent scenario, with the percentage gain of IDDL and FDDL gain over K-SVD and GDL

Noise	dB	K-SVD	GDL	FDDL	IDDL	IDDL gain [%]	FDDL gain [%]
Babble	0	6.17	6.13	6.23	**6.25**	**1.30**	0.96
	5	7.89	7.97	7.91	**7.99**	**0.25**	–0.75
	10	9.76	9.92	9.70	**9.93**	**0.10**	–2.26
	15	11.90	12.18	12.13	**12.25**	**0.57**	–0.41
Car	0	7.14	7.16	7.53	**7.60**	**6.15**	4.91
	5	8.55	8.58	8.86	**9.11**	**6.18**	3.16
	10	10.26	10.35	10.63	**10.73**	**3.67**	2.63
	15	12.57	12.69	12.76	**12.77**	**0.63**	0.54
Restaurant	0	6.52	6.48	6.54	**6.55**	**0.46**	0.30
	5	7.83	7.95	7.86	**7.96**	**0.13**	–1.14
	10	9.66	9.75	9.49	**9.77**	**0.21**	–2.73
	15	11.44	11.64	11.46	**11.85**	**1.80**	–1.57
Station	0	6.06	6.10	**6.25**	6.17	1.15	**2.40**
	5	7.91	8.04	**8.07**	8.03	–0.12	**0.37**
	10	9.88	10.02	9.96	**10.03**	**0.10**	–0.60
	15	11.96	12.09	11.95	**12.19**	**0.83**	–1.17
Train	0	7.57	7.50	7.70	**7.85**	**3.70**	1.68
	5	8.91	8.56	8.96	**9.02**	**1.23**	0.55
	10	10.30	10.46	10.74	**10.82**	**3.44**	2.60
Airport	0	6.65	6.54	6.74	6.73	1.20	**1.33**
	5	8.16	8.28	8.30	8.30	0.24	0.24
	10	10.22	10.19	10.13	**10.24**	**0.20**	–0.88
	15	12.25	12.31	12.29	**12.42**	**0.89**	–0.16
White	0	**7.11**	6.98	6.92	6.97	–1.97	–2.74
	5	**8.68**	8.49	8.44	8.54	–1.61	–2.84
	10	**10.56**	10.26	10.28	10.40	–1.52	–2.72
	15	**12.73**	12.28	12.63	12.41	–2.51	–0.79

Table 6
PESQ, speaker independent scenario, with the percentage gain of IDDL and FDDL over K-SVD and GDL

Noise	dB	K-SVD	GDL	FDDL	IDDL	IDDL gain [%]	FDDL gain [%]
Babble	0	1.87	1.89	1.94	**1.95**	**3.17**	2.57
	5	2.19	2.20	2.23	**2.23**	**1.36**	1.34
	10	2.46	2.51	**2.52**	2.51	0.00	**0.39**
	15	2.76	2.85	**2.85**	2.82	–1.05	0
Car	0	2.24	2.28	2.36	**2.40**	**5.26**	3.38
	5	2.43	2.49	2.55	**2.58**	**3.61**	2.35
	10	2.61	2.68	2.71	**2.75**	**2.61**	1.10
	15	2.82	2.93	2.93	**2.95**	**0.68**	0
Restaurant	0	1.87	1.88	1.91	**1.92**	**2.13**	1.57
	5	2.11	2.13	2.17	**2.17**	**1.88**	1.84
	10	2.44	2.47	2.49	**2.49**	**0.81**	0.80
	15	2.68	**2.78**	2.77	2.75	–1.08	**0.35**
Station	0	1.89	1.94	**1.98**	1.97	1.55	**2.02**
	5	2.23	2.29	**2.33**	2.32	1.31	**1.71**
	10	2.50	2.57	**2.59**	2.58	0.39	**0.77**
	15	2.74	2.81	**2.82**	2.80	–0.36	**0.35**
Train	0	2.32	2.23	**2.40**	2.37	2.16	**3.33**
	5	2.46	2.40	**2.55**	2.53	2.85	**3.52**
	10	2.52	2.61	**2.74**	2.73	4.60	**4.74**
Airport	0	1.94	1.93	**1.99**	1.97	1.55	**2.51**
	5	2.25	2.26	**2.30**	2.29	1.33	**1.73**
	10	2.52	2.53	**2.57**	2.55	0.79	**1.55**
	15	2.79	2.81	**2.85**	2.82	0.36	**1.40**
White	0	**2.39**	2.32	2.38	2.39	0.00	–0.42
	5	**2.63**	2.54	2.61	2.63	0.00	–0.76
	10	**2.84**	2.75	2.83	2.83	–0.35	–0.35
	15	**3.03**	2.95	3.03	3.02	–0.33	0

evaluate the degree of improvement that IDDL and FDDL (which are discriminative dictionary learning algorithms) offer over K-SVD and GDL (which are reconstructive DL), we reported, in the same table, the percentage gain of IDDL and FDDL over K-SVD and GDL (percentage of outperformance), which is calculated as:

$$IDDL_{GAIN}=\left(1-\frac{\left|\max\left(\text{fwSegSNR(KSVD)},\text{fwSegSNR(GDL)}\right)\right|}{\text{fwSegSNR(IDDL)}}\right)\cdot 100\%, \tag{23}$$

$$FDDL_{GAIN}=\left(1-\frac{\left|\max\left(\text{fwSegSNR(KSVD)},\text{fwSegSNR(GDL)}\right)\right|}{\text{fwSegSNR(FDDL)}}\right)\cdot 100\%. \tag{24}$$

We can see that the proposed IDDL algorithm performs better in terms of fwSegSNR in most cases (19 out of 27), but not in the case of white noise, as it is not a structured noise.

Table 6 shows PESQ for the different dictionary learning algorithms, with the IDDL and FDDL percentage gain over K-SVD and GDL, which is calculated from Eqs. (23) and (24), using PESQ instead of fwSegSNR. The results show that IDDL performs better in 9 out of 27 of the cases, while its performance is very close to that of E-FDDL in the remaining cases.

Tables 5 and 6 show that K-SVD is the best DL for the case of white noise, in terms of both performance measures, and no gain is achieved by IDDL nor FDDL.

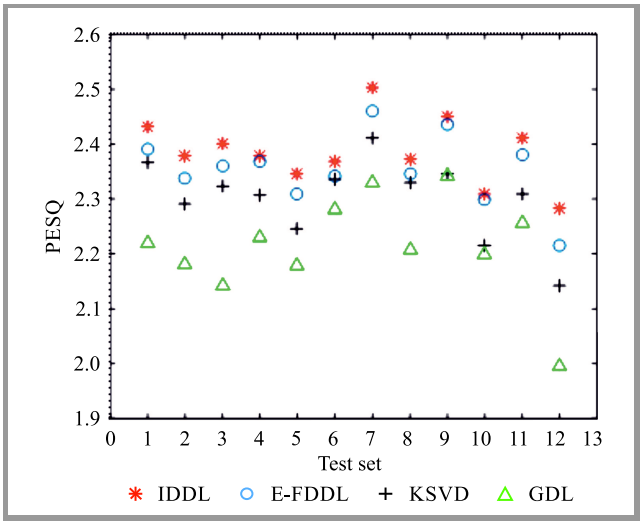

Fig. 3. PESQ over the different test sets.

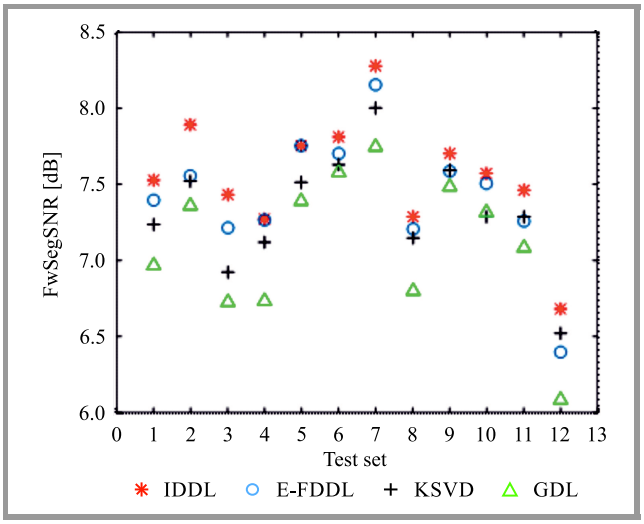

Fig. 4. fwSegSNR over the different test sets.

Figures 3 and 4 show fwSegSNR and PESQ, respectively, over all different test sets, in the case of car noise at 0 dB. We can see that IDDL outperforms all other investigated DL algorithms, over all test sets. We also noticed that the worst performance (lowest fwSegSNR and lowest PESQ) for all dictionaries is when the training set is all male, while the testing set is all female (test set number 12), while when the training set is all female and the testing set is all male (test set number 11), performance does not degrade, which might hint that the model learnt from female voices generalizes better than the model learnt from male voices (which needs to be investigated further in the future).

Table 7
DL training time in seconds

Number of atoms L	KSVD	GDL	FDDL	IDDL
300	**15**	44	52	20
600	**41**	58	175	57

Table 7 shows the different DL training times. We can see that K-SVD is characterized by the shortest DL time, while IDDL is ranked second. FDDL has the longest training time, because at the sparse code updating stage it enforces discrimination using Fisher discrimination criteria on the sparse codes, which is a costly sparse coding algorithm. Although Tables 5 and 6 show that IDDL offer performance that is very close to that of E-FDDL in terms of both performance measures, it has the advantage of lower complexity, and thus a short training time.

Table 8
Sparse coding time

Number of atoms L	Coding time [s]
300	0.008
600	0.03

Table 8 shows the different coding times for a single noisy frame using LARC, for different dictionary sizes. As expected, we notice that increasing the dictionary size (increasing the number of atoms L) increases the time needed to calculate the sparse codes $\mathbf{x}_i$ (which has a dimension of $2L$) of the amplitude spectrum of each noisy frame, at the enhancement stage, and thus increases the time needed to perform speech enhancement.

4.4. Convergence Analysis

We have studied empirically the convergence of the proposed dictionary learning through examining how all the IDDL sub-costs (speech distortion, noise distortion, speech confusion, noise confusion, and sub-dictionaries' coherence) change with the respective iterations (variable t in Algorithm 1, line 2). All reported figures relate to babble noise, with 0 dB. Figure 5 shows that speech and noise distortion decreases with the number of iterations. We can also see that speech distortion is smaller than

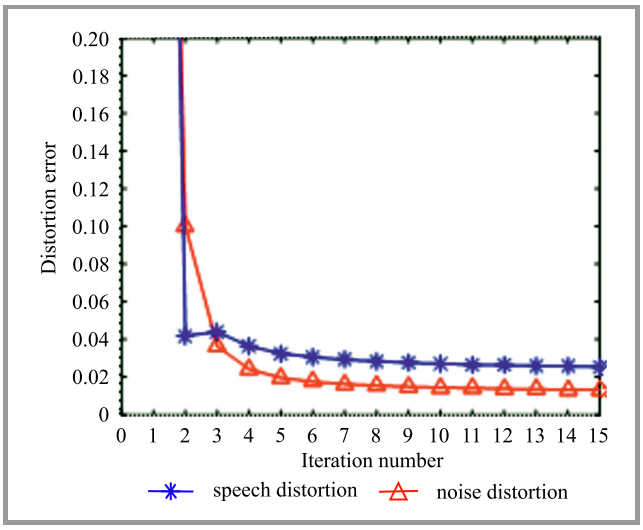

Fig. 5. Speech and noise distortion.

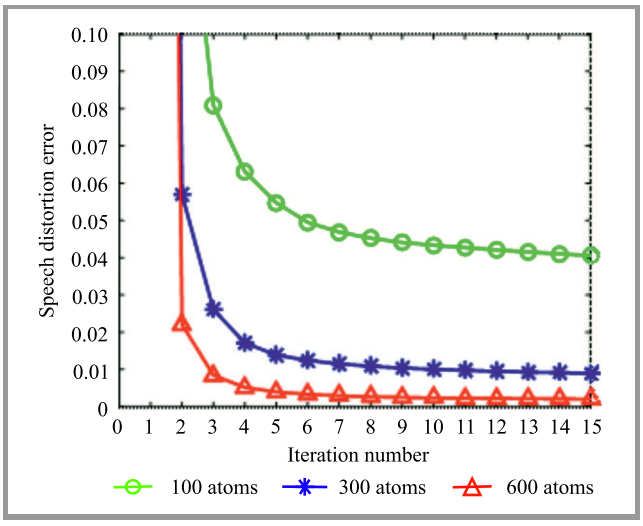

Fig. 6. Speech distortion for different dictionary sizes.

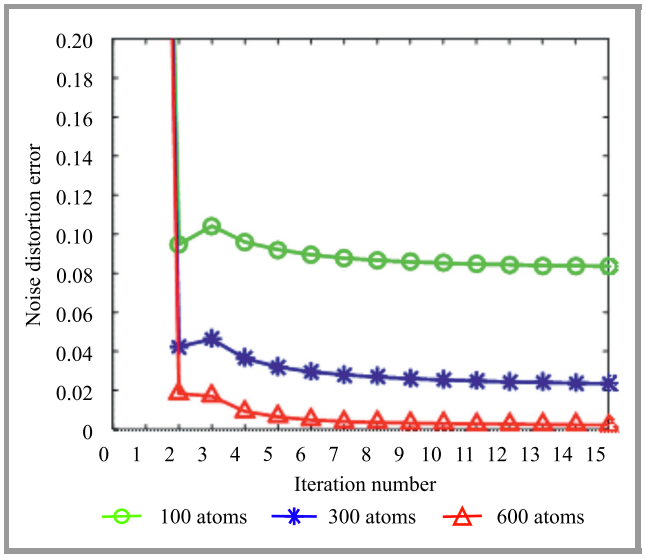

Fig. 7. Noise distortion for different dictionary sizes.

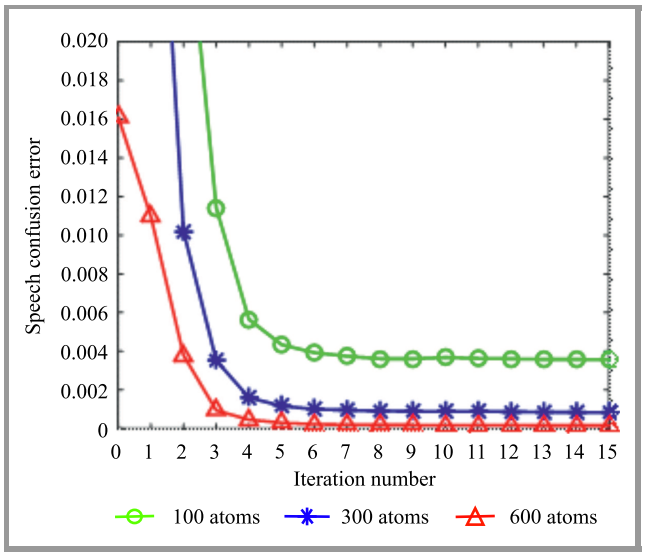

Fig. 8. Speech confusion error for different dictionary sizes.

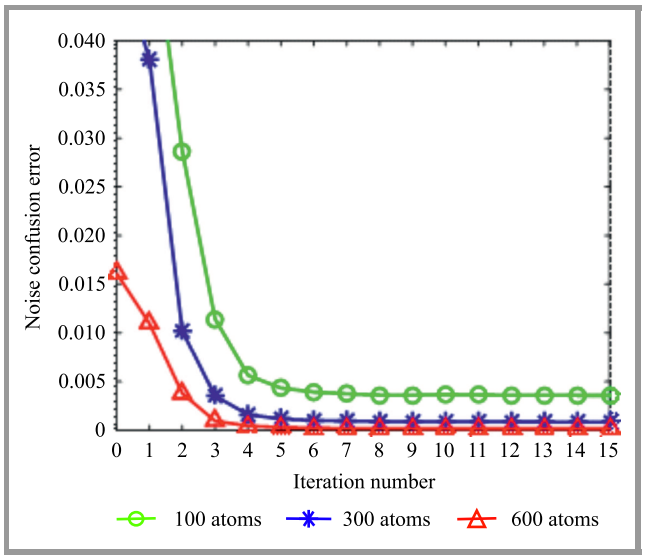

Fig. 9. Noise confusion error for different dictionary sizes.

noise distortion. This is because speech is more structured than noise.

Figures 6 and 7 show speech distortion and noise distortion for different number of atoms, respectively, and we can see that increasing the number of atoms decreases the distortion error, as the dictionary becomes richer, and thus has higher representation capability.

Figures 8 and 9 show the speech confusion error and noise confusion error. We can see that both speech and noise confusion errors achieve a considerable decrease with iteration number 3.

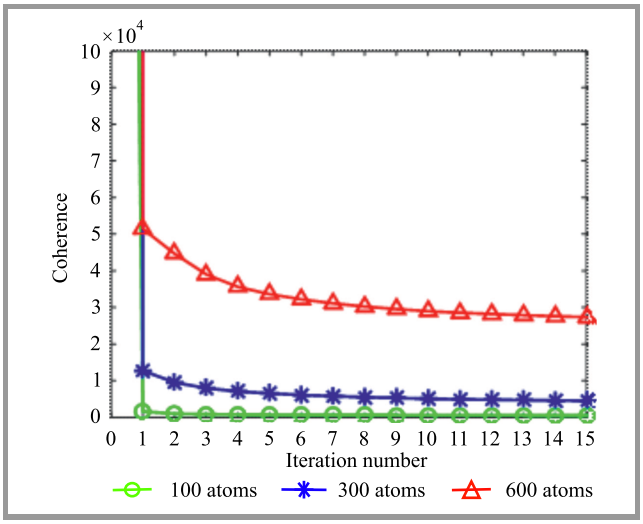

Fig. 10. Coherence between speech and noise sub-dictionaries.

Figure 10 shows the coherence between the noise and speech sub-dictionaries. We can see that increasing the number of atoms increases the coherence, as the minimum coherence increases with increasing the number of columns in any matrix.

5. Conclusion

In this paper we proposed a new algorithm to learn an incoherent discriminative dictionary called IDDL, used for the specific task of speech enhancement. The goal of the cost function is to minimize both "source distortion" and "source confusion" errors, in addition to reducing coherence between noise and speech sub-dictionaries. Performance of the proposed algorithm was evaluated using two objective measures: frequency weighted SNR: fwSegSNR and PESQ, to compare with well-known dictionary learning algorithms: K-SVD, GDL and FDDL. Experiments on the Noizeus dataset show that IDDL offers better performance in comparison to other studied DL in terms of both measures, in most of the cases, but not in the case of white noise. Performance of IDDL is close to that of E- FDDL in terms of both performance measures, but it has the advantage of having a notably shorter training time. The superior performance of IDDL makes it suitable for speech enhancement in the case of structured non-stationary noise, such as babble and car noise.

Acknowledgments

The authors would like to thank P. Loizou (R.I.P.) for publishing the implementations of fwSegSNR and PESQ objective measures. We thank Christian D. Sigg for providing an excellent implementation of LARC algorithm and GDL. We also thank Tiep Huu Vu for providing an excellent and efficient implementation of E-FDDL.

References

[1] S. Boll, "Suppression of acoustic noise in speech using spectral subtraction", *IEEE Trans. Acoust., Speech, Signal Process.*, vol. 27, no. 2, pp. 113–120, 1979 (doi: 10.1109/TASSP.1979.1163209).

[2] Y. Lu and P. C. Loizou, "A geometric approach to spectral subtraction", *Speech Commun.*, vol. 50, no 6. pp. 453–466, 2008 (doi: 10.1016/j.specom.2008.01.003).

[3] J. S. Lim and A. V. Oppenheim, "Enhancement and bandwidth compression of noisy speech", *Proc. of the IEEE*, vol. 67, no. 12, pp. 1586–1604, 1979 (doi: 10.1109/PROC.1979.11540).

[4] Y. Ephraim, "Statistical-model-based speech enhancement systems", *Proc. of the IEEE*, vol. 80, no. 10, pp. 1526–1555, 1992 (doi: 10.1109./5.168664).

[5] Y. Hu and P. C. Loizou, "A generalized subspace approach for enhancing speech corrupted by colored noise", *IEEE Trans. Speech Audio Process.*, vol. 11, no. 4, pp. 334–341, 2003 (doi: 10.1109/TSA.2003.814458).

[6] J. Sun, J. Zhang, and M. Small, "Extension of the local subspace method to enhancement of speech with colored noise", *Signal Process.*, vol. 88, no. 7, pp. 1881–1888, 2008 (doi: 10.1016/j.sigpro.2008.01.008).

[7] T. Sreenivas and P. Kirnapure, "Codebook constrained Wiener filtering for speech enhancement", *IEEE Trans. Speech Audio Process.*, vol. 4, no. 5, pp. 383–389, 1996 (doi: 10.1109/89.536932).

[8] S. Srinivasan, J. Samuelsson, and W. B. Kleijn, "Codebook driven short term predictor parameter estimation for speech enhancement", *IEEE Trans. Audio, Speech, and Language Process.*, vol. 14, no. 1, pp. 163–176, 2006 (doi: 10.1109/TSA.2005.854113).

[9] D. Y. Zhao and W. B. Kleijn, "HMM-based gain modeling for enhancement of speech in noise", *IEEE Trans. Audio, Speech, and Language Process.*, vol. 15, no. 3, pp. 882–892, 2007 (doi: 10.1109/TASL.2006.885256).

[10] N. Mohammadiha, R. Martin, and A. Leijon, "Spectral domain speech enhancement using HMM state-dependent super-Gaussian priors", *IEEE Signal Process. Lett.*, vol. 20, no. 3, pp. 253–256, 2013 (doi: 10.1109/LSP.2013.2242467).

[11] H. Veisi and H. Sameti, "Speech enhancement using hidden Markov models in Mel-frequency domain", *Speech Commun.*, vol. 55, no. 2, pp. 205–220, 2013 (doi: 10.1016/j.specom.2012.2242467).

[12] K. W. Wilson, B. Raj, and P. Smaragdis, "Regularized non-negative matrix factorization with temporal dependencies for speech denoising", in *Proc. of the 9th Ann. Conf. of the Int. Speech Commun. Association, Brisbane Interspeech 2008*, Brisbane, Australia, 2008, pp. 411–414.

[13] M. Sun, Y. Li, J. Gemmeke, and X. Zhang, "Speech enhancement under low SNR conditions via noise estimation using sparse and low-rank NMF with Kullback-Leibler divergence", *IEEE/ACM Trans. Audio, Speech, Lang. Process.*, vol. 23, no. 7, pp. 1233–1242, 2015 (doi: 10.1109.TASLP.2015.2427520).

[14] N. Mohammadiha, P. Smaragdis, and A. Leijon, "Supervised and unsupervised speech enhancement using nonnegative matrix factorization", *IEEE Trans. Audio, Speech, Lang. Process.*, vol. 21, no. 10, pp. 2140–2151, 2013 (doi: 10.1109.TASL.2013.2270369).

[15] C. D. Sigg, T. Dikk, and J. M. Buhmann, "Speech enhancement using generative dictionary learning", *IEEE Trans. Audio, Speech, Lang. Process.*, vol. 20, no. 6, pp. 1698–1712, 2012 (doi: 10.1109.TASL.2012.2187194).

[16] Y. Zhao, X. Zhao, and B. Wang, "A speech enhancement method based on sparse reconstruction of power spectral density", *Computers & Elec. Engin.*, vol. 40, no. 4, 2014, pp. 1080–1089 (doi: 10.1016/j.compeleceng.2013.12.007).

[17] Y. Luo, G. Bao, Y. Xu, and Z. Ye, "Supervised monaural speech enhancement using complementary joint sparse representations", *IEEE Signal Process. Lett.*, vol. 23, no. 2, pp. 237–241, 2016 (doi: 10.1109/LSP.2015.2509480).

[18] L. Zhang, G. Bao, J. Zhang, and Z. Ye, "Supervised single-channel speech enhancement using ratio mask with joint dictionary learning", *Speech Commun.*, vol. 82, no. C, pp. 38–52, 2016 (doi: 10.1016/j.specom.2016.06.001).

[19] T. W. Shen and D. P K Lun, "A speech enhancement method based on sparse reconstruction on log-spectra", *HKIE Trans.*, vol. 24, no. 1, pp. 24–34, 2017 (doi: 10.1080/1023697X.2016.1210545).

[20] M. Elad and M. Aharon, "Image denoising via sparse and redundant representations over learned dictionaries", *IEEE Trans. Image Process.*, vol. 15, no. 12, pp. 3736–3745, 2006 (doi: 10.1109/TIP.2006.881969).

[21] M. Aharon, M. Elad, and A. Bruckstein, "K-SVD: An algorithm for designing overcomplete dictionaries for sparse representation", *IEEE Trans. on Signal Process.*, vol. 54, no. 11, pp. 4311–4322, 2006 (doi: 10.1109/TSP.2006.881199).

[22] R. Rubinstein, M. Zibulevsky, and M. Elad, "Efficient implementation of the K-SVD algorithm using batch orthogonal matching pursuit", Technical Rep. CS-2008-08, Technion – Israel Institute of Technology, Haifa, Israel, 2008.

[23] K. Engan, S. O. Aase, and J. Hakon Husoy, "Method of optimal directions for frame design", in *Proc. IEEE Int. Conf. on Acoust., Speech, and Sig. Process. ICASSP'99*, Phoenix, AZ, USA, 1999, vol. 5 (doi: 10.1109/ICASSP.1999.760624).

[24] Y. Suo, M. Dao, U. Srinivas, V. Monga, and T. D. Tran, "Structured Dictionary Learning for Classification", 2014, arXiv:1406.1943.

[25] J. Mairal, F. Bach, J. Ponce, G. Sapiro, A. Zisserman, "Supervised dictionary learning", in *Advances in Neural Information Processing Systems 21*, D. Koller, D. Schuurmans, Y. Bengio, and L. Bottou, Eds. MIT Press, 2008, pp. 1033–1040.

[26] Q. Zhang and B. Li, "Discriminative K-SVD for dictionary learning in face recognition", in *Proc. 23rd IEEE Conf. on Comp. Vision and Pattern Recogn. CVPR 2010*, San Francisco, CA, USA, 2010, pp. 2691–2698 (doi: 10.1109/CVPR.2010.5539989).

[27] Z. Jiang, Z. Lin, and L. S. Davis, "Label consistent K-SVD: Learning a discriminative dictionary for recognition", *IEEE Trans. Pattern Anal. Mach. Intell.*, vol. 35, no. 11, pp. 2651–2664, 2013 (doi: 10.1109/TPAMI.2013.88).

[28] I. Ramirez, P. Sprechmann, and G. Sapiro, "Classification and clustering via dictionary learning with structured incoherence and shared features", in *Proc. 23rd IEEE Conf. on Comp. Vision and Pattern Recogn. CVPR 2010*, San Francisco, CA, USA, 2010, pp. 3501–3508 (doi: 10.1109/CVPR.2010.5539964).

[29] S. Kong and D. Wang, "A dictionary learning approach for classification: Separating the particularity and the commonality", in *Proc. 12th Eur. Conf. on Comp. Vision ECCV 2012*, Florence, Italy, 2012, pp. 186–199 (doi: 10.1007/978-3-642-33718-5_14).

[30] M. Yang, L. Zhang, and X. Feng, "Sparse representation based Fisher discrimination dictionary learning for image classification", *Int. J. of Computer Vision*, vol. 109, no. 3, pp. 209–232, 2014 (doi: 10.1007/s11263-014-0722-8).

[31] T. H. Vu and V. Monga, "Fast low-rank shared dictionary learning for image classification", in *IEEE Trans. on Image Process.*, vol. 26, no. 11, pp. 5160–5175, 2017 (doi: 10.1109/TIP.2017.2729885).

[32] J. A. Tropp, "Greed is good: algorithmic results for sparse approximation", *IEEE Trans. on Inform. Theory*, vol. 50, no. 10, pp. 2231–2242, 2004 (doi: 10.1109/TIT.2004.834793).

[33] Y. C. Pati, R. Rezaiifar, and P. S. Krishnaprasad, "Orthogonal matching pursuit: Recursive function approximation with applications to wavelet decomposition", in *Proc. of 27th Asilomar Conf. on Signals, Systems and Computers*, Pacific Grove, CA, USA, 1993 (doi: 10.1109/ACSSC.1993.342465).

[34] B. Efron, T. Hastie, I. Johnstone, and R. Tibshirani, "Least angle regression", *The Annals of Statistics*, vol. 32, no. 2, pp. 407–499, 2004 (doi: 10.1214/009053604000000067).

[35] S. Boyd, N. Parikh, E. Chu, B. Peleato, and J. Eckstein, "Distributed optimization and statistical learning via the alternating direction method of multipliers", *Found. and Trends in Machine Learn.*, vol. 3, no. 1, pp. 1–122, 2011 (doi: 10.1561/2200000016).

[36] A. Beck and M. Teboulle, "A fast iterative shrinkage-thresholding algorithm for linear inverse problems", *SIAM J. on Imaging Sci.*, vol. 2, no. 1, pp. 183–202, 2009 (doi: 10.1137/080716542).

[37] J. Mairal, F. Bach, J. Ponce, and G. Sapiro, "Online learning for matrix factorization and sparse coding", *J. of Machine Learn. Res.*, vol. 11, pp. 19–60, 2010, arXiv:0908.0050.

[38] "Noizeus: A noisy speech corpus for evaluation of speech enhancement algorithms" [Online]. Available: http://ecs.utdallas.edu/loizou/speech/noizeus/

[39] A. Rix, J. Beerends, M. Hollier, and A. Hekstra, "Perceptual evaluation of speech quality (PESQ) – A new method for speech quality assessment of telephone networks and codecs", in *Proc. IEEE Int. Conf. on Acoust., Speech, and Sig. Process.*, Salt Lake City, UT, USA, 2001, pp. 749–752 (doi: 10.1109/ICASSP.2001.941023).

[40] P. C. Loizou, *Speech Enhancement. Theory and Practice*. Boca Raton, FL, USA: CRC, 2013 (ISBN: 9781138075573).

[41] Y. Hu and P. C. Loizou, "Evaluation of objective quality measures for speech enhancement", *IEEE Trans. Audio Speech Lang. Process.*, vol. 16, no. 1, pp. 229–38, 2008 (doi: 10.1109/TASL.2007.911054).

[42] J. Ma, Y. Hu, and P. C. Loizou, "Objective measures for predicting speech intelligibility in noisy conditions based on new band importance functions", *J. Acoust. Soc. Am.*, vol. 125, no. 5, pp. 3387–3405, 2009.

[43] Noisex-92: Database of recording of various noises [Online]. Available: www.speech.cs.cmu.edu/comp.speech/Section1/Data/noisex.html

Dima Shaheen is a Ph.D. student at the Higher Institute for Applied Science and Technology HIAST, Damascus, Syria. She received her M.Sc. degree in Telecommunication Engineering in 2013 from HIAST. Her research interests include signal processing, speech processing, machine learning, information theory, and digital communication.

E-mail: dima.shaheen@hiast.edu.sy
Telecommunications Department
Higher Institute for Applied Science
and Technology HIAST
P.O. Box 31983 Damascus, Syria

Oumayma Al Dakkak received her Ph.D. in Electronic Systems from the Grenoble Institute of Technology (Institut polytechnique de Grenoble) in 1988. She is a Research Director at the Telecommunications Department, Higher Institute for Applied Science and Technology HIAST, Damascus, Syria. Her research interests include signal processing, speech processing, speech recognition, machine learning, and digital communication.
E-mail: oumayma.dakkak@hiast.edu.sy
Telecommunications Department
Higher Institute for Applied Science
and Technology HIAST
P.O. Box 31983 Damascus, Syria

Mohiedin Wainakh received his Ph.D. degree in Cybernetics and Information Theory in 1980 from the Kiev Polytechnic, Ukraine. Currently, he is a Research Director at the Telecommunications Department, Higher Institute for Applied Science and Technology HIAST, Damascus, Syria. His current research interests include digital communication, statistics, and information theory.
E-mail: mohiedin.wainakh@hiast.edu.sy
Telecommunication Department
Higher Institute for Applied Science
and Technology HIAST
P.O. Box 31983 Damascus, Syria

Paper

Interference Aware Routing Game for Cognitive Radio Ad-hoc Networks

Soodeh Amiri-Doomari, Ghasem Mirjalily, and Jamshid Abouei

Department of Electrical Engineering, Yazd University, Yazd, Iran

https://doi.org/10.26636/jtit.2018.110817

Abstract—Cognitive radio is a new communication paradigm that is able to solve the problem of spectrum scarcity in wireless networks. In this paper, interference aware routing game, (IRG), is proposed that connects the flow initiators to the destinations. A network formation game among secondary users (SUs) is formulated in which each secondary user aims to maximize its utility, while it reduces the aggregate interference on the primary users (PUs) and the end-to-end delay. In order to reduce the end-to-end delay and the accumulated interference, the IRG algorithm selects upstream neighbors in a view point of the sender. To model the interference between SUs, IRG uses the signal-to-interference-plus noise (SINR) model. The effectiveness of the proposed algorithm is validated by evaluating the aggregate interference from SUs to the PUs and end-to-end delay. A comprehensive numerical evaluation is performed, which shows that the performance of the proposed algorithm is significantly better than the Interference Aware Routing (IAR) using network formation game in cognitive radio mesh networks.

Keywords—aggregate interference, end-to-end delay, routing game, network formation game.

1. Introduction

Due to the ability of cognitive radio (CR) to solve the problem of spectrum scarcity, spectrum congestion and underutilization, Cognitive Radio Networks (CRNs) have been recognized as an outstanding technology [1]. Recently, researchers consider lower layers' challenges such as spectrum sensing, sharing, and spectrum mobility in infrastructure-based networks that use a base-station for considering the spectrum information [2]–[4]. Cognitive Radio Ad-Hoc Networks (CRAHNs) as a new class of CRNs without any central entity [5] have been considered recently from different aspects including spectrum sensing, spectrum mobility and the routing issue in the network layer of CRAHNs [6]–[9]. As demonstrated in [10], routing challenges in CRAHNs are classified into three main categories: channel-based [5]–[9], host-based [4], [11], and network-based [7], [12], [13] routing.

Channel-based challenges are related to the operating environment, such as channel availability and diversity. Authors in [5] present a geographical routing algorithm that addresses three main goals: PUs receiver protection from SU interference, joint spectrum and route selection, and provisioning of different routing modes. In the proposed scheme, each SU calculates its overlapping transmission range with the PUs transmitters' coverage to minimize the probability of PUs receivers on that area.

A spectrum-tree based on-demand routing protocol (STOD-RP) for CRAHNs has been proposed in [6]. It simplifies cooperation between spectrum decision and route selection by establishing a spectrum tree in each frequency band. Since this algorithm uses control packets, the system's overhead is significantly high.

Authors in [7] consider route diversity effects on the actual cost of the route and suggest an optimal routing metric for CRAHNs. The presented routing algorithm focuses on the end-to-end delay for delay sensitive applications.

A geographical routing algorithm for mobile SUs has been proposed in [8] to minimize the interference from SUs imposed on PUs. The proposed scheme jointly undertakes the path and channel assignments to avoid the PU's footprint. In [9] the geometrical approach to improve the spectrum utilization is used. This work takes into account three main factors: SUs' interference on PUs, SU network reliability, and computing Quality of Service (QoS) in both SU and PU networks. For minimizing the SUs' interference on the PUs, the routing scheme calculates the maximum transmission range based on the transmission power and the location of SUs and PUs.

Host-based challenges are related to the SUs such as mobility and minimizing the channel switching delay or back off delay.

A route switching game to address spectrum mobility and route switching issues in CRAHNs has been proposed in [11]. The cost of data flow is modeled as routing and switching costs. Routing costs correspond to the end-to-end delay and amount of energy consumption for relaying. Switching costs consider switching delay, back off delay and amount of energy consumption used for channel sensing and establishing new connections.

Network based challenges considers a tradeoff between the number of hop counts and other performance metrics such as interference, energy consumption and route robustness.

Article [12] proposes a new routing metric called cognitive transport throughput to capture the potential relay gain over next hop. The proposed scheme is based on the local channel usage statistics and selects the best relay node with the highest forwarding gain. In addition, a heuristic algo-

rithm is proposed to decrease the searching complexity of the optimal selection of channels and relays.
The routing algorithm in [13] is aware of the degree of connectivity of possible paths towards the destination. In the proposed scheme, the authors present a new CR metric based on the path stability and availability over time.
The authors in [14] develop a routing strategy for CR mesh networks based on the network formation game. This scheme by avoiding PU's region minimizes the aggregate interference from SUs to the PUs. It does not consider the geographical location of the destination in finding the routes.
The authors in [15] present a distributed dynamic routing protocol in multi-hop CR-based on the non-cooperative game theory where SUs minimize their interferences imposed on PUs.
In [16], the authors introduce the route robustness for the path selection in multi-hop CR networks. The algorithm selects some routes from a robust route set and specifies the spectrum of the selected routes in a way that the throughput of the system is maximized. The proposed strategy is not feasible in CRAHNs as it needs a global knowledge about the network's topology.
A spectrum and energy aware routing algorithms for CRAHNs based on the dynamic source routing has been proposed in [17]. Although, the proposed scheme can balance energy consumption and is able to reduce the routing overhead, it does not consider the problem of aggregate interference from SUs to PUs.

1.1. Contributions and Paper Organization

A main obstacle of getting a high performance of routing algorithm is the interferences [18], [19]. This is a major factor in determining the boundaries for the spectrum reuse. Network throughput has a direct relationship with the interference among links. Due to the negative impact of interference, the QoS of the network will be changed with the change of the routing patterns. Estimating the interference in a CRAHN is not an ordinary task. Therefore, proposing an efficient interference-aware routing algorithm that considers the interference measures to reduce its effects on each PU is a challenging task. Toward this goal, we define the PU's footprint as an area that no SU allowed to be turned on. According to the mentioned problem, we propose the interference aware routing algorithm for CRAHNs based on the network formation game (IRG).
In the proposed algorithm, a game theory model is used to connect the flow initiators directly or through SUs to the intended destinations optimally. The designed protocol is distributed, that avoids the problems of centralized algorithms. In contrast with the [14], proposed method selects an upstream neighbor that is close to the destination and out of the PU's region by geographical routing. In this way, we introduce the relay coefficient value (RCV) metric.
RCV helps to reduce the end-to-end delay and decreases the interference from SUs imposed on the PUs. The most important difference between proposed method and [14] is that this work considers the amount of interference between SUs and moreover it focuses on the physical interference model as in [20]. Another advantage of the proposed algorithm compared with [14] is the load balancing technique that leads to decrease the network congestion and also decreases the amount of aggregate interference on the PUs. Simulation results in four different scenarios show that the proposed protocol achieves a superior performance with reducing the normalized aggregate interference and the number of hop counts compared to [14].
The rest of this paper is organized as follows. Section 2 contains the system model description and assumptions. Section 3 introduces the proposed algorithm. In Section 4, the network formation game is presented. In Section 5, the performance of the proposed algorithm is evaluated. Finally, in Section 6, an overview of the results and some conclusion remarks are presented. For convenience, a list of key mathematical symbols used in this paper is provided in Table 1.

Table 1
System parameters

Symbol	Definition
$\mathbf{G}$	Network graph
$\mathbf{V}$	Set of SU nodes
$\mathbf{E}$	Set of edges (links) created between nodes
$l(i,j)$	Link from node i to node j
R_I	Interference range
R_T	Transmission range
C_{ij}	Capacity of link $l(i,j)$
num_i	Number of neighbor nodes of node i
t_i	Amount of generated traffic by node i in a unit of time
$p(i)$	Transmission power of node i
$t_{i,j}$	Amount of traffic from node i to node j in a unit of time
$P(f_k)$	Determined path for flow f_k
$d_{i,j}(t)$	Euclidean distance between nodes i and j
W	Bandwidth

2. System Model and Assumptions

2.1. Network Model and Assumptions

In this work, we consider a multi-hop CRAHN consisting of M stationary and location-aware SU nodes, denoted by $\{1, 2, \ldots, M\}$ and there are K stationary PUs indexed by $\{1, 2, \ldots, K\}$. All nodes are distributed randomly through-

out an A × A square area. We assume that there are N data flows $f_k = (n_{f_k}, D_{f_k})$, where $k = 1, 2, \ldots, N$ corresponds to k-th data flow, n_{f_k} and D_{f_k} are k-th flow initiator and k-th destination, respectively. Any flow initiator knows the location information of intended destination. SUs can acquire their own location information using the Global Positioning System (GPS) or other available localization services. Figure 1 shows proposed game strategy. There are six SUs and one PU deployed randomly in the area. The big circle represents the coverage area of PU. S and D represent the source and destination nodes, respectively. v_1 and v_4 could not participate in routing process because v_1 is in the coverage area of PU and v_4 is a downstream neighbor of S. Since node v_3 is further to the primary user compared to node v_2, node S selects v_3 as a next hop, because further node creates less interference on PU. In this work, the network is

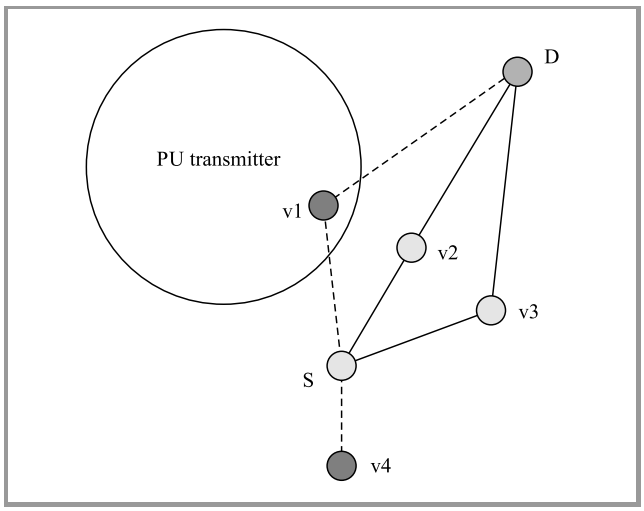

Fig. 1. Implementation of game strategy for $M = 6$ SUs distributed in the presence of the PU.

modelled by a directed graph $\mathbf{G} = (\mathbf{V}, \mathbf{E})$, where $\mathbf{V}$ represents M SU nodes and $\mathbf{E}$ denotes the set of links. We define a path for flow f_k as $P(f_k) = \{v_1^k, v_2^k, \ldots, v_{h-1}^k, v_h^k\}$, where h is the hop count and the nodes v_1^k and v_h^k correspond to the source and destination nodes, respectively.

2.2. Interference Model

Similar to [20], we consider two interference models: protocol model and physical model.

In protocol model, a transmission from node i to $j \underset{i,j}{\forall} \in \{1, 2, \ldots, M\}$ is successful if both of the following conditions are satisfied:

- $d_{i,j}(t) < R_T$, where R_T is the transmission range of SUs;
- any node k with $d_{k,j}(t) < R_I$ is not transmitting, where R_I is the interference range. On the other hand, a node may not send and receive at the same time and it cannot transmit to more than one node at the same time.

In physical model, suppose that node i wants to transmit to node j. The transmission is successful if:

$$SINR(i,j) = \frac{g(i,j)p(i)}{\eta W + \Sigma_{k \in \mathbf{V}, k \neq i,j} g(k,j)p(k)} \geq \sigma\,, \quad (1)$$

where η is the ambient Gaussian noise density, $g(i,j) = [d_{i,j}(t)]^{-\alpha}$ is the propagation loss from node i to node j where α is the path loss exponent, $p(i)$ is the transmission power of node i and $d_{i,j}(t)$ is the Euclidean distance between nodes i and j. A link $l(i,j)$ is available if the following conditions are satisfied:

- $SINR(i,j) \geq \sigma$,
- $d_{i,PU}(t) > R_I$ and $d_{j,PU}(t) > R_I$,

where $d_{i,PU}(t)$ and $d_{j,PU}(t)$ are the Euclidean distances between node i and PU, and node j and PU, respectively. The binary variable β_{ij} indicates the existence of a potential directed link from node i to j:

$$\beta_{ij} \triangleq \begin{cases} 1 & \text{, if there exist a potential link } l(i,j) \\ 0 & \text{, otherwise} \end{cases}. \quad (2)$$

According to the Shannon's formula [21], the capacity of link $l(i,j)$ is defined as:

$$C_{ij} = W \log_2(1 + SINR(i,j)) \quad (3)$$

The amount of traffic on node i must satisfy the following conditions:

$$t_i + \sum_{j \in \mathbf{V}} \beta_{ji} \times t_{j,i} - \sum_{j \in \mathbf{V}} \beta_{ij} \times t_{i,j} = 0 \quad (4)$$

$$t_{i,j} \leq C_{ij} \quad (5)$$

Equations (4) and (5) are the flow conservation constraints. In Eq. (4) outgoing flow should be equal to the sum of incoming flow and generated traffic. In Eq. (5) flow on each link cannot be bigger than its capacity.

Additionally, for minimizing the aggregate interference from SUs to the PU, primary user has a footprint where no SU is allowed to be turn on. When the SUs are outside the PU's footprint, they can utilize the cognitive functionalities to access the licensed spectrum. It is clearly predictable that with an increase in the number of secondary users M, the amount of aggregate interference is increased. The total interference to the primary user for a path $P(f_k)$ between v_1^k and v_h^k is given by:

$$I(P) = \sum_{i=1}^{h} p(i) L_i\,, \quad (6)$$

where $p(i)$ is the transmission power of node v_i^k, $L_i = d_{i,PU}^{-\alpha}$ is the propagation loss from SU to the PU where $d_{i,PU}$ is the Euclidean distance between node v_i^k and PU.

Figure 2 demonstrates the IRG interference model. There are a PU and three SUs deployed randomly in the area. The solid lines represent the channel interference from SUs to the PU, and the dotted lines show the channel interference from a SU to another SU.

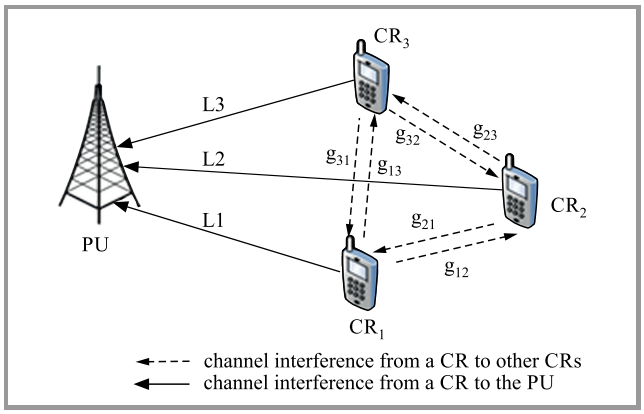

Fig. 2. System interference model when there are one PU and three SUs.

3. Interference Aware Routing Game for CR Ad-hoc Networks

Network formation game is a field of game theory that offers a suite of tools that may be used effectively in modeling the interaction among SU nodes in ad hoc networks to improve their payoffs [14], [22]. Game $g = \{\mathbf{V},\ \mathbf{S},\ U(a)\}$ has three main components: players, game strategy, and utility function. The proposed game components are defined as:

Definition 1. $\mathbf{V}$ shows a set of players or decision makers. Each player evaluates the resulting outcome through a payoff or "utility" function representing its objective. Interaction between the players is represented by the influence that each player has on the resulting outcome after other players have selected their actions. In the proposed algorithm, players are SUs, which establish a connection with their neighbors to route the traffic by focusing on minimizing the aggregate interference on PUs.

Definition 2. $\mathbf{S} = \{s_1 \times s_2 \times \cdots \times s_M\}$ is the strategy space. In fact, strategy is a decision to forward packets or not. SU nodes choose a strategy from their strategy space in response to other players' strategies. According to the sender (i.e. S) and destination (i.e. D) locations, only upstream neighbors (i.e. R), can forward packets. Choosing upstream neighbors, in the view point of S, leads to reduce the number of transmissions, end-to-end delay and the energy consumption. To specify the upstream neighbors, we define the $RCV(S,R,D)$ as:

$$RCV(S,R,D) = d_{S,D}(t) - d_{R,D}(t)\,, \tag{7}$$

where $d_{S,D}(t)$ and $d_{R,D}(t)$ show the Euclidean distance between source S and destination D and between relay R and destination D, respectively. We assume that each node knows the location information of its neighbors. In this case, each node sets its location information on the hello packet and broadcasts it.

To prevent the creation of loops in the network graph, it is necessary that if player j is connected to i already, player i cannot choose player j as its strategy. More precisely, if a link $l(j,i) \in \mathbf{E}$, then link $l(i,j) \notin \mathbf{E}$. To satisfy the above conditions, game strategy is defined as:

$$s_i = \{l(i,j) \in \mathbf{E} | j \in \mathbf{V} \setminus \{i\} \cup \lambda_i, RCV(i,j,D) > 0\}\,, \tag{8}$$

where λ_i is the set of nodes from which node i is accepted a link $l(j,i)$, i.e.

$$\lambda_i = \{j \in \mathbf{V} \setminus \{i\} | l(j,i) \in \mathbf{E}\}\,. \tag{9}$$

Definition 3. In the presented network formation game, each player has a utility that basically contributes every player in the network to improve its payoff by choosing a less congested node that is not only far from PU, but also near the destination. In fact, outcomes are determined by the particular strategy chosen by player i, s_i, and the strategies chosen by all of the other players in the game, $\mathbf{S}_{-i}$. The utility function in [14] is composed of barrier functions, interference temperature, link capacity and the amount of flow. By inspiration, we define the utility function of player i when it selects neighbor j as follows:

$$U(i,j) = \beta_{ij} \frac{RCV(i,j,D) \times C_{ij}}{\overline{E}_j t_{i,j} T_{Ij}}\,, \tag{10}$$

where $\overline{E}_j = \frac{1}{num_j+1}\left(E_j + \sum_{i=1}^{num_j} E_i\right)$ is the average current traffic load on node j and its neighbors in bits per seconds, num_j is the number of neighbor nodes of node j, $T_{Ij} = \frac{P_{Ij}}{k_B W}$ is the interference temperature of node j, P_{Ij} is the interference power in watts imposed by node j and k_B is the Boltzman's constant in J/K and E_i is the total traffic on node i. $\overline{E}_j$ caused to balance the load in the network and avoids the network congestion. If the area around the PU is quieter, the amount of aggregate interference will be decreased significantly.

4. Proposed Network Formation Algorithm

In this section, we proposed the network formation algorithm in details and some preliminary concepts are presented. When all SUs except i keep their own strategies $\mathbf{S}_{-i} = \{s_1, \ldots, s_{i-1}, s_{i+1}, \ldots, s_M\}$, the network graph is defined as $\mathbf{G}_{s_i, \mathbf{S}_{-i}}$. All players to improve their utilities choose appropriate strategies. For instance, player i selects strategy $s_i = l(i,j) \in \mathbf{S}_i$, player j may refuse to accept this connection if it reduces the utility of node j.

There are several approaches for the network formation game that are classified into two categories: myopic [14], [22] and far sighted [23]. The main difference between these two approaches is that in the myopic, the players employ their strategies based on the current state of the network. In other words, each player does not consider the future evolution of the network when it wants to maximize its payoff. However, in the far sighted algorithm, players adapt their strategies by predicting future strategies

of other players. For both types, well-known concepts of non-cooperative game theory can be used. The presented network formation algorithm which is summarized in Algorithm 1 is based on the myopic non-cooperative game.
Time axis is divided into slots with the fixed duration τ, each time slot is a round of the game. In each round, flow initiators generate a random number between 0 and 1, which indicates its priority. Each SU node utilizes its own strategy, $s_i^* \in \mathbf{S_i}$, to calculate its current utility by Eq. (10). If $U(\mathbf{G}_{s_i^*,\mathbf{S}_{-i}}) > U(\mathbf{G}_{s_i,\mathbf{S}_{-i}})$ strategy $s_i^* \in \mathbf{S_i}$ is a best response for a player $i \in \mathbf{V}$. To find the best response, players employ pairwise negotiations with their upstream neighbors. Assume that player i wants to form a new link with j. Adding a new link increases the amount of load on j. Therefore a link formation affects on utility of both nodes i and j. Hence, both nodes should consider the effect of link formation on their utilities before doing the actual formation. In this case, we consider the pairwise stability.

Definition 4. (pairwise stability): Under both following conditions, a network $\mathbf{G}$ is pairwise stable:

1. $l(i,j) \in \mathbf{E}, U_i(\mathbf{G}) \geq U_i(\mathbf{G} - l(i,j))$ and $U_j(\mathbf{G}) \geq \geq U_j(\mathbf{G} - l(i,j))$
2. $l(i,j) \notin \mathbf{E}$ if $U_i(\mathbf{G} + l(i,j)) \geq U_i(\mathbf{G})$ then $U_j(\mathbf{G} + + l(i,j)) < U_j(\mathbf{G})$.

In other words, by removing a link, amount of utility of both players i and j should be increased and also forming a new link should have a positive effect on both i and j utilities [24].

Algorithm 1: Proposed network formation algorithm

until converges to a final Nash equilibrium **do**

- **Random Prioritization of Flows:** Each flow initiator $n_{f_i} \in \mathbf{V}$, $i = 1, 2, \ldots, N$, randomly selects a number between [0, 1] that points out its priority.
- By the order in the previous step, each node n_{f_i} starts the network formation process:

1: n_{f_i} engages in pairwise negotiations with its upstream neighbors to measure its own utility by Eq. (10).
2: n_{f_i} replaces its current link to the destination with another link, if its utility increased.
3: n_{f_i} attaches some information to the hello packet and transmits it to the selected strategy (next hop node).

Based on the pairwise stability, flow initiators choose their best responses and leave the game until the next round, while its selected strategies enter the game. When the proposed network formation algorithm converges to the Nash equilibrium (NE), it reaches to a network where no player can change its strategy (current link).

Definition 5. Players cannot improve their own utilities by unilaterally changing the strategy at the equilibrium [14]. Therefore, a Nash graph is formed where the links chosen by each user are the best strategy.
In this model, player $i \in \mathbf{V}$ can choose its strategy $s_i = l(i,j) \in \mathbf{S_i}$ to improve its utility, while another player j can decline the i's request, if it leads to the utility reduction of node j. When no node in the network could change its payoff, the NE is achieved. In the proposed method, hello packets are sent until the network converges to the NE. The fields of one hello packet are shown in Table 2. When

Table 2
Fields of the hello packet

Fields	Descriptions
Des-Pos	Position of the destination node
Sender-Pos	Position of sender
$\overline{E_j}$	Average traffic load on sender node j
TTL	Limitation of hop-length of the path

node j is selected as the next hop, it attaches the following information to the hello packet:

- its own location information,
- average amount of its traffic load represented by $\overline{E}_j$,
- value of Time To Live (TTL) parameter.

The purpose of the TTL is to limit the number of hop counts in the selected path. After receiving a hello packet, a node checks the value of TTL. If it is zero and the node is not the destination, the node drops the hello packet. Otherwise, the node decreases the value of TTL by one.

Lemma 1: User i aims to optimize its own utility along its path to the destination rather than to have a control over the selection of other nodes.
Proof: User i only has control ability over its neighbor node, while other links are not controlled by node i. This means that node i cannot choose the full path directly and only can increase its payoff. To generate a multi-hop connection from flow initiator n_{f_i} to destination D_{f_i}, a selected node i needs to find a node in its neighborhood to connect as a next hop. In fact, SU i needs to choose a path that result in an optimal payoff. However, node i cannot choose the full path as together and it is not important the choice of other nodes. The path utility of user i can be expressed as a sum of utilities of all the nodes in the path. Denoting U_i^* as the optimal path utility of node i, we have:

$$U_i^* = \max\left(\sum_{n=i}^{h} U(n, n+1)\right), \tag{11}$$

where h is the hop count of path. Since each node in the path (n_{f_i}, D_{f_i}) maximizes its payoff, the path utility in

Eq. (11) can be rewritten as:

$$U_i^* = \max\left(U(i,i+1)\right) + \max\left(\sum_{n=i+1}^{h} U(n,n+1)\right) = \\ = \max\left(U(i,i+1)\right) + U_{i+1}^*. \quad (12)$$

5. Simulation Results

The performance of the proposed algorithm is evaluated and compared in different scenarios with the IAR algorithm [14] in terms of the end-to-end delay and the aggregate interference. For the scenarios under simulation, we show the effect of number of SU nodes, and the distance between flow initiators and destination, on the aforementioned performance metrics, and show the superiority of our proposed algorithm compared with the traditional IAR algorithm.

5.1. Simulation Setup

We consider a CRAHN in which M SU nodes are randomly distributed with the uniform distribution inside a square area with the size 400×400 m^2. M is selected from the set $\{50, 70, 90, 110\}$. We assume that there are K PUs in determined locations. There are five flow initiators that send their data to the intended destinations through the specified path P. For each data set, the location and traffic volume of each flow initiators (except n_{f_1}) are randomly selected. We assume that $R_T = 90$ m and $R_I = 180$ m.

In the simulations, we consider IEEE 802.11g standard. According to this standard, the physical layer is based on the Orthogonal Frequency Division Multiplexing (OFDM). Here, we consider the transmission rates of 6, 9, 12, 18, 24, 36 and 48 Mbps. In Eq. (1), η is the ambient Gaussian noise density, which is $k_B T$, where T is ambient temperature and k_B is Boltzmann constant. By considering $k_B = 1.38 \cdot 10^{-23}$ J/K, $T = 300$ K, $\eta = 414 \cdot 10^{-23}$ and $W = 20$ MHz.

In addition, each node computes its utility by Eq. (10). Each player to improve its utility saves the amount of its previous utility. To achieve the NE, players play in game while no SU can improve their utilities. We assume that each round of game is 20 s.

In the simulations, the data packet has an exponential distribution with mean 50 bytes. Finally, we compute the average of each performance metric over some runs where the corresponding 95% confidence intervals are also reported.

Figure 3 shows the convergence of the selected node when $M = 110$. As seen from Fig. 3, the amount of the utility in some iterations (before the proposed algorithm reaches to the NE point) follows decrease/increase behaviors. It is a well-known fact that in each iteration, a selected node intends to choose the best partner to connect in order to improve its utility. Hence, the selected node may not change its partner in some iterations. Therefore, the amount of its utility changes until the game reaches a steady state or the NE point.

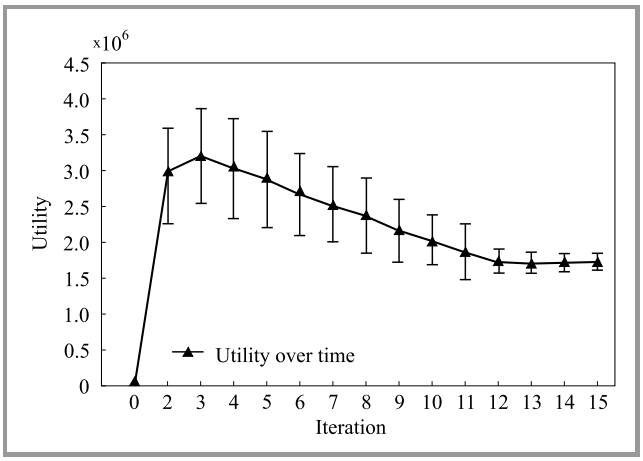

Fig. 3. Utility of a sample node over 15 iterations.

5.2. Evaluation and Comparison

First scenario: In this scenario, the number of SUs is selected from set $\{50, 70, 90, 110\}$ and there is one stationary PU located in (30, 374). Figure 4 compares the normalized aggregate interference of the proposed algorithm with that of the IAR in [14] for the first flow versus the different number of SUs. The normalized aggregate interference is defined as the amount of the aggregate interference, Eq. (6), imposed on the PU divided to the maximum value. As seen from Fig. 4, the proposed scheme displays a lower interference imposed to the PU when compared to the presented

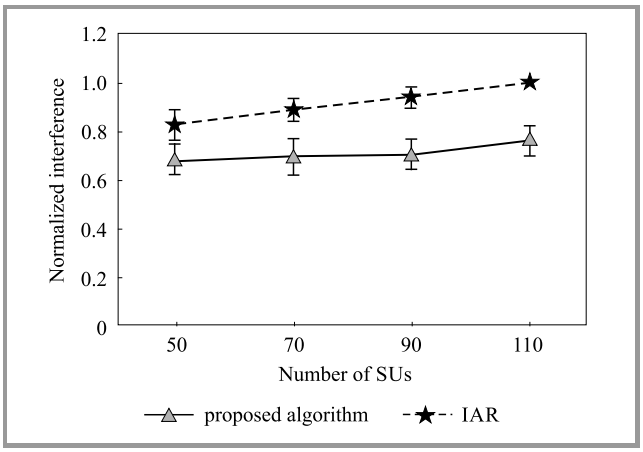

Fig. 4. Normalized interference versus different number of SUs in the proposed IRG and IAR algorithms.

algorithm in [14]. The minimum interference is achieved when the number of SUs is equal to 50. This enhancement comes from the $\overline{E}_j$ used in the proposed utility function. In fact, $\overline{E}_j$ causes the algorithm keeps away from routes that are located in the congested network area. More precisely, if the density of the flow in the region near the PU is high, the amount of the aggregate interference that secondary users create on the PU is increased significantly.

Figure 5 compares the number of hop counts (or equivalently end-to-end delay) between flow initiator n_{f_1} and destination D versus different number of SUs for both

algorithms. The interesting point from Fig. 5 is that in the proposed algorithm, RCV prevents packets to transmit to the downstream neighbors, thus, the end-to-end delay and the amount of energy consumption of the proposed scheme are reduced significantly when compared to the IAR algorithm.

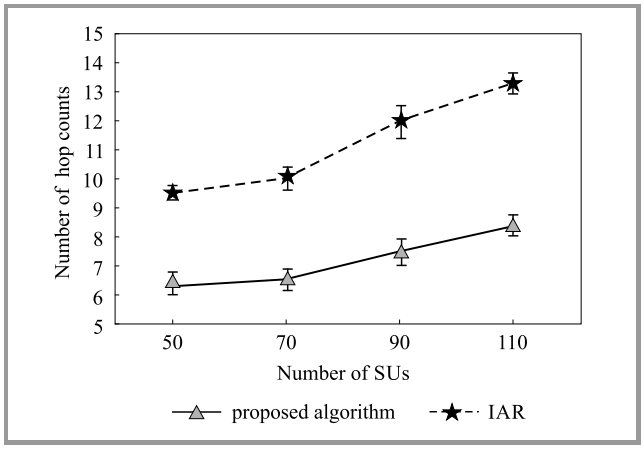

Fig. 5. Number of hop counts between n_{f_1} and D versus different number of SUs in the proposed IRG and IAR algorithms.

Second scenario: In this scenario, the number of SUs is fixed at $M = 110$, we set $K = 1$, PU is located in (30, 374), and the distance between flow initiator n_{f_1} and D is variable in the range of [50, 350]. Figures 6 and 7 provide a fair comparison between our algorithm and the IAR scheme in terms of the normalized aggregate interference and the end-to-end delay. Clearly, when the distance between n_{f_1} and D is low, the performances of both schemes are the same. The result comes from the fact that the route between source and destination will not include more nodes. However, by increasing the distance between the flow initiator and the destination, the number of hop counts is increased and the

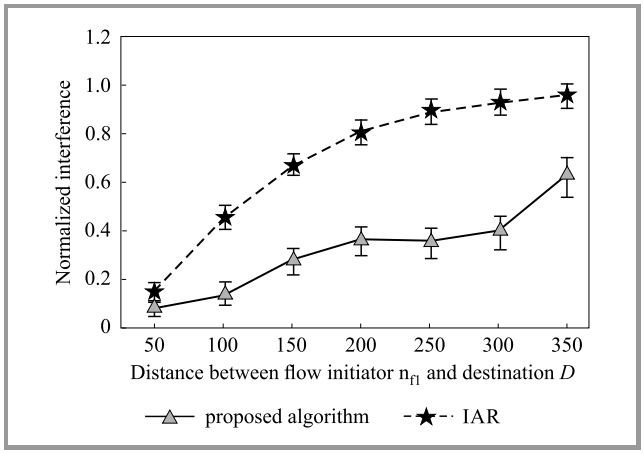

Fig. 6. Normalized interference versus different distances between n_{f_1} and D in the proposed IRG and IAR algorithms.

route consists of more SU nodes. Thus for both algorithms, the aggregate interference from more SUs which are transmitting in a unit of time is increased significantly.

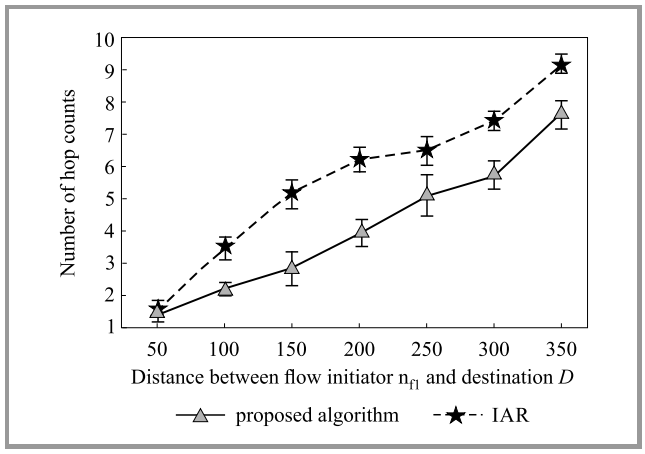

Fig. 7. Number of hop counts between n_{f_1} and D versus different distances between n_{f_1} and D in the proposed IRG and IAR algorithms.

Third scenario: In this scenario, we set $K = 2$, and the number of SUs is changed over the range $\{50, 70, 90, 110\}$. We follow the same performance metrics as in the first scenario to compare our proposed IRG scheme with that of

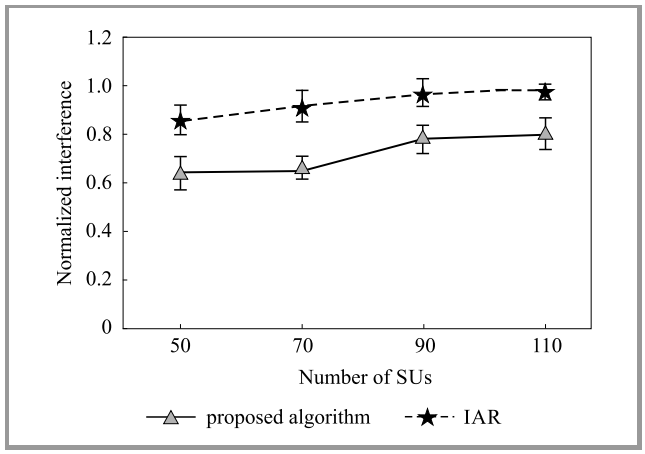

Fig. 8. Normalized interference when $K = 2$ vs. different number of SUs in the proposed IRG and IAR algorithms.

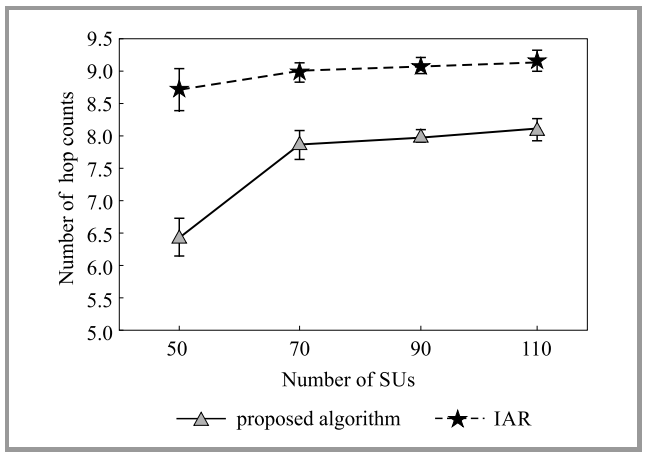

Fig. 9. Number of hop counts between n_{f_1} and D when $K = 2$ vs. different number of SUs in the proposed IRG and IAR algorithms.

the conventional IAR method when there are two PUs in determined locations (140, 187) and (30, 374). Similar to the first scenario, with an increase in the number of SUs, the amount of normalized interference imposed on both PUs is increased, and as a result, the number of hop counts grows, as respectively observed from Figs. 8 and 9.

Fourth scenario: To complete our simulation results, we evaluate the normalized aggregate interference and the end-to-end delay when physical inteference model is used and the link capacity is calculated by Eq. (3). Figures 10 and 11 show the results of the proposed algorithm in terms of the normalized interference and hop counts versus different number of SUs. The results are similar to the arguments as in Figs. 4 and 5. By increasing the number of SUs, the accumulated interference imposed on the PU and also the number of hop counts between the flow initiator n_{f_1} and destination D is increased significantly.

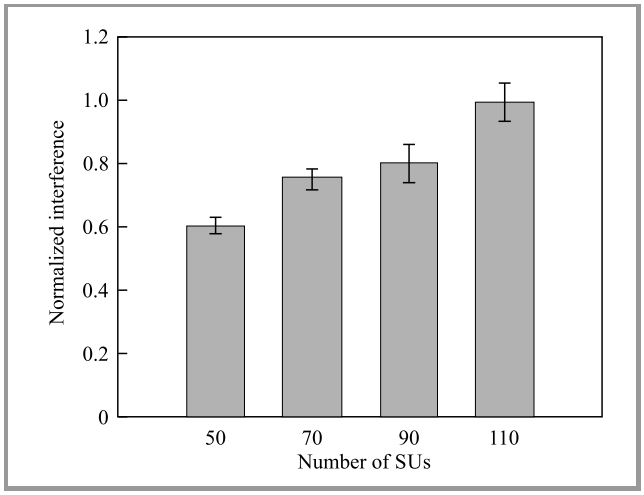

Fig. 10. Normalized interference given different number of secondary nodes in the proposed algorithm.

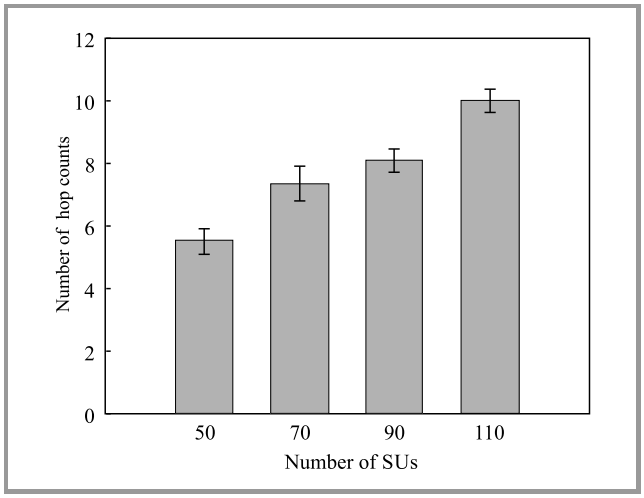

Fig. 11. Number of hop counts given different number of secondary nodes in the proposed algorithm.

6. Conclusion

In this paper, we used the game theory in CRAHNs to propose a new routing algorithm to control the interference and the number of hop counts. To this end, we formulated a network formation game among SUs and introduced a new utility function.

Using the proposed network formation algorithm, each SU can take a locally decision to optimize its utility by selecting a suitable strategy based on the myopic non-cooperative game. The proposed routing algorithm specifically mitigates the interference from SUs imposed on the PUs. Furthermore, to characterize the interference between SUs, we used the physical interference model. To select an appropriate neighbor, our game rule is to select an upstream neighbor in the view point of the sender nodes. We showed that the proposed algorithm avoids congested network zones and it forms at least one path from the flow initiators to the destinations. Simulation results showed that the proposed approach minimizes the aggregate interference and the number of hop counts between the flow initiator and the destination compared to the classical IAR [14] when the number of SUs is randomly selected over the set $\{50, 70, 90, 110\}$.

References

[1] S. Haykin, *Cognitive dynamic systems: perception-action cycle, radar and radio*. Cambridge: Cambridge University Press, 2012 (ISBN: 978-0521114363).

[2] C. Cormio and K. R. Chowdhury, "A survey on MAC protocols for cognitive radio networks", *Ad Hoc Networks*, vol. 7, no. 7, pp. 1315–1329, 2009 (doi: 10.1016/j.adhoc.2009.01.002).

[3] K. B. Letaief and W. Zhang, "Cooperative communications for cognitive radio networks", *Proceedings of the IEEE*, vol. 97, no. 5, pp. 878–893, 2009 (doi: 10.1109/JPROC.2009.2015716).

[4] Z. Li, F. R. Yu, and M. Huang, "A distributed consensus-based cooperative spectrum-sensing scheme in cognitive radios", *IEEE Trans. on Vehic. Technol.*, vol. 59, no. 1, pp. 383–393, 2010 (doi: 10.1109/TVT.2009.2031181).

[5] K. R. Chowdhury and I. F. Akyildiz, "CRP: A routing protocol for cognitive radio ad hoc networks", *IEEE J. on Selec. Areas in Commun.*, vol. 29, no. 4, pp. 794–804, 2011 (doi: 10.1109/JSAC.2011.110411).

[6] G.-M. Zhu, I. F. Akyildiz, and G.-S. Kuo, "STOD-RP: A spectrum-tree based on-demand routing protocol for multi-hop cognitive radio networks", in *Proc. IEEE GLOBECOM Telecommun. Conf.*, pp. 1–5, New Orleans, LA, USA, 2008 (doi: 10.1109/GLOCOM.2008.ECP.592).

[7] M. Caleffi, I. F. Akyildiz, and L. Paura, "OPERA: Optimal routing metric for cognitive radio ad hoc networks", *IEEE Trans. on Wireless Commun.*, vol. 11, no. 8, pp. 2884–2894, 2012 (doi: 10.1109/TWC.2012.061912.111479).

[8] K. R. Chowdhury and M. Felice, "Search: A routing protocol for mobile cognitive radio ad–hoc networks", *Comp. Commun.*, vol. 32, no. 18, pp. 1983–1997, 2009 (doi: 10.1016/j.comcom.2009.06.011).

[9] M. Xie, W. Zhang, and K.-K. Wong, "A geometric approach to improve spectrum efficiency for cognitive relay networks", *IEEE Trans. on Wireless Commun.*, vol. 9, no. 1, pp. 268–281, 2010 (doi: 10.1109/TWC.2010.01.090180).

[10] H. A. Al-Rawi and K.-L. A. Yau, "Routing in distributed cognitive radio networks: A survey", *Wireless Person. Commun.*, vol. 69, no. 4, pp. 1983–2020, 2013 (doi: 10.1007/s11277-012-0674-7).

[11] Q. Liang, X. Wang, X. Tian, F. Wu, and Q. Zhang, "Two-dimensional route switching in cognitive radio networks: A game-theoretical framework", *IEEE/ACM Trans. on Netw. TON*, vol. 23, no. 4, pp. 1053–1066, 2015 (doi: 10.1109/TNET.2014.2315194).

[12] Y. Liu, L. X. Cai, and X. S. Shen, "Spectrum-aware opportunistic routing in multi–hop cognitive radio networks", *IEEE J. on Selec. Areas in Commun.*, vol. 30, no. 10, pp. 1958–1968, 2012 (doi: 10.1109/JSAC.2012.121111).

[13] A. Abbagnale and F. Cuomo, "Gymkhana: a connectivity-based routing scheme for cognitive radio ad hoc networks", in *Proc. IEEE INFOCOM Conf. on Comp. Commun. Workshops*, pp. 1–5, San Diego, CA, USA, 2010 (doi: 10.1109/INFCOMW.2010.5466618).

[14] Z. Yuan, J. B. Song, and Z. Han, "Interference aware routing using network formation game in cognitive radio mesh networks", *IEEE J. on Selec. Areas in Commun.*, vol. 31, no. 11, pp. 2494–2503, 2013 (doi: 10.1109/JSAC.2013.131107).

[15] Q. Zhu, Z. Yuan, J. B. Song, Z. Han, and T. Basar, "Interference aware routing game for cognitive radio multi-hop networks", *IEEE J. on Selec. Areas in Comm.*, vol. 30, no. 10, pp. 2006–2015, 2012 (doi: 10.1109/JSAC.2012.121115).

[16] C.–F. Shih, W. Liao, and H.–L. Chao, "Joint routing and spectrum allocation for multi-hop cognitive radio networks with route robustness consideration", *IEEE Trans. on Wireless Commun.*, vol. 10, no. 9, pp. 2940–2949, 2011 (doi: 10.1109/TWC.2011.072011.101249).

[17] S. Kamruzzaman, E. Kim, D. G. Jeong, and W. S. Jeon, "Energy-aware routing protocol for cognitive radio ad hoc networks", *IET Commun.*, vol. 6, no. 14, pp. 2159–2168, 2012 (doi: 10.1049/iet-com.2011.0698).

[18] T. C. Clancy, "Achievable capacity under the interference temperature model", in *Proc. IEEE INFOCOM Int. Conf. on Comp. Commun.*, pp. 794–802, Anchorage, AL, USA, 2007 (doi: 10.1109/INFCOM.2007.98).

[19] S. Touati, H. Boujemaa, and N. Abed, "Outage probability analysis of optimal and suboptimal interference aware routing protocols for multihop underlay cognitive radio networks", *Trans. on Emerg. Telecommun. Technol.*, vol. 25, no. 7, pp. 736–744, 2014 (doi: 10.1109/INFCOM.2007.98).

[20] S. A. Doomari, G. Mirjalily, and J. Abouei, "Distributed game theory-based routing protocol for Cognitive Radio ad hoc networks", in *Proc. Int. Joint Conf. on Comp. Sc. and Softw. Engin. JCSSE*, Hatyai, Thailand, 2015, pp. 201–206 (doi: 10.1109/JCSSE.2015.7219796).

[21] C. E. Shannon, "A mathematical theory of communication", *ACM SIGMOBILE Mob. Comp. and Commun. Rev.*, vol. 5, no. 1, pp. 3–55, 2001 (doi: 10.1145/584091.584093).

[22] W. Saad, Z. Han, T. Basar, M. Debbah, and A. Hjorungnes, "Network formation games among relay stations in next generation wireless networks", *IEEE Trans. on Commun.*, vol. 59, no. 9, pp. 2528–2542, 2011 (doi: 10.1109/TCOMM.2011.062311.100046).

[23] J. Coimbra, G. Schütz, and N. Correia, "Energy efficient routing algorithm for fiber–wireless access networks: A network formation game approach", *Comp. Netw.*, vol. 60, pp. 201–216, 2014 (doi: 10.1016/j.bjp.2013.11.014).

[24] H. Khanmirza and N. Yazdani, "Strategic network formation game for energy consumption balancing", *Wireless Person. Commun.*, vol. 84, no. 2, pp. 841–865, 2015 (doi: 10.1007/s11277-015-2664-z).

Soodeh Amiri-Doomari received her B.Sc. degree in Electrical Engineering and her M.Sc. degree in Telecommunication in 2011 from Kerman University and Isfahan University of Technology (IUT) respectively. She is currently a Ph.D. candidate in the department of Electrical Engineering, Yazd University. Her research interests are in the area of wireless ad-hoc networks, sensor networks, cognitive radio, game theory and mobile cognitive radio.
E-mail: s.amiridoomari@stu.yazd.ac.ir
Department of Electrical Engineering
Yazd University
Daneshgah Blvd.
89195-741 Yazd, Iran

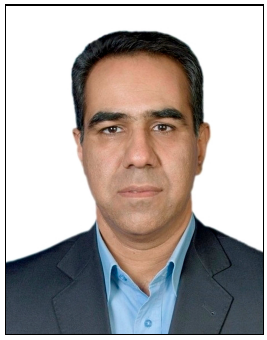

Ghasem Mirjalily received his Ph.D. degree in telecommunication engineering from Tarbiat Modarres University, Iran, in 2000. He was a visiting researcher at McMaster University, Canada, in 1998. Since 2000, he has been with Yazd University, Iran, where he is a full professor. Also, he is a senior member of IEEE. His interests include traffic engineering in wired and wireless networks.
E-mail: mirjalily@yazd.ac.ir
Department of Electrical Engineering
Yazd University
Daneshgah Blvd.
89195-741 Yazd, Iran

Jamshid Abouei received the B.Sc. degree in Electronics Engineering and the M.Sc. degree in Communication Systems Engineering both from the Isfahan University of Technology (IUT), Iran, in 1993 and 1996, respectively, and the Ph.D. degree in Electrical Engineering from the University of Waterloo in Waterloo, ON, Canada, in 2009. From 2009 to 2010, he was a Postdoctoral Fellow in the Multimedia Lab, in the Department of Electrical and Computer Engineering, at the University of Toronto, ON, Canada. Currently he is an Associate Professor in the Department of Electrical and Computer Engineering at the Yazd University. His research interests are in general areas of wireless ad hoc and sensor networks, with particular reference to energy efficiency and optimal resource allocations.
E-mail: abouei@yazd.ac.ir
Department of Electrical Engineering
Yazd University
Daneshgah Blvd.
89195-741 Yazd, Iran

Paper

Theoretical Investigation of Different Diversity Combining Techniques in Cognitive Radio

Rupali Agarwal[1], Neelam Srivastava[2], and Himanshu Katiyar[3]

[1] *Babu Banarasi Das National Institute of Technology & Management, Lucknow, Uttar Pradesh, India*
[2] *Rajkiya Engineering College, Kannauj, Uttar Pradesh, India*
[3] *Rajkiya Engineering College, Sonbhadra, Uttar Pradesh, India*

https://doi.org/10.26636/jtit.2018.124618

Abstract—In this paper, the performance of an energy detector in cognitive radio, using different diversity combining techniques, is evaluated. Among many diversity combining techniques, maximal ratio combining (MRC) gives the best results but at the cost of the highest complexity. To design a simpler receiver, it is suggested to use less complex combining techniques, i.e. switched diversity, which provides one of the least complex solutions to combat fading. The paper analyzes two switched diversity schemes, switch examine combining (SEC), and switch examine combining with post examining selection (SECp). A closed form expression determining the probability of detection using MRC, SEC and SECp is derived for various numbers of branches. Detection performance with different diversity combining techniques is compared and the complexity trade-off is observed.

Keywords—cognitive radio, complementary ROC, post examining selection, probability of detection, probability of false alarm, switch and examine combining.

1. Introduction

Cognitive radio (CR) is gaining attention in wireless scenarios as it enables the secondary user (SU) to efficiently utilize the free spectrum licensed to the primary user (PU), at a time when the spectrum is not being used [1]–[5]. This unoccupied or unutilized frequency band is known as a spectrum hole [6]. To find these holes, different sensing techniques are used [3], [7]. But fading is a problem in the wireless environment and due to this phenomenon the performance of PU detection degrades significantly.

In literature [8]–[15], space diversity is one of the solutions to mitigate the effect of fading. Diversity combining techniques [16] are then used to receive multiple copies of the signal generated by space diversity. Switched diversity and selection combining (SC) [17] are two most popular less complex diversity combining techniques. Selection of the diversity branch in SC is based on choosing the best signal among all which are received from different branches at the receiver [18]. The use of SC requires SNR estimation of all branches, hence switched diversity can be a simpler option for diversity combining. Switching from one diversity branch to another only when needed reduces receiver complexity [19]. There are two different strategies that can be used in switched diversity. One is switch and stay combining (SSC), in which the receiver selects another branch only if SNR of the current branch falls below the required threshold. The other strategy is switch and examine (SEC). The classic switch and SEC are used to take advantage of multiple diversity paths. SEC is also used with post examining selection (SECp) [20]. This scheme is similar to SEC, except one difference – it chooses the best path when no acceptable path is found after all paths have been tested.

In this paper the complexity detection performance of cognitive radio, using with different diversity combining techniques is compared and the complexity trade-off is observed. General expressions for probability of detection over the Rayleigh fading channel using MRC, SEC and SECp diversity combining techniques are derived.

2. System Model

In this paper the energy detection method is applied to the PU which is discussed in [21]. The received signal $r[n]$ can be defined as a binary hypothesis test as [21]:

$$r[n] = \begin{cases} z[n] & , H_0 \\ Hx[n] + z[n], & H_1 \end{cases}, \; n = 1,2,\ldots,N, \qquad (1)$$

where H is the channel coefficient that is considered as constant for a particular observation, i.e. for N samples. H_0 is the hypothesis test when noise only is present and H_1 is the hypothesis test when both noise and signal are present. $x[n]$ is the primary user signal component which is assumed to be an unknown deterministic signal, and $z[n]$ is the noise component which is assumed to be an additive white Gaussian noise (AWGN) having zero mean and variance σ^2.

3. Probability of Detection, Misdetection and False Alarm

3.1. Probability of False Alarm

As derived in [21] the probability of false alarm in AWGN channel is:

$$P_{fa} = \int_{\frac{\lambda}{\sigma^2}}^{\infty} \frac{1}{2^{\frac{N}{2}}\Gamma\left(\frac{N}{2}\right)} t^{\frac{N}{2}-1} \mathrm{e}^{-\frac{t}{2}} \mathrm{d}t = Q_{\chi_N^2}\left(\frac{\lambda}{\sigma^2}\right),\ \frac{\lambda}{\sigma^2} \geq 0, \quad (2)$$

$Q_{\chi_N^2}\left(\frac{\lambda}{\sigma^2}\right)$ can be written as [22]:

$$Q_{\chi_N^2}\left(\frac{\lambda}{\sigma^2}\right) = \begin{cases} 2Q\sqrt{\frac{\lambda}{\sigma^2}} & ,\ N=1 \\ 2Q\sqrt{\frac{\lambda}{\sigma^2}} + \frac{\mathrm{e}^{-\frac{\lambda}{2\sigma^2}}}{\sqrt{\pi}} & \\ \times \sum_{k=1}^{\frac{N-1}{2}} \frac{(k-1)!\left(\frac{2\lambda}{\sigma^2}\right)^{k-\frac{1}{2}}}{(2k-1)!} & ,\ N \text{ odd} \\ \mathrm{e}^{-\frac{\lambda}{2\sigma^2}} \sum_{k=0}^{\frac{N}{2}-1} \frac{\left(\frac{\lambda}{2\sigma^2}\right)^k}{k!} & ,\ N \text{ even} \end{cases}, \quad (3)$$

where $Q(.)$ is the complementary cumulative distribution function defined as:

$$Q(x) = \int_x^{\infty} \frac{1}{\sqrt{2\pi}} \mathrm{e}^{-\frac{t^2}{2}} \mathrm{d}t.$$

In the same work the probability of detection in AWGN channel is defined by:

$$P_d = Q_{\chi^2_{N(\gamma)}}\left(\frac{\lambda}{\sigma^2}\right) = \int_{\frac{\lambda}{\sigma^2}}^{\infty} \frac{1}{2}\left(\frac{1}{\gamma}\right)^{\frac{N-2}{4}} \mathrm{e}^{\frac{1}{2}(t+\gamma)} I_{\frac{N}{2}-1}\sqrt{\gamma t}\,\mathrm{d}t, \quad (4)$$

where λ is a predetermined threshold and instantaneous received SNR γ is defined as $\gamma = |H|^2\frac{\xi}{\sigma^2}$. Equation (4) can also be written using [23] for an even number of degrees of freedom as:

$$P_d = Q_{\frac{N}{2}}\left(\sqrt{\gamma}, \sqrt{\lambda'}\right), \quad (5)$$

where $\lambda' = \frac{\lambda}{\sigma^2}$ and $Q_m(.)$, the m-th generalized Marcum Q function [24] which is given by:

$$Q_m(\alpha,\beta) = \frac{1}{\alpha^{m-1}} \int_{\beta}^{\infty} x^m e^{-\frac{x^2+\alpha^2}{2}} I_{m-1}(\alpha x)\,\mathrm{d}x. \quad (6)$$

Equation (6) cannot be used for an odd degrees of freedom. For this case, it can be defined as [21]:

$$Q_{\chi^2_{N(\gamma)}}\left(\frac{\lambda}{\sigma^2}\right) = \sum_{k=0}^{\infty} \frac{\mathrm{e}^{-\frac{\gamma}{2}}\left(\frac{\gamma}{2}\right)^k}{k!} \int_{\lambda'}^{\infty} \frac{t^{\frac{N}{2}+k-1}\mathrm{e}^{-\frac{t}{2}}}{2^{\frac{N}{2}+k}\Gamma\left(\frac{N}{2}+k\right)}\mathrm{d}t$$
$$= \sum_{k=0}^{\infty} \frac{\mathrm{e}^{-\frac{\gamma}{2}}\left(\frac{\gamma}{2}\right)^k}{k!} \underbrace{Q_{\chi^2_{N+2k}}\left(\lambda'\right)}_{\text{Second term}}. \quad (7)$$

The second term is the right-tail probability of a central chi-square having $N+2k$ degrees of freedom.

3.2. Average Detection Probability

The probability of false alarm remains the same as given by Eq. (2) under any fading channel because it is formulated for the no signal transmission case and is independent of SNR. Hence the same formula can be used for upcoming sections as well. But to find out the probability of detection under the fading channel, Eq. (5) is averaged over the probability density function (PDF) of that particular channel. So, if the signal amplitude follows the Rayleigh distribution, then SNR γ follows an exponential PDF given by [25]:

$$f(\gamma) = \frac{1}{\overline{\gamma}}\mathrm{e}^{-\frac{\gamma}{\overline{\gamma}}},\ \gamma \geq 0, \quad (8)$$

where $\overline{\gamma}$ is the average received SNR.
The probability of false alarm remains the same as given by Eq. (2) under any fading channel because it is formulated for the no signal transmission case and is independent of SNR. So, the same formula can be used for upcoming sections as well. In the Rayleigh fading channel, the average probability of detection P_D for this case is evaluated by integrating Eq. (5) over Eq. (8) [25]:

$$\overline{P}_{d_{Ray}} = \int_0^{\infty} Q_{\frac{N}{2}}\left(\sqrt{\gamma}, \sqrt{\lambda'}\right) f(\gamma)\mathrm{d}\gamma$$
$$= \frac{1}{\overline{\gamma}} \int_0^{\infty} Q_{\frac{N}{2}}\left(\sqrt{\gamma}, \sqrt{\lambda'}\right)\mathrm{e}^{-\frac{\gamma}{\overline{\gamma}}}\mathrm{d}\gamma, \quad (9)$$

where $\overline{\gamma}$ is average SNR, and $f(\gamma)$ denotes the PDF of the fading channel (here PDF of the Rayleigh fading channel is taken).
Equation (9) can be written in the closed form [26]:

$$\overline{P}_{d_{Ray}} = \mathrm{e}^{-\frac{\lambda}{2}} \sum_{k=0}^{u-2} \frac{1}{k!}\left(\frac{\lambda}{2}\right)^k + \left(\frac{1+\overline{\gamma}}{\overline{\gamma}}\right)^{u-1}$$
$$\times \left(\mathrm{e}^{-\frac{\lambda}{2(1+\overline{\gamma})}} - \mathrm{e}^{-\frac{\lambda}{2}} \sum_{k=0}^{u-2} \frac{1}{k!} \frac{\lambda\overline{\gamma}}{2(1+\overline{\gamma})}\right). \quad (10)$$

For maximal ratio combining, scaling as well as cophasing of the signals is required and all the paths are optimally

combined at the receiver. The output SNR γ_t of the MR combiner is $\gamma_t = \sum_{l=1}^{L} \gamma_l$, where L is the total number of diversity branches and γ_l is the SNR of the individual branch. In MRC, the average probability of detection for AWGN channel is:

$$P_{dMRC} = Q_{LN/2}\left(\sqrt{2\gamma_t}, \sqrt{\lambda}\right). \tag{11}$$

The PDF of γ_t over i.i.d. Rayleigh branches for MRC is given by [9]:

$$f_{\gamma_{MRC}}(\gamma_t) = \frac{1}{(L-1)!\overline{\gamma}^L}\gamma_t^{L-1}\mathrm{e}^{-\frac{\gamma_t}{\overline{\gamma}}}. \tag{12}$$

The average probability of detection for MRC diversity scheme $\overline{P}_{dMRC}$ will then be calculated by averaging Eq. (11) over Eq. (12) and that comes out to be in closed form as:

$$\overline{P}_{d_{Ray_{MRC}}} = \alpha_1\left[Z_1 + \rho\sum_{n=1}^{L}\frac{\left(\frac{\lambda}{2}\right)^n}{2(n!)}{}_1F_1 \times\left(L; n+1; \frac{L\lambda\overline{\gamma}}{2L(1+\overline{\gamma})}\right)\right], \tag{13}$$

where:

$\alpha_1 = \frac{1}{L!2^{L-1}}\overline{\gamma}^{-L}$,

$$Z_1 = \frac{2^{L-1}(L-1)!\overline{\gamma}^{L+1}}{1+\overline{\gamma}}\mathrm{e}^{-\frac{\lambda}{2(1+\overline{\gamma})}}\left[\left(1+\frac{1}{\overline{\gamma}}\right)\left(\frac{1}{1+\overline{\gamma}}\right)^{L-1} \times\Im_{L-1}\left(-\frac{\lambda}{2(1+\overline{\gamma})}\right) + \sum_{n=0}^{L-2}(1+\overline{\gamma})^n\Im_n\left(-\frac{\lambda}{2(1+\overline{\gamma})}\right)\right],$$

$\rho = (L-1)!\left(\frac{2\overline{\gamma}}{1+\overline{\gamma}}\right)^L\mathrm{e}^{-\frac{\lambda}{2}}$.

The $\Im_n$ is Laguerre polynomial of degree n.

The probability of detection in the AWGN channel is defined by Eq. (5). The PDF of γ over L number of i.i.d. Rayleigh branches for SEC is given by Eq. [9]:

$$f_{\gamma_{SEC}}(\gamma) = \begin{cases}\left(1-\mathrm{e}^{-\frac{\gamma_T}{\overline{\gamma}}}\right)^{L-1}\frac{1}{\overline{\gamma}}\mathrm{e}^{-\frac{\gamma}{\overline{\gamma}}}, & \gamma < \gamma_T \\ \sum_{j=0}^{L-1}\left(1-\mathrm{e}^{-\frac{\gamma_T}{\overline{\gamma}}}\right)^j\frac{1}{\overline{\gamma}}\mathrm{e}^{-\frac{\gamma}{\overline{\gamma}}}, & \gamma \geq \gamma_T\end{cases}, \tag{14}$$

where γ_T is the switching threshold. The average probability of detection of switch and examine combining can be obtained by averaging Eq. (5) over Eq. (14) and comes out to be:

$$\overline{P}_{d_{SEC}} = \frac{1}{\overline{\gamma}}\mathrm{e}^{-\frac{\gamma}{\overline{\gamma}}}\left[\int_0^{\gamma_T}\left(1-\mathrm{e}^{-\frac{\lambda_T}{\overline{\gamma}}}\right)^{L-1}Q_{fracN2}\left(\sqrt{\gamma}, \sqrt{\lambda'}\right)\mathrm{d}\gamma + \int_{\gamma_T}^{\infty}\sum_{j=0}^{L-1}\left(1-\mathrm{e}^{\frac{\gamma_T}{\overline{\gamma}}}\right)^j Q_{\frac{N}{2}}\left(\sqrt{\gamma}, \sqrt{\lambda'}\right)\mathrm{d}\gamma\right]. \tag{15}$$

In the closed form Eq. (15) comes out to be:

$$\overline{P}_{d_{SEC}} = \left(1-\mathrm{e}^{-\frac{\gamma_T}{\overline{\gamma}}}\right)^{L-1}\left(\overline{P}_{d_{Ray}} - C\right) + \sum_{j=0}^{L-1}\left(1-\mathrm{e}^{-\frac{\gamma_T}{\overline{\gamma}}}\right)^j C, \tag{16}$$

where

$$C = \mathrm{e}^{-\frac{\gamma_T}{\overline{\gamma}}}Q_u\left(\sqrt{\gamma_T}, \sqrt{\lambda}\right) + \left(\frac{1+\overline{\gamma}}{\overline{\gamma}}\right)^{u-1} \times\mathrm{e}^{-\frac{\lambda}{2(1+\overline{\gamma})}}\left[1 - Q_u\left(\sqrt{2\gamma_T\frac{1+\overline{\gamma}}{\overline{\gamma}}}, \sqrt{\frac{\lambda\overline{\gamma}}{1+\overline{\gamma}}}\right)\right]. \tag{17}$$

3.3. Average Detection Probability for SECP

In CR, when no acceptable path is found after examining all the possibilities, the best path among all these unacceptable routes (with the highest SNR for data reception) is selected. Whereas in classical SEC, the switching-examining process is repeated until an acceptable path is found (i.e. with SNR greater than the threshold) or until all the routes have been examined. If all the paths are examined and no acceptable route is found, the receiver selects, in most cases, the last examined path [20]. In SECp, there is a predetermined threshold γ_T and any diversity path having SNR greater than this threshold is accepted. If no path is found having SNR greater than γ_T, the SECp receiver selects the path having the highest SNR. As such, SECp needs less path switching and fewer path estimations which results more complexity compared to the classic SEC method. But it shows a better performance that is proved later in this paper.

The PDF of γ over L no. of i.i.d. Rayleigh branches for SECp is given by [9]:

$$f_{\gamma_{SEC_p}}(\gamma) = \begin{cases}L\left(1-\mathrm{e}^{-\frac{\gamma}{\overline{\gamma}}}\right)^{L-1}\frac{1}{\overline{\gamma}}\mathrm{e}^{-\frac{\gamma}{\overline{\gamma}}}, & \gamma < \gamma_T \\ \left[1-\left(1-\mathrm{e}^{-\frac{\gamma}{\overline{\gamma}}}\right)^L\right]\frac{1}{\overline{\gamma}}\mathrm{e}^{-\frac{\gamma-\gamma_T}{\overline{\gamma}}}, & \gamma \geq \gamma_T\end{cases}. \tag{18}$$

The average detection probability of SECp can be obtained by averaging Eq. (5) over Eq. (18):

$$\overline{P}_{d_{SECP}} = I_1 + I_2, \tag{19}$$

where I_1 is given by:

$$I_1 = \frac{L}{\overline{\gamma}}\sum_{k=0}^{L}(-1)^k\frac{(L-1)!}{k!(L-k-1)!}[X_1 - X_2], \tag{20}$$

having

$$X_1 = \frac{\overline{\gamma}}{k+1}\mathrm{e}^{\frac{-\lambda'}{2}}\left[\left(1+\frac{2(1+k)}{\overline{\gamma}}\right)^{\frac{N}{2}-1}\left(\mathrm{e}^{\frac{\lambda'}{2(1+\frac{2(1+k)}{\overline{\gamma}}}} - \sum_{n=0}^{\frac{N}{2}-2}\frac{1}{n!}\frac{\lambda'}{2\left(1+\frac{2(1+k)}{\overline{\gamma}}\right)}\right) + \sum_{n=0}^{\frac{N}{2}-2}\frac{1}{n!}\left(\frac{\lambda'}{2}\right)^n\right], \tag{21}$$

$$X_2 = \frac{\overline{\gamma}}{1+k} \mathrm{e}^{-\frac{(1+k)\gamma_T^2}{\overline{\gamma}}} Q_{\frac{N}{2}}\left(\gamma_T, \sqrt{\lambda'}\right) + \frac{\overline{\gamma}}{2(k+1)} \times \left(1+\frac{2(1+k)}{\overline{\gamma}}\right)^{\frac{N}{2}-1} \mathrm{e}^{-\frac{\lambda'}{2}\frac{2(1+k)}{2(1+k)+\overline{\gamma}}} \times \left[1 - Q_{\frac{N}{2}}\left(\gamma_T\sqrt{1+\frac{2(1+k)}{\overline{\gamma}}}, \frac{\sqrt{\lambda'}}{\sqrt{1+\frac{2(1+k)}{\overline{\gamma}}}}\right)\right], \quad (22)$$

and I_2 has the expression given by:

$$I_2 = \left[1 - \left(1 - \mathrm{e}^{-\frac{\gamma_T}{\overline{\gamma}}}\right)^L\right] \mathrm{e}^{\frac{\gamma_T}{\overline{\gamma}}} C, \quad (23)$$

where C is defined by Eq. (17).

4. Results and Discussion

Here, the probability of detection for both SEC and SECp is evaluated using Monte Carlo simulation for the threshold SNR $\gamma_{th} = 18$ dB. Figure 1 illustrates SNR vs P_D over the Rayleigh fading channel for different diversity combining techniques (SEC, SECp, MRC) along with no diversity case. Here, the variation in probability of detection with respect to SNR is observed, and one may see from the graph that the probability of detection is higher for SECp than in the case of conventional SEC. Figure 2 also illustrates the same results for different numbers of samples, i.e. SECp performs better than SEC. Another finding of Fig. 2 is that the performance improves upon increasing N. In Fig. 3, a graph showing the probability of misdetection and the probability of a false alarm is plotted for a constant value of SNR. This graph is known as the complementary receiver operating characteristic (ROC) curve. Complementary ROC curves for different diversity combining techniques also show a better performance of the SECp technique, which is verified for different N in Fig. 4.

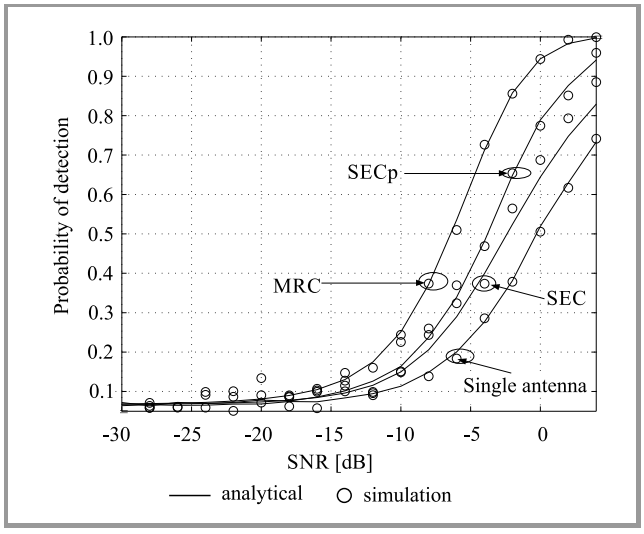

Fig. 1. SNR vs P_d curves over the Rayleigh fading channel for a single antenna and SEC, SECp, MRC diversity combining techniques for $L = 2$ with $\gamma_{th} = 8$ dB and $N = 10$.

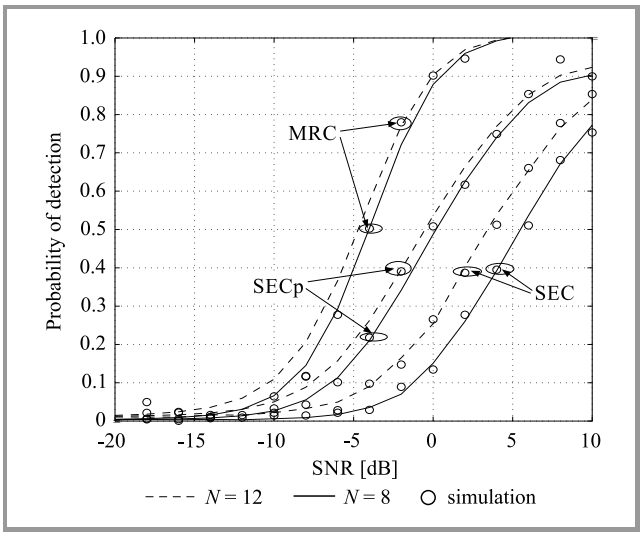

Fig. 2. SNR vs P_d curves over the Rayleigh fading channel with a single antenna and SEC, SECp ($L = 2$) diversity combining techniques having $\gamma_{th} = 8$ dB for different N.

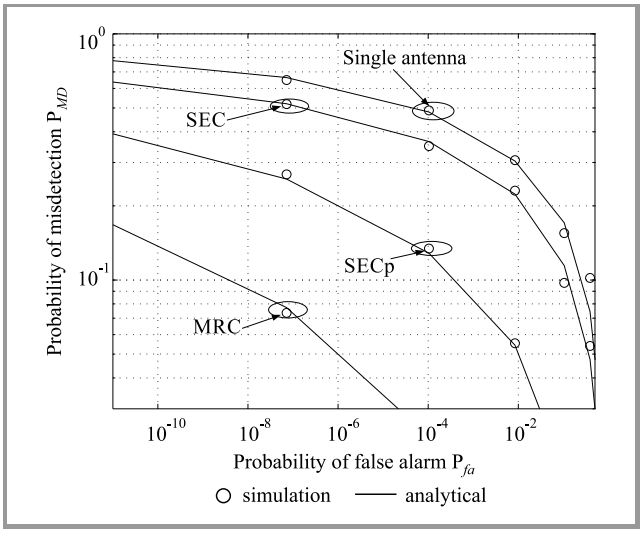

Fig. 3. Complementary ROC curves over the Rayleigh fading channel for a single antenna and SEC, SECp diversity combining techniques for $L = 2$ with $\gamma_{th} = 8$ dB, $\overline{\gamma} = 6$ dB, $N = 8$.

5. Conclusion

In this paper, performance analysis of different diversity combining techniques is conducted for cognitive radio scenarios. General formulas for the probability of detection using MRC, SEC and SECp diversity combining techniques over the Rayleigh fading channel are derived and results are cross-verified. Though MRC gives the best results, its hardware design is quite complex. If a less complex receiver design is required, switched diversity techniques may prove to be a better option. The performance of MRC is slightly better than SECp but the design of SECp is much simpler. It is shown that the same results are repeated for different numbers of samples. It is illustrated with the help of SNR vs probability of detection curves, as well as with

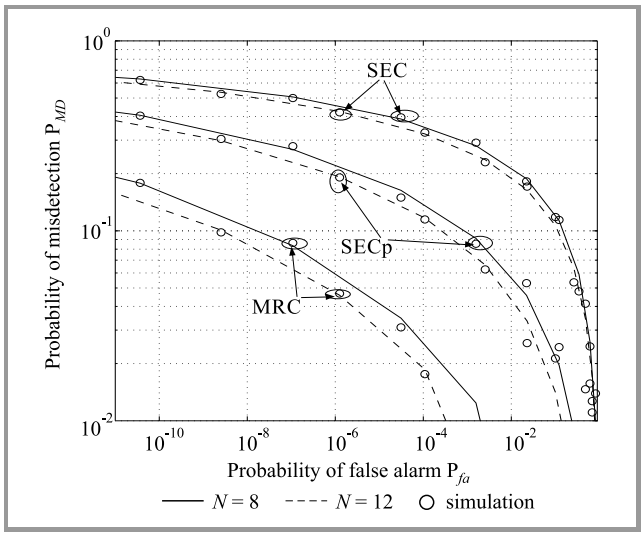

Fig. 4. Complementary ROC curves over the Rayleigh fading channel for a single antenna and SEC, SECp ($L = 2$) diversity combining techniques with $\gamma_{th} = 8$ dB, $\overline{\gamma} = 5$ dB for different N.

complementary ROC curves, that performance improves on increasing the number of samples. Performance improves also with additional branches. Performance of cognitive radio with no diversity is the lowest, and improves with the implementation of diversity combining techniques.

References

[1] K. R. Chowdhury, I. F. Akyildiz, and W.-Y. Lee, "CRAHNs: Cognitive radio ad hoc networks", *Ad Hoc Networks*, vol. 7, no. 5, pp. 810–836, 2009 (doi: 10.1016/j.adhoc.2009.01.001).

[2] B. H. Juang, J. Ma, and G. Li, "Signal processing in cognitive radio", *Proc. of IEEE*, vol. 97, no. 5, pp. 805–823, 2009 (doi: 10.1109/JPROC.2009.2015707).

[3] R. Balakrishnan, I. F. Akyildiz, and F. L. Brandon, "Cooperative spectrum sensing in cognitive radio networks: A survey" *Physic. Communic.*, vol. 4, no. 1, pp. 40–62, 2010 (doi: 10.1016/j.phycom.2010.12.003).

[4] M. C. Vuran, S. Mohanty, I. F. Akyildiz, and W.-Y. Lee, "Next generation/dynamic spectrum access/cognitive radio wireless networks: A survey", *Computer Networks*, vol. 50, no. 13, pp. 2127–2159, 2006 (doi: 10.1016/j.comnet.2006.05.001).

[5] A. Tkachenko, D. Cabric, and R. W. Brodersen, "Experimental study of spectrum sensing based on energy detection and network cooperation", in *Proc. 1st Int. Workshop on Technol. and Policy of Spectrum Sensing TAPAS 2006*, Boston, MA, USA, 2006, article no. 12 (doi: 10.1145/1234388.1234400).

[6] E. Hossain and V. Bhargava, *Cognitive wireless communication network*. New York: Springer, 2007 (ISBN: 978-0387688305).

[7] S. M. Mishra, D. Cabric, and R. W. Brodersen, "Implementation issues in spectrum sensing for cognitive radios", in *Proc. Conf. Record of the Thirty-Eighth Asilomar Conf. on Signals, Systems and Computers,*, Pacific Grove, CA. USA, 2004, pp. 772–776 (doi: 10.1109/ACSSC.2004.1399240).

[8] M. S. Alouini and M. K. Simon, "Performance analysis of generalized selective combining over Rayleigh fading channels", in *Proc. 1999 IEEE Communications Theory Mini-Conference*, Vancouver, BC, Canada, 1999, pp. 110–114 (doi: 10.1109/CTMC.1999.790247).

[9] M. K. Simon and M.-S. Alouini, *Digital Communication over Fading Channels*. Hobeken NJ: Wiley, 2nd edition, 2005 (ISBN: 978-0-471-64953-3).

[10] S. Ikki and M. H. Ahmed, "Performance analysis of cooperative diversity using equal gain combining (EGC) technique over Rayleigh fading channels", in *Proc. 2007 IEEE Int. Conf. on Commun.*, Glasgow, UK, 2007, pp. 5336–5341 (doi: 10.1109/ICC.2007.883).

[11] J. N. Laneman, D. N. C. Tse, and G. W. Wornell, "Cooperative diversity in wireless networks: Efficient protocols and outage behavior", *IEEE Transact. on Inform. Theory*, vol. 50, no. 12, pp. 3062–3080, 2004 (doi: 10.1109/TIT.2004.838089).

[12] M.-S. Alouini and A. J. Goldsmith, "A unified approach for calculating error rates of linearly modulated signals over generalized fading channels", *IEEE Transact. on Commun.*, vol. 47, no. 9, pp. 1324–1334, 1999 (doi: 10.1109/26.789668).

[13] T. Eng and L. B. Milstein, "Coherent DS-CDMA performance in Nakagami multipath fading", *IEEE Transact. on Commun.*, vol. 43, no. 2/3/4, pp. 1134–1143, 1995 (doi: 10.1109/26.380145).

[14] J. Hu and N. C. Beaulieu, "Closed-form expressions for the outage and error probabilities of decode-and-forward relaying in dissimilar Rayleigh fading channels", in *Proc. 2007 IEEE Int. Conf. on Communications*, Glasgow, UK, 2007, pp. 5553–5557 (doi: 10.1109/ICC.2007.920).

[15] H. Katiyar and R. Bhattacharjee, "Performance of two-hop decode-forward multi-antenna cooperative relaying in Nakagami-*n* fading channel", in *Proc. 2009 Annual IEEE India Conf. INDICON 2009*, Ahmedabad, Gujarat, India, 2009 (doi: 10.1109.INDCON.2009.5409478).

[16] D. Brennan, "Linear diversity combining techniques", *Proc of the IRE*, vol. 47, no. 6, pp. 1075–1102, 1959 (doi: 10.1109/JRPROC.1959.287136).

[17] A. Adinoyi, Y. Fan, H. Yanikomeroglu, H. Poor, and F. Al-Shaalan, "Performance of selection relaying and cooperative diversity", *IEEE Transact. on Wireless Commun.*, vol. 8, no. 12, pp. 5790–5795, 2009 (doi: 10.1109/TWC.2009.12.090138).

[18] T. S. Rappaport, K. L. Kosbar, W. H. Tranter, and K. S. Shanmugan, *Principles of Communication Systems Simulation with Wireless Applications*, Upper Saddle River, NJ: Prentice Hall, 1st edition, 2004 (ISBN: 978-0134947907).

[19] H. Katiyar, R. Bhattacharjee, and S. Darshi, "Outage performance of switch and stay combining scheme for multi-antenna relay network", in *Proc. 2010 Second UK-India-IDRC Int. Workshop on Cognit. Wireless Sys. UKIWCWS 2010*, New Delhi, India, 2010 (doi: 10.1109/UKIWCWS.2010.5724229).

[20] H.-C. Yang, M.-S. Alouini, "Improving the performance of switched diversity with post-examining selection", *IEEE Transact. on Wireless Commun.*, vol. 5, no. 1, pp. 67–71, 2006 (doi: 10.1109/TWC.2006.1576529).

[21] O. Altrad and S. Muhaidat, "A new mathematical analysis of the probability of detection in cognitive radio over fading channels", *EURASIP J. on Wireless Commun. and Network.*, no. 1, pp. 1–11, 2013 (doi: 10.1186/1687-1499-2013-159).

[22] I. E. Stegun and M. Abramowitz. *Handbook of Mathematical Functions with Formulas, Graphs, and Mathematical Tables*. New York: Dover, 1972 (ISBN: 978-0486612720).

[23] M. K. Simon, *Probability Distribution Involving Gaussian Random Variables: A Handbook for Engineers and Scientists*, International Series in Engineering and Computer Science. New York: Springer, 2002 (ISBN: 978-0387476940).

[24] I. S. Gradshteyn and I. M. Ryzhik, *Table of Integrals, Series and Products*. London: Academic Press Inc, 7th revised edition, 2007 (ISBN: 978-0123736376).

[25] R. Agarwal, N. Srivastava, and H. Katiyar, "Energy detection of unknown signals over Rayleigh fading channel for EGC and SSC diversity combining techniques", in *Proc. 2016 Int. Conf. on Emerging Trends in Electr. Electron. & Sustain. Energy Sys. ICETEESES*, Sultanpur, Uttar Pradesh, 2016, pp. 116–119 (doi: 10.1109/ICETEESES.2016.7581365).

[26] A. H. Nuttall, *Some integrals involving the Q SUB M function*. New London, CT: Naval Underwater Systems Center, 1974.

Rupali Agarwal received the B.Tech. degree from Inderprastha Engineering College, Ghaziabad, in 2005 and the M.Tech. degree from Harcourt Butler Technological Institute, Kanpur, in 2010, both in Electronics and Communication Engineering. From 2010 to 2011 she was Senior Lecturer of Electronics and Communication Engineering Department at Ambalika Institute of Management and Technology, Lucknow, Uttar Pradesh, India. She is currently working as Associate Professor in BBD National Institute of Technology and Management in the Department of Electronics and communication engineering, Lucknow, Uttar Pradesh, India. She has published over ten research papers in journals, and national and international conferences. Her research interests include wireless communication (specialized in channel modeling, cognitive radio and cooperative communication scheme).

E-mail: roopali.ipec@gmail.com
Babu Banarasi Das National Institute of Technology & Management
Lucknow, Uttar Pradesh, India 226010

Neelam Srivastava received the B.Eng. degree from M.M.M. Engineering College, Gorakhpur in 1985 and the M.Tech. degree from Institute of Technology, BHU, Varanasi, India in 1987 and Ph.D. degree in the area of Optical Communication at Lucknow University, Uttar Pradesh, India in 2004. She has been working at the Institute Institute of Engineering and Technology (IET), Lucknow, India for 25 years. At present she is a Director in Rajkiya Engineering College, Kannauj. She is an active member of many professional bodies like IEEE, IETE, IE, Board of Faculty of Engineering and Technology, Lucknow University. Her research interests include wireless and optical communication.

E-mail: neelam.srivastava@ietlucknow.ac.in
Rajkiya Engineering College
Kannauj, Uttar Pradesh, India 209732

Himanshu Katiyar received his B.Eng. degree in Electronics and Communication Engineering from M.I.T. Moradabad (M.J.P. Rohilkhand University, Bareilly), Uttar Pradesh, India in 2001, M.Tech. degree from Madan Mohan Malviya Engineering College, Gorakhpur (U.P. Technical University, Lucknow), Uttar Pradesh, India in 2004 and Ph.D. degree in the area of wireless communication at the Indian Institute of Technology (IIT), Guwahati, Assam India in 2011. From 2004 to 2005 he was lecturer in Electronics and Communication Engineering Dept. at SRMSCET, Bareilly, Uttar Pradesh, India and from 2005 to 2006 he was lecturer of Electronics and Communication Engineering Dept. at NIEC, Lucknow, Uttar Pradesh, India. From 2010 to 2017 he was Associate Professor at Babu Banarasi Das University, Lucknow, India. At present he is Associate Professor in the Electronics Engineering Dept. at Rajkiya Engineering College, Sonbhadra, Uttar Pradesh, India. His research interests include almost all aspects of wireless communications with a special emphasis on MIMO systems, channel modeling, infrastructure-based multihop and relay networks and cooperative diversity schemes.

E-mail: katiyarhimanshu@gmail.com
Rajkiya Engineering College
Sonbhadra, Uttar Pradesh, India 231206

Paper

Swarm Intelligence-based Partitioned Recovery in Wireless Sensor Networks

Gaurav Kumar and Virender Ranga

Department of Computer Engineering, National Institute of Technology Kurukshetra, Haryana, India

https://doi.org/10.26636/jtit.2018.121817

Abstract—The failure rate of sensor nodes in Heterogeneous Wireless Sensor Networks is high due to the use of low battery-powered sensor nodes in a hostile environment. Networks of this kind become non-operational and turn into disjoint segmented networks due to large-scale failures of sensor nodes. This may require the placement of additional high-power relay nodes. In this paper, we propose a network partition recovery solution called Grey Wolf, which is an optimizer algorithm for repairing segmented heterogeneous wireless sensor networks. The proposed solution provides not only strong bi-connectivity in the damaged area, but also distributes traffic load among the multiple deployed nodes to enhance the repaired network's lifetime. The experiment results show that the Grey Wolf algorithm offers a considerable performance advantage over other state-of-the-art approaches.

Keywords—connectivity restoration, meta-heuristics, relay node placement, wireless sensor networks.

1. Introduction

Heterogeneous wireless sensor networks (HWSNs) employ different types of nodes which differ from each other in terms of capabilities, load assigned to the nodes and coverage areas. HWSNs attract a large number of applications in the field of health, defense, agriculture, forest monitoring, etc. Moreover, HWSNs are well capable of operating in harsh and hostile environments without human intervention. However, it is a challenging task to simultaneously maintain coverage and connectivity in a harsh environment [1], [2].

It is a hard fact that sensor nodes (SNs) are more susceptible to failure in a harsh scenario and may drain battery power within a short span of time if unnecessary loads are assigned to them. Therefore, HWSNs require energy-constrained algorithms to perform operations in harsh environments. Segmentation or network partition is a classic, well-known problem affecting HWSNs. In a segmented network, SNs may not be able to communicate with other sensor relay nodes. This is a distributed problem, where computation is to be performed in different parts of the system and results need to be aggregated for the final action to be taken.

Restoration of lost connectivity in distributed, disconnected HWSNs is an example of diffusing computation, where it starts at one node of the distributed system and slowly transfers towards other parts. On the other hand, segments may be created by using relay nodes (RNs) due to large-scale failures of SNs (i.e. battery power exhausted) or due to a natural disaster. RNs are more powerful than SNs in terms of communication range and reserved battery backup. Therefore, relay node placement (RNP) in HWSNs is a cost effective and best-suited method to solve the network partition problem, simultaneously offering a fault tolerance mechanism. The relay node placement problem (RNPP) is NP-hard [3], [4]. RNs are expensive. Hence, a large number of RNs may increase the overall cost of a network. Each and every position of RNs in 2D renders different optimized solutions. The solution with a minimum RN count could be considered as an optimized solution for RNPP.

There are many techniques to solve RNPP in HWSNs. However, meta-heuristics are recognized as best-suited methods.

Meta-heuristics are problem independent and stochastic in nature to solve NP-hard and optimization problems. Some popular meta-heuristics include Particle Swarm Optimization (PSO) [5], Ant Colony Optimization (ACO) [6], or Genetic Algorithm (GA) [7]. A meta-heuristic may produce a promising solution for a given set of problems besides that it may also give the worst solution for another set. It totally depends on the choice of the meta-heuristic made based on the problem at hand. Therefore, there is a need to find a relevant metaheuristic approach which can produce favorable results for the selected set of problems.

All meta-heuristics performed the search process that was divided into two different phases: exploration and exploitation. Global searching is called exploration and local searching is known as exploitation. Exploration covers the whole solution space by diverging search agents in different directions. Exploitation is a local search and covers only a specific part of the solution space by converging towards a candidate position. Meta-heuristics can be classified into three various classes: swarm intelligence-based (SI), physics-based, and evolutionary algorithms (EAs) [8].

To solve RNPP, we use the Grey Wolf Optimizer (GWO) as a swarm intelligence-based technique enabling to find the optimal location of probable RNs. It is based on the hunting behavior of grey wolves.

The paper is organized as follows. Section 2 shows the related work concerned with RNPP. The system model and the problem statement are discussed in Section 3. Section 4 is completely devoted to GWO explanation. The proposed solution is described in Section 5. Section 6 discusses the pseudo code. Some well-established proposed solutions are compared with proposed solution in Section 7. Finally, the paper is concluded in Section 8.

2. Related Work

RNPP-related techniques used for repairing segmented HWSNs can be classified into two different categories, based upon the behavior of RNs within the network. The first category of approaches is related to the deployment of static RNs in the damaged portion of HWSNs. The second category is used for the deployment of mobile relay nodes which can relay data received from a group of sensor nodes or from nearby neighboring RNs to the base station (BS), which may be either mobile or stationary. The mobility of BS can be taken into consideration for improving transmission efficiency.

2.1. Deployment of Static Relay Nodes

Recently, Lee *et al*. [9] tackled RNPP by deploying RN using Steiner Points (SPs) and the convex hull approach. During the first phase, they find a convex hull on all disjoint segments, where each segment is represented by a representative node. Each representative node denotes the whole segment area as a single point in 2D. In the second phase, they proposed to find minimal sub-Steiner trees for every three neighboring terminal nodes. This procedure is followed repeatedly until two terminal nodes are left.

In [10], Lanza-Gutierrez *et al*. proposed six different multi-objective meta-heuristics (ABC, firefly algorithm, evolutionary algorithm with NBI-Tchebyff approach, non-dominated sorting genetic algorithm-II, strength pareto-evolutionary algorithm 2, variable neighborhood search). They evaluated all proposed solutions based on three objectives (average sensitivity area, network reliability, average energy cost) using the six meta-heuristics referred to above. Each objective is bound with an objective function that is being used as input for the meta-heuristics at hand.

The concept of the local search approximation algorithm is introduced by Ma *et al*. [11] and is also known as LSSA. They proposed a novel, connectivity aware, approximation-based approach for two-tiered HWSNs. They formed, with the help of a local search, a local set cover for different groups of sensor nodes. After that, they calculated a set cover for RNs based on the local set cover. They extended the same for the double relay node set cover.

The authors of [12] solve RNPP in static hybrid HWSNs with the help of PSO and integer, planning the average path length between sensors. They improve the efficiency of relay deployment because of a restricted search space of the integer, instead of the real number. Efficient deployment of RNs and BS may enhance the efficiency of the proposed solution.

Lloyd *et al*. [13] have proposed a solution to solve 1-tier as well as 2-tier RNPPs. Their proposed solution is used to find the optimal path for the single tier, and for RNs between every pair of sensors. The second approach is proposed for a 2-tier RNPP. Time complexity for the 1-tier solution proposed is shown to be a 7-approximation, and for 2-tier it is shown as $(4.5+\varepsilon)$-approximation and $(5+\varepsilon)$-approximation.

The authors of [14] proposed a game theory-based approach for RNPP. This approach is supposed to have a complete knowledge about the network (the number of failed nodes, the number of segmented parts and location of partitioned segments). Each segment is used as a player in the game in which each node is used as a payoff function. Game theory is a centralized approach. Therefore, each partition must know about the payoff function of all other partitions. At last, each player shares their payoff results to restore lost connectivity within the segmented network.

2.2. Deployment of Mobile Nodes

Mobility in HWSNs may be divided into two categories: batch movement and succeeding movement. In batch movement, a group of nodes moves towards another group of nodes for re-connection. The basic idea behind batch movement is to join two partitions by moving towards each other [15]. Succeeding movement is related to the movement of one or few RNs, performed in an awkward fashion, in order to repair the segmented network, e.g. [16] restore connectivity by succeeding movement of RNs to repair wireless sensor and actor networks (WSANs). The authors of [17] try to identify a node the removal of which may lead to network partition. After identification, the suggested algorithm starts connectivity restoration of the partitioned WSN. Wang *et al*. [18] introduced mobility in RNs as well as in BS and try to increase network lifetime in different environments, e.g. static network, WSN with a single mobile sink, and WSN with mobile RN.

The main advantage of deployment of mobile RNs is the ability to collect/send data from/to a large number of sensors. Mobile RNs in HWSNs enhance coverage, connectivity, fault tolerance and lifetime of the network. Akkya *et al*. [19] deployed mobile agents to re-connect segmented partitions of HWSNs. They proposed a mathematical model for deployment of RNs for a minimum traveling distance. The proposed solution is evaluated based on time required to reconnect the partitioned network and the total distance traveled by mobile RNs. The authors of [20] deploy mobile agents to receive/send sensed data from/to sensor/BS. The proposed solution saves energy of SNs by using mobile RNs to transmit the data to BS.

The authors of [21] proposed an algorithm to control the mobility of nodes to reduce energy consumption. The idea behind controlled mobility is based on covering the damaged part of WSN. The mobile RN restores connectivity in the no-connectivity area. Since moving a node for a long time may drain its battery power at a fast rate the proposed solution minimizes the maximum travel distance.

3. System Model and Problem Statement

In this paper, a flat structure of HWSN is considered on which SNs are deployed throughout a specific predefined area by using any node deployment strategy. Here, random deployment is taken. Sink node/BS is positioned at a predefined location to receive aggregated data. All network traffic flows towards BS to get useful information related to the environment being observed. When a large number of SNs fail, a number of disjoint, partitioned segments may be created. Figure 1a shows a segmented HWSN with seven disjoint segments and the damaged area. Thus, proposed approach is proposes to place RNs inside the damaged area to restore lost connectivity. Initially, one RN is assigned to every segment as a representative node which is denoted by Seg_i. Thus, there is a need to deploy at least N_{Seg} RNs for every disjoint segment (suppose we have N_{Seg} number of the disjoint segment).

The problem of placing relay nodes in the segmented area can be described as follows. Initially, segmentation is detected, with N_{Seg} number of disjoint segments. Initially, N_{Seg} is the number of RNs considered, with each of them working as a gateway node for their respective segment. For simplicity, it is assumed that every segment has an RN for the purpose of the experiment. That RN is denoted by Seg_i where $0 \leq i \leq N_{Seg}$. The range of RNs is considered to be as required, and is denoted by the symbol R_r. The range of RNs (R_r) may differ from the range of SNs (R_s) which is usually $R_r \geq R_s$. The proposed algorithm strives to find the near to optimal position and the minimum count of RNs by using the GWO meta-heuristic technique.

The research is based on the following assumptions:

- all SNs, as well as BS, are static,
- all RNs have an equal unit transmission range of R_r,
- HWSN uses its underlying routing protocol to relay data from source to destination,
- X-Y coordinates of all nodes are considered in integer space.

4. The Grey Wolf Optimizer

Grey wolves have a well-organized social hierarchy. Their hunting strategy can be used for solving the optimization problem. To complete the hunting process grey wolves move forward in a planned manner. The authors of [22] suggest various steps which are used by the wolves for hunting. All these are listed below:

- track, trail and trace,
- keep an eye, surround and hassle the target until it comes to rest,
- attack the prey.

In [8] authors give a model of all these procedures which can be used to solve many optimization problems. Presented solution uses the same technique to restore lost connectivity in a partitioned HWSN. As per the social hierarchy of grey wolves, solutions obtained from mathematical modeling are categorized into three fittest solutions. Alpha (α) is considered to be the best solution. Beta (β) and delta (δ) will be the second and the third fittest solution, respectively. The remaining solutions will be considered to belong to the omega (ω) set.

4.1. Surrounding Prey

To model the surrounding phase, the following equations are used to depict the behavior:

$$\vec{D} = \left|\vec{J} \cdot \vec{P}_w(i) - \vec{P}(i)\right| , \tag{1}$$

$$\vec{P}(i+1) = \vec{P}_w - \vec{K} \cdot \vec{D} , \tag{2}$$

where $\vec{D}$ indicates the distance between prey and wolf, $\vec{J}$ and $\vec{K}$ are the coefficient vector which is used to encircle the prey. Both of these play an important role during hunting. $\vec{P}_w$ and $\vec{P}$ is the position vector of the wolf and the prey, respectively, and i denotes an iterator.

The equation coefficient vectors $\vec{J}$ and $\vec{K}$ are given as follows:

$$\vec{J} = 2 \cdot \vec{l}_1 , \tag{3}$$

$$\vec{K} = 2\vec{k} \cdot \vec{l}_2 - \vec{k} , \tag{4}$$

where vector $\vec{k}$ is decreased from 2 to 0, and vectors $\vec{l}_1$, $\vec{l}_2$ are random vectors in $[0, 1]$.

4.2. Attacking Prey

One of the best capabilities of grey wolves is to make an estimation of the location of prey. Firstly, they encircle the prey and then attack it. Alphas are the most dominating wolves within the group and they steer the hunt. In the case of NP-hard problems, the solution space is very large and it is quite difficult to search for optimal solutions in polynomial time. GWO always strive to find three fittest or best solutions. Considering that alpha is the fittest, beta is the second best and delta is the third best solution, the following equations are used to show the behavior of alpha, beta, and delta:

$$\vec{D_\alpha} = \left|\vec{J_1} \cdot \vec{P_\alpha} - \vec{P}\right|, \vec{D_\beta} = \left|\vec{J_2} \cdot \vec{P_\beta} - \vec{P}\right|, \vec{D_\delta} = \left|\vec{J_3} \cdot \vec{P_\delta} - \vec{P}\right| , \tag{5}$$

$$\vec{P_1} = \vec{P_\alpha} - \vec{K_1} \cdot \vec{D_\alpha}, \vec{P_2} = \vec{P_\beta} - \vec{K_2} \cdot \vec{D_\beta}, \vec{P_3} = \vec{P_\delta} - \vec{K_3} \cdot \vec{D_\delta} , \tag{6}$$

$$\vec{P}(i+1) = \frac{\vec{P_1} + \vec{P_2} + \vec{P_3}}{3} . \tag{7}$$

The pseudo code of GWO is shown as Algorithm 1.

Algorithm 1. Grey wolf optimizer algorithm

```
procedure GWO(initial population)
    Initialize the population of grey wolf agents P_d(d =
    1,2,...,n)
    Initialize all coefficient vectors k, K and J
    P_α ← First best possible solution
    P_β ← Second best possible solution
    P_β ← Third best possible solution
    while (i < max number of iterations) do
        for each search agent do
            Update possible location of current search
            agent by using Eq. (7)
        end for
        Update coefficient vectors k, K and J
        Calculate the fitness of all search agents
        Update position vectors P_α, P_β and P_δ
        i ← i + 1
    end while
    return P_α                    ▷ Return the best solution
end procedure
```

5. The Proposed Solution

We have considered a well-connected network in the simulation, which is converted into segmented portions after a large-scale failure of SNs. It leads to the creation of multiple, disjoint segments within the network. A 2D vector of the locations of disconnected segments is used as population size for the proposed solution and generates the probable location of prey. This is an iterative process and each iteration has its own solution, because the number of segments keeps changing continuously. The proposed GAIN solution is mapped with the GWO algorithm, as: all disconnected segments are treated as grey wolves. By using the current location of wolves, the probable location of prey is found. The location of prey is continuously updated with coefficient vectors, as discussed in Section 4. The observed location of prey is used for relay node placement between different segments to recover lost connectivity. The proposed solution is executed in different phases as shown below:

- locate the position of initial RNs,
- neighbor discovery,
- populating RNs,
- termination phase.

In the first phase, RNs are considered as representative nodes for all disjoints segments. Their locations are observed as discussed in Subsection 5.1. The transmission range of RNs (i.e. R_r) is considered to be the radius of the circle made by the coverage field of any RN. Therefore, any RN can cover a distance of $2R_r$ in all directions. The second phase is concerned with finding the neighboring segments with the help of the deployed RNs. In the third phase, the proposed algorithm strives to populate RNs in the damaged region by using different rounds. In each round, one best RN position is returned by the presented solution. The calculated location is abbreviated as the current relay node location for the respective round. The relay placed at the said location is called current relay. The current relay node strives to find representative nodes within its range. Now, nodes within the range of each other become neighboring nodes. All connected nodes in the segment are denoted by only one representative node for the simplicity of the algorithm. In the fourth phase (i.e. termination phase), the algorithm terminates when condition $N_{Seg} \leq 2$ is met, where N_{Seg} represents a number of disjoint segments in the network. Finally, if only one segment is left, connectivity has been restored successfully. If two segments are left, then there is a need to populate some additional RNs on the basis of the Euclidean distance between them, as discussed and shown in Eq. (8). The detailed description of the proposed GAIN solution is described in the following subsections.

5.1. Locate the Position of Initial RNs

Whenever the BS observes a sudden decrease in the amount of information sensed from the deployed network, it identifies a large-scale failure of SNs. The proposed solution is required to find relevant positions for populating representative nodes Seg_i where i represents the number of segments. Considering all segments have their own representative RN as a gateway for the segmented part, any communication within the segments would be possible only through these RNs. Figure 1a represents an example of a partitioned network with its seven representative nodes denoted by Seg_1 to Seg_7. The solution takes X-Y locations of all representative nodes as an input and produces a relay count. In addition, to identify the minimum distance between any two points, GAIN uses Euclidean distance given by:

$$ED_{(x_1,y_1)(x_2,y_2)} = \sqrt{(x_1-x_2)^2+(y_1-y_2)^2}\ , \qquad (8)$$

where $ED_{(x_1,y_1)(x_2,y_2)}$ denotes the Euclidean distance between two points (x_1,y_1) and (x_2,y_2).

5.2. Neighbor Discovery

In this phase, we consider a set of representative nodes obtained from the first phase. After that, each segment discovers its neighboring segments, as explained in Algorithm 2. After placing initial RNs, some of the segments find other segments to be within their transmission range and list those segments as their neighboring segments. Figure 1a shows an example of seven initial segments. Each segment is denoted by a single RN and it is referred to as a representative node for all nodes of the respective segment. Each representative RN is denoted by $Seg_i(x,y)$, where Seg_i is the segment number with its coordinate (x,y). As calculated in the simulation, X-Y coordinates of all segments are as Seg_1: $(50,12)$, Seg_2: $(79,23)$,

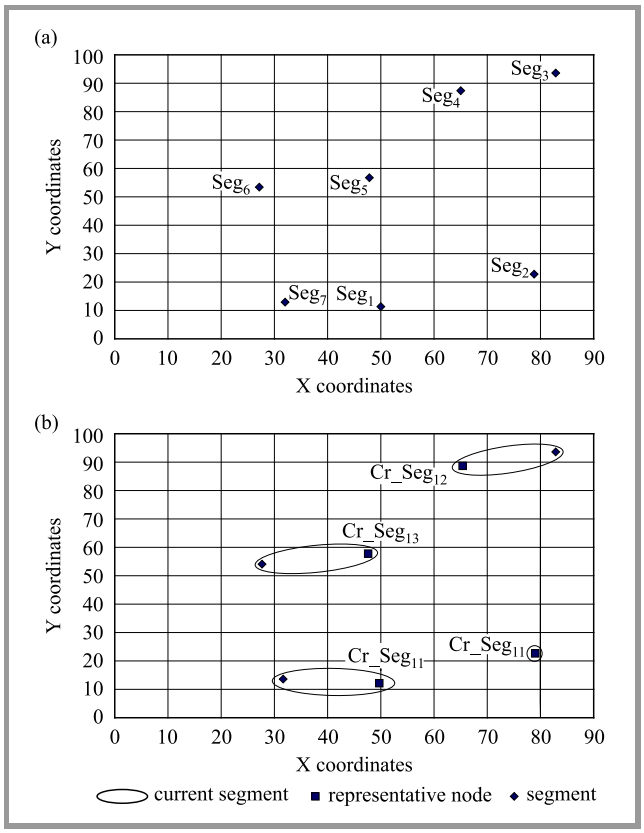

Fig. 1. Representing initial two steps of GAIN: (a) showing initial position of each segment Seg_i, and (b) showing neighboring segments where $R_r = 15$ m.

Seg_3: $(83,94)$, Seg_4: $(65,88)$, Seg_5: $(48,57)$, Seg_6: $(27,54)$ and Seg_7: $(32,13)$. After the placement of representative nodes within every segment, the proposed solution will increase the communication range of the respective segments due to the large communication range of RNs, albeit some of the segments do not require additional relays to establish communication between disjoint segments. The Euclidean distance between two segments (representative nodes) can be calculated as two points (x_1,y_1) and (x_2,y_2) in the X-Y plane. These points will be the neighbors of each other when these two points satisfy equality $R_r \leq ED_{(x_1,y_1)(x_2,y_2)}$. In this way, neighboring points will be combined into a single segment which is shown in Fig. 1b. It can be observed that Seg_1 joins Seg_7, Seg_3 joins Seg_4, Seg_5 joins Seg_6 and Seg_2 have no neighboring segment and converted it into current segments $Cr_{Seg_{14}}$, $Cr_{Seg_{12}}$, $Cr_{Seg_{13}}$, $Cr_{Seg_{11}}$, respectively.

This step adds an extra boost to the proposed algorithm to solve the network partition problem, and it is really helpful in reducing the number of deployed RNs. It is observed in the simulation that the total number of relay nodes would be always greater than or equal to the initial number of segments. This relation can be shown as $Count\_Relay \geq N_{Seg}$ where $Count\_Relay$ denotes the total number of relays requiring restoring connectivity within a disconnected WSN. After completion of the neighbor discovery phase, some of the segments combine with their neighboring segments and the rest of them are termed as current segments. The current segments are represented by $Cr_{Seg_{ij}}$, where i denotes the iteration number and j simply denotes the current segment number. Each segment may or may not have its neighbors, for e.g. Seg_2 does not have any neighboring nodes and segments Seg_1, Seg_4, Seg_5 have one neighboring node, i.e. Seg_7, Seg_3, Seg_6, respectively, as depicted in Fig. 1b.

5.3. Populating RNs

The third step of the proposed solution is executed in rounds. In each round, RN position is calculated and the observed position is represented by RN_i, where i denotes the respective iteration number. The proposed GAIN solution generates a convex hull over the representative nodes of the current segments $Cr_{Seg_{ij}}$. Due to the random and stochastic nature of RNs, their positions come out of the transmission range of all the segments. To remove this side effect, we incorporate the convex hull algorithm that uses the Graham scan algorithm [23]. The proposed solution continuously checks whether the calculated point lies inside the convex hull or not. If it lies inside the convex hull, then we proceed to the next iteration, otherwise the algorithm discards the candidate position and puts it into the

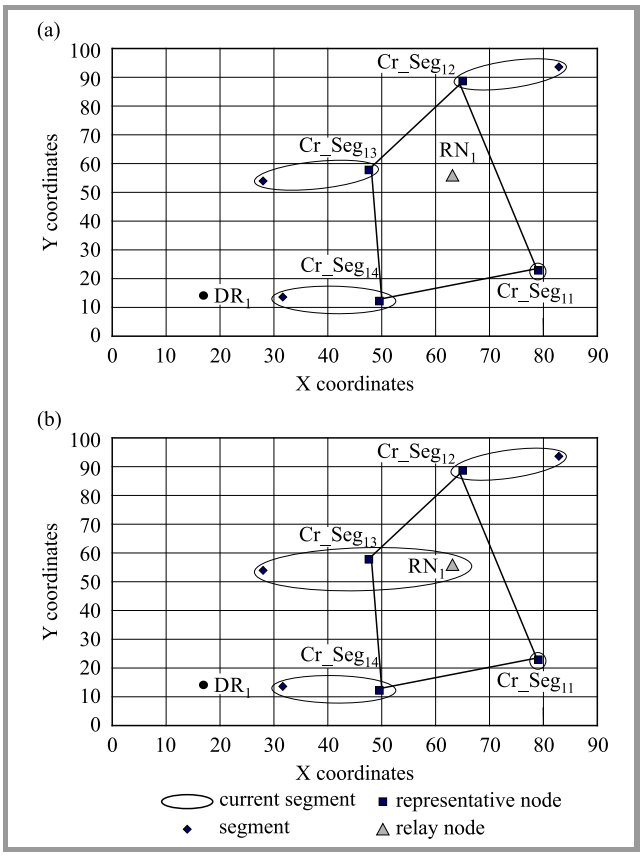

Fig. 2. First iteration of placing relay node placement by GWO: (a) shows a convex hull made by current segments, the first RN $RN_1(63,56)$ and the discarded relay $DR_1(17,14)$, and (b) current segment Cr_{Seg_3} is within the range of RN RN_1.

category of discarded RNs, represented by DR1, as shown in Fig. 2a.

The first iteration scenario has been shown in Fig. 2b. Here, one discarded RN position $DR_1(17,14)$, which lies outside the convex hull and one accepted RN position $RN_1(63,56)$ which lies inside the convex hull are shown. Sometimes only one, and sometimes a higher number of executions is required. Therefore, time-related complexity may be increased. However, GAIN shows better results compared with state-of-the-art solutions. The proposed algorithm strives to find segments within the range of RN RN_1. Again, the solution uses Eq. (8), where coordinates (x_1,y_1) represent the position of the RNs and (x_2,y_2) shows the coordinates of current segments. If any two current segments satisfy relation $ED_{(x_1,y_1),(x_2,y_2)} \leq 2R_r$, then both of these segments are considered within the range of each other. The same scenario can be seen in Fig. 1b, which shows that RN_1 is within the communication range of current segment $Cr_{Seg_{13}}$, so these two segments combine into a single segment.

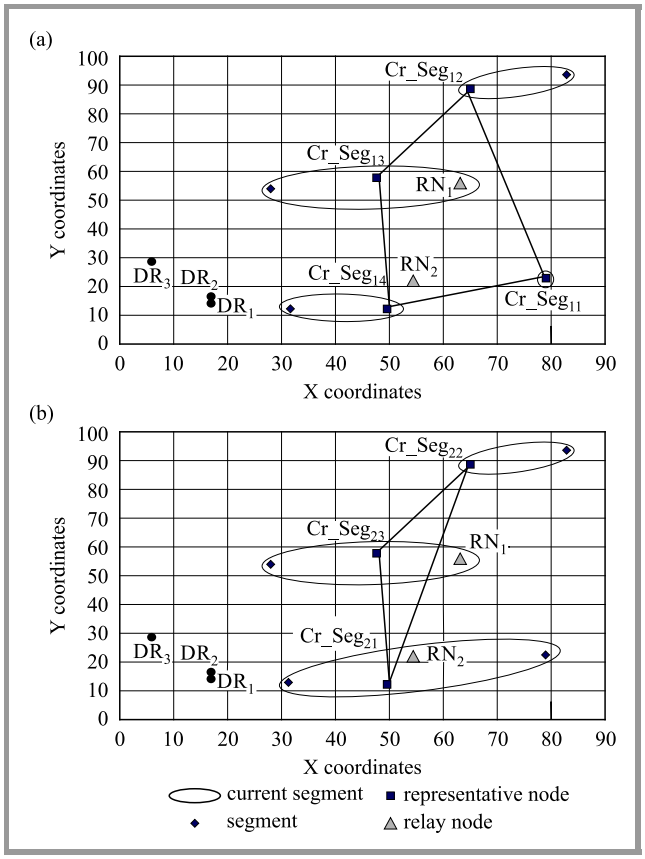

Fig. 3. Second iteration of placing relay node placement by GWO: (a) shows discarded relays $DR_2(17,16)$ and $DR_3(6,28)$ and second RN $RN_2(55,21)$, and (b) RN RN_2 combines current segments Cr_{Seg_4} and Cr_{Seg_1}

We obtain two discarded relays $DR_2(17,16)$ and $DR_3(6,28)$, after the second iteration of the proposed solution due to its random nature (as shown in Fig. 3a). In the third attempt, GAIN is able to find a relevant position for RN $RN_2(55,21)$ which lies inside the convex hull of the respective current segments. The solution considers α as the best solution, so it tries to produce an output which is favorable for the first input in the population. But this side effect can be removed by using the convex hull approach. GAIN forces RNs to populate inward the damaged area. Figure 3b shows that current segments Cr_{11} and Cr_{14} combine into a single current segment Cr_{21}.

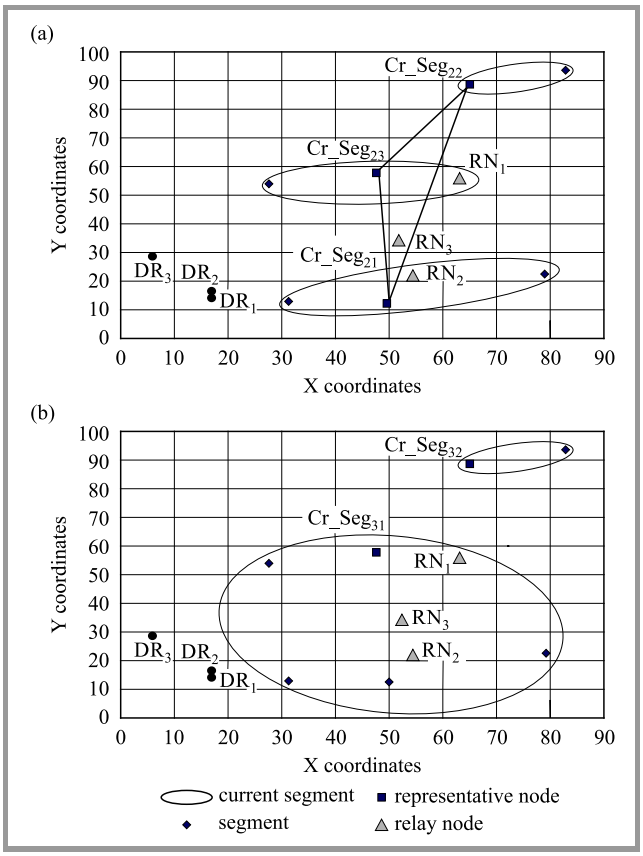

Fig. 4. Third iteration of placing relay node by GWO: (a) location of RN $RN_3(52,34)$ is found using GWO, and (b) RN RN_3 combines current segments Cr_1 and Cr_3.

The proposed solution generates three current segments after the execution of the second iteration – Cr_{21}, Cr_{22}, Cr_{23}. In the third round, GAIN produces another RN position $RN_3(52,34)$ which is able to communicate with current segments Cr_{21} and Cr_{23} by satisfying equation Eq. (8) and tries to restore lost connectivity as shown in Fig. 4a. Here, RN_3 will act as a gateway or bridge between both these segments. Figure 4b represents only two current segments Cr_{31} and Cr_{32}. Therefore, it is considered as a terminating condition.

5.4. Termination Phase

Termination phase is the last step of the proposed algorithm. The solution always checks for the remaining number of disconnected segments, because it is an iterative approach and it reconnects segments in the same manner. If two or fewer segments are left, the algorithm enters its termination

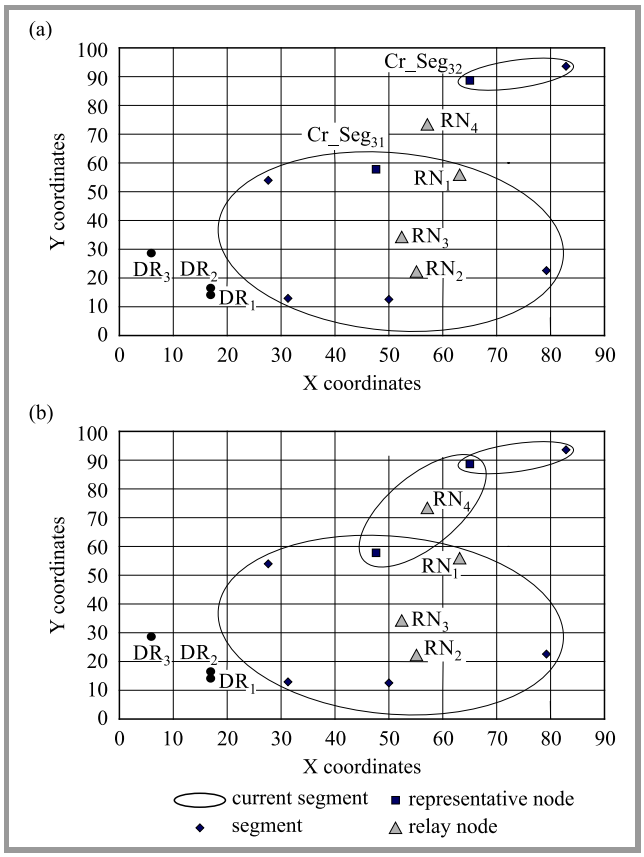

Fig. 5. Termination condition because only two current segments are left: (a) fourth RN $RN_4(57,73)$ has been placed manually, and (b) RN RN_4 combines both of the remaining segments.

phase. In the termination phase, it is considered that if one segment is left only, then connectivity has been restored. If two segments are left, then the algorithm finds the number of RNs required for restoration of connectivity by using the equation listed in the GAIN Algorithm 2 (lines 33–36). The relevant positions of RNs can be found by using the Euclidean distance between last two segments. Figure 5a shows that RN RN_4 has been placed between current segments $Cr_{Seg_{31}}$ and $Cr_{Seg_{32}}$. The position is somewhere along the line that joins these two segments. Figure 5b shows that disconnected segments can communicate with each other using RN RN_4 as a bridge.

5.5. Discussion on Degree of Novelty

The proposed algorithm has the power to generate an efficient and well-connected network topology. GAIN populates RNs in the inward direction of the damaged area. This generates a simple and efficient topology. The final topology generated is shown in Fig. 6. Some important observations may be inferred from the resulting topology, and are explained below:

- Connectivity is an important factor of any network topology. It shows its ability to handle failures. If network connectivity is high, then it can bear a large number of failures, up to a threshold limit. The resulting topology shown in Fig. 6 indicates that nodes on the edge of the network or terminal nodes are characterized by high connectivity (bi-connectivity). When a failure occurs, it does partition the network due to its high degree of connectivity.

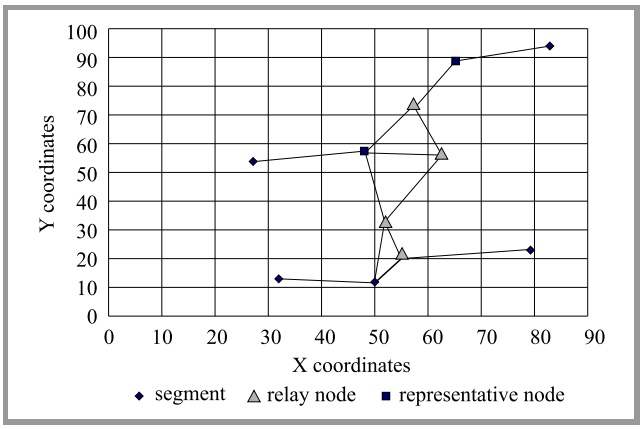

Fig. 6. Resulting topology calculated with GAIN.

- Distributed traffic load is the backbone of any network topology, because any network which has a centralized traffic load may suffer from continuous failures of the central part. Presented topology has no central point of failure, however. Instead of centralized load shown in Fig. 6, it is characterized by traffic load distributed among all nodes within the network. Therefore, it helps enhance the overall lifetime of the network.

6. Discussion on Pseudo Code of Proposed Solution

In this section, we explain the pseudo code of the proposed GAIN solution, which is shown in Algorithm 2. This pseudo code is divided into different parts based on the phases of GAIN. GAIN maintains a 2D array S for the coordinates of representative nodes and an integer variable, *Count_Relay* to hold the total number of RNs. The integer variable N_{Seg} shows the number of disjoint segments within the partitioned network. Lines 3–9 show the neighbor discovery phase. Line 5 is the main part of the neighbor discovery phase. If Seg_i and Seg_j satisfy this condition, then these two segments become the neighbors of each other. The iterative process for populating RNs is shown in lines 10–32. Line 12 computes the convex hull over the representative nodes of current segments. Line 13 calculates the candidate position of RN for the current round. Next, the solution checks for the position of the current RN. If it lies inside the convex hull, then it is put into the acceptable list. Otherwise, it is included in the list of discarded RNs. The same scenario is depicted in lines 14–31. Each candidate RN position has some segments within its communication range. If these segments are in the range of the current RN, then it is considered as a new segment, as

Algorithm 2. GAIN pseudocode

```
1: procedure GAIN(Area, N_Seg, R_r)
2:     Initialize array S[N_Seg][2] and Count_Relay ← 0;
3:     for i ← 0 to N_Seg do
4:         for j ← i+1 to N_Seg do
5:             if Euclid_Dist(S[i][0], S[i][1], S[j][0],
               S[j][1]) < 2R_r then
6:                 Join segment j-th with segment i-th and
                   remove it from array S.
7:             end if
8:         end for
9:     end for                                  ▷ Discovery
10:    while S have more than 2 points do
11:        Initialize Cr_Relay[2];
12:        CH ← Compute a convex hull of all points in S
13:        Cr_Relay ← GWO(S);
14:        if check Cr_Relay lie inside convex hull CH then
15:            Count_Relay++;
16:            Initialize C_Seg_in_Range ← 0 and 2D vec-
               tor Seg_in_Range;
17:            for i ← 0 to N_Seg do
18:                if Euclid_Dist(S[i][0], S[i][1],
                   Cr_Relay[0], Cr_Relay[1]) < 2R_r then
19:                    Seg_in_Range ← S[i] and
                       Count_Seg_in_Range++;
20:                end if
21:            end for
22:            if C_Seg_in_Range==0 then Create a new
               segment by using current relay
23:            else
24:                if C_Seg_in_Range==1 then Add cur-
                   rent relay to respective segment
25:                else
26:                    for i ← 1 to Seg_in_Range.size() do
27:                        Join all segments together and
                           remove those from S instead of
                           of first one.
28:                    end for
29:                end if
30:            end if
31:        end if
32:    end while
33:    if S have two point then
34:        Temp ← (Euclid_Dist(S[0][0], S[0][1], S[1][0],
           S[1][1]) − 2R_r)/(2R_r);
35:        Count_Relay ← Count_Relay + Temp;
36:    end if  ▷ To obtain the required number of RN to
       connect last two segments
37: return Count_Relay
38: end procedure
```

explained in line 22 of Algorithm 2. If the segments are in the range of the current RN, then they are added to the list of current RNs of the respective segment (line 24). If the number of segments within the range of the current relay exceeds one, then all these segments are joined together and represented as a single segment (lines 26–27).

Algorithm 3. Euclidean distance between two points in X-Y plain

```
1: procedure Euclid_Dist(x_1, x_2, y_1, y_2)
2:     a ← | x_1 − x_2 |^2
3:     b ← | y_1 − y_2 |^2
4:     return √(a+b)
5: end procedure
```

For initiating the termination condition, we check the count of remaining segments. If it is lower than 3, then the algorithm enters the termination phase, implemented by means of lines 33–36. These lines calculate the number of remaining RNs requiring joining, by calculating the Euclidean distance between them.

7. Performance Evaluation and Comparison

In this section, the performance and effectiveness of GAIN are discussed. Comparison with state-of-the-art algorithms is also explained. The GAIN algorithm is implemented and simulated in Java. The experiment results show that the proposed solution identified the lowest count of RNs as a number of segments increased. The total number of RNs and the number of disconnected segments are proportional to each other. So, these two factors are very important. Our objective is to find the minimum number of relay counts. Table 1 shows the parameters used in the simulation to analyze its performance.

Table 1
Simulation parameters

Parameter	Value
Area	1000×1000 m
Nodes	100–500
Total number of partition	5–9
Communication range of RNs	50–325 m
Number of placed RNs	5–45

7.1. Performance Metrics

For the purpose of the experiment, we have considered a variable range of RNs with a fixed number of partitioned segments. We have also taken a variable number of partitioned segments for a variable range of RNs. The following listed metrics are used to validate performance:

- Number of segments (N_{Seg}) – a large value of (N_{Seg}) may increase the requirements related with connectivity, which would result in a large number of RNs required – *Count_Relay*. As discussed earlier in Section 5, the total count of relay nodes is always greater than or equal to the number of partitioned segments. Hence, this metric has a direct impact on the minimum number of RNs.

- Transmission range of RN (R_r) – a longer transmission range directly affects the total count of RNs. R_r exerts a direct impact on performance. Our experiment results show that a longer communication range may be considered for getting better results. The minimum number of RNs required to ensure inter-segment connectivity is directly influenced by inter-segment connectivity.
- Total count of RNs $(Count\_Relay)$ – this parameter is directly related to the deployment cost of the network, as a minimum relay count is preferred. It shows the estimated performance advantage of the proposed approach in comparison with other algorithms.

7.2. Comparative Approaches

This section provides an overview of some well-known and recently published algorithms. Considering the metrics described above, our objective is to solve the network partition problem and to propose an efficient approach to the issue at hand. In this section a brief introduction of four other RNPP solutions is discussed. The first algorithm generates a convex hull and calculates the Steiner point for every three neighboring nodes repeatedly, until two segments are left (ORC [9]). The second algorithm uses the Steiner minimum tree with the minimum number of Steiner points to find the location of RNs for restoration of global connectivity in WSN (STP-MSP [24]). The third algorithm forms the minimum spanning tree which is based on a single-tiered RNP (MST-1tRN [13]). The last algorithm studies the problem of the connected single cover, where each SN is covered by a single RN (1CSCP [25]).

- ORC – this approach seeks to form the minimum Steiner tree on the convex hull to populate RNs. It is an iterative process and is completed in different stages. Authors of ORC [9] proposed a heuristic based on the convex hull and populated RNs inwards from the boundary of the convex hull. In each iteration, the convex hull is formed and Steiner points for every set of three neighboring nodes are found considering Steiner points of the previous iteration as an input for the next iteration to form convex hull. ORC uses the k-LCA approach [26] to solve the Steiner tree problem.
- STP-MSP – this algorithm follows the concepts of the minimum spanning tree (MST) and the Steiner tree point (STP). The combination of these two approaches results in a fully connected WSN. STP-MSP considers P terminals which have no connectivity and it strives to find an MST formed by these P terminal nodes. Regarding a constant R, STP-MSP forms an edge p_1p_2 between two points p_2 and p_2 and inserts $\lceil \frac{|p_1p_2|}{R} - 1 \rceil$ a number of Steiner points, where R is the transmission range of the relay.
- MST-1tRN – initially, the MST-1tRN algorithm uses a set of sensor nodes, $S = (s_1, s_2, s_3, \ldots, s_n)$ and some other constants r and R as the range of SNs and RNs, respectively. It strives to compute MST T_S generated by set S. It then tries to steinerize that MST to obtain an (r,R)-constrained Steiner tree by populating RNs on each edge of MST T_S.
- 1CSCP – the 1CSCP algorithm is totally based on the concept of the connected single cover problem. It seeks to find the location of a minimum number of RNs and ensures that each SN is covered by at least one RN. RNs are placed so that a connected network can be generated by using these RNs, and that BSs be reachable. A connected network of RNs is called a minimum connected single cover graph.

7.3. Simulation Results and Comparison

The simulations prove the concepts used in respective research work. The GAIN algorithm is simulated in the Java environment, with multiple configurations. Each configuration has a different number of segments N_{Seg} and a varying transmission range of RNs R_r. All SNs are randomly placed in the area of interest (i.e. 1000×1000 m). The transmission range of RNs varies from 50 m to 325 m and the value of N_{Seg} assumes 5, 6, 7 and 8. All experiment results are taken into consideration, with their average equaling 30 individual results.

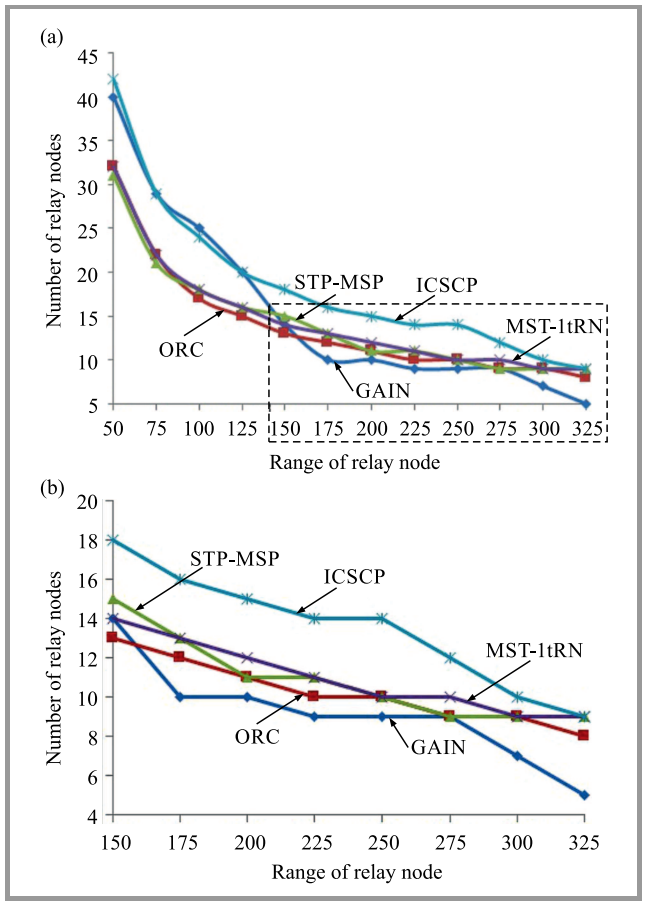

Fig. 7. GAIN vs. other algorithms. The lower figure is a magnified version of the rectangle area in the upper chart.

The performance of GAIN is studied with other four comparative algorithms in terms of the total RN count required to restore lost connectivity of a partitioned WSN, for various ranges of RNs. For all results, shown in Fig. 7, N_{Seg} is taken as a constant value of 5. Figure 7a shows that proximity is an important factor in a disconnect network. It has been observed that the RN count decreases as the range increases. While studying the impact of the large value of R_r, it has been shown that the total count of RNs is largely influenced by the value of R_r. The transmission range of RNs R_r and the number of RNs required to restore connectivity are inversely proportional to each other, which means that as range increases, the count of RNs decreases and vice-versa. The same relation can be depicted in Figs. 7a-b. The performance of GAIN decreases slightly compared to other algorithms for a low transmission range of RNs, due to the random nature of GWO. It tries to find an optimal location by considering all segments at a time. However, in Steiner points-based algorithms, the candidate RN location is found by considering only a few nodes at a time. As seen in Fig. 7a, for the value of R_r from 50 to 150 m, GAIN produces a larger number of RN locations, outperforming ORC. Generally, in a real time application, the value of R_r is to equal 200 or more than 200. Hence, Fig. 7a shows that for the transmission range of 150–325 m, the proposed solution renders better results than ORC, STP-MSP, MST-1tRN, 1CSCP in terms of the total RN count. Figure 7b is a magnified version of Fig. 7a, showing the results in greater detail. For a large value of R_r, GAIN populates RNs inwards from the outer edge of the first convex hull. At the outset, GAIN consistently outperforms all other comparative algorithms, for a large value in the range of 200–325 m.

In the subsequent simulation results, the range of RN is considered to be a constant value, i.e. equals 200 m. Here we simulate GAIN for various numbers of segments, to see the impact of a large-scale failure, where the value of N_{Seg} increases by leaps and bounds. Figure 8a shows the results of four different experiments, with the number of segments varying from 5 to 8. GAIN consistently outperforms other algorithms, because of a large transmission range of RN. Meanwhile, it can be observed that as segmentation increases by one, the required number of RNs increases sharply. Apart from this, we also observed one thing – GAIN can also restore connectivity for a large scale failure, where the number of partitioned segments is large. But other algorithms are not able to populate RNs in such a large-scale type of failure.

Figure 8b shows the experiment results only for GAIN, but with various numbers of disconnected segments considered. This figure depicts the relation between the number of segments and the range of RN. It can be concluded that when the transmission range of RN is high, the number of segments does not affect the final count of RNs (i.e. *Count_Relay*). Despite the large value of N_{Seg} GAIN consistently maintains the minimum number of RNs. Instead of this, when there is a slight change in the value of N_{Seg} and

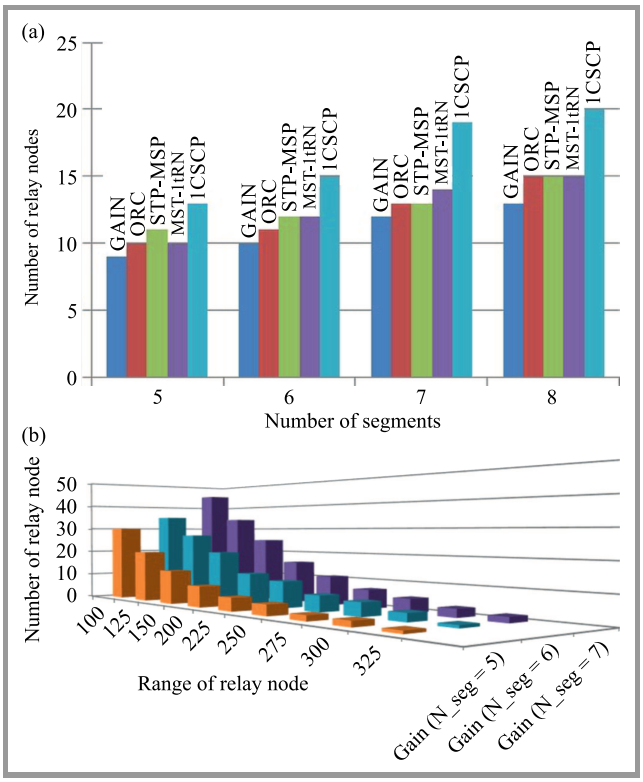

Fig. 8. Comparison of GAIN and other algorithms ($R_r = 200$) (a) and comparison of GAIN results for varying numbers of segments (b). (For color pictures visit www.nit.eu/publications/journal-jtit)

with a low value of R_r, the final count of RN *Count_Relay* increases quickly. This simulation is performed for three different values of N_{Seg} equaling 5, 6 and 7. At last, we conclude, based on the results of the experiments, that GAIN's performance is favorable in comparison with other comparative approaches, for a large value of R_r. GAIN shows a below-benchmark performance for a low value of R_r, due to the randomness of GWO.

8. Conclusion and Future Scope

Generally, HWSNs operate in a harsh and hostile environment, where SNs are more susceptible to failures. A large-scale failure of SNs results in the creation of a partitioned network. Disjoint segments are no more able to communicate with other. Therefore, we proposed the grey wolf optimizer algorithm to repair the segmented heterogeneous wireless sensor network and to restore lost connectivity within the disjoint HWSN. The proposed approach operates in rounds, and in each round one RN position is returned. If the candidate position is inside the convex hull, then it is considered as an acceptable RN position, otherwise we discard it. When the number of remaining segments falls below three, then the situation is considered to be the terminating condition of GAIN. In the termination phase, the position of RNs is calculated with Euclidean equality.

We evaluate the performance of GAIN and compare it with other well-known algorithms of similar nature. The simulation results have confirmed that our proposed solution outperforms other algorithms and populates a minimum number of nodes for a large communication range of RNs. The resultant topology shows a good connectivity with balanced traffic loads. In the future, we will be working to test the proposed solution on a real testbed.

References

[1] V. Ranga, M. Dave, and A. K. Verma, "Network partitioning recovery mechanisms in WSANs: A survey", *Wireless Personal Commun.*, vol. 72, no. 2, pp. 857–917, 2013 (doi: 10.1007/s11277-013-1046-7).

[2] V. Ranga, M. Dave, and A. K. Verma, "Relay node placement for lost connectivity restoration in partitioned wireless sensor networks", *in Proc. Int. Conf. on Electron. and Commun. Syst. ECS 2015*, Bacelona, Spain, 2015, pp. 170–175.

[3] V. Ranga, M. Dave, and A. K. Verma, "Relay node placement to heal partitioned wireless sensor networks", *J. of Comp. & Elec. Engin.*, vol. 48, no. C, pp. 371–388, 2015 (doi: 10.1016/j.compeleceng.2015.09.014).

[4] G. Kumar and V. Ranga, "Meta-heuristics for relay node placement problem in wireless sensor networks", in *Proc. 4th Int. Conf. on Parallel, Distrib. and Grid Comput. PDGC 2016*, Waknaghat, India, 2016, pp. 375–380 (doi: 10.1109/pdgc.2016.7913180).

[5] J. Kennedy, "Particle swarm optimization", in *Proc. of Int. Conf. on Neural Netw. ICNN'95*, Perth, WA, Australia, 1995, pp. 1942–1948 (doi: 10.1109/ICNN.1995.488968).

[6] M. Dorigo, M. Birattari, and T. Stutzle, "Ant colony optimization", *IEEE Comput. Intell. Mag.*, vol. 1, no. 4, pp. 28–39, 2006 (doi: 10.1109/MCI.2006.329691).

[7] E. Bonabeau, M. Dorigo, and G. Theraulaz, *Swarm Intelligence: From Natural to Artificial Systems*, 1st ed. Oxford University Press, 1999 (ISBN: 978-0195131598).

[8] S. Mirjalili, S. M. Mirjalili, and A. Lewis, "Grey wolf optimizer", *Adv. in Engin. Software*, vol. 69, pp. 46–61, 2014 (doi: 10.1016/j.advengsoft.2013.12.007).

[9] S. Lee and M. Younis, "Optimized relay node placement for connecting disjoint wireless sensor networks", *Comp. Netw.*, vol. 56, no. 12, pp. 2788–2804, 2012 (doi: 10.1016/j.comnet.2012.04.019).

[10] J. M. Lanza-Gutierrez and J. A. Gomez-Pulido, "Assuming multiobjective metaheuristics to solve a three-objective optimisation problem for relay node deployment in wireless sensor networks", *Appl. Soft Comput.*, vol. 30, no. C, pp. 675–687, 2015 (doi: 10.1016/j.asoc.2015.01.051).

[11] C. Ma, W. Liang, M. Zheng, and H. Sharif, "A connectivity-aware approximation algorithm for relay node placement in wireless sensor networks", *IEEE Sensors J.*, vol. 16, no. 2, pp. 515–528, 2016 (doi: 10.1109/JSEN.2015.2456931).

[12] C. Zhao and P. Chen, "Particle swarm optimization for optimal deployment of relay nodes in hybrid sensor networks", in *IEEE Congr. on Evolut. Comput. CEC 2007*, Singapore, 2007, pp. 3316–3320 (doi: 10.1109/CEC.2007.4424899).

[13] E. L. Lloyd and G. Xue, "Relay node placement in wireless sensor networks", *IEEE Trans. on Computers*, vol. 56, no. 1, pp. 134–138, 2007 (doi: 10.1109/TC.2007.250629).

[14] I. F. Senturk, S. Yilmaz, and K. Akkaya, "A game-theoretic approach to connectivity restoration in wireless sensor and actor networks", in *Proc. IEEE Int. Conf. on Commun. ICC 2012*, Ottawa, ON, Canada, 2012, pp. 7110–1714 (doi: 10.1109/ICC.2012.6364848).

[15] P. Basu and J. Redi, "Movement control algorithms for realization of fault-tolerant ad hoc robot networks", *IEEE Network*, vol. 18, no. 4, pp. 36–44, 2004 (doi: 10.1109/MNET.2004.1316760).

[16] A. A. Abbasi, M. Younis, and K. Akkaya, "Movement-assisted connectivity restoration in wireless sensor and actor networks", *IEEE Trans. on Parallel and Distrib. Syst.*, vol. 20, no. 9, pp. 1366–1379, 2009 (doi: 10.1109/TPDS.2008.246).

[17] K. Akkaya, F. Senel, A. Thimmapuram, and S. Uludag, "Distributed recovery from network partitioning in movable sensor/actor networks via controlled mobility", *IEEE Trans. on Computers*, vol. 59, no. 2, pp. 258–271, 2010 (doi: 10.1109/TC.2009.120).

[18] W. Wang, V. Srinivasan, and K.-C. Chua, "Using mobile relays to prolong the lifetime of wireless sensor networks", in *Proc. 11th Ann. Int. Conf. on Mob. Comput. and Network. MobiCom 2005*, Cologne, Germany, 2005, pp. 270–283 (doi: 10.1145/1080829.1080858).

[19] M. Y. Sir, I. F. Senturk, E. Sisikoglu, and K. Akkaya, "An optimization-based approach for connecting partitioned mobile sensor/actuator networks", in *Proc. IEEE Conf. on Comp. Commun. Worksh. INFOCOM WKSHPS 2011*, Shanghai, China, 2011, pp. 525–530 (doi: 10.1109/INFCOMW.2011.5928869).

[20] R. C. Shah, S. Roy, S. Jain, and W. Brunette, "Data MULEs: Modeling a three-tier architecture for sparse sensor networks", in *Proc. of 1st IEEE Int. Worksh. on Sensor Netw. Protocols and Appl.*, Anchorage, AK, USA, 2003 (doi: 10.1109/SNPA.2003.1203354).

[21] G. Wang, G. Cao, T. La Porta, and W. Zhang, "Sensor relocation in mobile sensor networks", in *Proc. IEEE 24th Ann. Joint Conf. of the IEEE Comp. and Commun. Soc. INFOCOM 2005*, Miami, FL, USA, 2005, vol. 4, pp. 2302–2312 (doi: 10.1109/INFCOM.2005.1498517).

[22] C. Muro, R. Escobedo, L. Spector, and R. Coppinger, "Wolf-pack (Canis lupus) hunting strategies emerge from simple rules in computational simulations", *Behavioural Processes*, vol. 88, no. 3, pp. 192–197, 2011 (doi: 10.1016/j.beproc.2011.09.006).

[23] R. L. Graham, "An efficient algorithm for determining the convex hull of a finite planar set", *Inform. Process. Lett.*, vol 1, no. 4, pp. 132–133, 1972 (doi: 10.1016/0020-0190(72)90045-2).

[24] X. Cheng, D.-Z. Du, L. Wang, and B. Xu, "Relay sensor placement in wireless sensor networks", *Wireless Networks*, vol. 14, no. 3, pp. 347–355, 2008 (doi: 10.1007/s11276-006-0724-8).

[25] D. Yang, S. Misra, X. Fang, G. Xue, and J. Zhang, "Two-tiered constrained relay node placement in wireless sensor networks: Efficient approximations", in *Proc. 7th Ann. IEEE Commun. Soc. Conf. on Sensor Mesh and Ad Hoc Commun. and Netw. SECON 2010*, Boston, MA, USA, 2010, pp. 1–9 (doi: 10.1109/SECON.2010.5508241).

[26] G. Robins and A. Zelikovsky, "Tighter bounds for graph Steiner tree approximation", *SIAM J. on Discrete Mathem.*, vol. 19, no. 1, pp. 122–134, 2005 (doi: 10.1137/S0895480101393155).

Gaurav Kumar received his B.Tech. degree in Computer Science and Engineering from Gautam Buddh Technical University Lunckow in 2012 and M.Tech. degree in Computer Engineering from NIT Kurukshetra Haryana, India in 2017. Currently, he is working as Assistant Professor in University Departments, Rajasthan Technical University, Kota Rajasthan. His interest areas are fault tolerance in Wireless sensor networks, Internet of Things, and Big Data.

E-mail: gngauravnain@gmail.com
Department of Computer Engineering
National Institute of Technology Kurukshetra
Haryana, India

Virender Ranga received his Ph.D. degree from Computer Engineering Department of National Institute of Technology, Kurukshetra, Haryana, India in 2016 followed by M.Tech. degree in 2004, and B.Tech. degree in 2001. He has published more than 50 research papers in various International SCI Journals in the area of computer communications as well as reputed international conferences. Presently, he is an Assistant Professor in the Computer Engineering Department since 2008. He has been conferred by Young Faculty Award in 2016 for his contributions in the field of computer communications. He is an active reviewer of many reputed journals of IEEE, Springer, Elsevier, Taylor & Francis, Wiley and Inder-Science. His research areas include wireless sensor and ad-hoc networks, data science, IoT security and FANET security.

E-mail: virender.ranga@nitkkr.ac.in
Department of Computer Engineering
National Institute of Technology Kurukshetra
Haryana, India

Paper

Non-crossing Rectilinear Shortest Minimum Bend Paths in the Presence of Rectilinear Obstacles

Shylashree Nagaraja

Department of Electronics & Communication Engineering, Rastreeya Vidyalaya College of Engineering, Bengaluru, Karnataka, India

https://doi.org/10.26636/jtit.2018.120417

Abstract—The paper presents a new algorithm to determine the shortest, non-crossing, rectilinear paths in a two-dimensional grid graph. The shortest paths are determined in a manner ensuring that they do not cross each other and bypass any obstacles present. Such shortest paths are applied in robotic chip design, suburban railway track layouts, routing traffic in wireless sensor networks, printed circuit board design routing, etc. When more than one equal length non-crossing path is present between the source and the destination, the proposed algorithm selects the path which has the least number of corners (bends) along the path. This feature makes the path more suitable for moving objects, such as unmanned vehicles. In the author's scheme presented herein, the grid points are the vertices of the graph and the lines joining the grid points are the edges of the graph. The obstacles are represented by their boundary grid points. Once the graph is ready, an adjacency matrix is generated and the Floyd-Warshall all-pairs shortest path algorithm is used iteratively to identify the non-crossing shortest paths. To get the minimum number of bends in a path, we make a modification to the Floyd-Warshall algorithm, which is constitutes the main contribution of the author presented herein.

Keywords—Floyd-Warshall algorithm, rectilinear non-crossing shortest paths, rectilinear obstacles.

1. Introduction

The problem of non-crossing shortest paths is well researched and several algorithms are described in literature, i.e. [1]–[3]. In general, the shortest paths reduce the time and cost of communication. Non-crossing paths are essential in VLSI chip track layouts, printed circuit board routing, robotic motion control [4], [5], etc.

Obstacles are natural and common in graphs representing geometrical/geographical scenarios In a printed circuit board layout, the components act as obstacles for the routing paths. Similarly, in transportation layouts, obstacles and prohibited zones are very common. In such a situation, we have to find optimal paths which avoid the obstacles and bypass them to reach the destination. Several algorithms have been presented to find the shortest paths in the presence of obstacles, which are modeled as rectangles, rectilinear polygons and general polygons [6]–[11]. In this paper, a new method to bypass the obstacles without touching them is presented.

Bends or corners are unavoidable in graphs which have obstacles and other physical constraints, or when a direct link fails. The presence of bends along the paths reduces velocity of moving objects and increases energy consumption. In physical implementation, the cost of such paths is higher as well. Therefore, the author's aim is to ensure a minimum number of bends.

Let us consider a scenario where several shortest paths of equal length exist between a pair of nodes in a rectilinear graph. Among these shortest, equal paths, the path that has the lowest number of bends is called the rectilinear minimum bend shortest path (MBSP) [6]. First, we find the MBSP between a given source-destination pair. If more than one such MBSP is present, we take one of them. The objective is to find MBSPs between K distinct source-destination pairs. This results in K distinct MBSPs, one for each source-destination pair. Additionally, the paths should be distinct, disjoint and non-crossing. In the proposed method, each source-destination pair contributes a single optimal path. We have K such paths corresponding to K such pairs. This is not the same as the first K-shortest paths for a single source-destination pair. When obstacles are present in the graph, the paths should not touch the obstacles but should avoid and bypass them. The given region where the paths have to be determined is discretized by a uniform square grid of a suitable size. Then, the constrained paths are determined on the undirected graph using the well-known Floyd-Warshall algorithms from the graph theory.

Even though multi-criteria optimization methods [12], [13] can be used to solve this MBSP problem, they are more complex and experience difficulty in getting the best weights for combining multiple criteria into a single one. The weights depend on the size and layout of the graph. The paper provides a comparison of the proposed method with the bi-criteria optimization method.

2. Basic Symbols Notations and Assumptions

The geometric region under consideration is represented by a square mesh grid which covers the entire region as shown in Fig. 1. A planar graph $\mathbf{G}(\mathbf{V},\mathbf{E})$ is constructed

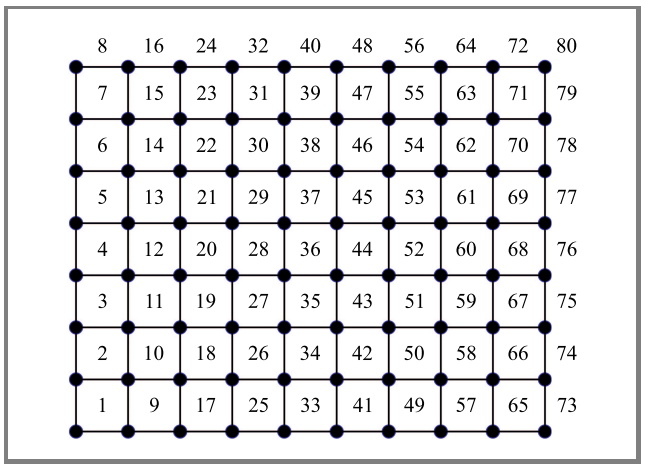

Fig. 1. Grid graph numbering scheme: width in terms of grid points $= W = 10$, height in terms of grid points $= H = 8$.

from the grid. The grid points are the vertices (nodes) of the graph and the grid lines are the edges of the graph. The number of grid points along width of the graph is W, and that along the height is H. Thus, the total number of vertices (grid points) represented by n is, $n = WH$. The total number of links would be $(W-1)H + (H-1)W$.

2.1. Node Numbering

The n nodes of the graph are numbered from 1 to n, column-wise, starting from the bottom left corner, as shown in Fig. 1. After numbering a column from its bottom to top, the next column is numbered further from its bottom to top, and so on. In each column, as we traverse from its bottom to top, the node numbers increase by one for each successive node. On the other hand, along each row, the node numbers increase by H as we traverse successive nodes from left to right. Thus, in Fig. 1, as we traverse from left to right, along any row, the node numbers increase by 8, successively. Here $H = 8$. The node numbers act as node IDs. A horizontal or a vertical line segment is denoted by the beginning and ending of that segment. Thus, for example, in Fig. 1, segments $2 \rightarrow 10$ and $80 \rightarrow 8$ are horizontal segments, whereas, $1 \rightarrow 2$ and $80 \rightarrow 73$ are vertical segments. The minimum length of a horizontal line segment, in terms of the difference between its end node IDs, is H. For example, for the line segment $2 \rightarrow 10$, the length is $10 - 2 = 8 = H$. This property applies to all horizontal segments. Since the minimum length is H, an important characteristic of horizontal segments is that they have lengths greater than or equal to H. For vertical segments, the minimum and the maximum lengths (in terms of the end node differences) are 1 and $H-1$, respectively. For example, for the minimum vertical segment $1 \rightarrow 2$, its length is $2 - 1 = 1$. For the maximum vertical segment $73 \rightarrow 80$, the length is $80 - 73 = 7 = H - 1$. Thus, for vertical segments, the maximum length is $H-1$ which means the lengths are less than H. These properties are essential to check for the existence of bends (corners) along a path, as described later. The vertex set V of the graph is $\{1 : n\}$.

2.2. Node Connectivity and Edge Weights

4-connectivity for all the nodes (vertices) is used. This means that each non-border node is connected to its 4 immediate neighbors: north, south, east and west. The four corner nodes of the graph have 2 connections each. Non-corner border nodes have 3 corners each. Thus, the graph is a one-hop network. The nodes which are more than one hop are not connected directly at all. The weights (effective distances) for the connecting edges are taken as one. In this paper, the terms weight and length are used synonymously. Thus, the length of an edge is the same as the weight of that edge. The weights for the edges between directly unconnected nodes are set to infinity. All edge weights are positive. Thus, an edge weight of ∞ means no direct connection. Therefore, the elements of the adjacency matrix are either 1 or ∞.

2.3. Adjacency Matrix

The adjacency (connectivity) matrix of the graph is represented by $\mathbf{A}$. The size of matrix $\mathbf{A}$ is $n \times n$. The element $\mathbf{A}(i,j)$ of the adjacency matrix gives the weight of the edge (link) between node i and node j. The diagonal elements of $\mathbf{A}$ are taken as ∞, to prevent self-loops. The graph is an undirected graph. Therefore, $\mathbf{A}(i,j) = \mathbf{A}(j,i)$ and $\mathbf{A}$ is symmetric. An edge can allow the flow in either direction. When i and j are connected $\mathbf{A}(i,j) = 1$, else, $\mathbf{A}(i,j) = \infty$. The number of 1s in row i of $\mathbf{A}$ gives the number of edges leaving node i, and the number of 1s in column i gives the number of edges entering node i. Since our graph is a 4-connected grid graph, the maximum number of 1s in a row or column is 4. As an example, consider a 3×3 grid graph of nine nodes represented by $\mathbf{G}$, as:

$$\mathbf{G} = \begin{bmatrix} 3 & 6 & 9 \\ 2 & 5 & 8 \\ 1 & 4 & 7 \end{bmatrix}.$$

The corresponding adjacency matrix $\mathbf{A}$ will be:

$$\mathbf{A} = \begin{array}{c} \\ 1 \\ 2 \\ 3 \\ 4 \\ 5 \\ 6 \\ 7 \\ 8 \\ 9 \end{array} \begin{array}{c} \begin{array}{ccccccccc} 1 & 2 & 3 & 4 & 5 & 6 & 7 & 8 & 9 \end{array} \\ \begin{bmatrix} \infty & 1 & \infty & 1 & \infty & \infty & \infty & \infty & \infty \\ 1 & \infty & 1 & \infty & 1 & \infty & \infty & \infty & \infty \\ \infty & 1 & \infty & \infty & \infty & 1 & \infty & \infty & \infty \\ 1 & \infty & \infty & \infty & 1 & \infty & 1 & \infty & \infty \\ \infty & 1 & \infty & 1 & \infty & 1 & \infty & 1 & \infty \\ \infty & \infty & 1 & \infty & 1 & \infty & \infty & \infty & 1 \\ \infty & \infty & \infty & 1 & \infty & \infty & \infty & 1 & \infty \\ \infty & \infty & \infty & \infty & 1 & \infty & 1 & \infty & 1 \\ \infty & \infty & \infty & \infty & \infty & 1 & \infty & 1 & \infty \end{bmatrix} \end{array}.$$

In general, in $\mathbf{A}$, the rows, as well as the columns of the corner nodes, have 2 ones, those of the non-corner border nodes have 3 ones and those of the inside nodes have 4 ones.

Thus, the nodes are characterized by direct connectivity, immediately along north↔south and east↔west axes. The nodes have no immediate diagonal connectivity. This is an important requirement to ensure the non-crossing property of the shortest paths. Because of this 4-connectivity, all connected paths from the source node to the destination node have to be rectilinear.

2.4. Objective

Given the source-destination node pairs $(s_i - t_i)$ for $i = 1$ to K, the main objective is to find K shortest paths $\mathbf{P}(s_i,t_i)$'s which are disjoint, having a minimum number of bends and which do not touch any obstacles present in the graph.

3. Properties of Paths

A simple path from the source node s to the destination node t is a series of connected edges from s to t through the intermediate nodes without any loops. Hereafter, for brevity and convenience, we refer to simple path(s) by the term path(s). Let the sequence of intermediate nodes along a specific path from s to t be, $v_1, v_2, \ldots, v_m$. Then, the entire path including s and t is represented by $\mathbf{P}(s,t)$, such as:

$$\mathbf{P}(s,t) = [\, s, v_1, v_2, \ldots, v_m, t]\,. \tag{1}$$

$\mathbf{P}(s,t)$ is an array of nodes. With m intermediate nodes, the size of the array is $m+2$, which is same as the number of nodes in $\mathbf{P}(s,t)$. The length of the path is the sum of the edge weights along the path from s to t. From Eq. (1), one can see that the number of edges connecting s to t is $m+1$, that is one less than the size of the array $\mathbf{P}(s,t)$. In this case, the weights of all the connecting edges are 1s. Therefore, the total weight of the path is $m+1$ itself. The total weight of the path is also called the length of the path or path length. When the path length is short, then the corresponding travel cost is also lower.

3.1. Shortest path

When there are several paths from s to t, that path which has the minimum path length is the shortest path. The number of shortest paths can be more than one. Then, the path lengths of these are minimum and equal.

3.2. Rectilinear property of paths

Our graph is a square grid graph and all the edges are either parallel to x axis or y axis. Since a path is a chain of edges, the edges making up the path are parallel to the Cartesian coordinates. Then the path is rectilinear, because each edge of the path is either parallel to x or y, i.e. each edge is either vertical or horizontal.

3.3. Non-crossing Property of Paths

To understand the non-crossing property of the paths, we introduce a theorem on the non-crossing constraint.

Theorem 1. In a square grid graph, node-disjoint paths do not cross each other. *Proof.* In the presented scheme, all paths are rectilinear. Consider two paths $\mathbf{P}(s_1,t_1)$ and $\mathbf{Q}(s_2,t_2)$, where the source and the destination nodes s_1, t_1, s_2, t_2 are all disjoint. Let $E_P(a,b)$ be any edge that belongs to $\mathbf{P}(s_1,t_1)$ and similarly let $E_Q(c,d)$ be any edge that belongs to $\mathbf{Q}(s_2,t_2)$. Now, consider the geometrical intersection of edges $E_P(a,b)$ and $E_Q(c,d)$. When both of them are horizontal or both of them vertical, they are parallel

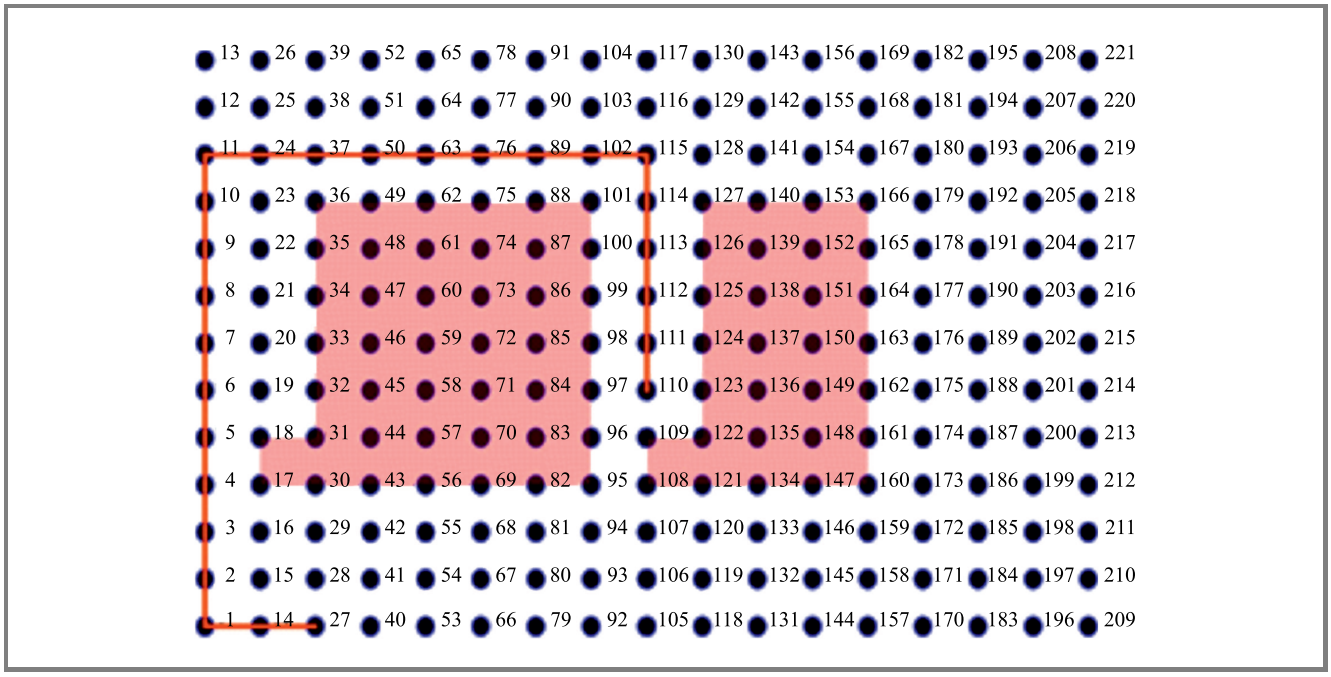

Fig. 2. Obstacles bounded by grid points marked by shaded areas.

and cannot meet each other. Therefore, the condition for the intersection is that one of them has to be horizontal while the other one vertical. In our grid graph, vertical and horizontal edges meet only at nodes (see Fig. 1). Hence, the two edges can meet only at one of the nodes. This node is obviously the common node for both the edges. Therefore, the condition for the intersection of $E_P(a,b)$ and $E_Q(c,d)$ is that they should have a common node or the paths should not be disjoint. On the other hand, if $E_P(a,b)$ and $E_Q(c,d)$ are node-disjoint, they cannot meet each other. Since the paths are made up of a series of edges, if the edges of the respective paths cannot meet, then the two paths also cannot intersect. This argument can be extended to all possible paths. Therefore, if paths are node-disjoint, they cannot intersect each other. Based on Theorem 1, determination of non-crossing paths boils down to that of finding node-disjoint paths.

3.4. Representation of Obstacles in the Graph

Obstacles are those regions in the graph which should be avoided by the paths. The paths should not touch the obstacles and have to bypass them if necessary to reach the destination. In this grid graph, the boundaries of the obstacles are marked by the grid points (nodes of the graph), as shown in Fig. 2. Since obstacle boundaries are represented by the grid points of the square grid graph, the obstacles are rectilinear polygons. The obstacle can be in the form of polylines, as shown by the line in Fig. 2. We can also specify certain grid points as obstacles. Then, all points along the line and the isolated obstacle points are excluded or made inaccessible while finding the shortest paths.

3.4.1. Exclusion (or marking out) of a specific node

Exclusion of a specific node is done by setting the weights (distances) of all incident edges of that node to infinity. Then, the edges entering or leaving that node have ∞ as their weight. Therefore, the shortest path algorithm will exclude that node, because if included, the total length (weight) would become ∞. Let the node to be excluded be J, where $J \in \{1:n\}$. Then the weights of all incident edges leaving J are given by the elements of row J of the adjacency matrix $\mathbf{A}$. Similarly, the weights of incident edges entering J are given by the elements of column J of $\mathbf{A}$. Therefore, the elements of row J and column J have to be set to ∞. Before setting the elements to ∞, matrix $\mathbf{A}$ is saved in a temporary matrix **Atemp**, which can be used to restore J as explained later. Thus, the exclusion operation is carried out as:

$$\mathbf{Atemp} = \mathbf{A}\,, \tag{2}$$

$$\mathbf{A}(J,:) = \infty\,. \tag{3}$$

Here, the colon notation is used to represent all elements of row J. Similarly the weights of incident edges entering J are set to ∞ as:

$$\mathbf{A}(:,J) = \infty\,, \tag{4}$$

Here, $\mathbf{A}(:,J)$ represents all the elements of column J. Thus, use of Eqs. (3)–(4) alters the adjacency matrix $\mathbf{A}$ such that node J is excluded or **marked out** while searching for the shortest path. Nodes belonging to the obstacles are permanently marked out. But in our method, certain nodes are **marked out** temporarily in the present iteration, to be restored in the later iterations as will be explained later.

3.4.2. Inclusion or mark-in of a node that was excluded earlier

Inclusion or **mark-in** of node J which was marked out earlier is done by restoring the elements of row J and column J from $\mathbf{A}$ as:

$$\mathbf{A}(J,:) = \mathbf{Atemp}(J,:)\,, \tag{5}$$

$$\mathbf{A}(:,J) = \mathbf{Atemp}(:,J)\,. \tag{6}$$

3.5. Node-disjoint K Shortest Paths

Determination of node-disjoint shortest paths is a well-known NP-complete problem [6]. To overcome this, Yen's iterative method [7] is used, which is sufficient for engineering applications. Given K distinct source-destination node pairs (s_i,t_i) for $i=1$ to K, we first find the shortest path from s_1 to t_1. Then, the nodes along the first shortest path are made inaccessible for the next iteration, by setting the weights of all incident edges of those nodes to infinity (**marked-out** operation), as given by Eqs. (2)–(3). Next, we find the second shortest path. Again, make the involved nodes inaccessible by setting the relevant incident edge weights to infinity (**marked-out** operation) and so on, until we determine K shortest disjoint paths. In this method, the next iteration will exclude those nodes which have been already covered by the previous paths. We use Floyd-Warshall all pairs shortest path algorithm for determining the individual shortest paths. The reason for using this algorithm is described later.

3.6. Bends in a Path

Consider a path $\mathbf{P}(i,j)$ from source i to destination j. Let k be an intermediate node along the path, as shown in Fig. 3. Symbol, k (lowercase) is used for intermediate nodes in the Floyd-Warshall algorithm. This k is different from the uppercase K which represents the number of shortest paths. Now, $\mathbf{P}(i,k)$ and $\mathbf{P}(k,j)$ are the two segments of $\mathbf{P}(i,j)$ joined at node k. The two segments can be perpendicular, as in Fig. 3a, or collinear (no bend), as in Fig. 3b.

3.6.1. Checking for a bend at *k*

For the existence of a bend in a path, one line segment should be horizontal and the other one has to be vertical and vice-versa. As explained earlier, the condition for the segment $\mathbf{P}(i,k)$ to be horizontal is, its end node difference $\text{abs}(i-k)$ should be greater than or equal to H. That is, $\text{abs}(i-k) \geq H$. The condition for segment $\mathbf{P}(k,j)$ to be

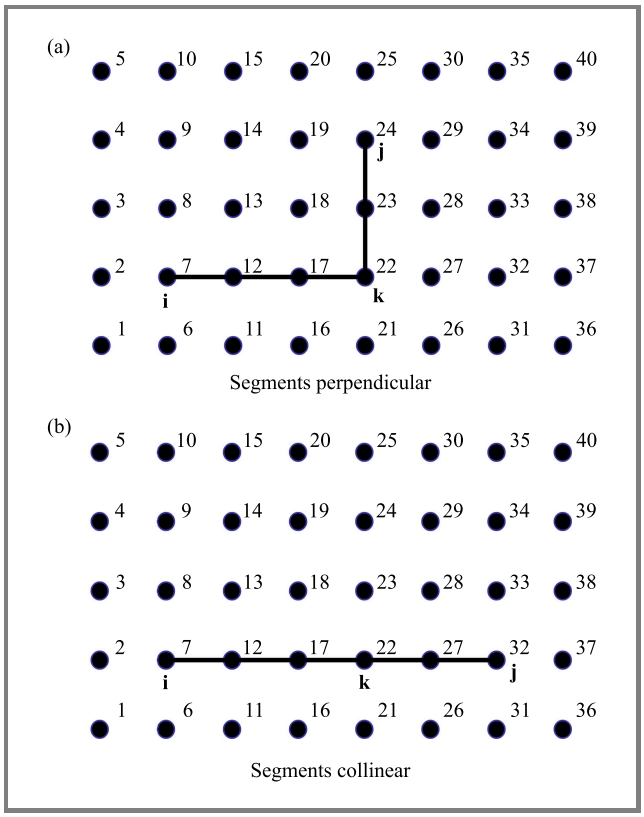

Fig. 3. Two possible paths from node i to node j via k.

vertical is, $\text{abs}(k-j) < H$. These two conditions can be expressed as:

$$\begin{cases} \text{abs}(i-k) \geq H \text{ , if } \mathbf{P}(i,k) \text{ is horizontal} \\ \text{abs}(k-j) < H \text{, if } \mathbf{P}(k,j) \text{ is vertical} \end{cases}. \quad (7)$$

Constraint (7) gives the condition for $\mathbf{P}(i,k)$ and $\mathbf{P}(k,j)$ to be perpendicular. They can also be perpendicular when $\mathbf{P}(i,k)$ is vertical and $\mathbf{P}(k,j)$ is horizontal. This condition can be expressed as:

$$\begin{cases} \text{abs}(i-k) < H \text{ , if } \mathbf{P}(i,k) \text{ is vertical} \\ \text{abs}(k-j) \geq H \text{, if } \mathbf{P}(k,j) \text{ is horizontal} \end{cases}. \quad (8)$$

If either constraint (7) or (8) holds true, then $\mathbf{P}(i,k)$ and $\mathbf{P}(k,j)$ are perpendicular. Constraints (7) and (8) are combined using OR logic and the combined logical constrain is written as:

$$G = \big(\text{abs}(i-k) \geq H \text{ \&\& } \text{abs}(k-j) < H\big) \\ || \ \big(\text{abs}(i-k) < H \text{ \&\& } \text{abs}(k-j) \geq H\big). \quad (9)$$

Here, && is the logical AND operator, || is the logical OR operator and G is a logical variable. $\mathbf{P}(i,k)$ and $\mathbf{P}(k,j)$ are perpendicular if G given by Eq. (9) is true, else they are collinear. In Fig. 3, $G =$ true for the path shown in Fig. 3a and $G =$ false for the path shown in Fig. 3b.

4. Modified Floyd-Warshall Algorithm

The main contribution of this paper is the modification of the Floyd-Warshall all pairs shortest path algorithm to take care of the 90° bends (corners) along the paths.

4.1. Basic Principle

Consider two different paths $\mathbf{P}(s,a,t)$ and $\mathbf{Q}(s,b,c,d,e,f,t)$ from source s to destination t, as shown in Fig. 4. Here, $\mathbf{P}(s,a,t)$ has one bend at a, while $\mathbf{Q}(s,b,c,d,e,f,t)$ has 5 bends at b,c,d,e,f.

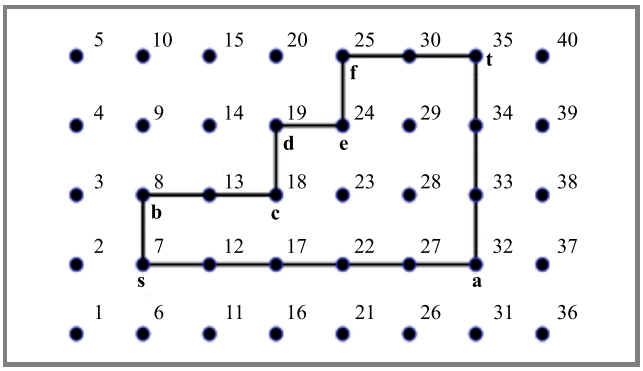

Fig. 4. Two different paths having the same length, but different number of bends.

In the square grid graph of Fig. 4, every connecting edge has a weight 1 and the paths are rectilinear. Therefore, the lengths of the two paths are the same and equal 8, even though the number of bends in each path is different. In this case, the shortest path algorithm can choose either path **P** or path **Q**, with equal preference. But our objective is to select **P** against **Q**, because of a lower number of bends in **P**. To achieve this objective, *corner weights* are introduced in addition to edge weights.

4.1.1. Corner weights

We assign a very small weight (compared to the edge weight) ε to each corner (or bend). Thus, the corner weight is represented by ε. Now, while calculating the total length of a path, both the edge weights and the corner weights are added. This total length is called the augmented length of a path. A very low corner weight is chosen, so that while comparing two paths of different total edge weights, it does not play any significant role. On the other hand, while comparing two different paths of equal total edge weight, the corner weights play a decisive role.

4.1.2. Selection of corner weight ε

Let the possible estimated maximum number of bends (corners) along a lengthy path in the graph be denoted by *mnb*. Then the total corner weight would be $mnb \cdot \varepsilon$. This value should be less than one hop weight, so that the addition of corner weight does not affect the relative weights of paths

under comparison. Therefore, ε should be chosen such that, $mnb \cdot \varepsilon < 1$. That is, choose ε as:

$$\varepsilon = \frac{1}{mnb} \tag{10}$$

Thus, ε depends on the size and layout of the graph.

4.1.3. Augmented path length

The total length of a path considering both the edge weights and corner weights is defined as the augmented path length (APL). Thus for a given path:

APL = "sum of edge weights along the path"
+ "sum of corner weights along the path".

Therefore, a rectilinear path with a lower number of corners will have a lower APL. For example, in Fig. 4, the APL of path $\mathbf{P}(s,a,t)$ is $8+\varepsilon$, because it has one corner, whereas that of path $\mathbf{Q}(s,b,c,d,e,f,t)$ is $8+5\varepsilon$, because it has 5 corners.

Algorithm 1: Floyd Warshall all pair shortest path

$[\mathbf{D}, \mathbf{Next}] = \text{FWAPSP1}(\mathbf{A}, H, n)$

1: **For** each edge (u,v)
2: $D[u][v] \leftarrow A[u][v]$; // $A[u][v]$ is same as $A(u,v)$.
3: $Next[u][v] \leftarrow v$;
4: **End for**
5: **For** $k = 1$ to n
6: **For** $i = 1$ to n
7: **For** $j = 1$ to n
8: **If** $D[i][j] > D[i][k] + D[k][j]$
// update for minimization
a: $D[i][j] \leftarrow D[i][k] + D[k][j]$;
b: $Next[i][j] \leftarrow Next[i][k]$;
// Modification to check for a 90° bend
c: $G = (\text{abs}(i-k) >= H \text{ \&\& } \text{abs}(k-j) < H)$
$||(\text{abs}(i-k) < H \text{ \&\& } \text{abs}(k-j) >= H$;
If (G==true)
$D[i][j] \leftarrow D[i][j] + \varepsilon$;
End if
// Modification end
9: **End if**
10: **End for** // j
11: **End for** // i
12: **End for** // k

Since APLs take care of both the edge weights and corner weights, we use APLs instead of just edge weights, in the shortest path algorithm. Then the algorithm determines the shortest paths with minimum number of bends.

4.2. Floyd-Warshall Algorithm with Corner Weights

The modified Floyd-Warshall algorithm is given as Algorithm 1. On input, it takes adjacency matrix **A**, graph height **H**, number of nodes n and corner weight value ε. On output, it gives the shortest path length (distance) **D** matrix and **Next** matrix. Algorithm 1 is named as Floyd Warshall all pair shortest path (FWAPSP1), and it is written in the form of a function.

Algorithm 2: Function FWAPSP2

$[\mathbf{F}, \mathbf{Next}] = \text{FWAPSP2}(\mathbf{D}, H, n)$

1: **For** each edge (u,v)
2: $F[u][v] \leftarrow D[u][v]$; // $[u][v]$
3: $Next[u][v] \leftarrow v$;
4: **End for**
5: **For** $k = 1$ to n
6: **For** $i = 1$ to n
7: **For** $j = 1$ to n
8: **If** $F[i][j] > F[i][k] + F[k][j]$
// update for minimization
a: $F[i][j] \leftarrow F[i][k] + F[k][j]$;
b: $Next[i][j] \leftarrow Next[i][k]$;
// Modification to check for a 90° bend
c: $G = (\text{abs}(i-k) >= H \text{ \&\& } \text{abs}(k-j) < H)$
$||(\text{abs}(i-k) < H \text{ \&\& } \text{abs}(k-j) >= H$;
d: **If** (G==true)
$F[i][j] \leftarrow F[i][j] + \varepsilon$;
End if
// Modification end
9: **End if**
10: **End for** // j
11: **End for** // i
12: **End for** // k

D matrix gives the minimum APL connected paths between all pairs of nodes. In Algorithm 1, we see that the update of $D[i][j]$ and $Next[i][j]$ (steps 8a and 8b) occur before the augmentation of $D[i][j]$ by the corner weight ε. Therefore, matrix **D** and **Next** will not fully and truly reflect the overall connectivity of the paths taking the APLs into account. Hence, we have to recalculate new **D** and **Next**, based on $D[i][j]$'s instead of $A[i][j]$'s. Even though, the **Next** matrix calculated from FWAPSP1 is not directly used further, it is retained as a formality. The recalculation of matrices **D** and **Next** is implemented in Algorithm 2. On input, it takes

connectivity matrix **D**, graph height H and n. On output, it gives updated shortest path length (distance) **F** matrix and **Next** matrix.

Checking for a bend in the path at k, an intermediate node between i and j, is straightforward in the Floyd-Warshall algorithm compared to Dijkstra, because both the terms on the RHS of step 8a (update for minimization) of FWAPSP1 or FWAPSP2 are an addition of two sub-paths $\mathbf{P}(i,k)$ and $\mathbf{P}(k,j)$. Therefore, the constraint term G, as given by Eq. (9) can be easily constructed, but, in Dijkstra, it is not the case.

4.3. Main Algorithm

The objective is to determine K number of rectilinear non-crossing shortest minimum bend paths (RNMBP) in the presence of rectilinear obstacles. The main algorithm uses Algorithm 1 and 2 to implement RNMBP. Initially, the given obstacles are **marked out** in the adjacency matrix **A**.

Algorithm 3: RNMBP

1: Get the matrix **A** for the given graph with obstacles marked out, use Eqs. (2) and (3)
2: Find the K shortest paths for the given (s,t) ignoring the non-crossing property using unmodified Floyd-Warshall algorithm
3: Get the sorted (s,t) pair based on the lengths of the shortest paths obtained in step 2
4: **Atemp** $=$ **A** // store **A** for the future use
5: Set $i = 1$ // start with the first pair
6: Mark out (s,t) nodes for indices greater than i as obstacles. // we do not want the present path to pass // through those higher indices (s,t) nodes
7: Get **D** using, $[\mathbf{D},\mathbf{Next}] = \text{FWAPSP1}(\mathbf{A},H,n)$. // the return value **Next** is not used
8: Get **Next** using, $[\mathbf{E},\mathbf{Next}] = \text{FWAPSP1}(\mathbf{D},H,n)$
9: **If** $\mathbf{E}(s_i,t_i) = \infty$ go to step 12 // this path not exists
10: Reconstruct the path $\mathbf{P}(s_i,t_i)$
11: Mark out all the nodes along this path.
12: Mark in (restore) the marked out (s,t) node pairs using **Atemp**
13: Increment i for the next iteration as $i = i+1$
14: **If** $i > K$ exit, **Else** go to step 6
15: Exit

4.3.1. Order of processing

In a graph, a longer path creates more obstacles for the succeeding paths than a shorter path. Consider the example of two paths shown in Fig. 5.

The longer line is between 3–38 nodes and the shorter one is between 24–22. If the longer line is drawn first as in Fig. 5a, it covers the entire graph horizontally. Therefore, the second shorter line cannot be drawn without crossing the first line. Hence the non-crossing property cannot be satisfied. On the other hand, if the shorter line is first, the obstacle created is small and the second longer line can be drawn satisfying the non-crossing property, as shown in Fig. 5b.

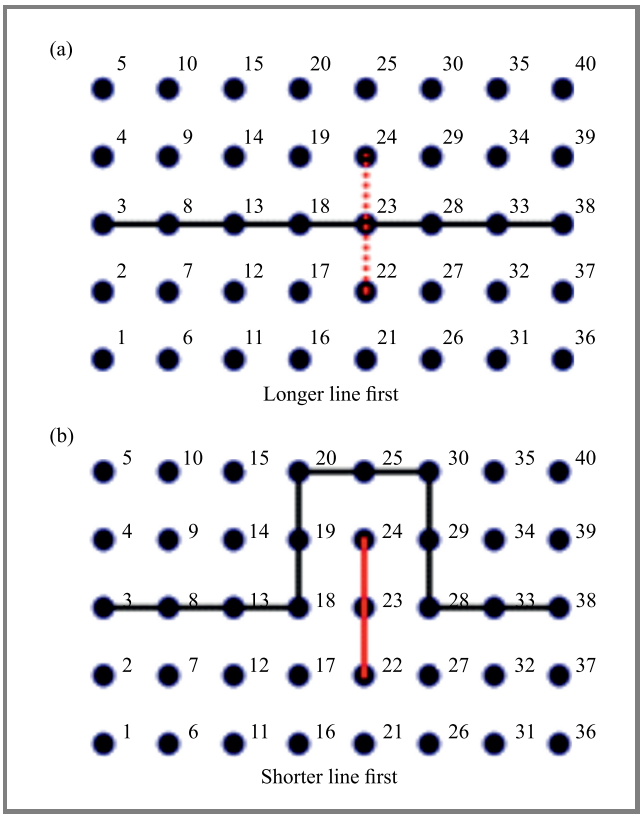

Fig. 5. The effect of order of preference.

Therefore, among the K shortest paths to be determined, we process them in the increasing order of their lengths. Initially, the shortest lengths of all K paths are determined considering the non-crossing (node disjoint) property. Then the corresponding (s,t) pairs are sorted in the increasing order of their lengths. Then, the sorted (s,t) list is processed one after another, as described in Subsection 3.5.

Now, $\mathbf{P}(s_i,t_i)$ for $i = 1$ to K gives the K shortest non-crossing minimum bend paths. Since algorithm RNMB uses the modified Floyd-Warshall algorithm, the time complexity is $O(n^3)$. The path reconstruction function has a complexity of $O(n)$.

4.4. Experimental Results

Several examples are solved using RNMBP. Because of the limited space, all results are not presented.

Example 1. Here, $W = 17$, $H = 13$ and $K = 7$. The total number of nodes $n = 17 \times 13 = 221$ and $\varepsilon = 0.001$,

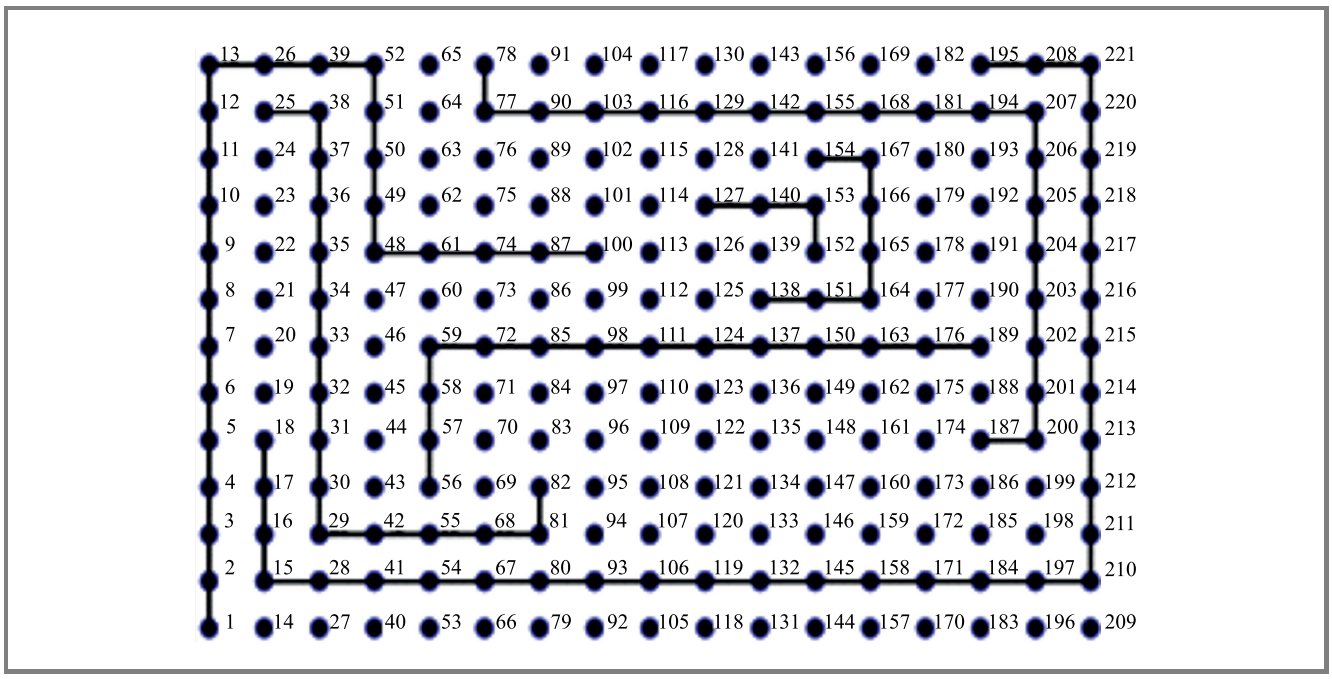

Fig. 6. Seven non-crossing shortest paths identified by RNMBP.

which corresponds to $mnb = 1000$. The $(s-t)$ pair set is taken as:

$$(s-t) = \{\ (78-187), (189-56), (127-152), (195-18), (82-25), (154-138), (1-100)\ \}$$

This example has no obstacles.
The shortest paths are found using RNMBP. The 7 non-crossing paths are shown in Fig. 6. The full path and the lengths are shown in Table 1.

Example 2. This is an example with rectilinear obstacles. Here, $W = 17$, $H = 13$ and $K = 2$. The total number of nodes $n = 17 \times 13 = 221$ and $\varepsilon = 0.001$. The $(s-t)$ pair set is taken as:

$$(s-t) = \{(1-73), (164-196)\}.$$

The two shortest paths avoiding the obstacles are found using RNMBP and are shown in Fig. 7.

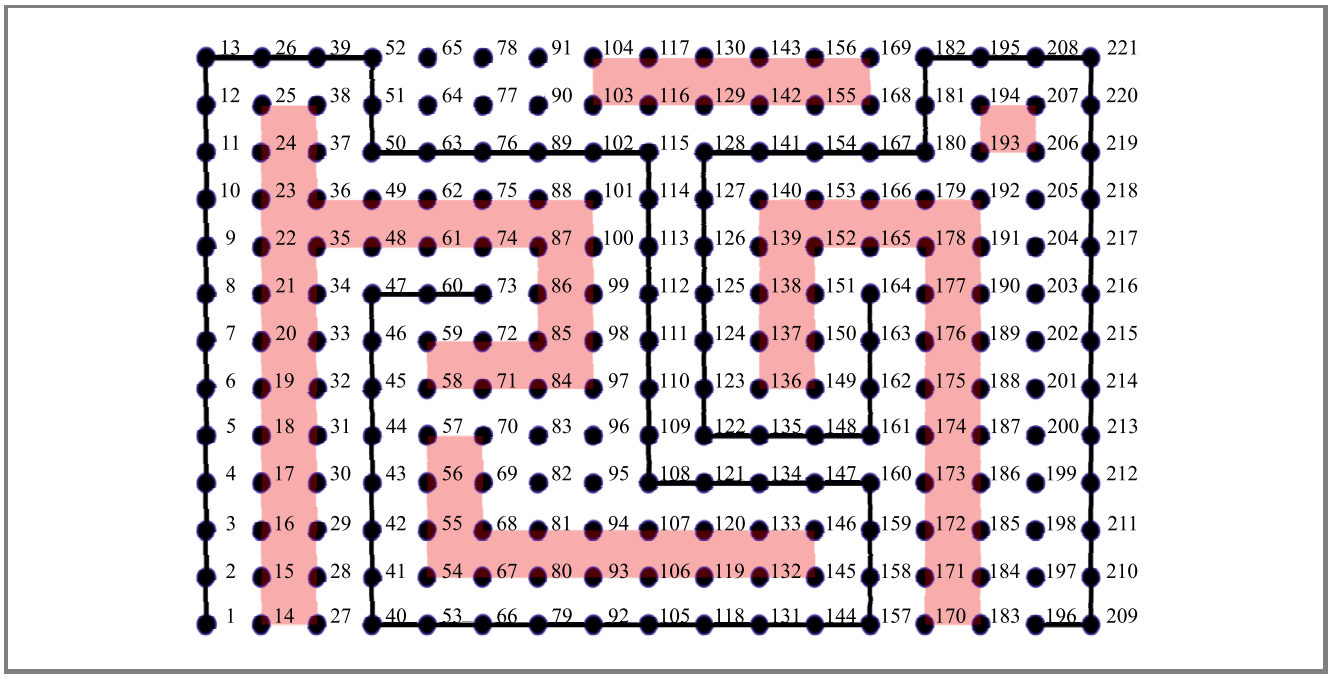

Fig. 7. Two non-crossing shortest paths avoiding obstacles identified by RNMBP.

Table 1
Nodes along the path and path lengths

i	$(s_i - t_i)$	Nodes along the full path	Path length
1	127–152	[127 140 153 152]	3
2	154–138	[154 167 166 165 164 151 138]	7
3	189–56	[189 176 163 150 137 124 111 98 85 72 59 58 57 56]	13
4	82–25	[82 81 81 68 55 42 29 30 31 32 33 34 35 36 37 38 38 25]	17
5	1–100	[1 2 3 4 5 6 7 8 9 10 11 12 13 13 26 39 52 51 50 49 48 48 61 74 87 100]	25
6	78–187	[78 77 77 90 103 103 116 129 142 155 168 181 194 207 206 205 204 203 202 201 200 200 187]	22
7	195–18	[195 208 221 220 219 218 217 216 215 214 213 212 211 210 210 197 184 171 158 145 132 119 106 93 80 80 67 54 41 28 15 16 17 18]	33
The total length of all paths = 120			

In Fig. 7, the paths do not touch the obstacles. The RNMBP algorithm can be modified so that the paths may touch the obstacle boundaries but should not cross them.

5. Comparison with Other Methods

In the proposed RNMBP algorithm, minimization of the number of bends, as well as the length of a path, is done simultaneously using the modified, well-known Floyd-Warshall algorithm, whereas in [6], the authors determine the shortest staircase-path first and then use the push-and-drag method to reduce the number of bends. The algorithm given by [6] is relatively more complex than the presented method wherein pushing and dragging are not required.

In the proposed algorithm, the obstacles are taken care of by simply marking out (excluding) the corresponding boundary nodes. In [6], an extra graph called the boundary graph is created, which unnecessarily increases complexity. In [7], track graphs are created to take care of obstacles. In [8], induced points and multiple paths are generated before getting the final path. In [9], extreme points and edges of the obstacles are determined first. In this case, additional processing of the obstacles is not required. In Lee's algorithm [10], wave-front propagation is used throughout the graph until the target node is reached which is a tedious process. In [11], a visibility graph is created to take care of the obstacles. There is no need to create additional graphs here.

In the next step, a time complexity comparison with bi-objective optimization is researched. Let us consider an example, where $K = 7$ and $\varepsilon = 0.001$. The width $W = 10$ and height H is varied from 20 to 60 in steps of 5. Therefore, $n = W \times H$ varies from 200 to 500 in steps of 50. The problem is solved using the bi-objective optimization (BiOO) method [13], as well as RNMBP. The length of the path and the number of bends along the path are expressed by functions $L(\mathbf{x})$ and $B(\mathbf{x})$, respectively, where $\mathbf{x}$ is the binary decision vector [13]. The scalarized objective function $F(\mathbf{x})$ is taken as:

$$F(\mathbf{x}) = \lambda \cdot L(\mathbf{x}) + (1 - \lambda) \cdot B(\mathbf{x}), \tag{11}$$

λ is set at 0.5 to give equal weightage to both criteria. The BiOO (minimization of $F(\mathbf{x})$) is carried out using binary integer programming. The time taken by BiOO, as well as RNMBP, for different values of n (total number of nodes in the graph) is shown in Fig. 8.

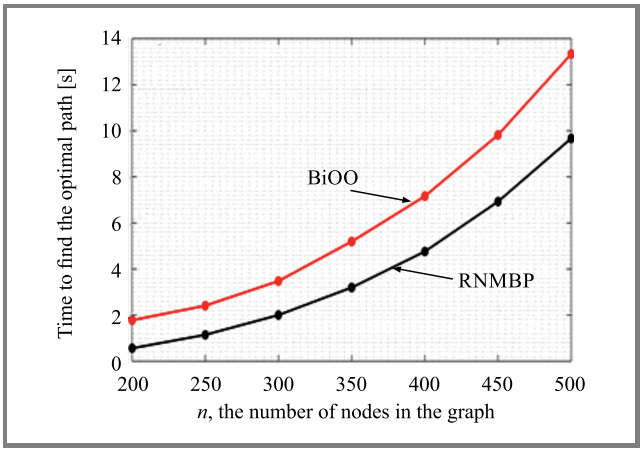

Fig. 8. Time taken versus the number of nodes.

From Fig. 8, we see that the RNMBP method takes substantially less time compared to the BiOO method. Of course, the times taken are machine-dependent and are relative only.

6. Conclusions

A new algorithm is presented to determine K shortest non-crossing minimum bend paths in the presence of obstacles, in a square grid graph. A simple and novel technique is adopted to minimize the number of bends in the shortest path by introducing corner weights and augmented path lengths in the modified Floyd-Warshall algorithm. Obstacles and non-crossing requirements are handled by **marking out** the respective nodes. Our RNMBP algorithm has a time complexity of $O(n^3)$ and is simple to implement. Even then, its task completion time is substantially lower than that of the BiOO method.

References

[1] A. Madkour, W. G. Aref, F. U. Rehman, M. Abdur Rahman, and S. Basalamah, "A Survey of Shortest-Path Algorithms" [Online]. Available: https://arxiv.org/abs/1705.02044 (accessed 6 July 2017).

[2] S. Eriksson-Bique *et al.*, "Geometric *k*-shortest paths", in *Proc. 26th Ann. ACM-SIAM Symp. Discrete Algorithms SODA'15*, San Diego, CA, USA, 2015, pp. 1616–1625 (doi: 10.1137/1.9781611973730.107).

[3] J. S. B. Mitchell, "Geometric shortest paths and network optimization", in *Handbook of Computational Geometry* J.-R. Sack and J. Urrutia (ed.). Amsterdam: Elsevier Science B.V., 1998, pp. 633–701 (doi: 10.1016/B978-044482537-7/50016-4).

[4] N. S. P. Hyun, P. A. Vela, and E. I. Verriest, "A New framework for optimal path planning of rectangular robots using a weighted L_p norm", *IEEE Robotics and Automation Let.*, vol. 2, no. 3, pp. 1460–1465, 2017 (doi: 10.1109/LRA.2017.2673858).

[5] N. Qingbin, "Research on robot obstacle avoidance and path tracking under dynamically unknown environment", in *Proc. 2017 IEEE 2nd Adv. Inform. Technol., Electronic and Automation Control Conf. IAEAC*, Chongqing, China, 2017, pp. 2607–2610 (doi: 10.1109/IAEAC.2017.8054496).

[6] C. D. Yang, O. Z. Lee, and C. K. Wong, "On bends and lengths of rectilinear paths: A graph-theoretic approach", *Internat. J. Comput. Geom. Appl.*, vol. , no. 1, pp. 61–74, 1992 (doi: 10.1142/S0218195992000056).

[7] Y. E. Wu, E. Widmayer, M. D. E. Schlag, and C. K. Wong, "Rectilinear shortest paths and minimum spanning trees in the presence of rectilinear obstacles", *IEEE Trans. Comput.*, vol. C-36, no. 3, pp. 321–33, 1987 (doi: 10.1109/TC.1987.1676904).

[8] M. de Berg, M. van Kreveld, B. J. Nilsson, and M. H. Overmars, "Shortest Path Queries in Rectilinear Worlds", *Int. J. of Computat. Geom. & Applic.*, vol. 2, no. 3, pp. 287–309, 1992 (doi: 10.1142/S0218195992000172).

[9] D. T. Lee and F. P. Preparata, "Euclidean shortest paths in the presence of rectilinear barriers", *Networks*, vol. 14, no. 3, pp. 393–410, 1984 (doi: 10.1002/net.3230140304).

[10] E. M. Arkin *et al.*, "The shortest path to a segment and quickest visibility queries", in *Proc. 31st Int. Symp. on Computat. Geometry SoCG*, Eindhoven, The Netherlands, 2015, pp. 658–673 (doi: 10.4230/LIPIcs.SOCG.2015.658).

[11] K. L. Clarkson, S. Kapoor, and P. M. Vaidya, "Rectilinear shortest paths through polygonal obstacles in $O(n(\log n)^2)$ time", in *Proc. 3rd Annual ACM Sympos. Comput. Geom.*, Waterloo, ON, Canada, 1987, pp. 251–257 (doi: 10.1145/41958.41985).

[12] Z. Tarapata, "Selected multicriteria shortest path problems: An analysis of complexity, models and adaptation of standard algorithms", *Int. J. of Applied Mathem. and Computer Science*, vol. 17, no. 1, pp. 269–287, 2007 (doi: 10.2478/v10006-007-0023-2).

[13] Y. Sun and M. X. Lang, "Bi-objective optimization for multi-modal transportation routing planning problem based on Pareto optimality", *J. Ind. Eng. Manag.* vol. 8, no. 4, pp. 1195–1217, 2015 (doi: 10.3926/jiem.1562).

Shylashree Nagaraja received her B.Eng. degree in Electronics and Communication from VTU, Karnataka, India in 2006. She received her M.Tech. degree in VLSI Design and Embedded Systems from VTU, Karnataka, India, in 2008. She received her Ph.D. degree from VTU, Karnataka, India in 2016. She received Best PhD Thesis Award for the year 2016–2017 in Electronics & Communication Engineering form BITES. She is also an Associate Professor at the ECE Department, Rastreeya Vidyalaya College of Engineering, Bengaluru, Karnataka, India. She is an author or co-author of more than twenty papers on the subjects of cryptography, computer networks and VLSI.
E-mail: shylashashi@gmail.com, shylashreen@rvce.edu.in
Department of Electronics & Communication Engineering
Rastreeya Vidyalaya College of Engineering
Mysuru Road
Bengaluru 560059
Karnataka, India

Information for Authors

Journal of Telecommunications and Information Technology **(JTIT)** is published quarterly. It comprises original contributions, dealing with a wide range of topics related to telecommunications and information technology. **All papers are subject to peer review**. Topics presented in the JTIT report primary and/or experimental research results, which advance the base of scientific and technological knowledge about telecommunications and information technology.

JTIT is dedicated to publishing research results which advance the level of current research or add to the understanding of problems related to modulation and signal design, wireless communications, optical communications and photonic systems, voice communications devices, image and signal processing, transmission systems, network architecture, coding and communication theory, as well as information technology.

Suitable research-related papers should hold the potential to advance the technological base of telecommunications and information technology. Tutorial and review papers are published only by invitation.

Manuscript. TEX and LATEX are preferable, standard Microsoft Word format (.doc) is acceptable. The authors JTIT LATEX style file is available:
http://www.nit.eu/for-authors

Papers published should contain up to 10 printed pages in LATEX authors style (Word processor one printed page corresponds approximately to 6000 characters).

The manuscript should include an abstract about 150200 words long and the relevant keywords. The abstract should contain statement of the problem, assumptions and methodology, results and conclusion or discussion on the importance of the results. Abstracts must not include mathematical expressions or bibliographic references.

Keywords should not repeat the title of the manuscript. About four keywords or phrases in alphabetical order should be used, separated by commas.

The original files accompanied with pdf file should be submitted by e-mail: redakcja@itl.waw.pl

Figures, tables and photographs. Original figures should be submitted. Drawings in Corel Draw and PostScript formats are preferred. Figure captions should be placed below the figures and can not be included as a part of the figure. Each figure should be submitted as a separated graphic file, in .cdr, .eps, .ps, .png or .tif format. Tables and figures should be numbered consecutively with Arabic numerals.

Each photograph with minimum 300 dpi resolution should be delivered in electronic formats (TIFF, JPG or PNG) as a separated file.

References. All references should be marked in the text by Arabic numerals in square brackets and listed at the end of the paper in order of their appearance in the text, including exclusively publications cited inside. Samples of correct formats for various types of references are presented below:

[1] Y. Namihira, Relationship between nonlinear effective area and mode field diameter for dispersion shifted fibres, *Electron. Lett.*, vol. 30, no. 3, pp. 262–264, 1994.

[2] C. Kittel, *Introduction to Solid State Physics*. New York: Wiley, 1986.

[3] S. Demri and E. Orłowska, Informational representability: Abstract models versus concrete models, in *Fuzzy Sets, Logics and Knowledge-Based Reasoning*, D. Dubois and H. Prade, Eds. Dordrecht: Kluwer, 1999, pp. 301–314

Biographies and photographs of authors. A brief professional authors biography of up to 200 words and a photo of each author should be included with the manuscript.

Galley proofs. Authors should return proofs as a list of corrections as soon as possible. In other cases, the article will be proof-read against manuscript by the editor and printed without the author's corrections. Remarks to the errata should be provided within one week after receiving the offprint.

A copy of the JTIT is provided to each author of paper published.

Journal of Telecommunications and Information Technology has entered into an electronic licencing relationship with EBSCO Publishing, the worlds most prolific aggregator of full text journals, magazines and other sources. The text of *Journal of Telecommunications and Information Technology* can be found on EBSCO Publishings databases. For more information on EBSCO Publishing, please visit www.epnet.com.

(*Contents Continued from Front Cover*)

INSTYTUT ŁĄCZNOŚCI
PAŃSTWOWY INSTYTUT BADAWCZY

Editorial Office

National Institute
of Telecommunications
Szachowa st 1
04-894 Warsaw, Poland

tel. +48 22 512 81 83
fax: +48 22 512 84 00
e-mail: redakcja@itl.waw.pl
http://www.nit.eu

JOURNAL OF TELECOMMUNICATIONS AND INFORMATION TECHNOLOGY 3/2018